NMED/DOE/AIP-95/3

Characterization of Environmental Radiation and Radioactivity Near Albuquerque, New Mexico

By
John Michael Hostak
New Mexico Environment Department

In Cooperation with
the University of New Mexico,
Environmental Radiation Measurements Laboratory
Dr. Robert D. Busch, Director

May 1995

DOE Oversight Bureau
New Mexico Environment Department
2044-A Galisteo Street, P.O. 26110
Santa Fe, New Mexico 87502

Characterization of Environmental Radiation and Radioactivity Near Albuquerque, New Mexico

By
John Michael Hostak,
New Mexico Environment Department

In Cooperation with
the University of New Mexico,
Environmental Radiation Measurements Laboratory
Dr. Robert D. Busch, Director

May 1995

Characterization of Environmental Radiation and Radioactivity near Albuquerque, New Mexico

By
John Michael Hostak

Executive Summary

May 1995

Characterization of
Environmental Radiation and Radioactivity
near Albuquerque, New Mexico

by
John Michael Hostak

EXECUTIVE SUMMARY

The characterization of environmental radiation in a given locality is an important consideration in both siting and decommissioning nuclear facilities, the assessment of consequences of current operations and past releases from nuclear facilities or activities, and in understanding the relative risk that environmental radiation poses to public health and the environment. The primary objective of this study was to characterize the relative contributions of natural and man-made radioactivity at a variety of locations near Albuquerque, New Mexico. The quantitation methods employed were all based on gamma-radiation detection, including: soil sampling with gamma-ray spectroscopy, environmental thermoluminescent dosimeters, and the use of a high pressure ionization chamber. These methods have the advantage of relative ease of use with minimal laboratory preparation.

Typical numerical values and ranges for radionuclides in soil and *in situ* exposure rate measurements were evaluated. Geometric and harmonic means for the measurement parameters over the entire study area follow: ^{226}Ra, 1.15 and 1.12 pCi/g; ^{214}Bi, 1.19 and 1.16 pCi/g; ^{235}U, 0.06 pCi/g (both) ; ^{238}U, 1.80 and 1.65 pCi/g; ^{232}Th, 1.40 and 1.37 pCi/g; ^{40}K, 15.5 and 15.3 pCi/g; ^{137}Cs, 0.18 and 0.14 pCi/g; TLD Rates, 11.4 μR/h (both); and HPIC rates, 13.0 μR/h (both). The values for ^{238}U and ^{232}Th series nuclides, as well as ^{137}Cs and exposure rates were higher on the slopes of the Sandia and Manzano Mountains and Central Highlands than in the Albuquerque Basin. ^{40}K maxima were associated with the western foothills and bajadas associated with mountain front outwash from igneous rocks. Higher values for ^{238}U and ^{232}Th series nuclides are associated with source rock type and elevated ^{137}Cs correlated with meteorologic patterns.

Results for soil activities and exposure rate measurements compared favorably with various literature sources including the results of surveillance and characterization efforts related to nuclear facilities currently operating or planned in New Mexico.

TABLE OF CONTENTS

LIST OF TABLES
(in Appendix I)

LIST OF FIGURES

1. INTRODUCTION

The characterization of environmental radiation has developed as an integral operational Health Physics task, accompanying the explosive development of defense and commercial nuclear capabilities in the United States since the late 1940's. Such characterization is an important consideration in the siting and decommissioning of nuclear facilities, the assessment of consequences of current operations and past releases from nuclear facilities, and in understanding the relative risk that environmental radiation may pose to public health and the environment. Increasing public health concern has been placed on the process of remediating facilities and land areas that were purposefully or incidentally contaminated by radioactive materials as a consequence of civilian and military nuclear activities. Among the most difficult and potentially controversial features of that process is the establishment of enforceable cleanup standards and their relationship to background radiation levels (1,2,3).

The United States has emerged as a leader within the global nuclear community in the areas of dismantling, decontamination, and remediation of nuclear facilities in the private and public sectors, as well as evaluation and design of nuclear waste repositories. This has been conditioned in part by the waning of the commercial nuclear power industry, the aging of power reactors with respect to their design lives, and the industry's increasingly pressing need for transient and permanent nuclear waste storage capacity. Moreover, with the cessation of the Cold War, the Nation's weapons complex has accelerated the processes of decommissioning portions of its weapons-based facilities and seeking non-defense industrial missions for its remaining nuclear assets. Increased activity is also occurring in the processes of assessing and mitigating uncontrolled radioactive waste sites and contaminated lands from past activities in the weapons complex. All of these processes can have the effect of increasing the environmental radiation source term. The extent to which those radiation levels may increase and result in impacts on public health and the environment must be evaluated by comparison to some baseline, reflecting both natural and anthropogenic radiation contributions.

1.1 Radiation Sources in the Vicinity of Albuquerque, NM

Government owned facilities throughout New Mexico have figured prominently in the development of the nation's nuclear defense capabilities since the beginning of the "nuclear age". Elements of all the processes described above are occurring

simultaneously at Department of Energy (DOE) and Department of Defense (DOD) facilities on Kirtland Air Force Base (KAFB) near Albuquerque, New Mexico. To be sure, the United States Government does not own the only operating Albuquerque area facilities that manage radioactive materials and wastes. The largest Nuclear Regulatory Commission (NRC) licensee in New Mexico is also located in the Albuquerque area: the University of New Mexico including its extensive medical facilities. There are numerous other small NRC licensees in the Albuquerque area such as nuclear medicine facilities, medical and industrial radiographic operations, and other miscellaneous source owners. A preliminary inventory of NRC licensees that are potential radioactive dischargers within the immediate Albuquerque vicinity, as well as in surrounding areas that may exert local impacts, has been documented (4). NRC regulated facilities in Albuquerque and throughout New Mexico are licensed through the New Mexico Environment Department under its Radiation Protection Regulations (5). While their contribution to the radiation environment can not be ignored wholesale, that aggregate contribution is expected to be relatively small compared to the various government facilities established at Kirtland Air Force Base. These include reactors, accelerators, irradiators, facilities for destructive testing of nuclear materials and devices, long-term mixed and radioactive waste storage, spent nuclear fuel storage, and approximately seventy uncontrolled radioactive waste or land contamination areas (6,7,8,9,10).

The reconsolidation of the U.S. nuclear weapons complex and search for new missions for old facilities is expected to significantly augment the number of Albuquerque area DOE nuclear facilities and their resultant effluent and waste streams. Two impending initiatives are the relocation of neutron generator manufacturing facilities from Pinellas, FL, to Sandia National Laboratories in Albuquerque, NM, and the retrofitting of the Sandia Annular Core Research Reactor and Hot Cell Facilities to accommodate the industrial-scale manufacture of the medical imaging isotope, $^{99}Mo(^{99m}Tc)$ (11). As New Mexico's most populous and fastest growing area, the pressure to open dwindling public land and water resources near Albuquerque for development is expected to create mounting pressure on one of the largest aggregate land holders in the area, Kirtland Air Force Base including its various tenants, to further decommission facilities and remediate radioactive contamination in the environment from past defense activities.

Additional attention has been drawn to environmental radiation sources in the Albuquerque area as a result of several studies showing naturally occurring radon (^{222}Rn) concentrations in residential air and ground water which are

elevated with respect to current guidelines and proposed regulations (12,13,14,15). Ground water provides the sole public drinking water supply for Albuquerque.

1.2 Study Design and Experimental Approach

The ultimate study goal was to improve the general understanding of the geographic distribution of environmental radiation and radioactivity in the study area. It is fervently hoped that the results of this study are of practical value for a number of potential end-users. The results were intended to have particular value for entities overseeing the operations and impacts of nuclear facilities in the region, including the New Mexico Environment Department (NMED). An incidental value is the demonstration of the capabilities developed at the University of New Mexico's Environmental Radiation Measurement Laboratory (ERML) to characterize radioactivity and radiation in or arising from environmental media.

This study represents an exploration of radioactivity and radiation characteristics of the environment in the vicinity of Albuquerque, New Mexico. The term *exploration* is used advisedly. The study incorporated populations of sampling and monitoring locations that were as extensive as practicable for its duration, but could not be said to have originated from a statistically *designed* sampling or monitoring program, as defined in the most strict sense (16). Such programs are designed for specific objectives that include characterization of small-scale hazardous waste sites for remedial action. The objective of our study was much broader: to search for discernible trends in distributions of environmental radiation and radioactivity. The author took the best advantage of opportunities to locate sampling and monitoring points incidental to oversight activities involving radiological surveillance and assessment programs at Sandia National Laboratories (SNL) and the Inhalation Toxicology Research Institute (ITRI). In that sense, the design of sampling and monitoring may be said to have been judgmental in character. This approach also allowed for comparisons to existing facility monitoring programs and their data sets. To our knowledge, an extensive geographic characterization study that includes the objective of determining a baseline for potential radioactive contamination has been performed only once in New Mexico by an organization external to an agency of the U. S. Government. That study was the New Mexico Environmental Improvement Division's (now New Mexico Environment Department) Statewide WIPP Transportation Corridor (Roadside) Study (17). The radiochemical soil analysis data from that study were statistically reduced as an ancillary feature of this study.

Quantitative positioning data were not readily available for the Roadside study, so the radiochemical results are treated as statewide summaries.

The instrumental techniques used to characterize radiation and radioactivity in this study were all based on gamma-ray measurement. Thus, they enjoy all the advantages and suffer from all the limitations inherent to gamma-ray detection methods. The primary limitation concerns finding suitable gamma-emitting primary or daughter nuclides with energies and yields amenable to clear detection and analysis. Advantages of the methods include rapid detection, relative ease of use, and limited laboratory preparation of samples. The techniques employed included the use of high sensitivity thermoluminescent dosimeters deployed in the environment, soil sampling and analyses by laboratory gamma-spectroscopy, and the use of a portable high pressure ionization chamber as an environmental survey instrument. The study was augmented by use of a global positioning instrument and other geographical information sources, as well as research into environmental characteristics that might influence local distributions.

1.3 Regional Setting

To create an environmental perspective in which to interpret the results of this study, it is necessary to define geographic limits for the region and illustrate pertinent regional characteristics. The study region is illustrated in Figure 1, which also identifies soil sampling locations and gives the approximate study region boundaries in degrees latitude and longitude. As may be seen, much of the study effort was focused in and around KAFB. The region which includes and surrounds the Albuquerque Metropolitan Area is located in north-central New Mexico. While largely concentrated in Bernalillo County, the study region overlaps into Sandoval County in the north, Santa Fe County in the east, and Valencia County in the south.

1.3.1 Geologic Setting

The study region is located within the Albuquerque-Belen Basin, a gross tectonic subsidence feature of the Rio Grande Rift. The latter has also been described as the Rio Grande Trough. The Rio Grande Rift comprises a string of such structural basins bordered by series of *en echelon* fault blocks, extending from central Colorado to northern Mexico in the northern extreme of the Basin and Range Province of North America (18). While included in the province, the Rift is structurally distinguishable as a failed rift arm.

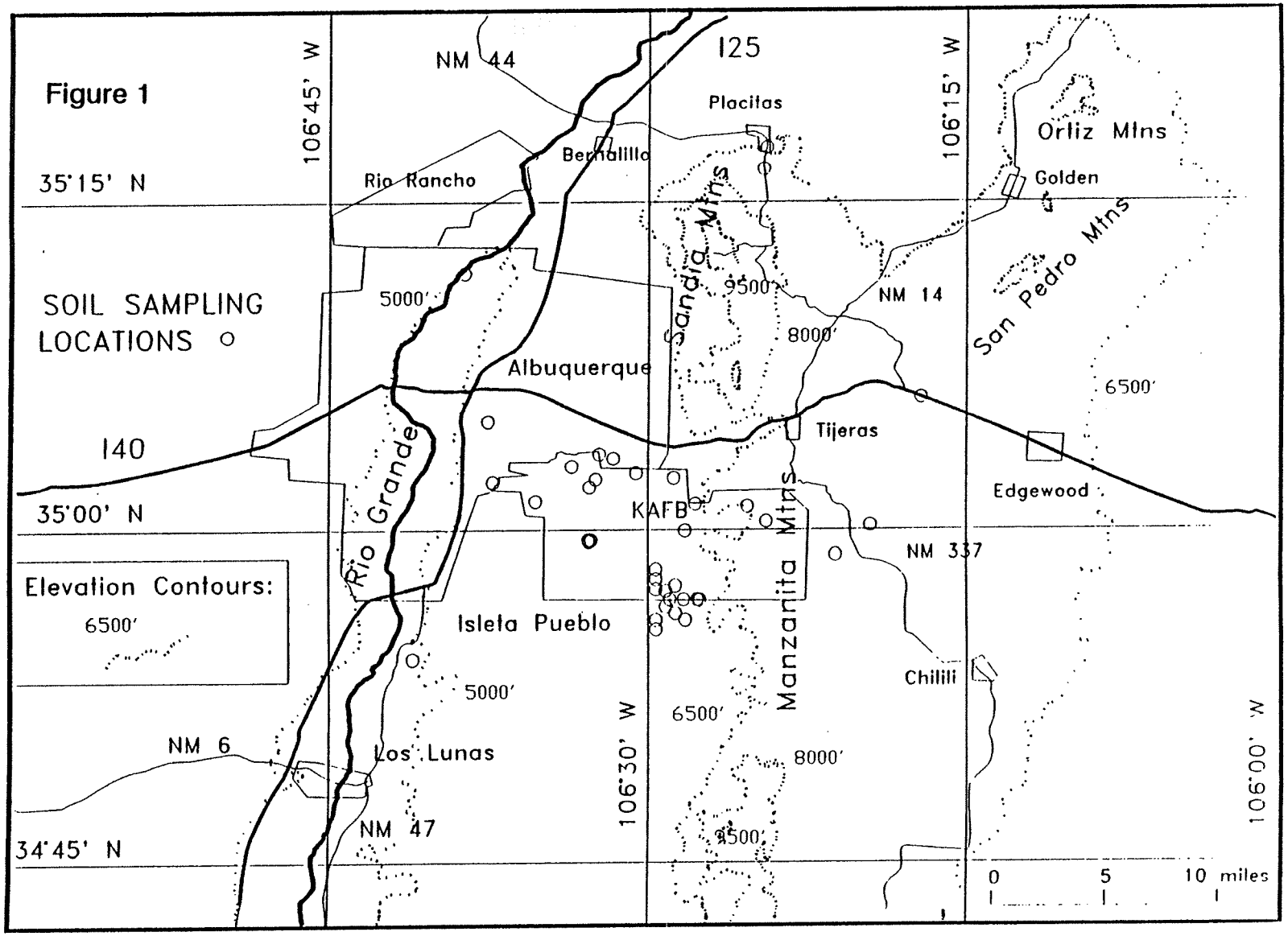
Figure 1
SOIL SAMPLING LOCATIONS
Elevation Contours:
6500'
35°15' N
35°00' N
34°45' N
106°45' W
106°30' W
106°15' W
106°00' W
NM 44
125
140
NM 14
NM 337
NM 6
NM 47
Placitas
Bernalillo
Rio Rancho
Albuquerque
Tijeras
Edgewood
KAFB
Isleta Pueblo
Los Lunas
Chilili
Orliz Mtns
Golden
Sandia Mtns
San Pedro Mtns
Manzanita Mtns
Rio Grande
5000'
6500'
8000'
9500'
0
5
10 miles

The Albuquerque-Belen Basin encompasses about 2100 square miles in north-central New Mexico. The basin may be further divided into two distinct geohydrologic regions, termed northern and southern half-grabens (19,20,21). Sediments accumulated on the graben floor vary in depth from less than a few feet near the mountain escarpments to as much as 21,000′ at basin center, below the Rio Grande. The subsurface geology, geochemistry and hydrology of the basin have been the wellspring of continuing energetic scientific investigations and are discussed in greater detail in a variety of sources (19,20,21,22,23). Much of this activity has been fueled by the dwindling availability of ground water resources that provide the sole source of potable water in an area experiencing accelerated urban development and population growth. Geology and geomorphology vary widely within the basin, and structural complexity increases with approach toward the eastern basin margin, including extensive faulting. Probable Holocene movement has been documented on several basin faults, a condition sufficient to meet NRC *capable fault* criteria (18,24,25,26). The Albuquerque Basin is seismically active, with relatively frequent earthquakes of low magnitude (27,28,29). The basin may be prone to significant vertical and horizontal ground accelerations of 0.32 *g* and 0.48 *g*, respectively (30). Vertical displacement of buried sediments can contribute additional detritus to local soil development (31,32).

The study region may be further divided into distinct physiographic subunits for convenience, as follows. Proceeding from west to east, the study region includes the Albuquerque West Mesa area on the sprawling Llano de Albuquerque, underlain by basalt over a significant area, the west river terraces, the inner Rio Grande valley floodplain, the east river terrace and the East Mesa areas which are dissected by east-west trending arroyos, and the steep escarpments of the Sandia and Manzano Mountain Ranges, which rise to create the eastern boundary of the basin and are dissected primarily by east-west trending canyons. The eastern extreme of the study region terminates in the Central Highlands, beyond the crestlines of the mountain ranges and outside the boundary of the basin. The majority of the study area is located on the sloping piedmont plain of coalescing alluvial fans (bajadas) and river terraces in the northern half-graben, sweeping westward from the Manzano and Sandia Mountains at elevations between 5000 and 6500 feet above mean sea level (5000′-6500′ MSL). Significant elevation changes over the region are roughly indicated in Figure 1 by hatched lines on 1500′ intervals. A greater level of physiographic detail has not been included in these figures for the sake of simplicity and ease of interpretation. The reader may find greater detail in numerous excellent regional references used

references used in the study for interpretation and construction of simplified maps, including Figure 1 (33,...45).

A variety of soil types may be found across the study region, reflecting the various processes of sedimentation and soil development. Soil types may be divided into four generally consistent categories related to local geomorphology and physiographic regions as described in their areas of occurrence (18,19,22,45,46). These include:

1.) Soils of alluvial and colluvial origin that form nearest to their source rocks, representing the least degree of geochemical and physical weathering (youngest soils), occurring in areas of steep uplift on the eastern escarpments and incised canyons, northern extreme of the Sandias, and in the eastern Central highlands;

2.) Piedmont-slope alluvium, ranging from fine grained sandy loams to coarser-grained sands, found on the east and west mesas of the region including younger alluvial fan deposits as well as relatively thin mantling of sediments over pediments and basalt flows;

3.) Valley-border alluvium, derived from local outwash, stream-borne sediments and eolian deposition in the inner Rio Grande valleys, including locally extensive incised river terrace and arroyo deposits found in the east and west terrace areas;

4.) River alluvium deposits of the Rio Grande channel and floodplains, varying widely in terms of source rock origin and in grain size including clays, silts, sands and gravels.

The geological ages of these surficial deposits range from Holocene to middle Pleistocene epochs. A variety of source rocks have contributed the original mineral constituents of the soils (47,48). From the east side of the escarpment proceeding west are the coalescing alluvial fan deposits (bajada) deposits derived from the outcropping rocks of the Sandia and Manzano (Manzanita) Ranges. Source rocks providing the bulk of material in the basin include the Precambrian acid intrusive and extrusive rocks and their altered forms: Granite of the Sandia Mountains, biotite granite, granite gneiss, and meta-rhyolites, as well as Precambrian metamorphic rocks: amphibolite, schist, quartzite, and greenstone, and contribution from Pennsylvanian rocks including the Madera Limestone and cherts, siltstones and sandstone conglomerates of the Sandia Formation. Grain size generally decreases with increasing distance from the mountain fronts, reflecting the higher degree of mechanical decomposition and weathering of

the original mineral constituents. Components of these deposits include gravels, quartz and potassium feldspar sands, and micaceous silt fines. At the mouth of Tijeras Canyon, dividing the Sandia and Manzano Ranges, are outcrops of red Permian Abo Sandstone and the heterogeneous Madera Limestone which contribute to local sediments, as well as those carried during flow events through Tijeras Arroyo to the west. To the north of the Sandias, Mesozoic rocks are heavily eroded into a system of deep canyons. These include Jurassic age Morrison Formation sediments and range lithologically from shale to sandstone. The tipped fault block mountain ranges are largely capped by the east dipping Madera Limestone, which is expected to contribute a majority of detrital material to the soils of Central Highlands, Las Huertas Canyon and Sandia Peak locations within our study region. The Madera Limestone as a group may also contain interbedded micaceous or feldspathic shales, sandstone, and occasionally arkosic conglomerates. Outcrops of decomposing Precambrian granites were also encountered on the approach to the peak via Las Huertas Canyon. Reworked sedimentary materials of varying origins are found on the west mesa as stream, terrace, and eolian deposits. Floodplain deposits reflect the local source rock composition of the eastern bajadas, but also contain sediments reflecting volcanic and metamorphic rock derived debris, originating upriver in the northern highlands.

The most prominent surface hydrologic feature of the Albuquerque-Belen basin is the Rio Grande River. A number of arroyos contribute flow and sediments to the Rio Grande within the basin. The largest tributary to the Rio Grande in the study region is Tijeras Arroyo, which accepts storm water run-off from most of the surface drainage features on KAFB. Discharge from Tijeras Arroyo to the Rio Grande occurs via the Albuquerque Municipal Arroyo Flood Control Authority (AMAFCA) Channel System. Notable surface drainage features also occur separately on the southern portion of KAFB which are presumed to discharge to playa lakes on the University of New Mexico land grant to the west of KAFB (49). KAFB facilities that may influence flow in these features include the SNL Coyote Test Field, SNL Technical Areas Three and Five (TA III, TA V) and various SNL Environmental Restoration and U.S. Air Force Installation Restoration sites. Flow in all area drainage features, including the reach of Tijeras Arroyo that traverses KAFB, is ephemeral, dependent on rainfall events and facility discharges. Perennial flow in Tijeras Creek ordinarily disappears by infiltration into arroyo bed sediments at varying distances to the northeast of KAFB. There is some small contribution of ground water to surface flow from springs and seeps on the margins of the Arroyo del Coyote which is tributary to Tijeras Arroyo. Isolated surface drainage features also occur at the southern extreme of KAFB,

discharging any surface flow from ITRI facilities and southern SNL Environmental Restoration sites southward to Isleta Pueblo. SNL and ITRI facilities may also indirectly influence surface water quantity and quality in the Rio Grande through discharge of liquid wastes to the City of Albuquerque Publicly Owned Treatment Works (POTW).

1.3.2 Climate

Climatologically, the Albuquerque Basin is variably xeric. Average annual rainfall increases with elevation (from west to east) from less than ten inches to more than sixteen inches annually (50). Sandia Peak receives on the order of twenty to thirty inches per year. The majority of atmospheric moisture arrives in the Rio Grande Trough, including the Albuquerque Basin, from the Gulf of Mexico as summer monsoons. Greater than fifty percent (50%) of annual precipitation occurs as rainfall from July to September, when storm fronts bearing Gulf moisture from the east move inland. Winter precipitation may also approach the basin from the east as storm gyres arrive from the south bearing moisture from sources including the Gulf of California and Pacific Ocean. As a consequence, wet deposition rates of atmospherically dispersed materials should increase from west to east in the basin, and with increasing altitude due to orographic effects (51). Radioactive materials dispersed in the upper atmosphere, such as fallout from past above-ground weapons testing, may therefore be preferentially deposited on the eastern slopes of the Manzano and Sandia Mountain Ranges, resulting in lesser deposition in the basin that lies beyond the mountain rain shadow. Additional microclimatic factors which are influenced by the north-south trending mountain ranges include warmer conditions on the west flanks as compared to east flanks due to insolation occurring later in the day. As an influence on soil development, higher runoff on the west flanks is associated with thinner soils.

Other annual trends in basin meteorologic conditions were evaluated for the recent past twelve years. Gradual springtime warming is reported from the National Weather Service (NWS) monitoring station at the Albuquerque International Airport, with freezing days that may extend into late April (52). This, and the later occurrence of maximal rain conditions, limits the beginning of the growing season for non-irrigated native vegetation, moving peak growth conditions and primary production yields to late summer or early fall. Average diurnal shifts in temperature of 12° C to 15° C have been consistently reported, varying from nighttime thermal inversions to daytime temperature highs. The fairly wide temperature shifts coupled with canyon topography may

power diurnal shifts in wind direction as great as 180° in some parts of the study region, due to phenomena that are sometimes termed the *chimney effect* or wind drainage. This and other topographically influenced behavior is likely to limit the general utility of Albuquerque Airport NWS data for predicting the direction of wind driven atmospheric dispersion of effluents from all potential DOE, DOD, and NRC discharge sources or contamination sites in the region.

1.3.3 Habitat and Vegetative Cover

The observation of biotic habitats and vegetative patterns provides cues that were useful in characterizing trends in physical processes in the environment. In particular, the greater rainfall to the east of the basin and with increasing altitude was also reflected by the change in biotic communities in the study region. Vegetation also contributes to soil development and characteristics to a significant extent. Community designations used hereafter are consistent with those of Brown and Lowe (53), as best interpreted from the author's field observations. The piedmont/bajada region is dominated by a mixture of the Plains and Great Basin Grassland (P&GBGrl) and Great Basin Conifer Woodland (PJWdl) communities to an elevation of about 7500' MSL. The grassland community components of the piedmont-bajadas, mesas and terraces consist largely of short grass plains of grama, wheatgrass, three-awn, muhly, galleta and buffalo grass, while the woodland community components consist of piñon and juniper trees interspersed with grasses as above and various forbs and shrubs including sage, saltbrush, winterfat, and rabbitbrush, more often associated with the Great Basin Desert Scrub (GBDScr) community. Other plants occur that are more associated with the Semidesert Grassland (SDGrl) community including various cacti, dropseed and burro grass. Extensive local replacement by snakeweed, soaptree yucca, cholla, and Russian thistle attest to various rangeland disturbances, including the historical use of the range for grazing livestock. With increasing elevation into the Manzano and Sandia Ranges, these communities grade into the Rocky Mountain Montane Conifer Forest (RMMCF) characterized by ponderosa pine, Gambel oak, and New Mexico locust, as well as aspen in fire replacement areas. This community is also interspersed with perennial bunchgrasses, tufted hairgrasses, and forbs including sedges, cinquefoil, yarrow, vetch, and dandelion. This assemblage separately characterizes the Subalpine Grassland (SAGrl) community. At the highest elevations, primarily on the eastern slope approaches to Sandia Peak and Manzano Peak, the woodland communities grade into the Rocky Mountain Subalpine Conifer Forest (RMSCF), containing Englemann and blue spruces, corkbark fir and aspen

in fire replacement stands. Shallow ground water subirrigation in canyons and the Rio Grande Valley enhances the development of riparian woodland or *bosque* conditions. These woodlands represent distinct sub-communities within the larger community framework. Much of the original riparian habitat in the study area has been converted to agriculture and urban development; human exploitation of the valley including urban pueblo culture predates the continuous occupation by European settlers by many hundreds of years. Remaining bosque is notable for extensive stands of native cottonwood, desert willow, and mesquite, as well as exotic replacement species such as tamarisk and russian olive. Bernalillo County is home to at least 14 species of rare or sensitive plant species, many of which may be preserved in the lesser impacted areas of KAFB, Isleta Pueblo, and adjoining USFS holdings (54,55).

1.3.4 Population and Land Use

The largest population center in the study area is Albuquerque, NM. The 1990 census for the Albuquerque metropolitan area accounts for a population of approximately 502,100 persons, with a total Albuquerque Basin population of approximately 563,600 persons (56). Approximately 570,000 people are estimated to reside within the study region that extends eastward from the basin to the central highlands. Land use in portions of the study area within and in the immediate surroundings of Albuquerque is dominated by urban patterns of residential, commercial, and industrial development. However, a significant portion of the remaining basin is dedicated to open range grazing of beef cattle, milk production from dairy cattle primarily in feedlots, open range grazing of sheep and goats, and food- and feed-crop production. A 1988 agricultural census indicated that there were approximately 32,000 head of beef cattle and 7,300 head of dairy cattle within an 80 km radius of nuclear facilities on KAFB (57,58). Pastoral agriculture continues to be an important environmental dosimetric pathway consideration in the study area. The KAFB subregion of the study comprises about 53,000 acres in south-central Bernalillo County including 20,450 acres that have been withdrawn from the United States Forest Service (USFS). Intense development of the northern portion of KAFB grades rapidly to the south into sparser distribution of facilities with larger intervening undeveloped buffer areas. The bulk of operating nuclear facilities are located in the more southerly areas of KAFB. Contamination areas are more widely distributed, largely found in the eastern KAFB and USFS withdrawn areas, and throughout the central and southern portions of the base (6,7,8,9,10).

2. PROCEDURES

In this section we discuss the methods, materials, tools, and instrumentation used in the field and laboratory, the expected sources of potential variability introduced into the various methodologies, as well as the techniques used to reduce analytical data and assure the validity of results through maintaining the quality of all stages of the effort.

2.1 Site Location Data

The locations of soil samples, thermoluminescent dosimeters, and pressurized ion chamber measurements were fixed in the field using a NAV PRO MARK V Global Positioning System (GPS) carrier phase code receiver from Magellan Systems, San Dimas, CA. The GPS is a system of satellites maintained by the United States Air Force to provide navigational data for the Department of Defense. The GPS receiver was first initialized at the author's residence near Albuquerque. Altitude data within one meter is required to be input during initialization of the receiver for accurate and precise horizontal positioning, thus a second initialization was performed at the well-defined benchmark of the highest nearby elevation, Sandia Peak at 10678 feet above mean sea level (10678' MSL). The location also provided a relatively unlimited field of view and low relative horizons. Location data were obtained as degrees latitude and longitude with a horizontal accuracy of 12 meters in autonomous operation, improved to 5 meters using field differential. Altitude was also obtained from the GPS as orthometric height (feet above mean sea level). All values were compared for accuracy to their approximate locations and altitudes on United States Geological Survey Topographic Maps for the region of study (33,...44). GPS derived altitude data as height above geoidal suffered from the greatest variability. The combined data sources were used to generate all of the geographic figures in this study.

2.2 Soil Sampling and Analysis

Soil sampling provides the most direct means of determining concentrations and distributions of radionuclides in the environs of nuclear facilities. It is not, however, the most sensitive technique for measuring small incremental changes in environmental radioactivity that might result from routine operational releases under controlled conditions from nuclear facilities. Nonetheless, the importance of soil sampling as a primary monitoring tool can not be underestimated. Soil acts as an integrator and reservoir of

relatively long-lived radionuclides that may be remobilized through a variety of environmental processes and pose new threats to human health and spread of environmental contamination. The general rationale for soil sampling site selection has been discussed above to some extent. The choice of sampling locations was made as a subset of locations sampled routinely or as part of special studies by Albuquerque area DOE facilities' monitoring programs. Concentrated sampling was made in the vicinity of two general areas that represent the highest radiation ground-shine components of all KAFB area facilities as determined by remote sensing, surrounding SNL Technical Areas III/V and ITRI (59). The soil sampling program was further supplemented by locations chosen to provide more extensive geographic coverage as well as altitude correlation. The soil sampling locations are included in the map titled Figure 1.

2.2.1 Sampling Protocol

The soil sampling and sample management protocol were designed to conform to United States Environmental Protection Agency (EPA) and Nuclear Regulatory Commission (NRC) guidelines and recommendations (60,61,62,63,64). Sampling was performed at 38 locations to reflect the upper surface of the soil to a depth of 5 cm, which is expected to be the most sensitive indicator of radioactive contamination. The near surface layer of soil is also that which is most dynamic in terms of transformation by biogeochemical and physico-chemical weathering processes. Several European studies performed in the aftermath of the Chernobyl disaster have demonstrated the tendency for recently deposited fallout nuclides, notably ^{137}Cs, to remain most concentrated in the upper few centimeters of both soil and submerged lacustrine sediments (65,66,67,68). Experience with the disposal of liquid radioactive waste to earthen sumps also shows a tendency toward retention of ^{137}Cs in the shallowest depths of exposed soils (69). Studies of deposition of fission products from historical fallout onto soils in Chile and the western United States, including New Mexico, have shown overwhelmingly that ^{137}Cs remains concentrated in the shallower soil levels when not subjected to burial by additional sediments (70,71). There is additional evidence that naturally occurring radionuclides such as uranium and thorium may be relatively concentrated in near-surface soil layers, largely due to interactions with soil organic matter (72). Other studies in New Mexico indicate that the concentrations of natural radionuclides do not appear to vary greatly with moderate depth from the surface where the soils are largely depleted in organic matter (73,74). Those studies also indicated that ^{137}Cs deposited on sedimentary surfaces from atmospheric

fallout tends to remain associated with the original surface layers, even after burial by successive sediment deposition events.

To obtain samples representing the surface, soils were obtained using a sod cutter constructed from a welded stainless steel pipe flange with an effective sampling depth and radius of 5 cm. The cutting edge of the flange had been machined into a bevel to facilitate soil penetration. The sod cutter was pressed into the ground sequentially at four sublocations chosen within a meter radius of a central point at each established sampling location to circumscribe four subsample volumes. The four subsamples represented a total pre-disturbance soil volume of 1570 cm^3, encompassing a horizontal surface area of 3.14×10^{-2} m^2. For very loose sandy soils, as were found at most locations within the boundaries of the Albuquerque Basin, the contents of each subsample were removed by scooping out the circumscribed soil volume with a stainless steel trowel, holding the sod cutter in place. For cohesive soils, as were found at most locations east of the basin boundary, the soil plugs were loosened from the surrounding and underlying soil by first gently rotating the sod cutter in place, and pulling out an intact soil plug.

The four samples from each location were composited into a fresh, gallon-size plastic "zip-lock" bag, sealed with clean duct tape and were labelled directly onto the bag with an indelible marking pen using a ten digit sample identification number. The protocol for numerical identification was, in order of inscription, the last two digits of the year, the two digit month, two digit day followed by the four digit hour and minute of sampling from the twenty-four hour clock. The identity of the sample, site name, description of the soil type, environmental conditions, survey instrument readings, and any positioning data were entered into a bound logbook to constitute a permanent record. Some positioning and radiation survey data were obtained at dates subsequent to the sampling.

Physical characterization of soil samples in the field was limited to visual examination of general soil properties, such as predominant grain size and correlation with geologic-geomorphic settings for inference of potential source rocks. More exact petrographic analysis was considered to be outside the scope of the current study. The secured and labelled sample container was placed into a second fresh plastic bag and sealed as before. The bag was placed inside a clean plastic cooler for transport to the next sampling site and eventually to the laboratory for analysis. A custody form was drafted to track each batch of soil samples from field through analysis.

Control of potential sample cross contamination was managed by several means. Manipulation of sampling equipment and materials was performed using latex surgical gloves. The sample bagging procedure also provided a barrier to sample cross contamination. Decontamination of the sampling equipment, sod cutter and trowel, was performed between sampling sites by wiping off soiled surfaces with a clean paper towel, followed by spraying with a mild solution of Liquinox© detergent in distilled-deionized water and gentle scrubbing. This was followed by rinsing with distilled-deionized water and air drying.

A necessary quality assurance measure was the establishment of a sample duplication frequency to evaluate the field efforts. The fraction of any total monitoring effort allocated to quality assurance depends on various factors including the scope of the effort, natural variability and distribution of analytes of concern, available knowledge regarding sampling and analytical procedures, and the relationship between practical detection levels and any risk-based action levels (63,64). The question of natural variability and distribution in the region of interest was a central question in our exploratory effort. Environmental characteristics and processes that introduce variability to the radionuclide concentrations in soil include the source rock from which the sediments are derived, the degree of weathering of mineral components, the erosional and depositional environment or geologic setting, solution and evaporation processes governed by occurrence of water, soil development including the incorporation of organic components, and variability in patterns of introduction of foreign radionuclides, such as temporal and spatial variability in deposition from atmospheric fallout. The ultimate quality assurance objective centers on creating a design that achieves a desired level of data quality while best utilizing available resources. The quality assurance requirements for an exploratory study need not be as stringent as those imposed for strict site definition. There is abundant experience to demonstrate that 5% field duplication of samples will, in general, provide adequate quality control for determining variance between samples representing the same approximate site; expectations of improving precision to less than about ± 20% for environmental samples is, in all likelihood, unrealistic (63). Thus, 5% was the frequency of field sampling duplication that was applied in this study. A summary of soil samples including field and laboratory duplicates is presented with positioning data and characteristics of the soil and geologic settings in Tables 1 and 2.

2.2.2 Laboratory Analysis

Procedures for the preparation and analysis of soils were designed to conform with NCRP, EPA, NRC and DOE(EML) guidelines and recommendations (75,...79). Sufficient quantities of soil from each sample were transferred from their original sample container into tared, quart aluminum cans during the initial phase of analysis, and into tared, liter polyethylene Marinelli beakers during the latter phase. The cans and beakers were provided precleaned by the manufacturers and had not been used previously in ERML. The cans or beakers containing the soil samples were weighed and placed into a convection oven to dry for at least 24 hours at 96-98° C.

After drying, the samples were immediately removed to be weighed. Capping and sealing of aluminum can samples were performed thereafter by tapping the can lids into place with a mallet and placing a bead of latex sealant around the junction. Marinelli beaker samples were sealed by placement of the tight fitting lid onto the beaker, and wrapping several revolutions of vinyl tape around the junction. This was done in order to seal the beakers adequately to minimize radon escape, while leaving the beakers in a condition so that they might be easily reused. The latter was not generally possible for aluminum cans which become deformed in the process of sealing and reopening.

The sealed samples were held for ingrowth of ^{222}Rn and ^{220}Rn and their daughters for a period of no less than twenty days from sampling. Contrary to conventional wisdom, such long hold-up times may not be strictly necessary. It has been shown that counting of a soil sample 2 to 6 hours after sample sealing and again up to 8 days thereafter will not result in significant count differences (80). Apparently, the soil disturbance involved in sampling and mild handling does not significantly perturb radon daughter equilibria in soil samples. Radon and its daughters appear to remain trapped in the fine structure of the soil matrix, although they may be released by more aggressive treatment such as acid digestion or muffling.

Gamma-spectral analysis of soil samples was performed at ERML using a 25% efficient P-type coaxial high purity germanium (HPGe) detector with 120 cm^2 of active area, 1.9 keV resolution at 1.33 MeV, and a 48:1 peak-to-Compton ratio. The detector's upper surface is covered by a 0.020" thick beryllium window with a transmission coefficient of approximately 95% at 5.9 keV. The Model GMX-25190-P detector was obtained from EG&G ORTEC Instrumentation, Oak Ridge, TN.

Peak analysis was performed using the ORTEC MAESTRO/OMNIGAM software package. A typical spectrum of dominant soil nuclide gamma peaks appeared as shown in Figure 2 (81). The influence of natural uranium constituents in the soils was simulated by the spectrum of depleted uranium contaminated soil in Figure 3 (81).

Performance checks for system quality assurance included periodic energy and efficiency calibrations to fixed geometry gamma standards and background counts. Short duration backgrounds and two-point energy calibrations of the detection system were performed at the beginning of each sample count or approximately daily. Energy calibration was achieved using a ^{22}Na button check source of approximately 1 μCi, placed on top of the can or beaker containing a soil sample. The geometric effect of this procedure appeared to improve the agreement between source and sample calibrations. Energy calibrations remained fairly linear over the entire energy range of interest at about 2 channels per keV. Background counts were performed using surrogate samples containing ordinary Hawaiian cane sugar in quantities equivalent to that of a typical sample. In this way, the influence of sample shielding on the penetration of gamma background in the counting environment could be taken into effect. The surrogate backgrounds generally yielded lower background count rates than those using an empty chamber. Longer background counts, of two to four days in duration, were performed on an average frequency of once every five weeks to provide robust data for background correction and detection level determination. Efficiency calibrations (counts per gamma) were performed on a frequency of once every three to four weeks. The calibrations were performed using a multinuclide standard source obtained from Isotope Products Laboratories, Burbank, CA. The efficiency standard was provided as a liter volume Marinelli beaker containing 1608.6 g of clean 50-70 mesh sand, into which nine gamma-emitting radionuclides were uniformly dispersed. A certificate of calibration for the source and its implicit National Institute of Standards and Testing (NIST) traceability is maintained at ERML. Twelve separate energy peaks were produced by the standard, ranging from 0.088 MeV (88 keV) to 1.836 MeV (1836 keV).

Efficiency calibrations performed over three months were grouped and analyzed, as summarized in Figures 4 and 5. The analyses include representation of the data as a power function fit and as a least squares fit with stepwise linear regression. The stepwise least squares representation accounted for 97.8% of variance at a correlation of 98.9%, while the power function accounted for 94.4% of variance at 97.2% correlation. Efficiency as a function of energy showed very little variation over the counting period. A number of

Figure 2: Typical Soil Spectrum, Major Constituents

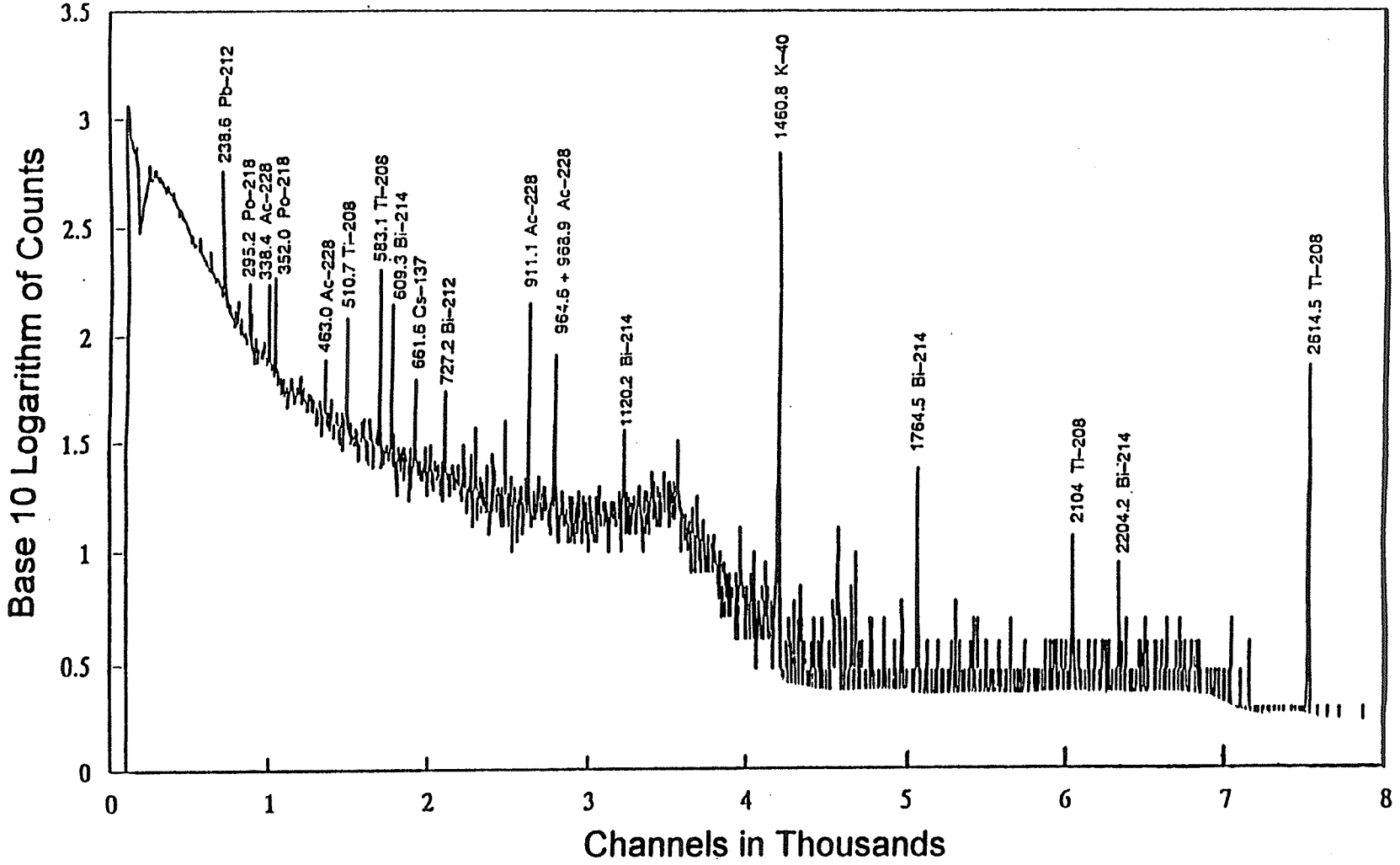

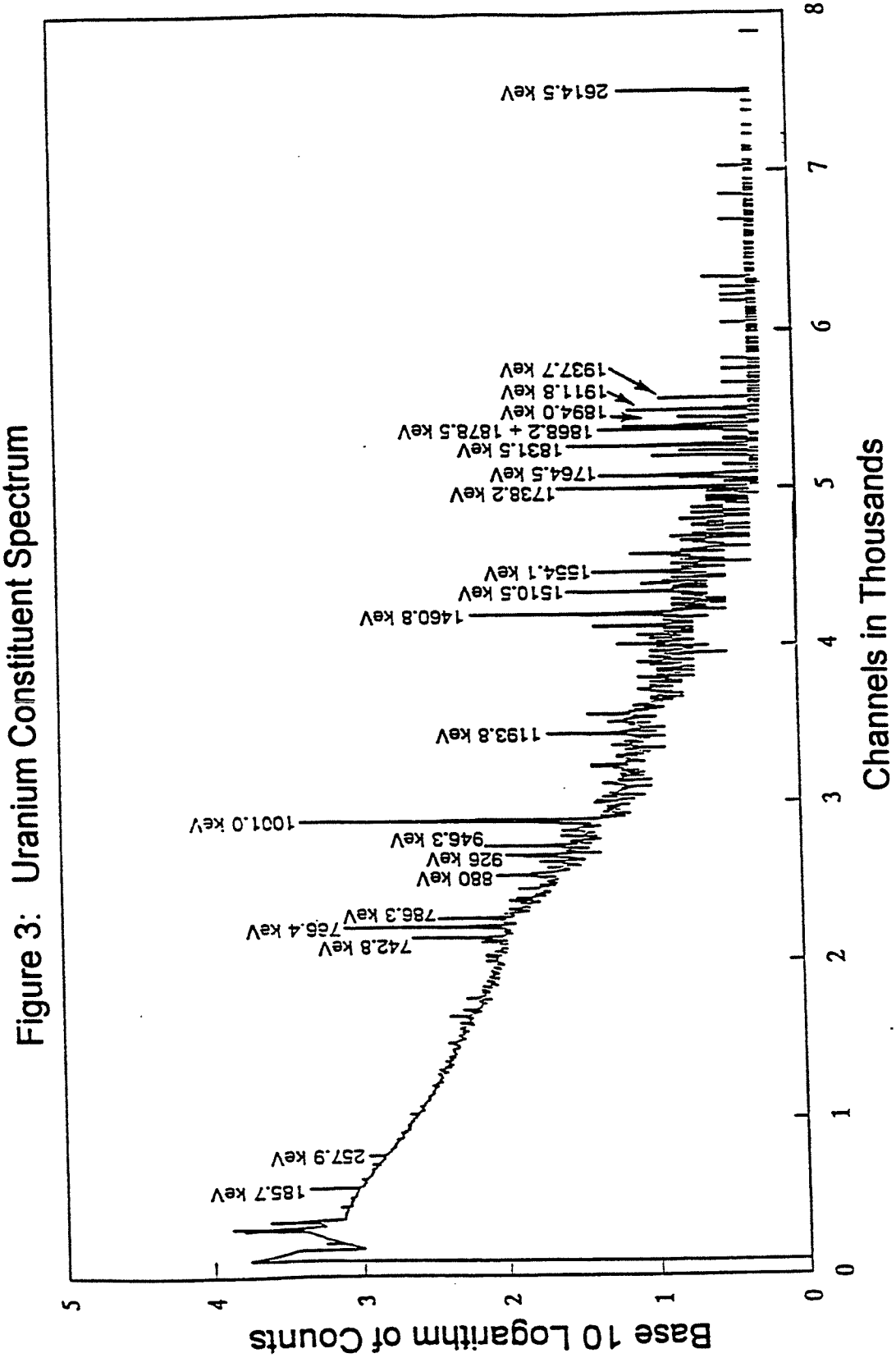

Figure 3: Uranium Constituent Spectrum

Figure 4

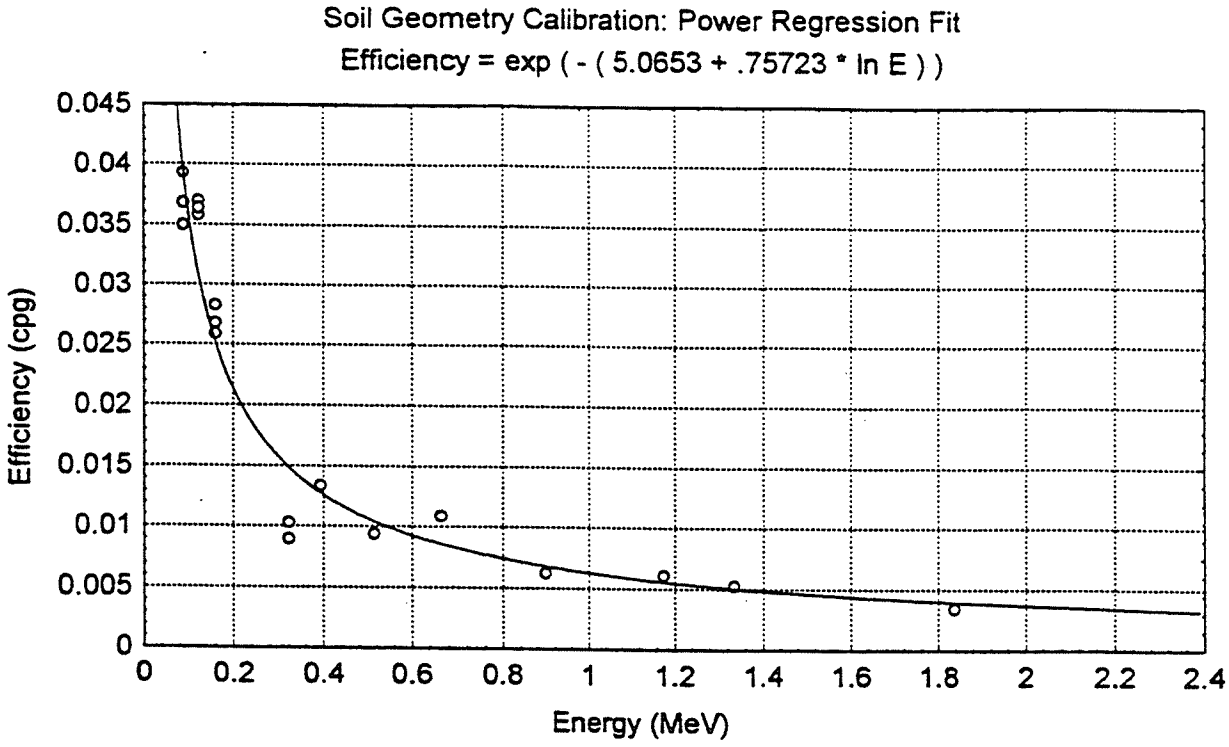

Figure 5

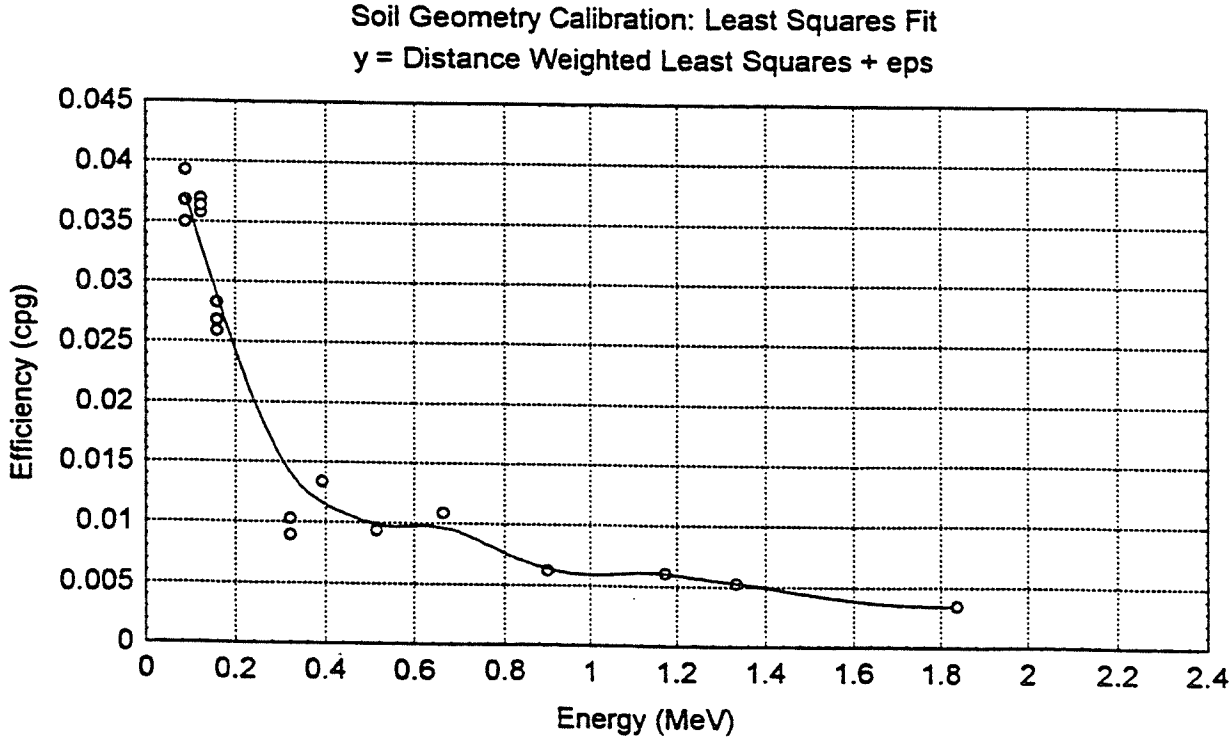

sample counts were performed in aluminum can geometry prior to obtaining this calibration source. The germanium detector used is very sensitive to differences in source geometries, as is typical of small detectors. Three soil samples counted in aluminum cans were transferred to Marinelli beakers, and recounted to generate a calibration conversion. The count rates of seventeen of the strongest peaks ranging from 187 keV to 2617 keV from each sample were compared between the two geometries to generate peak-by-peak ratios. A final ratio of aluminum can to Marinelli counts of 0.41 ± 0.09 was found, which exhibited no discernible energy dependence over the energy range examined. This ratio was used to convert all aluminum can results to Marinelli geometry calibration equivalence. The comparison is depicted in Figures 6 and 7.

Prepared samples were placed into the sample chamber over the detector, and the low-background, graded lead and copper shield was closed around the chamber. Counting was initiated using an IBM-compatible personal computer loaded with a multichannel analyzer card and the supporting ORTEC spectral analysis software. The operating voltage for the detector system was maintained at 2500 V. Count times often met or exceeded the operational recommendation of 60,000 seconds (69), but the test of counting time adequacy was whether sufficient counts were obtained in all regions of interest to yield good statistical characteristics. That count value was taken equal to or greater than about 1000, yielding a theoretical Poisson coefficient of variance of ≤ 3%. Count durations as live time are included in Tables 1 and 2 for each sample. The spectra were examined for all detectable peaks and compared to forty seven routine peak energies derived from the natural radioisotope chain spectra. The routine peak energies are listed with their identities, yields and typical counting efficiencies in Table 3. Nuclide data were compiled from a number of sources (82,...87). Count data were reduced to soil activity concentrations using a computational spreadsheet devised by the author. This included conversion using the available nuclide data and calibration efficiencies, current background subtraction, and calculations of lower levels of detection.

Lower levels of detection were calculated for each energy peak with an appropriate background component in each analysis by the method of Currie (87), i.e.:

$$LLD \equiv 0.11\ BEA + 0.5[(3.29)\ \sigma_B \sqrt{\eta}\ /(YEVT)]$$

where: LLD is the lower level of detection,
BEA is the blank equivalent activity in pCi/g,
σ_B is the Poisson expected deviation found as the square root of blank counts,

Figure 6

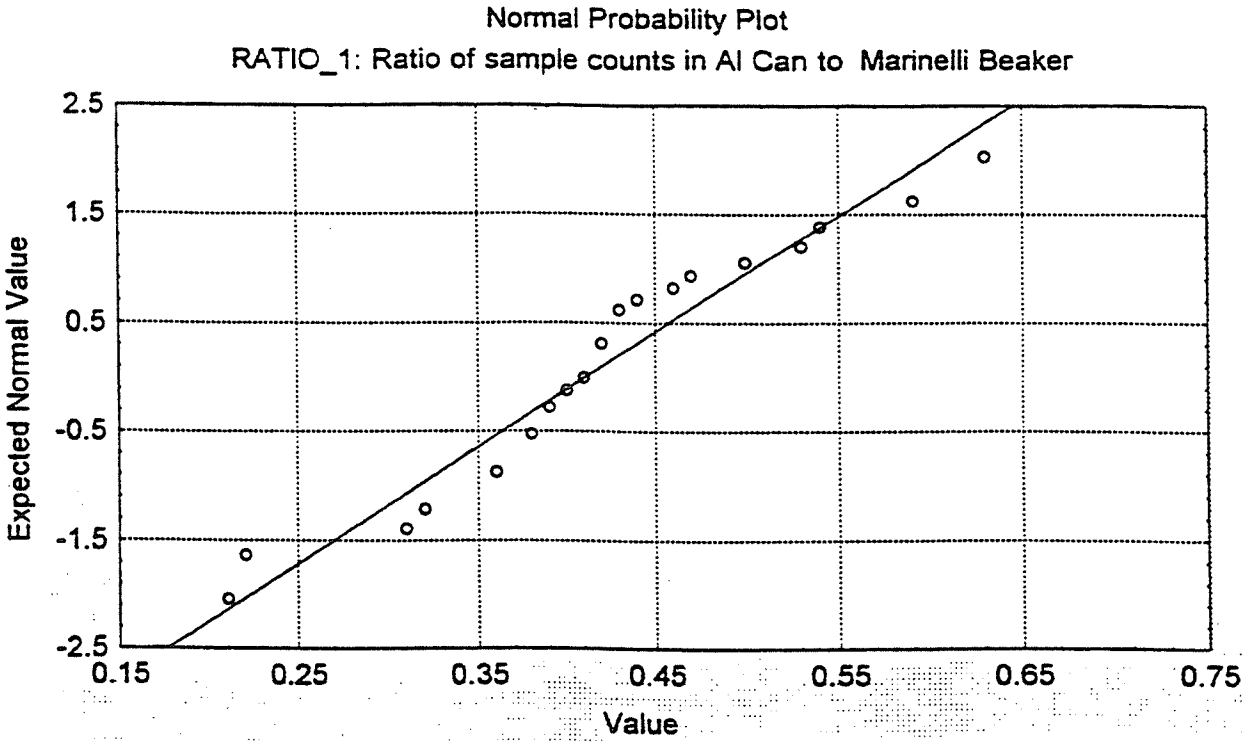

Figure 7

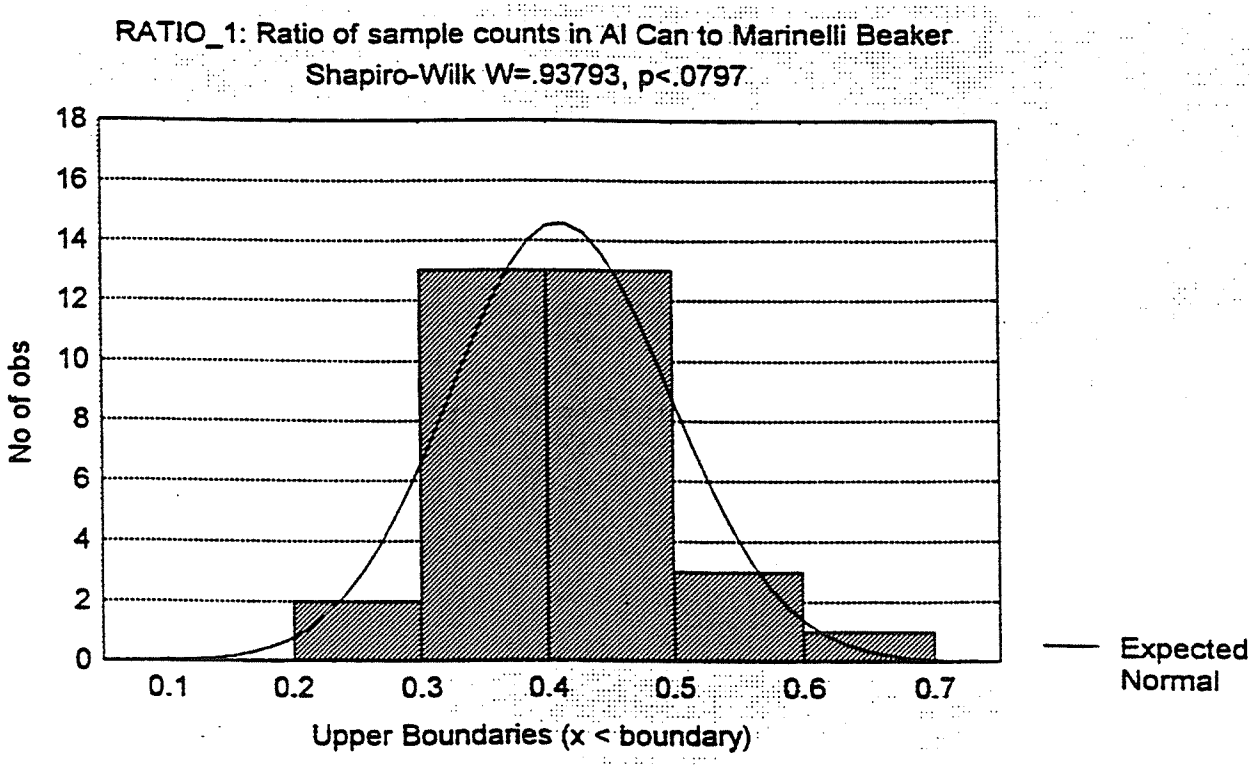

Y is the gamma yield at the given energy per disintegration, analogous to chemical yield,

E is the counting efficiency in counts/disintegration,

V is the sample mass in grams,

T is the effective counting time, given as the measurement time Δt, for long half-lived components and their daughters in equilibrium ($\lambda t < 1$), and,

η is given as $1 + (\Delta t/\Delta t_B)g_A$,

where: Δt_B is the background count time, and,

g_A is a factor that accounts for changes in the calibration factor, given the value of unity in our case.

The correction for the aluminum can counting geometry was applied *a priori* to the input data for the LLD. Only 24 to 36 of the total scanned regions yielded sufficient background counts in well defined peaks to calculate a lower level of detection (LLD) for the sample analysis. Of these, a smaller number of unique or high yield energy peaks were used for final activity quantitation. Reported non-detectable (ND) values arose only when neither manual or software-based methods could clearly discern the presence of a peak in a given region of interest. An additional statistical test of detection was based on a magnitude of counting uncertainty, σ_c, such that $2\sigma_c \geq$ total net counts in the region was interpreted as undetected. Statistically undetected peak counts (designated ND), where the presence of a peak could be demonstrated however poorly fitted, were used as the best estimates for purposes of summations and averaging.

The GMX series detectors have an extended low energy efficiency range that verges very closely to zero energy as approached from the right before falling abruptly to a minimum. As a practical matter, the low energy ranges of all sample spectra and background spectra were heavily populated with characteristic U, Th, Pb, Bi, and Ra x-rays, as well as higher energy peak interferences, superimposed on a sizeable bremsstrahlung and Compton scattering continuum, rendering any attempts to resolve and quantify low energy peaks from the sample problematic. One presumed non-x-ray energy peak was consistently seen at about 120-125 keV. Primary peaks in the ERML counting environment that might account for this include ^{234}U at 120.9 and ^{227}Ac at 122.4, a daughter of ^{235}U. Reactor fuel which has been enriched in ^{235}U also tends to be become enriched in another light uranium isotope: ^{234}U. The likelihood of appreciable quantities of ^{227}Ac building up in chemically purified uranium fuel is somewhat less plausible; its immediate predecessor, ^{231}Th, has a 32,500 year half-life. Both uranium species are naturally occurring, and are present in building and shielding materials surrounding the counting

environment. Predominant source materials, based on activity, in ERML include ^{137}Cs and ^{60}Co. The observed value falls significantly far from the expected values for double or single escape peaks from either of these sources, and the potential influence of the sources has not been demonstrated on the basis of regular detection of primary peaks. The precise origin of this peak remains a point of conjecture, but its deleterious effect, along with the accompanying x-ray noise, on low energy peak resolution and quantitation remains the same.

Nuclide quantitation peaks for final reporting were chosen after exhaustive review of the available peaks in the useable count window, designated to range from about 0.15 to 2.8 MeV. For each sample count, all detected daughter peaks in the ^{226}Ra and ^{232}Th series were averaged using gamma-yield weighting and compared to the results of counting in the peak regions of highest yield for each series: ^{214}Bi at 609.3 keV and ^{212}Pb at 238.6 keV, respectively. While the ^{212}Pb peak has minor competition from two other nearby peaks, ^{224}Ra at 241 keV and ^{214}Pb at 241.9 keV, there appeared to be sufficient distance between the centroids of the multiplet peaks that the MAESTRO/OMNIGAM analysis was capable of discriminating their influence through the process of setting background subtraction regions. Thus the 238.6 keV peak derived activities agreed favorably, though sometimes conservatively, to values obtained for other ^{232}Th daughters. The ^{212}Pb peak at 238.6 keV was ultimately chosen for quantitation and reporting to optimize statistical detection based on the peak's high relative gamma yield and counting efficiency. ^{235}U and ^{226}Ra were quantified using fixed fractions of the counts for the 186 keV peak. Based on average values for relative natural abundances of uranium isotopes, gamma yields of the two radionuclides and assuming the equilibrium relationship for ^{238}U and ^{226}Ra, it can be shown that approximately 60% of the peak counts can be attributed to ^{226}Ra, and 40% can be attributed to ^{235}U. This was tested by comparison of activities derived from ^{226}Ra and ^{214}Bi peak counts, deriving a counting case-by-case ratio, and testing the entire population for a normal statistical distribution. A soil activity concentration ratio for ^{226}Ra:^{214}Bi of 0.96 ± 0.08 was found to hold over the entire data set of forty two total soil counts. The graphical results of that comparison can be seen in Figures 8 and 9. ^{137}Cs, ^{238}U as ^{234m}Pa, and ^{40}K were quanitified using full-energy gamma peaks at 661.7 keV, 1001 keV, and 1462 keV, respectively. There is some disagreement in the literature between the abundance values for the ^{234m}Pa peak, ranging over a factor of two (89). An intermediate value of 0.008 gammas/disintegration was used for our analyses.

Figure 8

Normal Probability Plot for the Distribution of
Trimmed Ra-226 to Bi-214 Soil Activity Concentration Ratios
in the Vicinity of Albuquerque, NM

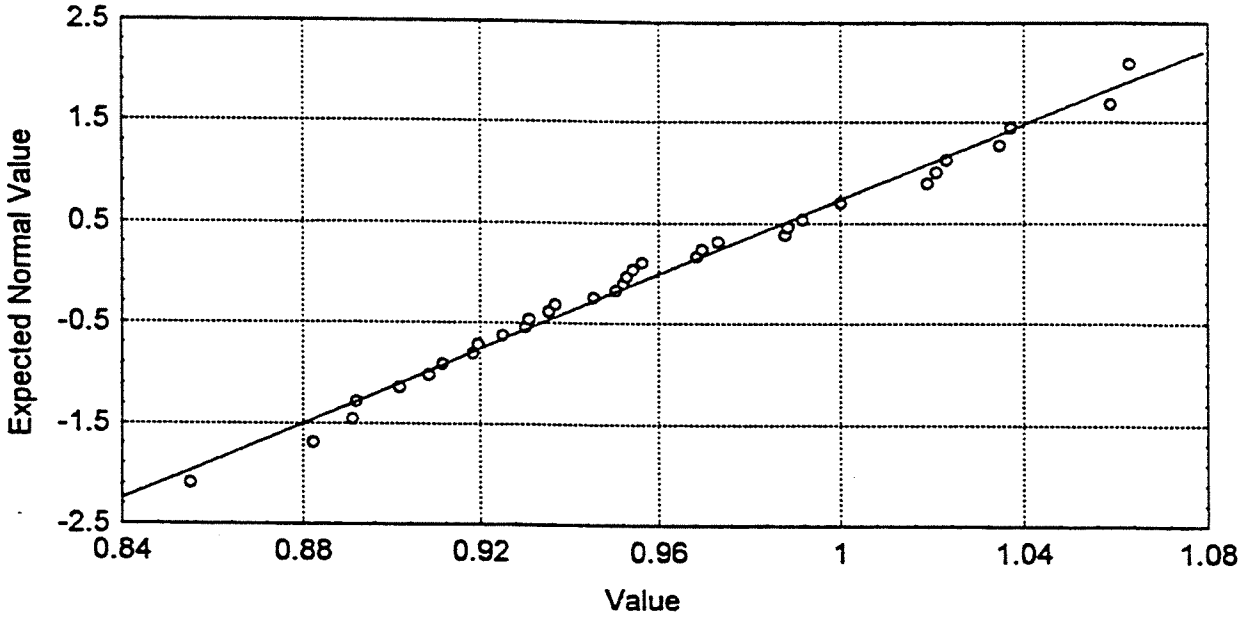

Figure 9

Distribution of Trimmed Ra-226 to Bi-214 Soil Activity Concentration Ratios
K-S d=.08861, p> .20; Lilliefors p> .20
Shapiro-Wilk W=.97851, p<.7671

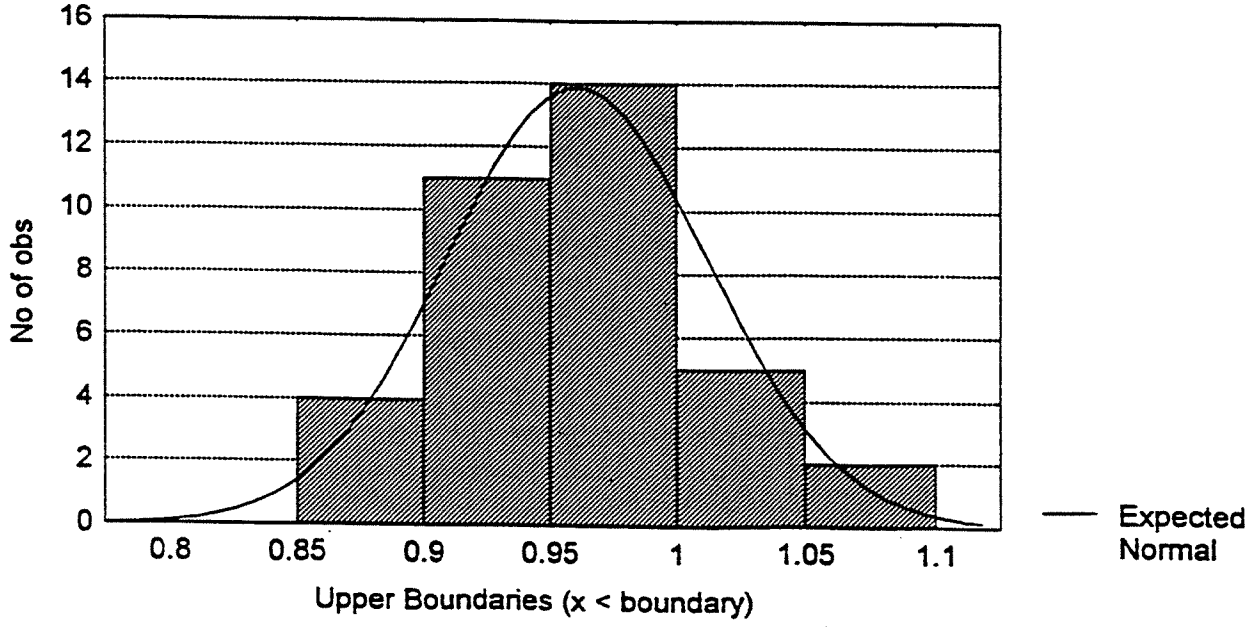

The method employed to evaluate individual counting and general analytical uncertainties remains to be discussed. The MAESTRO/OMNIGAM gamma peak analysis method is based on a Gaussian fit to the detected peak, and fitting of a baseline to subtract out the Compton continuum. Excellent discussions of the complexities of pulse-height distribution analysis in HPGe and Ge(Li) spectra, including the Gaussian fitting approach, may be found in a number of sources (90,91,92). Using the Gaussian approach, the software generates fitted gross and net count areas within a spectral region of interest, and a standard deviation for the net portion of the fitted peak. This standard deviation was reported in the study in lieu of the theoretical Poisson standard deviation since the fitted deviation was deemed to be more representative of the uncertainty in peak fitting analysis. Total error for the peak count was reported as the deviations for sample and background counts added in quadrature. Analytical duplicates, separate from field duplicates, were also performed at a frequency of 5% to evaluate analytical uncertainties. Additional performance checks included interlaboratory comparison and EPA performance evaluation unknowns as external laboratory evaluation standards (ELESs). The ELESs were provided and analyzed as dispersed in water, a dissimilar medium, so comparison to soil analysis was not exact. Results for the analytical effort are included in Tables 4,5,6 and 7.

2.3 *In situ* Environmental Exposure Rate Measurements

The methods used for quantitation of environmental radiation included a long-term study using thermoluminescent dosimeters deployed at various locations in the vicinity of Albuquerque, NM, and short-term deployment of a high pressure ion chamber (HPIC) at a greater number of field locations. Anticipated sources of environmental variability are common to both methods, and are discussed collectively following field and laboratory procedural development.

2.3.1 Thermoluminescent Dosimeters

With one exception, all thermoluminescent dosimeters (TLDs) were deployed at environmental locations that are also monitored by SNL or ITRI. The total distribution of TLDs encompassed a more extensive area than soil sampling in the study region, as may be seen in Figure 10. The study employed Panasonic 814 Environmental TLD badges and the Panasonic UD-716A Automated TLD Reader from Matushita Industrial Equipment Co., Ltd., Osaka, Japan. Each TLD badge contained three elements of the high sensitivity thermoluminescent phosphor,

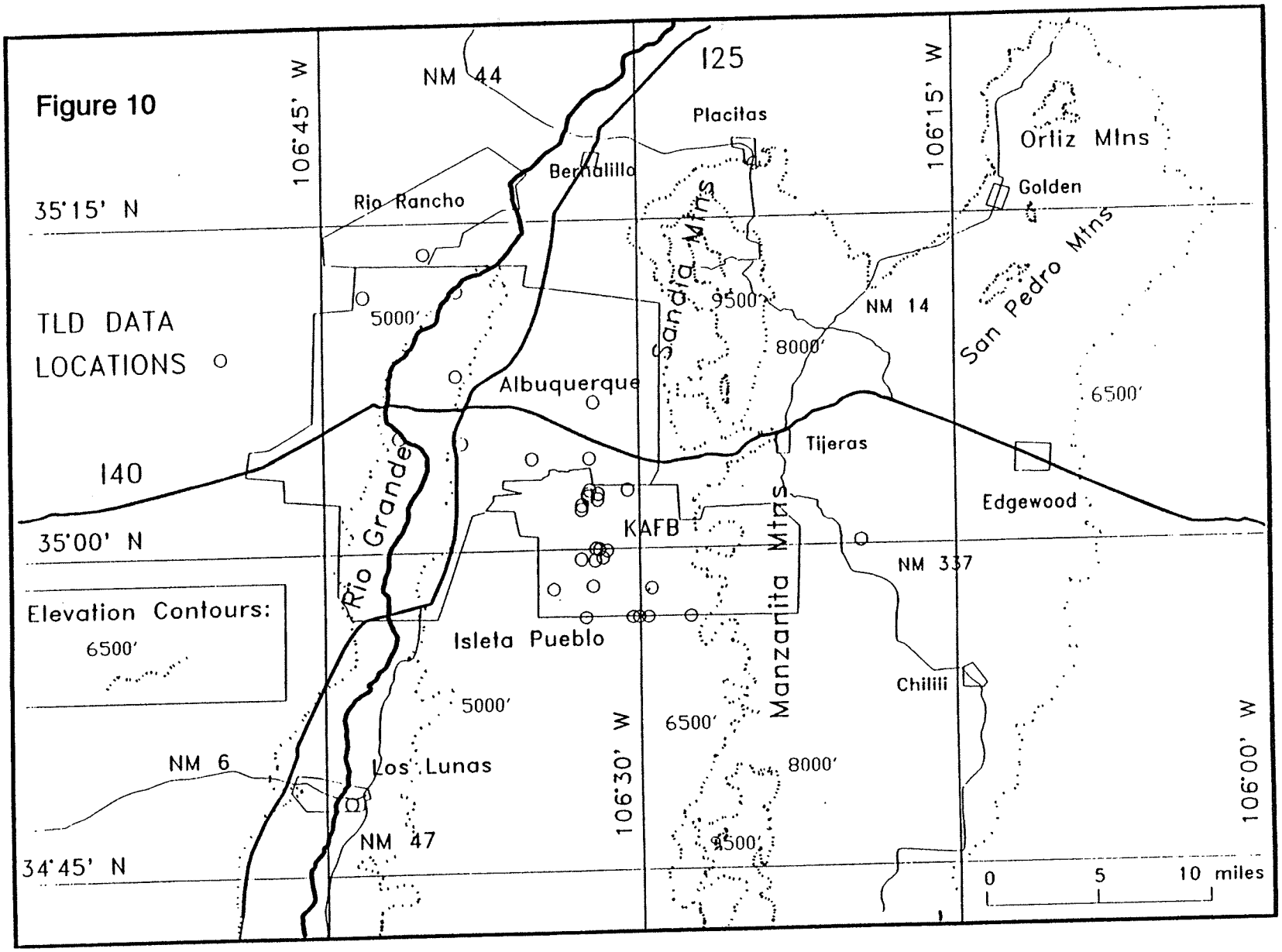
Figure 10
106°45' W
NM 44
125
Placitas
106°15' W
Orliz Mtns
Bernalillo
Golden
35°15' N
Rio Rancho
Sandia Mtns
San Pedro Mtns
TLD DATA
LOCATIONS
5000'
9500'
NM 14
8000'
Albuquerque
6500'
Tijeras
140
Rio Grande
KAFB
Edgewood
35°00' N
Manzanita Mtns
NM 337
Elevation Contours:
6500'
Isleta Pueblo
Chilili
5000'
6500'
106°30' W
106°00' W
NM 6
Los Lunas
8000'
NM 47
9500'
34°45' N
0
5
10 miles

thulium activated calcium sulfate: $CaSO_4(Tm)$, filtered by 1000 mg/cm^2 of lead and plastic. The phosphor is intended for use in gamma dosimetry only. The phosphor is dispersed as a powder in teflon and encased in polyimide on a plastic substrate which is inserted into a plastic badge for deployment. The outer badge contains the additional filtering material.

The TLD card within the badge is mechanically removed and replaced by the automated TLD reader. The prepared TLD phosphor is well protected from humidity and other moisture, contamination, visible or UV light stimulation, and the effects of oxygen on phosphor response during radiant thermal read-out. All of these factors may contribute spurious TLD signals and concomitant loss of latent dose information. Details of the preparation, sensitivity and relative field hardiness of the $CaSO_4(Tm)$ TLD phosphor may be found in extensive discussions elsewhere (93,94,95). A fourth element intended for mixed-field beta-gamma dose measurement, composed of $LiB_4O_7(Cu)$ filtered by 14 mg/cm^2 of plastic, was also included in each TLD badge, but its readings were not used in our study. The greater sensitivity of the $CaSO_4(Tm)$ elements (about thirty times) and straightforward analysis of the unmixed gamma field for monitoring and calibration purposes delimited our scope of interest.

The TLD monitoring program procedures were designed and performed to conform with the guidelines and recommendations of the American National Standards Institute (ANSI), National Bureau of Standards (now NIST), EPA, NRC, DOE, and the manufacturer's instructions (96,...101). TLDs were deployed at each location in the field, mounted at one meter from ground surface on a post. The posts were constructed from ten foot lengths of thin-walled, 3/4" diameter polyvinyl chloride (PVC) plastic sprinkler tubes, obtained from a local building supplier, cut in half and inserted into the ground to a depth of approximately two feet in a small-diameter hole made using a San Angelo digging bar. This method was chosen for several reasons. The tubes were relatively inexpensive, straight, flexible, easily installed in a durable but non-permanent fashion, and contained no ferrous materials that might contribute small exposures from ubiquitous ^{60}Co contamination in steels.

Ferrous materials in the deployment configuration were generally minimized. These included short lengths of garden twist-tie (thin wires imbedded in plastic to prevent corrosion) used to affix the TLDs to the outside of the tube, threaded through holes drilled in each tube, and the springs which are included in the polyethylene TLD holder provided by Panasonic. It was assumed that the few milligrams of steel in

the wires and springs would have negligible relative effect on the measured TLD exposures. PVC plastic and polyethylene are low average atomic number (low-Z) materials that were not expected to significantly shield or contribute gamma exposure.

Two TLDs were installed on each tube, facing the same direction, with their collective midpoint at one meter. Thus, each location had a subpopulation of six $CaSO_4$(Tm) TLD elements from which a measurement mean and uncertainty could be derived. TLD field deployment and exchanges were performed every approximate ninety days, from Second Quarter, 1993 to Second Quarter, 1994. Field exchanges were accompanied by at least two TLDs designated as deployment controls. The deployment controls were annealed at the same time as the environmental TLDs and laboratory controls. After annealing, the TLDs were allowed to rest for about twenty four hours prior to field deployment to reduce the spurious effects of residual delayed thermoluminescence. After accompanying the TLD field deployment, the deployment controls were returned to a shielding cell that was constructed from low-activity lead bricks at ERML.

ERML is located within the lowest average exposure rate portion of a highly shielded facility, the UNM Nuclear Engineering Laboratory. Sources of radiation which might influence stored TLD controls include UNM's 5 W maximum reactor including any fuel source or neutron capture gamma-rays, influx of cosmic rays, the ^{60}Co irradiator source referred to above, various source materials stored in the source vault, and natural materials used in building structure and shielding. The lead TLD shielding cell wall thickness exceeded the ANSI recommendation of 5 cm by a factor of at least two, except for an aperture provided for placement and removal of TLDs. The aperture, which measured approximately 8 cm by 8 cm in area, was covered with only 5 cm thickness of lead for ease of removal. TLDs were placed in the cell's inner compartment at the greatest possible distance from the covered aperture. Laboratory controls were placed in the cell directly after annealing, where they remained for the duration of the quarter. Field deployed TLDs were routinely retrieved and read at the end of each quarter along with deployment and laboratory controls. Glow curves and raw data were obtained for the three $CaSO_4$(Tm) elements of each TLD. The raw data were then converted to equivalent exposure rates using exposure calibrations and fading corrections, discussed below.

A group of 50 TLDs were annealed at the mid-point of the deployment quarter to be irradiated for calibration. Ten TLDs were designated travel controls to be given no direct irradiation, and eight TLDs each were irradiated to calculated exposure rates ranging from 5 to 40 mR, with travel controls

treated as zeros. Calibration was performed at the SNL Gamma and Neutron Irradiation Range. Documentation of the operating procedures and a full description of the facilities may be found elsewhere (102,103). Irradiation was performed using a ^{137}Cs disk source with an initial activity of 14 Ci on June 24, 1983. The source rests on a moveable platform in a concrete well 9" in radius and 35' in total depth. The source is moved automatically within the well to a desired depth to deliver the required exposure over a specified time. TLDs were placed on a wheeled platform which was moved horizontally over the irradiation well at a fixed height using a manually operated chain drive. The TLDs remained in place for the duration of the specified exposure, and were wheeled back manually upon the human operator's recognition of the audible alarm of an external timing device. Exact exposure times may vary based on the operator's response time with an estimated. The vertical location of the source is calculated by computer based on source strength, source-to-target distance in air, and transmission through a steel plate at the apex of the well.

Like most high sensitivity phosphors, $CaSO_4(Tm)$ is notoriously energy dependent in its response. Thus, the use of a ^{137}Cs source for irradiation may not be optimal; a ^{226}Ra source might be preferred for environmental measurements, particularly the ground-shine component of exposure. Gamma-rays of the ^{226}Ra series, along with those of the ^{232}Th series and ^{40}K, contribute from 50% to 70% of the total environmental exposure rate (1,78,104). Response as sensitivity in $CaSO_4(Tm)$ for exposure to the approximate 200 keV energy of ^{226}Ra is greater, on the order of 5%, than response to exposure at the 662 keV energy for ^{137}Cs (101). However, as shielded with lead, the manufacturer reports an actual *decrease* in response per exposure at 250 keV relative to ^{137}Cs, on the order of 5-10%. The actual average energy for the natural soil gamma spectrum will vary as a function of primary radionuclide concentrations and the degree of daughter retention in the soils, as well as the concentration of radon daughters in the atmosphere surrounding the detector. A typical *in situ* gamma spectrum was depicted in Figure 2. The results of five TLD calibrations against ^{137}Cs over the lifetime of the project were grouped for analysis, and are summarized in Figure 11. The high pressure ionization chamber measurements and average field TLD measurements were paired for linear regression analysis to compare their relative responses, as depicted in Figure 12.

Additional performance indicators requiring evaluation included TLD fading and angular or directional dependence. TLD fading was evaluated in two ways: as laboratory controlled fading of calibration exposures, and as environmental fading

Figure 11

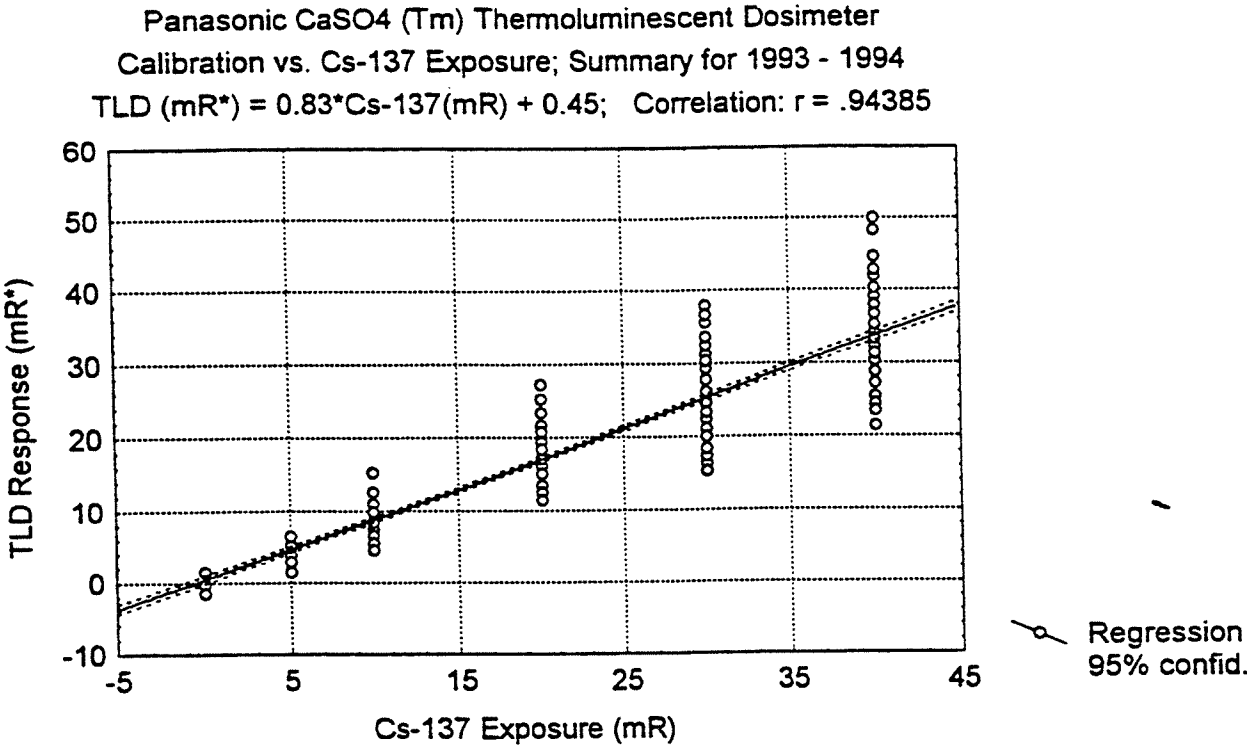

Figure 12

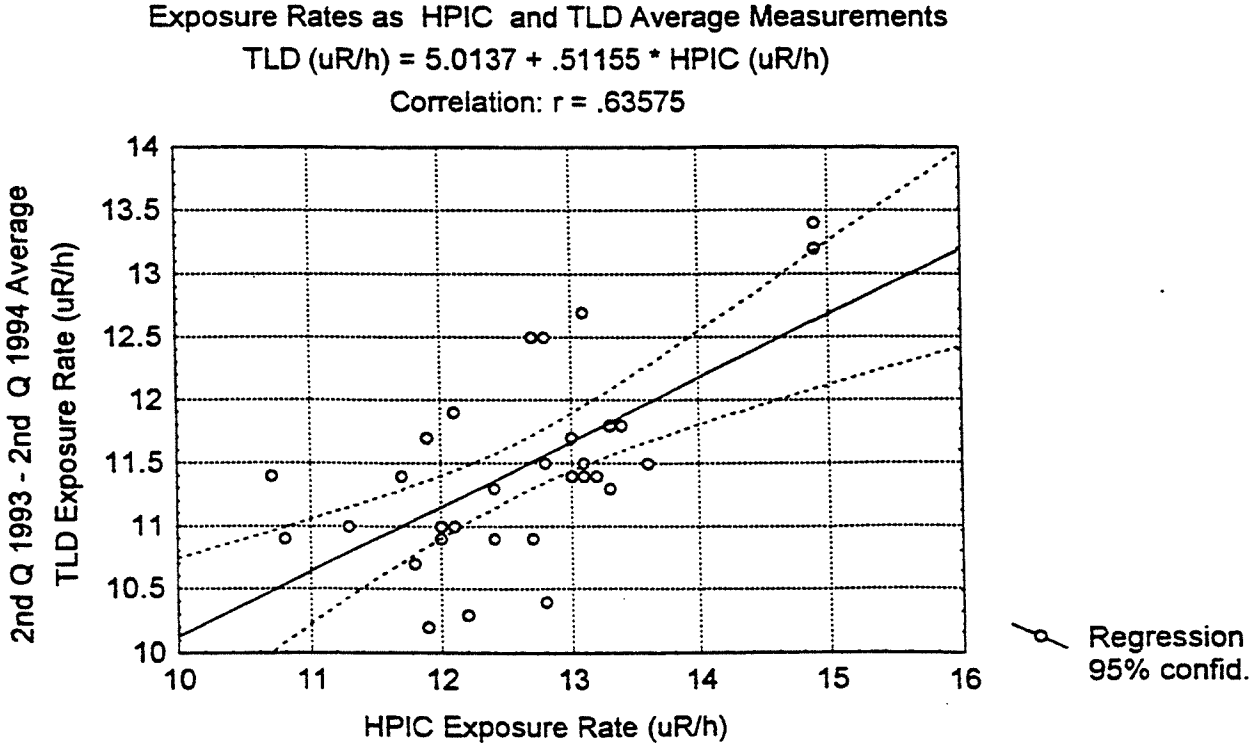

using successively longer field deployments in the same period. Laboratory controlled fading was estimated by irradiating a calibration set of TLDs, as described above, dividing the set into two groups: one group to be read immediately and another to be stored at a relatively low background location for reading at the end of the deployment cycle, 45 days later. By comparing slopes of zero corrected best fit regression lines for TLD response versus exposure, it was estimated that fading of about 4% occurs in the first 1.5 months under controlled storage conditions.

A second experiment to address fading under environmental conditions was devised in the first deployment cycle, Second Quarter, 1993. Historically, the second quarter of the year is the period of maximal daily insolation for Albuquerque conditions of latitude and meteorology with an average of about 680 langleys (50). A subset of eleven locations was chosen for multiple exposure cycles lasting one month, two months and three months, within the cycle. An aspect of complexity introduced in evaluating environmental fading by this method is the range of exposure rate variability over a cycle, to the extent that it may be resolved by the measurement technique. In an effort to minimize the effects due to that range of variation, one month exposures were followed in sequence by two month exposures. The exposure rates normalized to μR/h for full and sub-cycles were then analyzed. The results of the analysis are included in Table 8. The bulk of fading appeared to occur within the first two months. From the analysis, it was inferred that an average 6.5% total fading occurs in field deployed TLDs. This value was introduced thereafter as a correction factor for the reported quarterly TLD results.

Directional dependence of TLDs was assessed in the environment over a deployment period of 77 days during Second Quarter, 1994. This was expected to allow sufficient time for environmental fading to equilibrate. A population of 40 TLDs was deployed at an open ground location on Kirtland Air Force Base, distant from any structures or artificial radiation producing facilities. Four TLDs each were installed on each of ten posts in the cardinal compass directions: north, south east and west. The north TLD was installed on each post by first comparing magnetic north on a compass with "solar" north. The latter was found by aligning a plumb shadow, assured by using a spirit level, that fell from a slender digging bar at precisely mid-day with each post. The analytical conclusions are discussed later under Results.

The dearth of prescribed element correction factors (ECFs) for a reference set of TLDs introduced an element of uncertainty during the instrumental phase (reading) of the TLD

effort. The manufacturer asserted a maximum error in measurement reproducibility without ECFs of about 15% (101). We attempted to compensate for this effect by the deployment of multiple TLDs at each location for mean and error estimation, and averaging TLD responses over the five deployment cycles for purposes of method comparison. The tolerance for error allowed in the ANSI standard for environmental deployment is 30% at the 95% confidence limit, and the tolerance for laboratory error at a total exposure equivalent to 10 μR/h over the field cycle (about 22 mR total exposure) is 10% at the 95% confidence limit. The generation of ECFs requiring exposure of reference TLDs in a well-defined and uniform field is part of an ongoing project at UNM, separate from this effort. It should be noted, however, that "rank correction factors", or RCFs, for elements within the TLD card are encrypted into the bar code on the TLD by the manufacturer to correct for response when read by the UD-716A reader. RCFs are established by a similar but more general one-time calibrated exposure of at least one TLD element to ^{137}Cs. The performance of field deployed TLDs relative to the ANSI recommendations is discussed under the Results section.

2.3.2 High Pressure Ion Chamber Measurements

The majority of sites monitored by soil sampling and TLDs were also surveyed using a high pressure ionization chamber (HPIC), as seen in Figure 13. Procedures for application of the HPIC were devised to conform with NCRP, ICRU, AEC, and NRC (draft) guidelines and recommendations, as well as the manufacturer's instructions for use and electronic performance verification (104,...109).

The instrument employed was a Reuter-Stokes RS-112 HPIC, consisting of an 8 liter sphere composed of 304 stainless steel with a wall thickness of 0.120", containing 25 atmospheres of high purity argon gas. Of two resistors installed within the RS-112 electrometer circuit to convert charge collection to a digital exposure rate measurement, only the low range (0-500 μR/h) R903 resistor was utilized under environmental conditions. The 20 mV per μR/h sensitivity of the R903 resistor was verified through the shadow shield exposure technique, as specified by the manufacturer, at ERML using an approximately 1.3 mCi ^{226}Ra source supplied by the UNM Physics Department (109). Primary electronic calibration of the instrument against a reference standard may be performed periodically by the manufacturer, but was outside the expertise as well as the authority of the author. A performance cross-check against Colorado State University's HPIC was performed at ERML, showing agreement at ambient exposure levels within 1.0%.

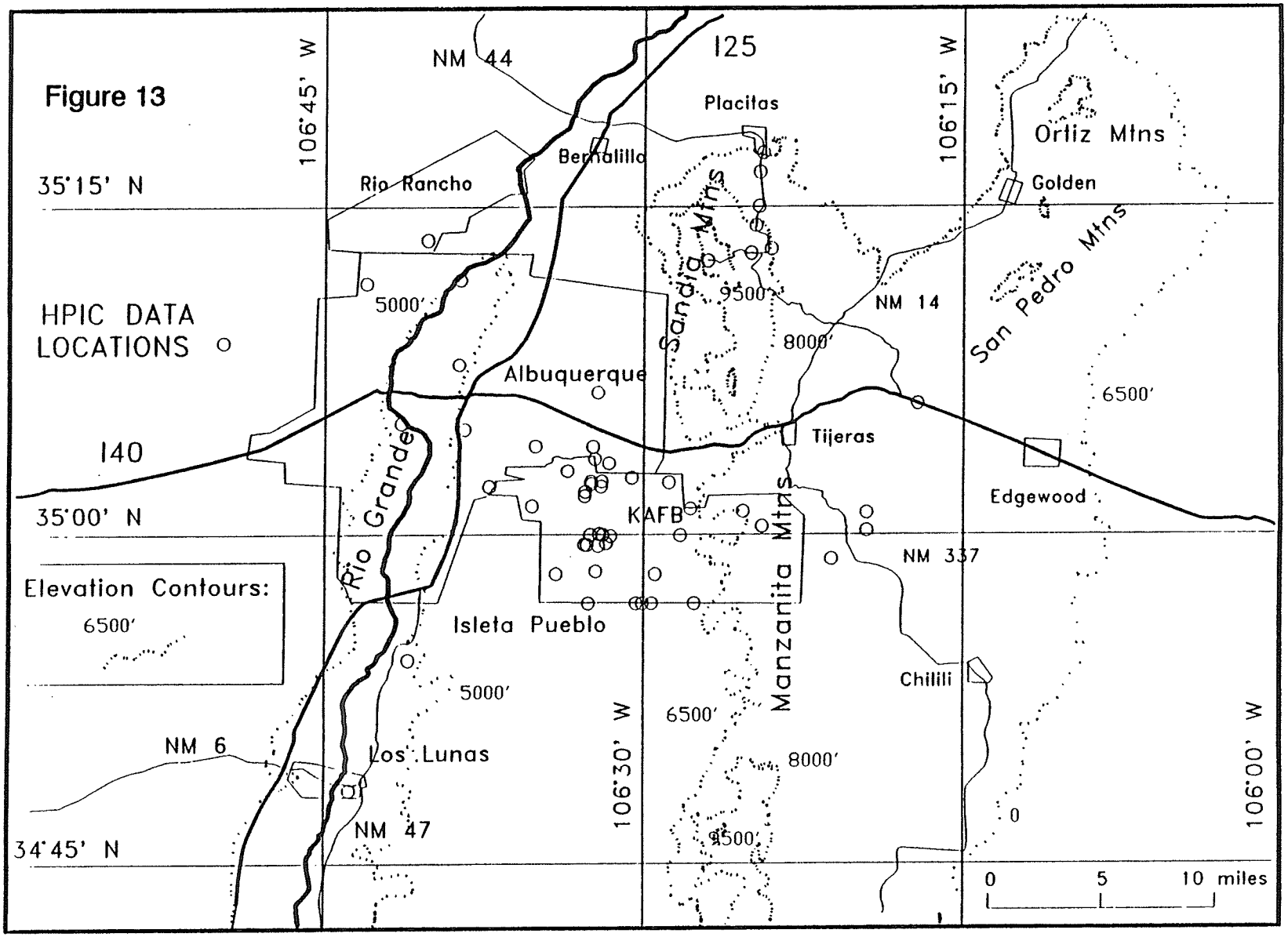
Figure 13
106°45' W
NM 44
125
Placitas
106°15' W
Ortiz Mtns
Bernalillo
35°15' N
Rio Rancho
Golden
HPIC DATA
LOCATIONS
5000'
Sandia Mtns
9500'
NM 14
San Pedro Mtns
8000'
Albuquerque
6500'
Tijeras
I40
Edgewood
35°00' N
KAFB
Rio Grande
NM 337
Elevation Contours:
6500'
Isleta Pueblo
Manzanita Mtns
Chilili
5000'
6500'
106°30' W
106°00' W
NM 6
Los Lunas
8000'
NM 47
9500'
34°45' N
0
0 5 10 miles

The high-Z materials in the walls of the HPIC impart an appreciable energy dependence to the instrument. The HPIC is on the order of 5% more sensitive at the energy for ^{226}Ra, about 200 keV, than at the energy of the primary calibration standard: ^{137}Cs at 662 keV (109). Since the difference in response was relatively slight, the uncorrected measurements were reported. This convention was also intended to maintain a consistent comparison with the TLD measurements, which were also calibrated to ^{137}Cs exposure.

To obtain additional horizontal and altitude associated data, HPIC measurements were performed at eight additional locations not associated with soil sampling or TLD deployments. The HPIC was deployed at one meter from ground surface at each monitored location. The HPIC's field of influence from terrestrial materials has been estimated to have a horizontal radius of about 60 feet in typical field deployment (59). The HPIC was operated for no less than 5 minutes and no more than two days at any given location. The measurements of highest frequency were performed for durations of 15 to 30 minutes. Continuous operation of the HPIC over a TLD field cycle was not practical at any of the TLD deployment or soil sampling sites. HPIC measurements were replicated periodically at six sites over five months, and one location was monitored continuously with collection of fifteen minute data averages for two days. HPIC replicate coefficients of variation ranged from 1% to 5%, and the continuous fifteen minute measurements varied by 0.8%. The raw replicate deviation values ranged from 0.1 to 0.7 $\mu R/h$.

2.3.3 Sources of Environmental Variability

Expected sources of temporal variability for the *in situ* gamma-ray exposure measurements arising from natural processes included variations in radon immersion concentrations and variations in the cosmic-ray intensities. Natural sources of spatial variability within a fixed time frame included the radioactive constituents of the underlying substrate, local diffusion of radon, and altitude controlled variability in cosmic-ray intensity. Both temporal and spatial exposure variation in exposure measurements may have in addition been influenced by effluents or emanations from nuclear facilities or events. Spatial and temporal effects were examined in the current study, and are discussed later under Results.

Outdoor radon concentrations may vary both diurnally and seasonally, controlled primarily by conditions that minimize vertical mixing of the surface air layer with the upper atmosphere such as nighttime thermal inversions and thermal inversions associated with high pressure-clear night sky

conditions (110). Wide diurnal temperature inversions in the study area were discussed previously under "Climate". Prolonged thermal inversions occur periodically throughout the winter months in Albuquerque, visibly apparent as a bounding layer of air pollutants (50). Environmental conditions that may also affect radon evolution from soil include soil moisture and vegetative cover (111,112). Seasonal soil drying results in a decreased barrier to diffusion through the loss of water from intergranular spaces. Vegetative cover may affect soil gas transport through the combined action of soil drying and the increased soil porosity resulting from root growth and decay. The major source of moisture available to soils in the Albuquerque area is rainfall. While rains may occur at any time of year, over half of Albuquerque area rainfall normally occurs between late July to early September, and sustained windy periods usually occur in March and April (50,51,52). Soil drying in the Albuquerque area would be expected to increase during the low humidity periods of late winter and spring. During these periods, soils are impacted by increasing air temperatures, wind driven evaporation, and evapotranspiration accompanying increased plant growth (51,53,113,..116). Radon's seasonal contribution to *in situ* gamma-ray measurement may thus be anticipated to increase during the periods of prolonged thermal inversion in winter and during the spring and summer warming periods preceding the monsoon rains.

Seismic activity may also enhance radon emanation through the disturbance of terrestrial materials (117). Seismic activity in the basin has been discussed above. Its contribution to radon emanation and the resultant effects on exposure rate measurement are no more cyclically predictable than the occurrence of earthquakes.

Cosmic-ray intensity introduces an element of temporal exposure rate variability that may be predicted from periodic trends. The predominant components of cosmic radiation in the lower terrestrial atmosphere are muons, electrons, and muon-mediated ionized air molecules. Neutrons make up a lesser fraction. The secondary cosmic-ray particles may produce gamma-rays affecting ground-based detection through interaction with atmospheric and terrestrial materials, and particle decay via electromagnetic cascades (78). Energy deposition in terrestrial materials from the muon component averages about 8 keV/cm (104). The primary cosmic gamma-ray component has little terrestrial effect: less than 10% reach even the highest montane altitudes (118). The indirect contribution of cosmic-rays to total free-air exposure in Second Quarter 1993 ranged from about 6.0 to 6.5 μR/h for the piedmont and terrace altitudes (5300′ to 6000′ MSL) in the basin (59). The cosmic-ray contribution to exposure rate

measured at the altitude of Sandia Peak may be expected to be double the basin value (107).

It has been consistently demonstrated that an inverse relationship exists between cosmic ray intensity as measured by ground-based neutron and muon detection, and solar surface activity as measured by sunspot numbers (119). The cosmic-ray modulating effects correlated with sunspot activity occur cyclically, displaying a quasi-periodicity of 11 years. Superimposed on the 11-year cycle is a 22 year cycle of variation due to changes in the solar magnetic cycle that also results in modulation of cosmic-rays incident on the surface of the earth (120,121). It is believed that the physical causes for the cyclical phenomena lie in the electrodynamic alteration of the heliosphere, and the associated effects on the behavior of the solar winds in modulating primary cosmic-ray particles. Cosmic-ray muon intensity measured on earth, correlated with high gamma-ray background, recovers completely near each solar activity minimum, while neutron maxima appear to recover more slowly. Sunspot numbers in the current solar activity cycle, SAC 22, displayed maxima beginning in July 1989 and August 1990, with the lowest monthly mean neutron monitor counting rates in the historic record obtained in June 1991. Based on recent National Oceanic and Atmospheric Administration (NOAA) solar radio flux and sunspot number data, overall solar activity was near the approximate mid-point of decline for SAC 22 by the beginning of 2nd quarter 1993 when the TLD program commenced, i.e., the approximate mid-point of recovery for muon intensity (122). By Second Quarter, 1994, it is expected that solar modulation of cosmic ray intensity would also be moderate. It is anticipated that cosmic-ray intensity would recover well before the predicted 1997 sunspot number minimum. Given the previous considerations, the net effect of cosmic-ray activity on environmentally deployed TLDs should have been a slight increase over the study duration.

Without regard to the individual sources of variability, it is doubtful whether annual changes of less than about 11 mR, or hourly changes of less than 2 μR/h, are statistically significant; those values have been suggested as minima for all measurements due to natural variability (123).

3. RESULTS AND DATA TREATMENT

Upon completion of laboratory analytical operations, data reduction, and qualification, summaries were tabulated of the raw results derived from each of the techniques in the multimedia effort. The various summaries are discussed in the context of their techniques below. In addition, the populations of analytical data for each of the various techniques and parameters were entered with geographic data to create three-dimensional surface projections and contour plots to facilitate the inference of regional trends. Since there was insufficient information to support the use of krigging or other geostatistical biasing techniques, a least squares fitting algorithm was used to produce the projections and contours in all cases. An unfortunate but unavoidable consequence of this was the inference of specific regional trends where a dearth of data exists. These regions are readily apparent in the contour plots, and literal interpretation of the *steepness* of the depicted contours should not be impled. The analytical data were further treated statistically to evaluate the behavior of the sampled populations. Data analysis and treatment were performed to conform to EPA recommendations (64).

3.1 Soil Sampling and Analysis Results:

Raw results for ^{226}Ra, ^{235}U, ^{232}Th, and ^{214}Bi in soils are given in Tables 4 and 5. Results are given in Tables 6 and 7 for ^{137}Cs ^{238}U, and ^{40}K in soils, along with the HPIC readings and estimated ground-shine exposure components arising from the major nuclides in $\mu R/h$. The ground-shine component of exposure was estimated by a method described in NCRP 94, using fixed conversion values multiplied by the activity concentration values for the uranium and thorium series nuclides and ^{40}K (104). The uranium series soil activity values required for multiplication were actually taken from the ^{226}Ra series. This was done since the vast majority of gamma-rays in the uranium series derive from radium and its daughters, and there appeared to be disequilibrium between U and Ra activity concentrations in virtually all of the soil samples analyzed. The ground-shine estimates expressed as fractions of the HPIC measurements agreed well with the approximate range of 50% to 70% of total free-air exposure given in the literature (1,78,104). The highest relative ground-shine exposure fractions were associated with areas of highest radium series soil activities. The geographic and statistical trends for each soil activity parameter are given below. Following the technique specific observations are statistical summaries for all analyzed measurement parameters.

3.1.1 ^{226}Ra and ^{214}Bi in Soils

The geographic distribution for ^{226}Ra soil activity concentrations found as 60% of the 186 keV peak region counts is depicted as a three-dimensional projected surface in Figure 14, and as iso-concentration contours in Figure 15. It was apparent from these figures that a dramatic increase in ^{226}Ra in soils occurs with approach to the easternmost sampling points. This trend is also visible in the complementary Figures 16 and 17 for ^{214}Bi, although the concentration values are somewhat greater overall than those for ^{226}Ra. This may be an artifact of the fixed average fractions used to differentiate between ^{226}Ra and ^{235}U counts under the same peak area, suggesting a slight underestimation resulted from applying the radium fraction convention. In any event, the results of the spatial presentation suggest that there are distinguishable regional trends in the distribution of radium series nuclides. Several values in the eastern portion of the study region, east of the dividing Sandia and Manzano Mountain Ranges, were sufficiently high to suggest that they derived from separate populations. Soil activity concentrations of nuclides in the ^{226}Ra subseries ranged from approximately 0.8 to 1.4 in the inner basin, while values lying outside the basin ranged from about 1.3 to 2.7 pCi/g.

To examine the statistical characteristics of the two related data sets, box-and-whisker diagrams, normal and log-normal probability plots, and population distribution fittings were evaluated. Among these techniques, probability plotting has been strongly recommended to test the homogeneity of sample populations (64). The results of applying these analyses suggested that the easternmost data points might indeed derive from a population distinct from the remaining data. To further evaluate this, a standard outlier test using one-sided critical T_n values was performed for the entire data set at the 5% risk of false rejection level for both raw and log-transformed data (124,125). Only one value from each of the log-transformed data sets was trimmed by this method. Those values derived from the same exceptionally high activity location, as measured by both gamma-spectroscopy and inferred by *in situ* HPIC measurement. Since many natural processes can be shown to be best described with lognormal distributions, this model was assumed and tested, and appeared to generate the best distribution for the remaining data (16). The relative fit of the data to normal and lognormal distributions was evaluated in several ways. First, the spread of data was inspected using box-and-whisker diagrams for the trimmed and untrimmed normal and log-transformed data, as depicted in Figures 18 and 19. Slight skew of outlier trimmed data to the right is reduced by log-transformation. Skew and kurtosis were evaluated by estimating the third and fourth moments

Figure 14

Spatial Distribution of Ra-226 Soil Activity Concentrations
in the Vicinity of Albuquerque, NM

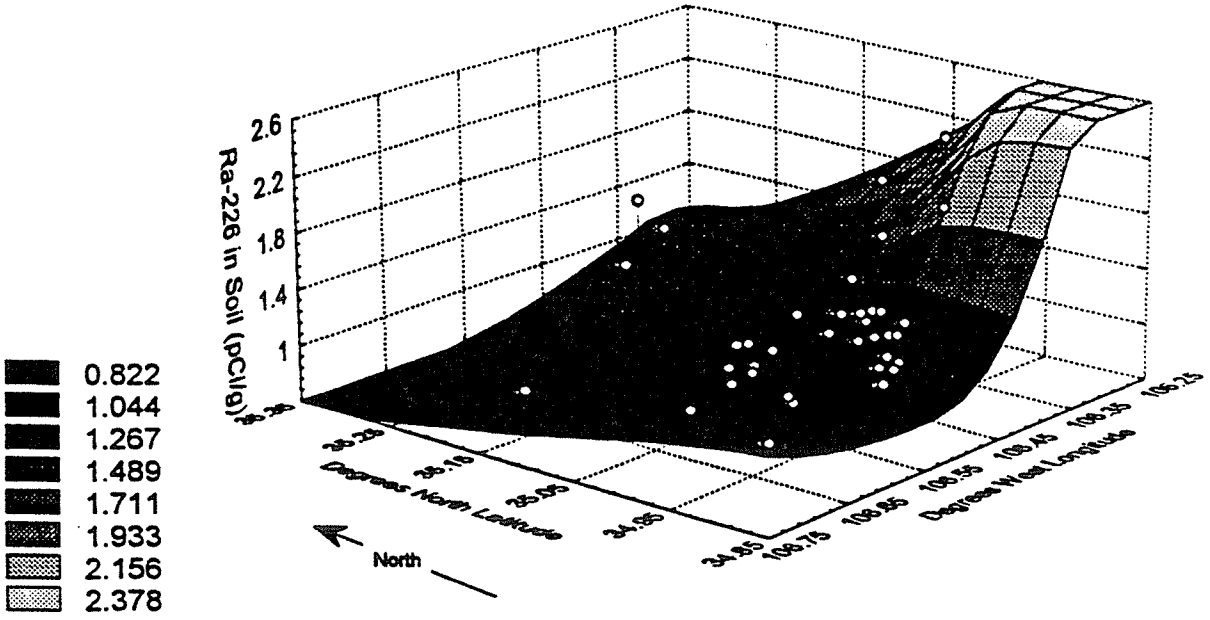

Figure 15

Spatial Distribution of Ra-226 Soil Activity Concentrations
in the Vicinity of Albuquerque, NM

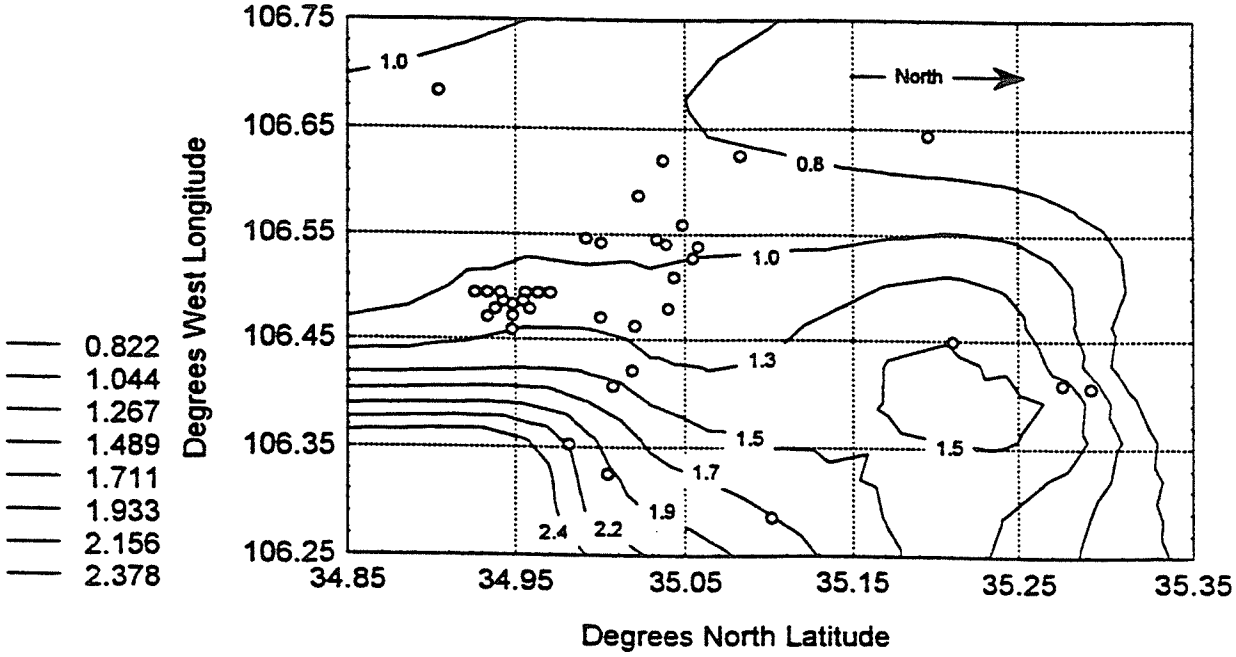

Figure 16

Spatial Distribution of Bi-214 Soil Activity Concentrations
in the Vicinity of Albuquerque, NM

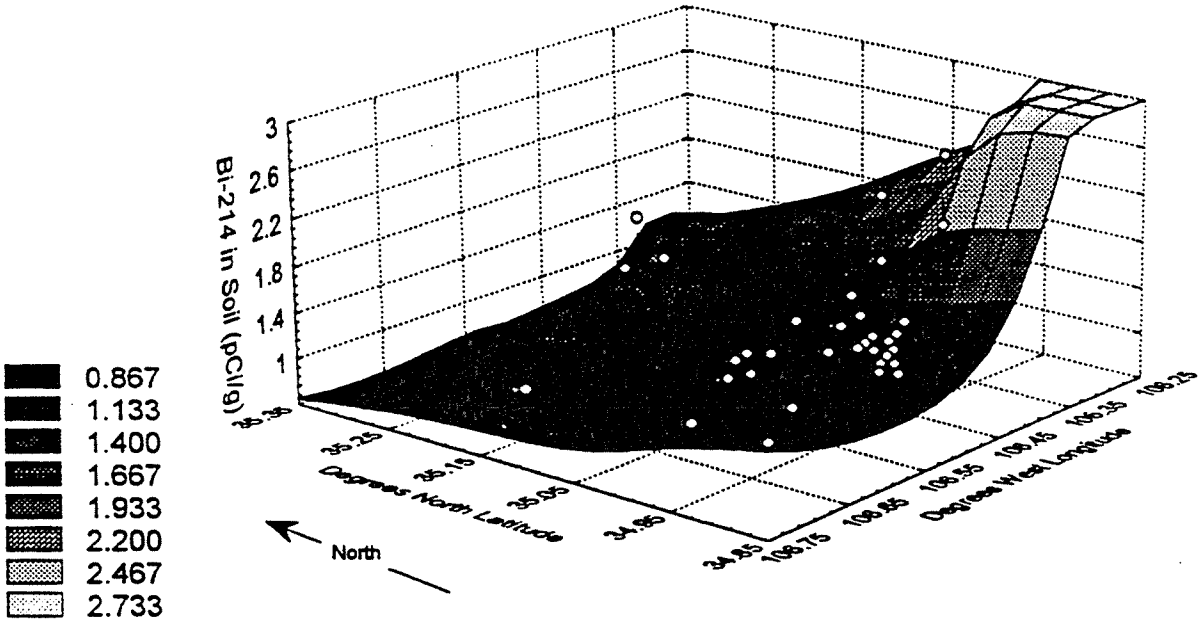

Figure 17

Spatial Distribution of Bi-214 Soil Activity Concentrations
in the Vicinity of Albuquerque, NM

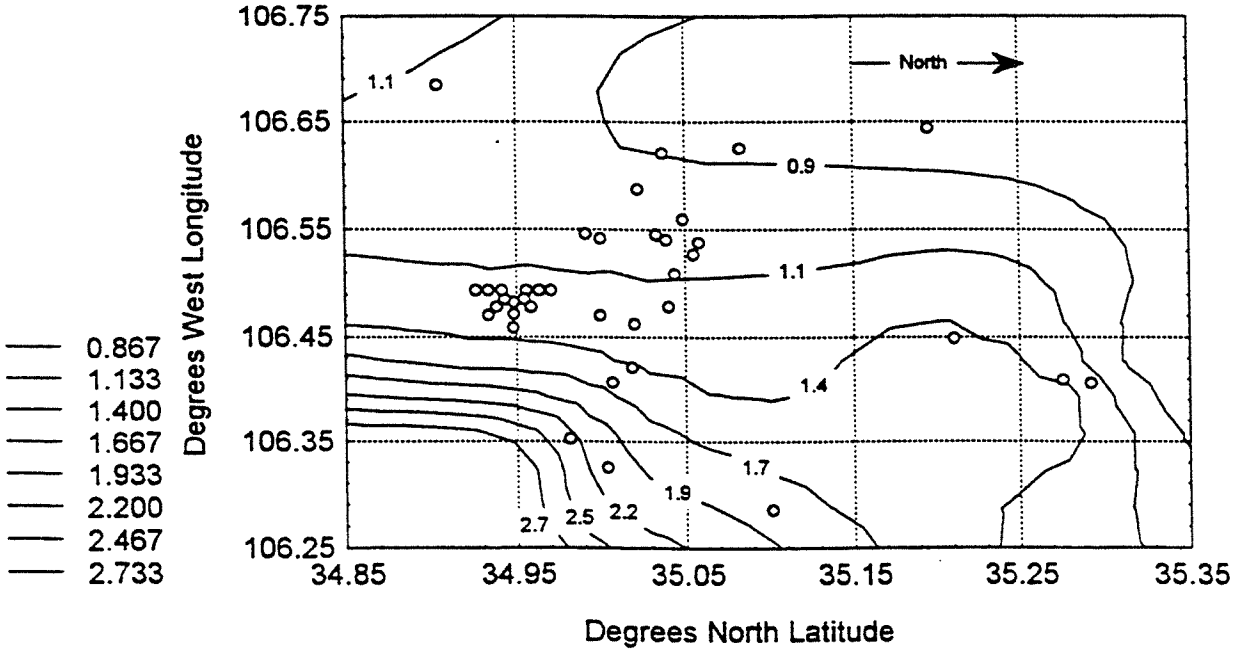

Figure 18

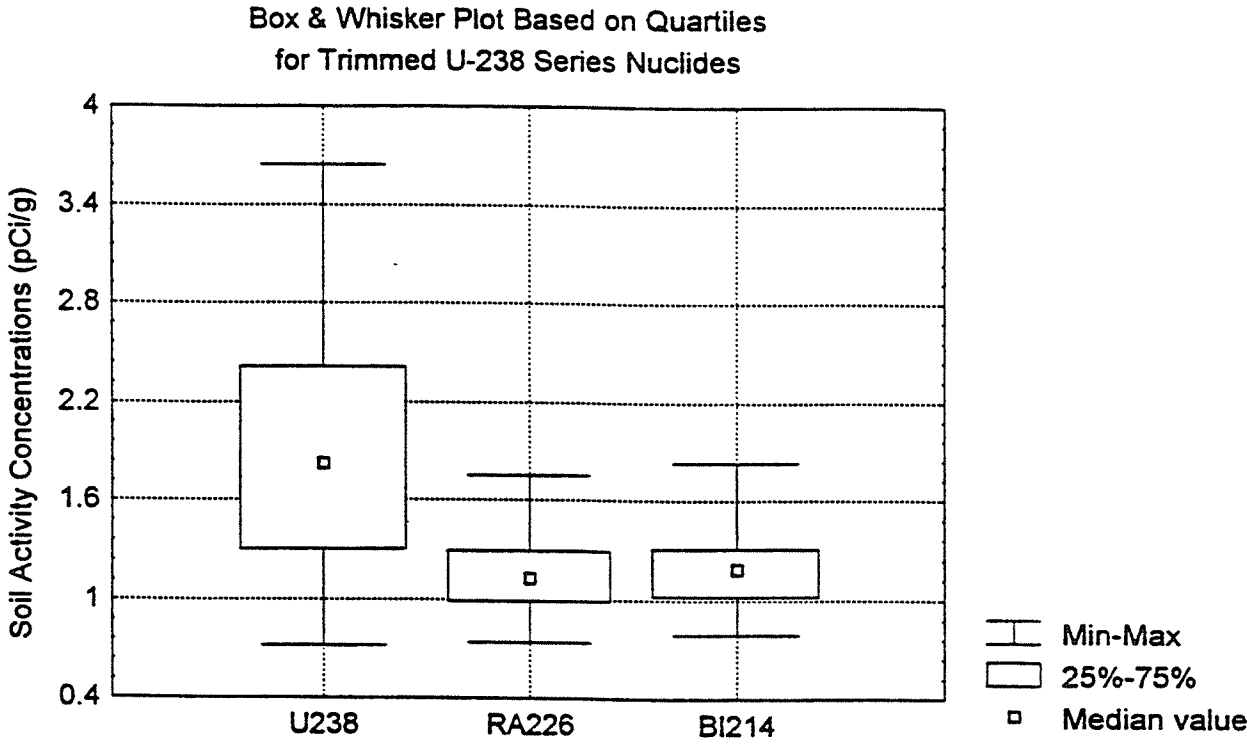

Figure 19

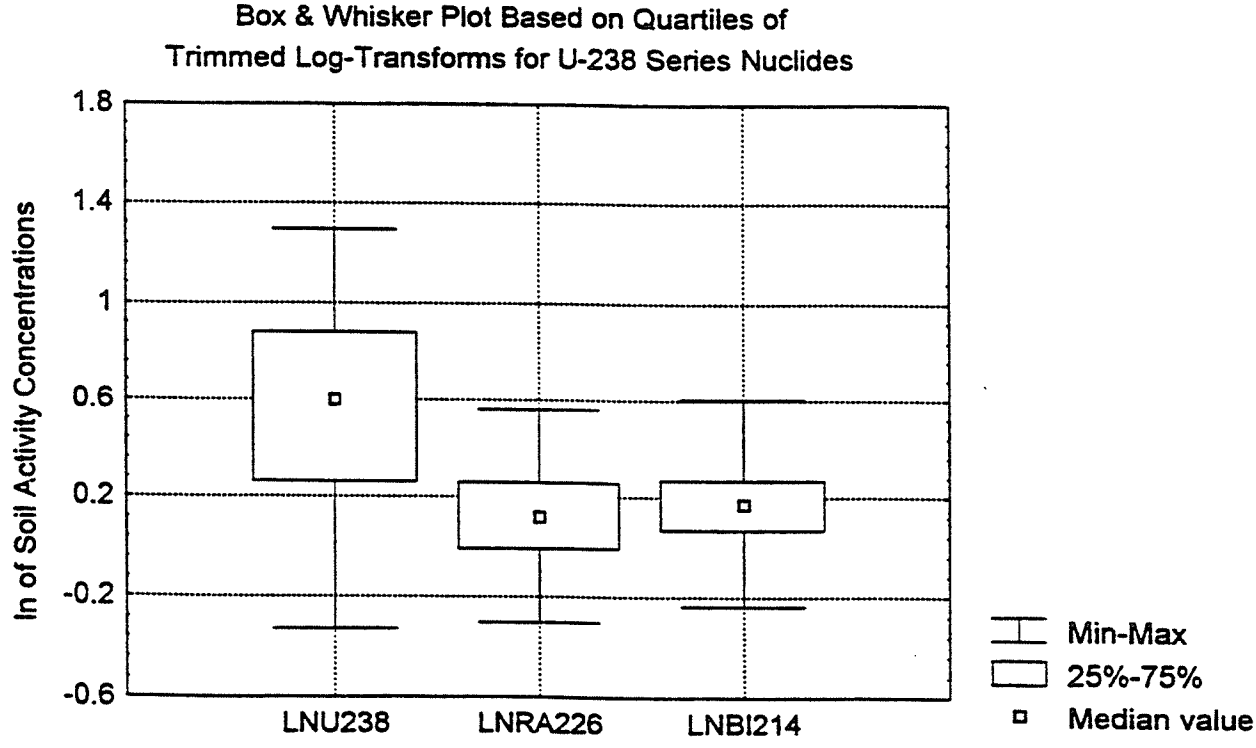

about the population mean: γ_1 and γ_2 (126). Kurtosis, a measure of the heaviness of data in the tails of an assumed distribution, was of minimal utility since the data sets were relatively sparse. The resultant effects of trimming and transformation on data distribution were further tested via the Shapiro-Wilkinson W parameter, Chi-square, Lilliefors' test, and the Kolgorov-Smirnov single-sample test. Normal probability plots and normal histograms representing the data as optimized by trimming and log-transformation for ^{226}Ra can be seen in Figure 20 and 21, and for ^{214}Bi in Figures 22 and 23. These figures also indicate the results for various statistical tests.

Since log-transformation of data may mask subtle trends, it was deemed prudent to inspect the distributions of raw, untransformed values as well. Figures 24 and 25 represent the distribution of trimmed untransformed data for the two nuclides, respectively. Numerical analysis of the plots indicated multiple modes, and the appearance of the plots suggested a vestige of at least one other sample population distributed around an elevated relative mean. The arithmetic means of the initial raw population data of 1.20 ± 0.32 pCi/g for ^{226}Ra and 1.25 ± 0.34 pCi/g for ^{214}Bi were refined to respective geometric means of 1.12 ± 0.26 pCi/g and 1.19 ± 0.26 pCi/g. These values are expected to best reflect the majority of locations within the study region. The relative successes of ^{226}Ra and ^{214}Bi counting were examined by generating a normal probability distribution for the ratio of soil activity concentrations, as shown previously in Figures 8 and 9. The relatively good fit to a normal distribution encourages the use of the 186 keV count fractioning technique, suggesting that the ratio varies around a mean value by random effects without internal bias. ^{226}Ra counts at 186 keV yielded soil activity concentrations of about 96% compared to those yielded by ^{214}Bi counts at 609 keV. This average value was not altered by data trimming, although trimmed data are represented in the figures and yielded slightly higher sample deviations than untrimmed data.

3.1.2 ^{235}U in Soils

The analytical process described above was also applied to evaluate spatial and statistical distributions of ^{235}U in soil. ^{235}U soil activity concentrations were found from gamma-spectral analysis as 40% of 186 keV counts. Based on our previous observations, the ^{235}U activities were expected to be slightly over-estimated, on the order of 6%. Since the data had already been used to calculate ^{226}Ra soil activity concentrations, they had effectively lost a degree of freedom, so the soil activity estimates were truncated to the number of

Figure 20

Normal Probability Plot for the Distribution of
Trimmed Log-Transformed Ra-226 Soil Activity Concentrations
in the Vicinity of Albuquerque, NM

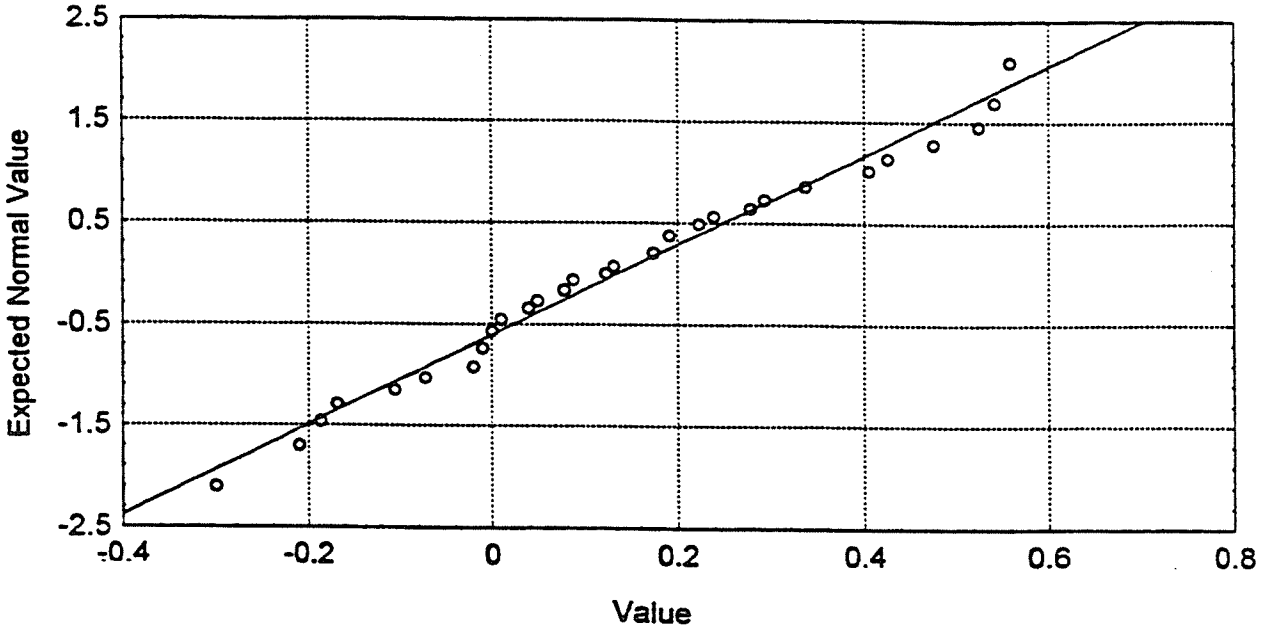

Figure 21

Distribution of Trimmed (ln) Ra-226 Soil Activity Concentrations
K-S d=.07806, p> .20; Lilliefors p> .20
Shapiro-Wilk W=.97162, p<.5493

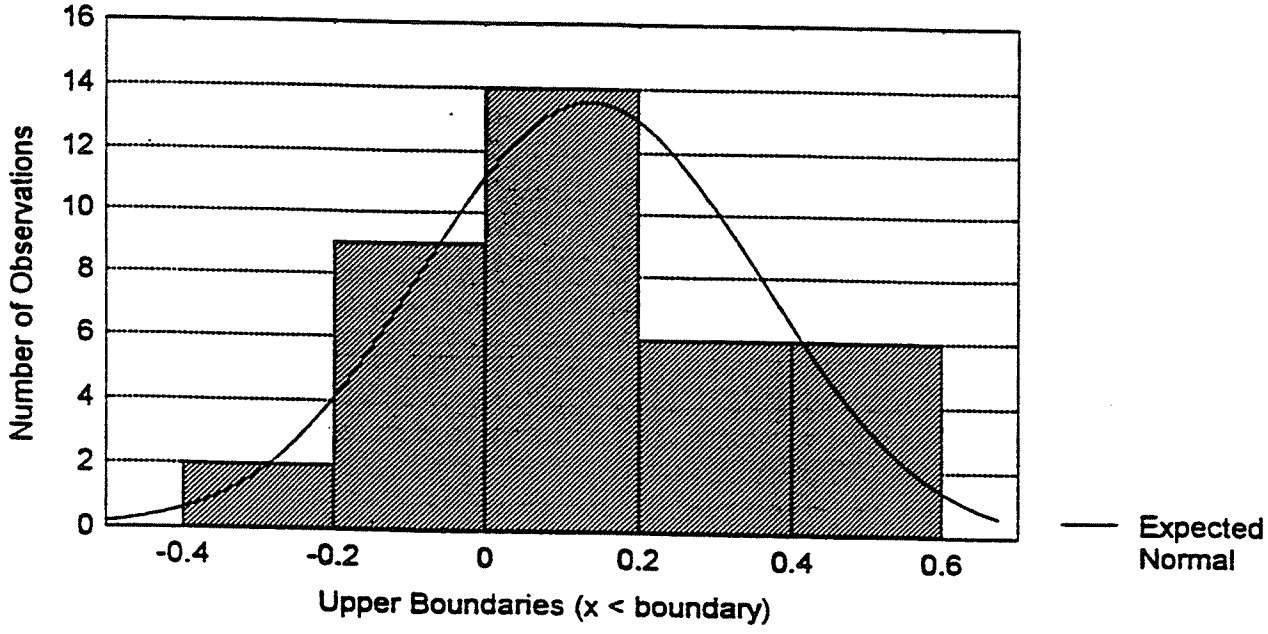

Figure 22

Normal Probability Plot for the Distribution of
Trimmed Log-Transformed Bi-214 Soil Activity Concentrations
in the Vicinity of Albuquerque, NM

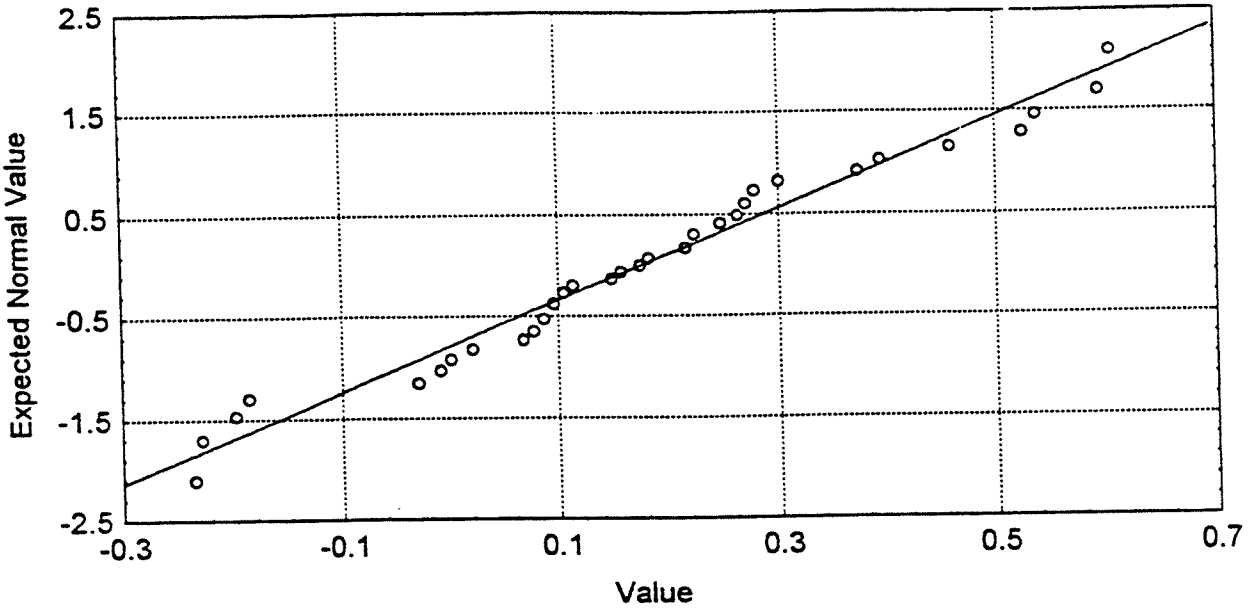

Figure 23

Distribution of Trimmed (ln) Bi-214 Soil Activity Concentrations
K-S d=.09998, p> .20; Lilliefors p> .20
Shapiro-Wilk W=.96099, p<.2850

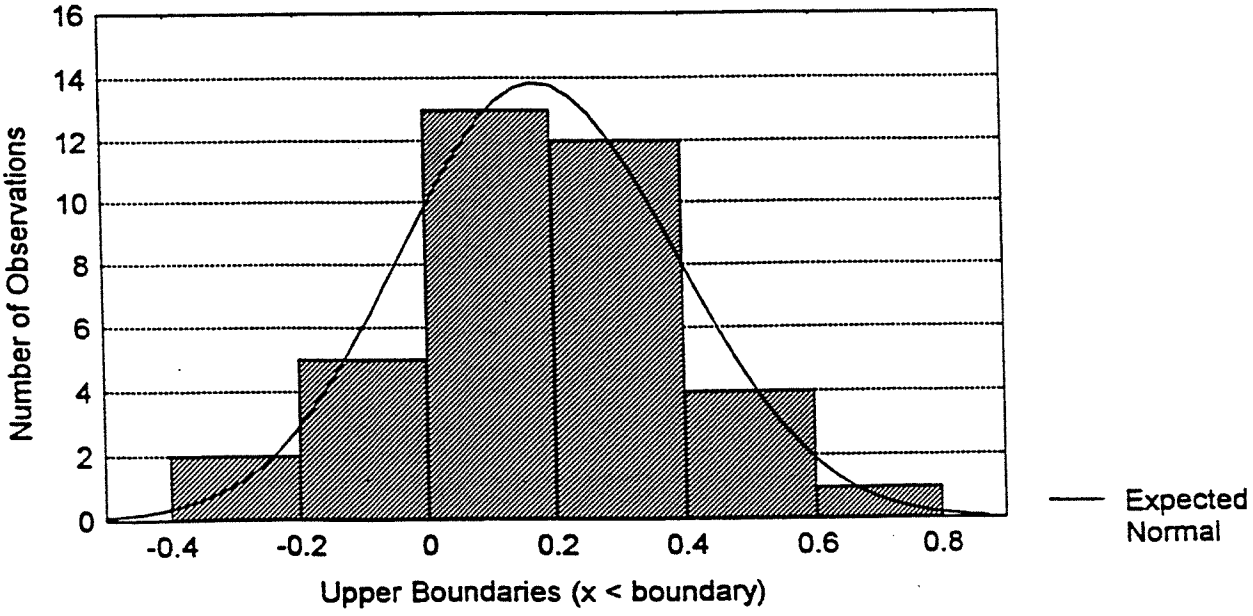

Figure 24

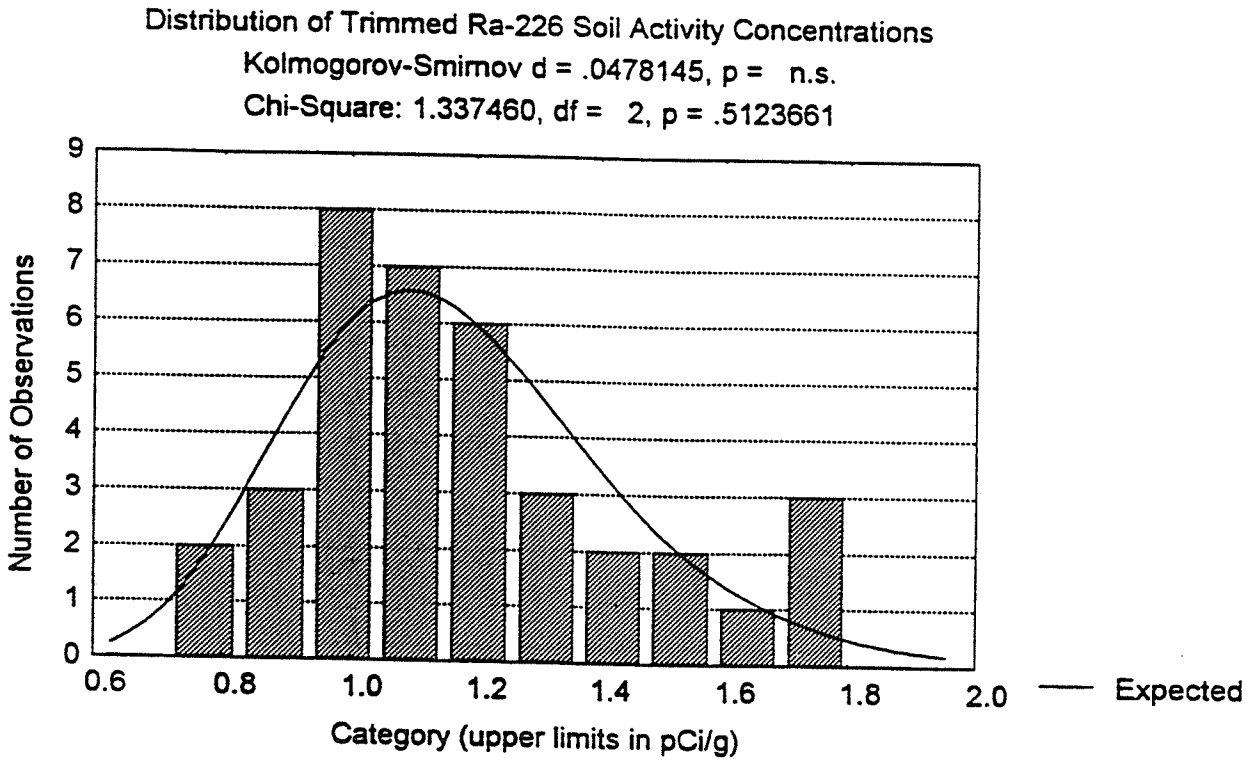

Figure 25

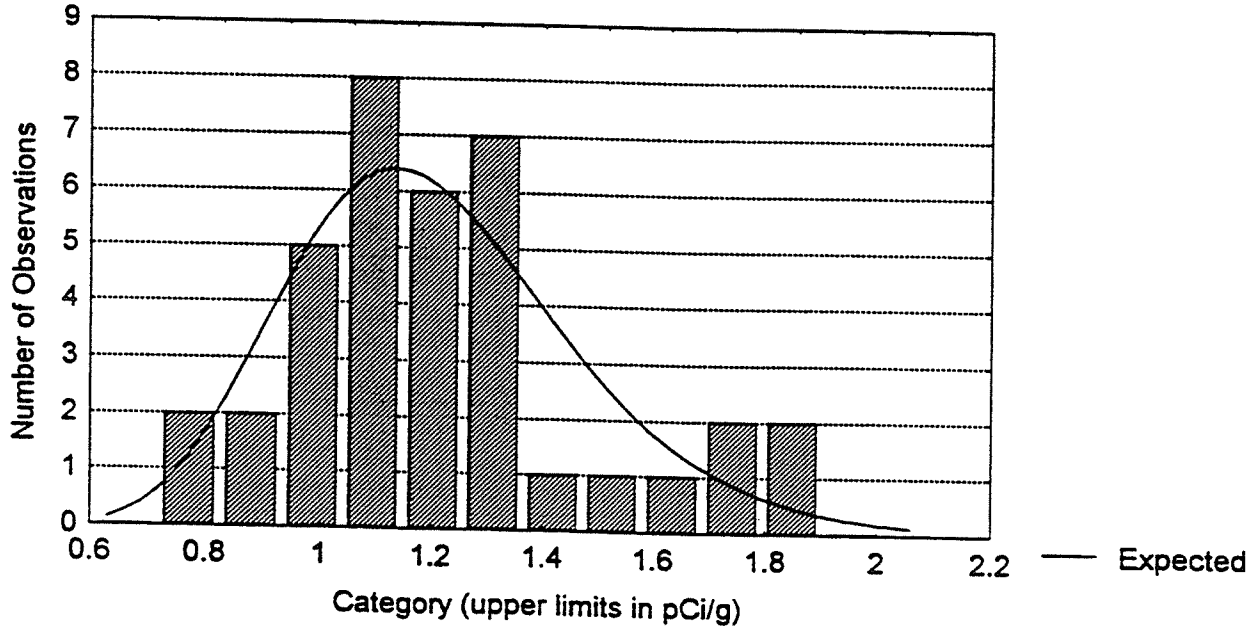

decimal places reported for ^{226}Ra. Because the ^{235}U soil activity estimates were necessarily derivative, it was anticipated that their distribution would closely mimic the trends observed for ^{226}Ra. This is apparent to some extent in the surface and contour maps in Figures 26 and 27. Inner basin values for ^{235}U soil activity concentrations ranged from less than 0.05 to more than 0.06 pCi/g, while values beyond the escarpment ranged from about 0.07 to 0.12 pCi/g.

The significant-figure truncation convention appeared to have the effect of producing a more markedly right-skewed (or positively skewed) data distribution, as may be observed in Figure 28. Log-transformation reduced the degree of right data skew to a lesser degree than was observed for ^{226}Ra and ^{214}Bi, as may be seen in Figure 29. Use of critical T_n values to determine outliers in the log-transformed data set resulted in rejection of one data point at the 5% risk level, also associated with the anomalously high activity and exposure rate location discussed previously. That data point is readily apparent in the lognormal probability plot depicted in Figure 30 as the point of greatest magnitude and distance from the fitted normal line. The distribution of trimmed raw values are depicted in Figure 31, which did not replicate the bimodal appearance of the ^{226}Ra plot, and exhibits the strong positive (right) data skew characteristic of a lognormal distribution.

3.1.3 ^{238}U in Soils

Counting data for ^{238}U, as mentioned above, was found by counting in the low gamma-abundance region centered at 1001 keV. This produced the fewest recognizable peaks in the spectra analyzed. Fitting of the available peaks was performed by developing regions about the 1001 keV line that yielded resolutions on the order of 2 keV through iteration of software recognition and operator manipulation. The high detection uncertainty is reflected in the higher overall LLDs found for this peak, recorded in Tables 6 and 7. Non-detected results were found in ten of thirty eight sample cases, mainly in the aluminum can geometry counts. The values for these non-detected peaks were estimated for distribution analysis by using the LLD. This is one of several defensible methods that may be used for population estimation that prevents left-censoring of the data (16,64,127). The limitation on reporting of sample population means is that the actual sample population values are *less than* those found by this technique. The sample means are, in turn, estimates of "true" but unattainable universal population values. This level of qualification (i.e., less than) is implicit in all further reporting of ^{238}U data in this study.

Figure 26

Spatial Distribution of U-235 Soil Activity Concentrations
in the Vicinity of Albuquerque, NM

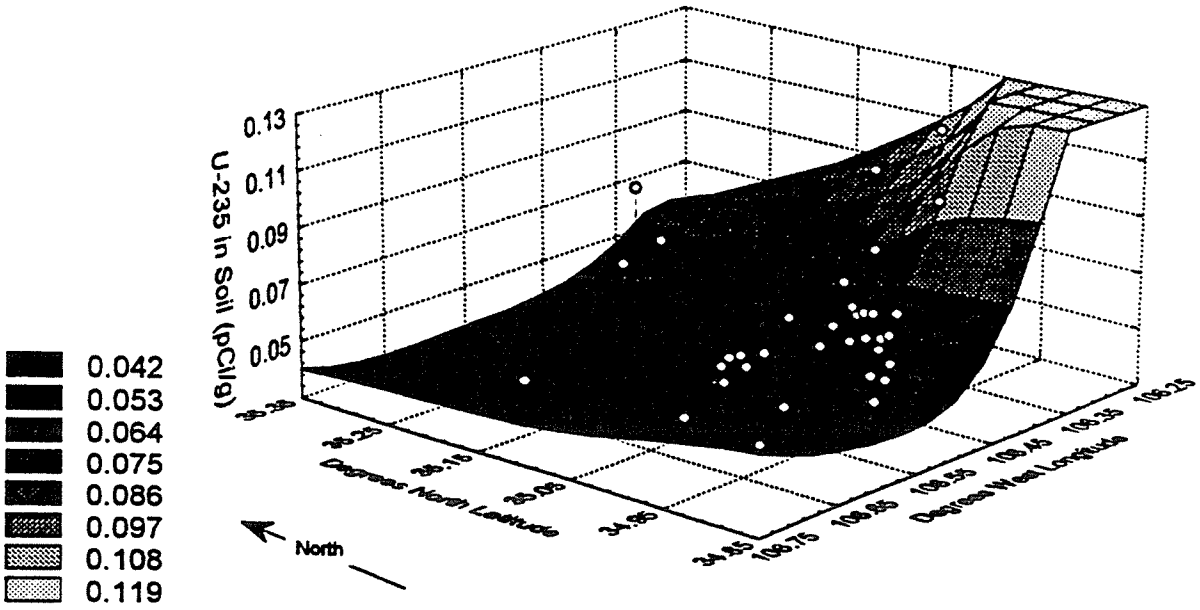

Figure 27

Spatial Distribution of U-235 Soil Activity Concentrations
in the Vicinity of Albuquerque, NM

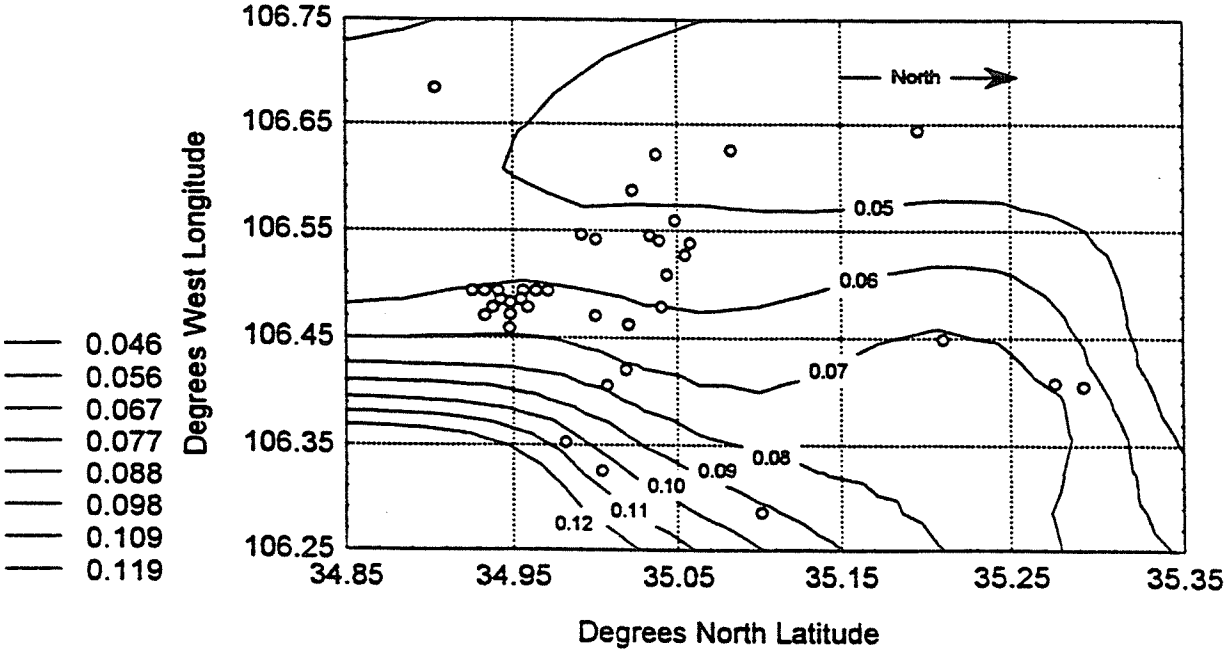

Figure 28

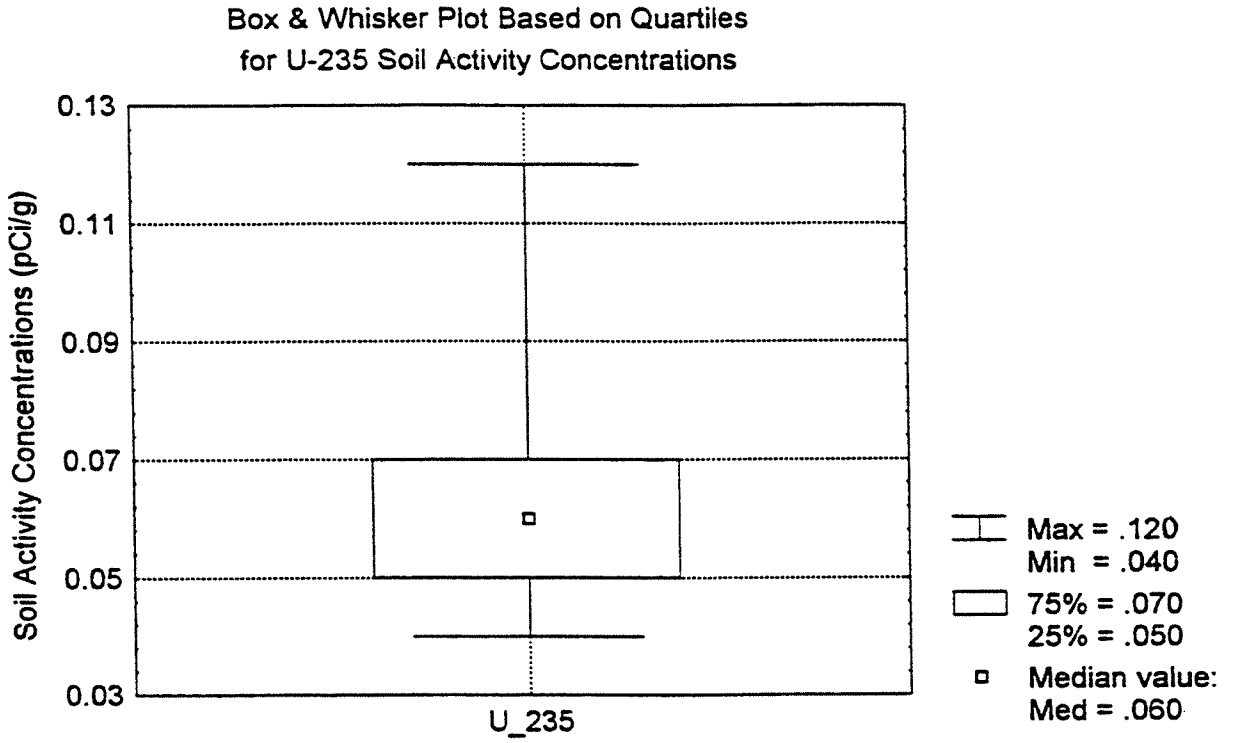

Figure 29

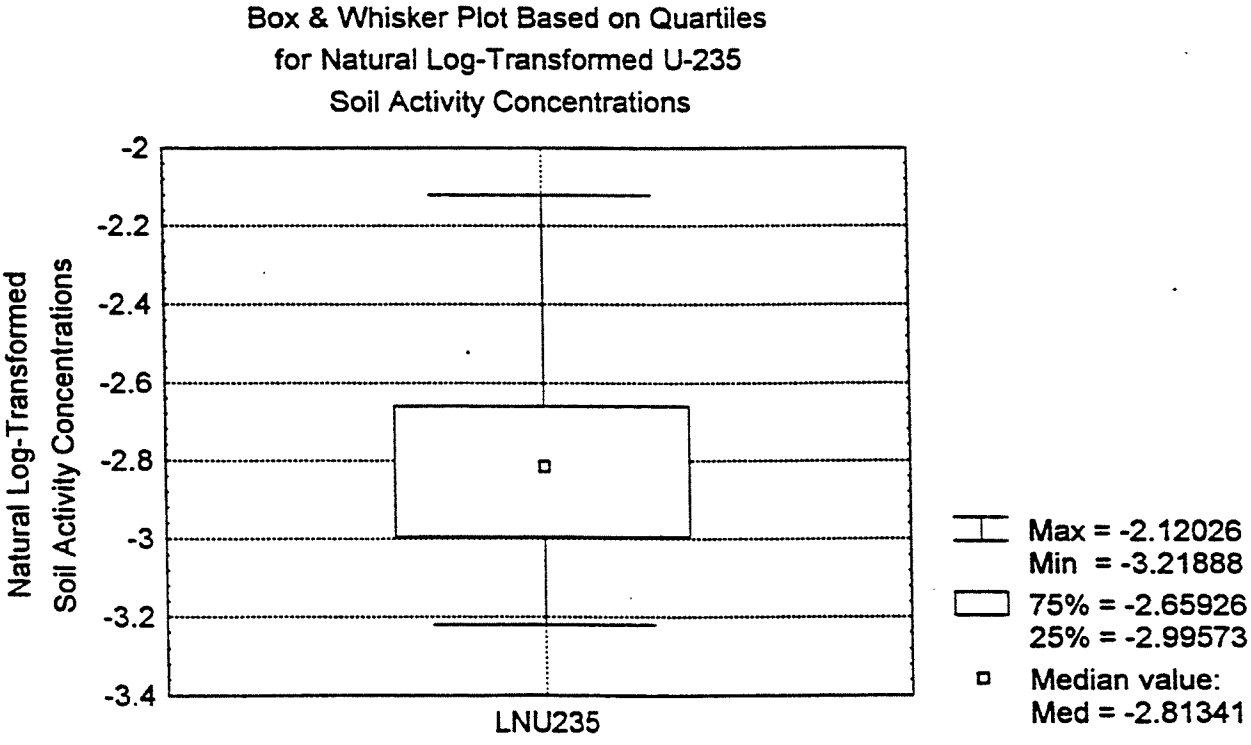

Figure 30

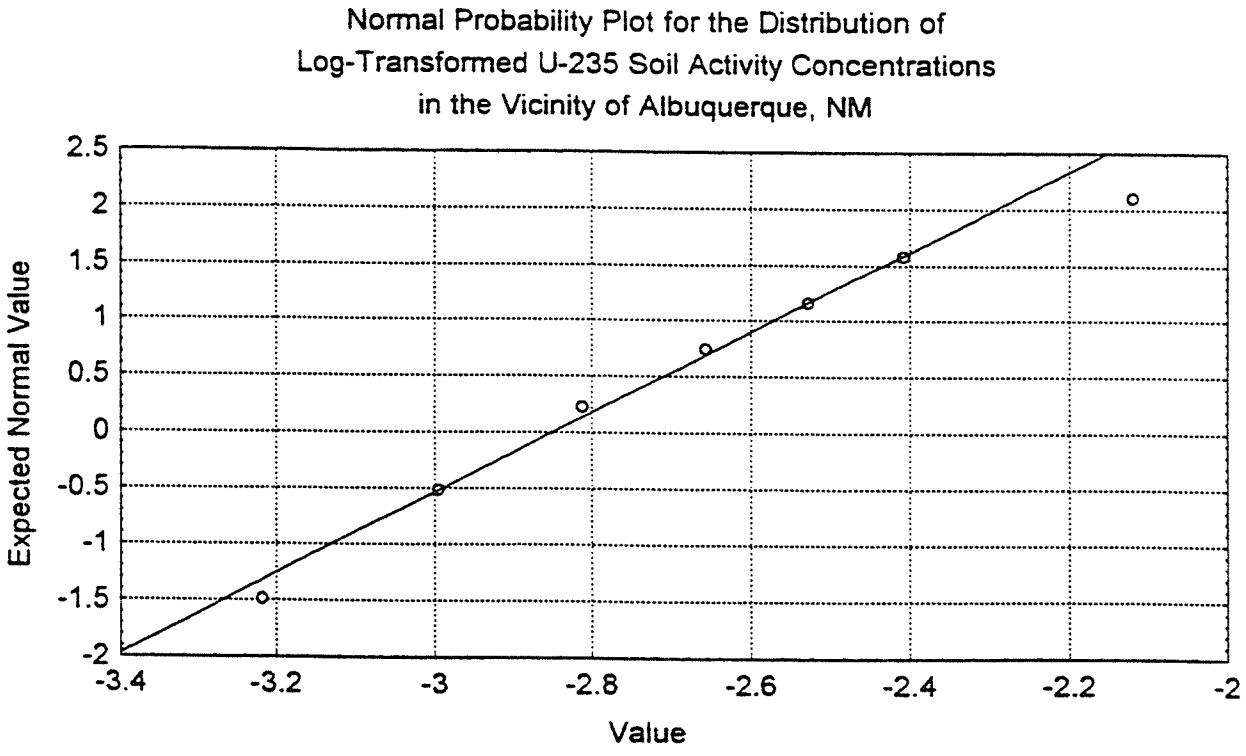

Figure 31

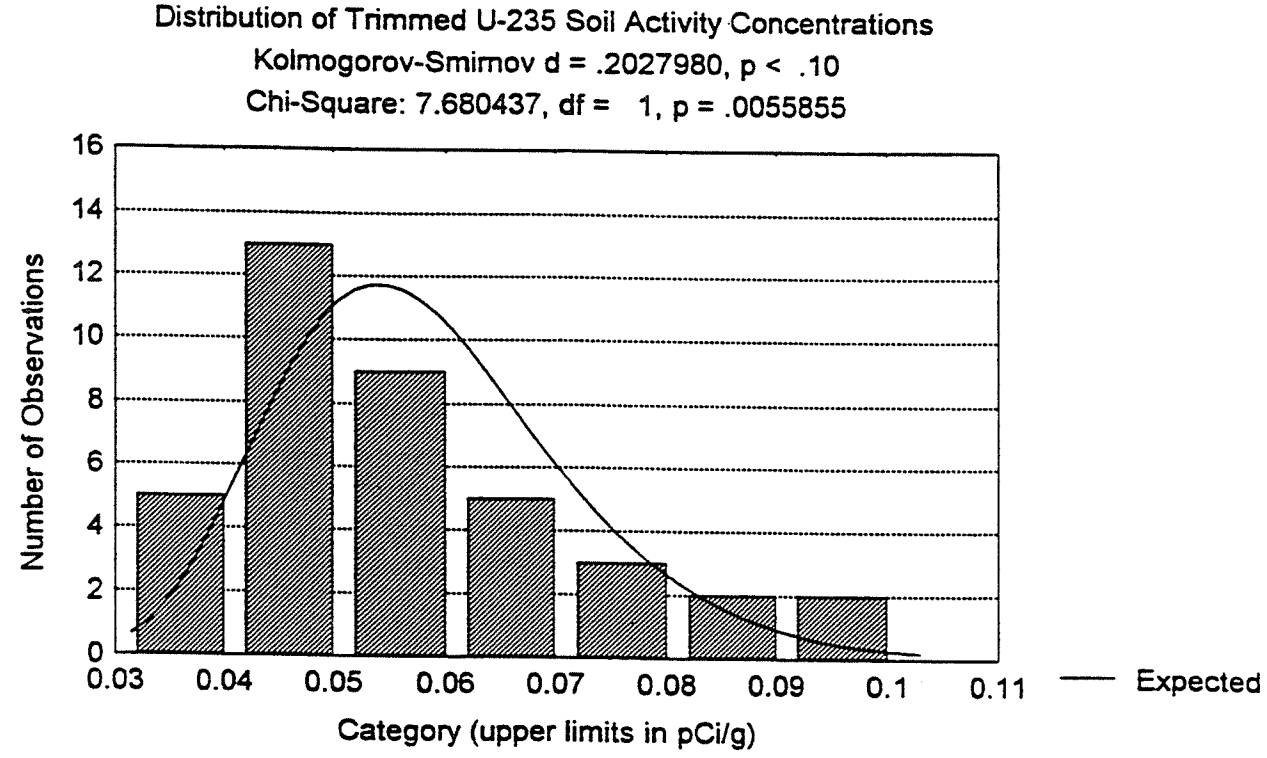

The spatial distribution of ^{238}U in the study area soils is depicted as a surface and as contours in Figures 32 and 33, respectively. The effect of flattening the data distribution exercised by the incorporated LLDs is apparent, but the trends previously observed for ^{238}U series (^{226}Ra subseries) nuclides were preserved, as would be predicted. Higher values were generally found in the Central Highlands and Sandia Range north slope and peak areas, outside the basin boundaries. Those values ranged from about 2.3 to 3.3 pCi/l. By contrast, the basin values range from about 0.9 to 1.9 pCi/l. On the whole, ^{238}U values were greater than comparable values for ^{226}Ra subseries daughters, suggesting the influence of geochemical factors leading to decay disequilibrium in the soil samples. The average U:Ra ratio was 1.65 ± 0.62 for the trimmed data set. The ratio data evinced a reasonably close fit to a normal distribution with a small degree of positive skew, as is shown in Figures 34 and 35.

The sequential process of evaluating the sample population through outlier discrimination and log-transformation also resulted in improvement of statistical distribution characteristics. A critical T_n test yielded one outlying value at the evaluated 5% risk level. This value was not associated with the otherwise high activity and exposure rate location in the Central Highlands, but was nearest a SNL environmental restoration site contaminated with depleted uranium. The same data value also showed an unusually high U:Ra ratio by comparison to the critical T_n. As was apparent in Figures 18 and 19, right skew for the trimmed ^{238}U data set suggests a lognormal distribution. A normal probability plot and histogram of the log-transformed data may be seen in Figures 36 and 37. This may be compared to distributions of the untransformed data in Figures 38 and 39. Mutlimodality of the distribution is suggested in the latter figures, but was not readily apparent in the numerical analysis. Comparing the Shapiro-Wilkinson W statistic evaluated for the raw data distribution in Figure 38 and log-transformed data distribution in Figure 37 suggests that log-transformation improved the apparent statistical behavior of the data set.

3.1.4 ^{232}Th in Soils

The spatial distribution of ^{232}Th in soils, as measured by the daughter ^{212}Pb, suggested a smoother increase with westward approach to the eastern slopes of the Manzano Mountains in the western extreme of the Central Highlands. This may be seen in Figures 40 and 41. Unlike the uranium isotopes and radium subseries nuclides, a separate concentration high is not evident in the northeast contours of

Figure 32

Spatial Distribution of U-238 Soil Activity Concentrations
in the Vicinity of Albuquerque, NM

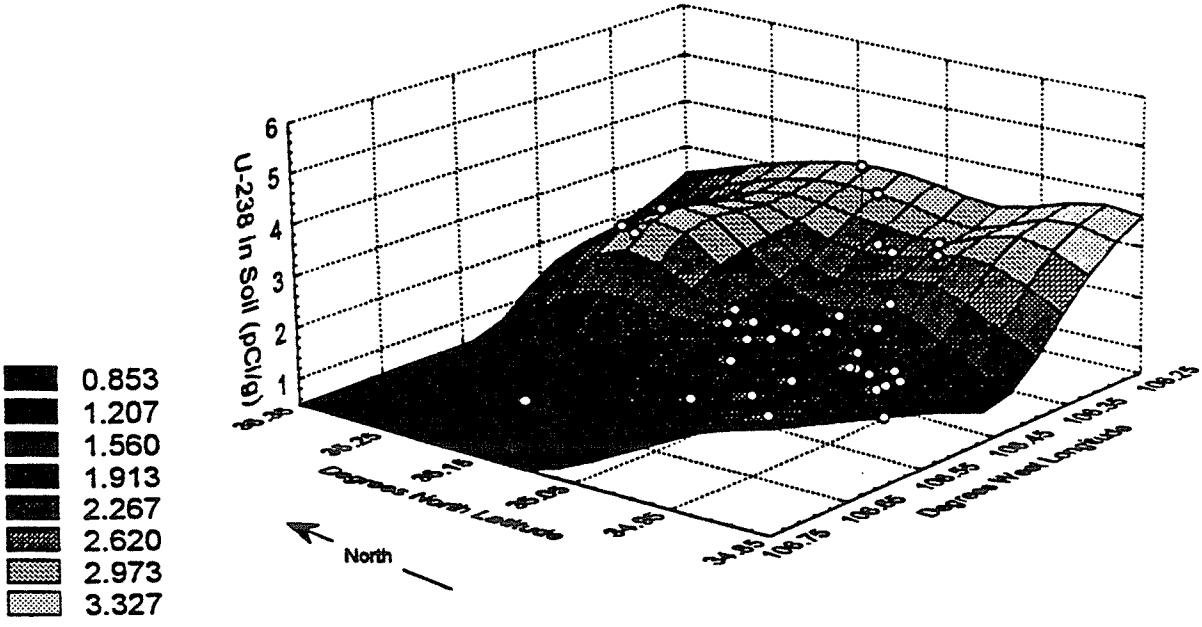

Figure 33

Spatial Distribution of U-238 Soil Activity Concentrations
in the Vicinity of Albuquerque, NM

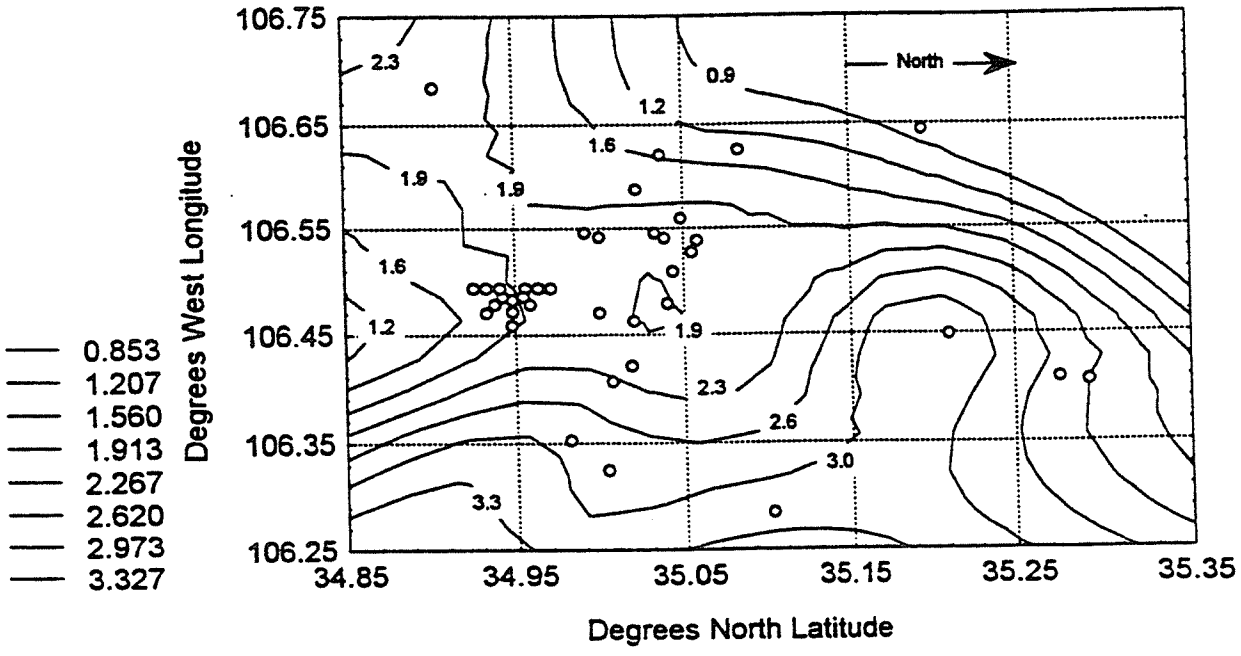

Figure 34

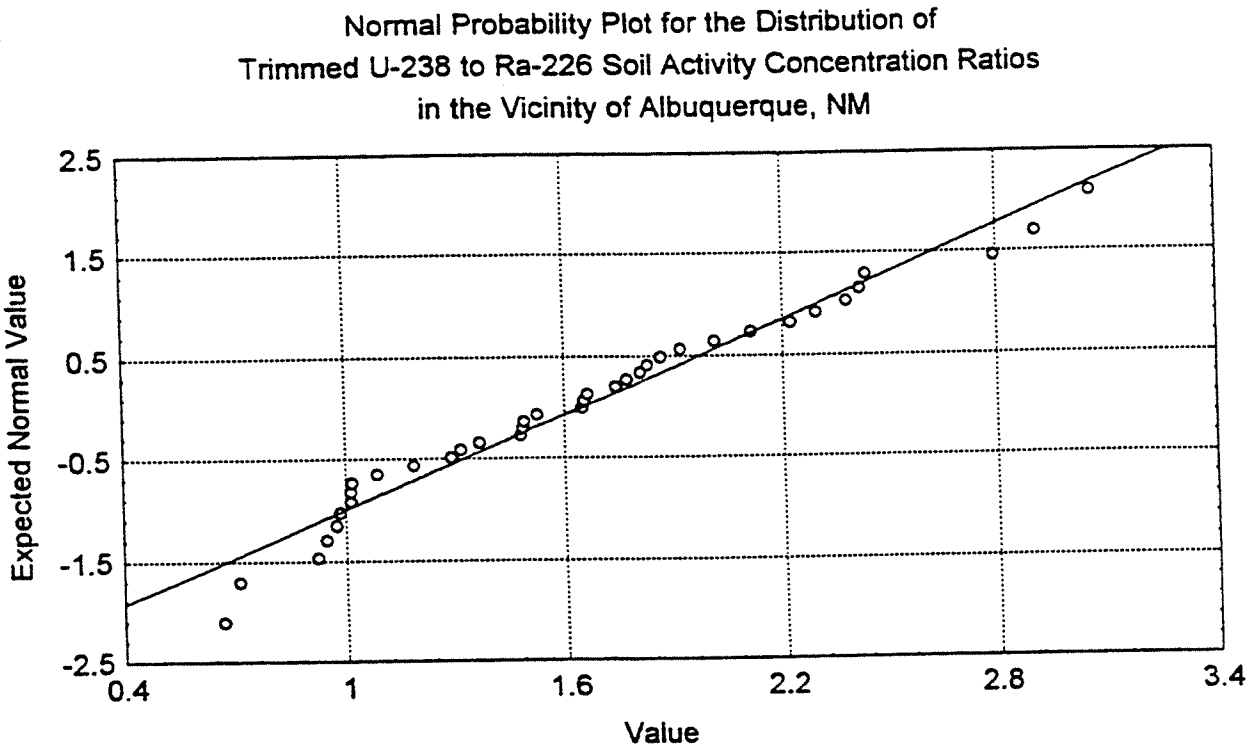

Figure 35

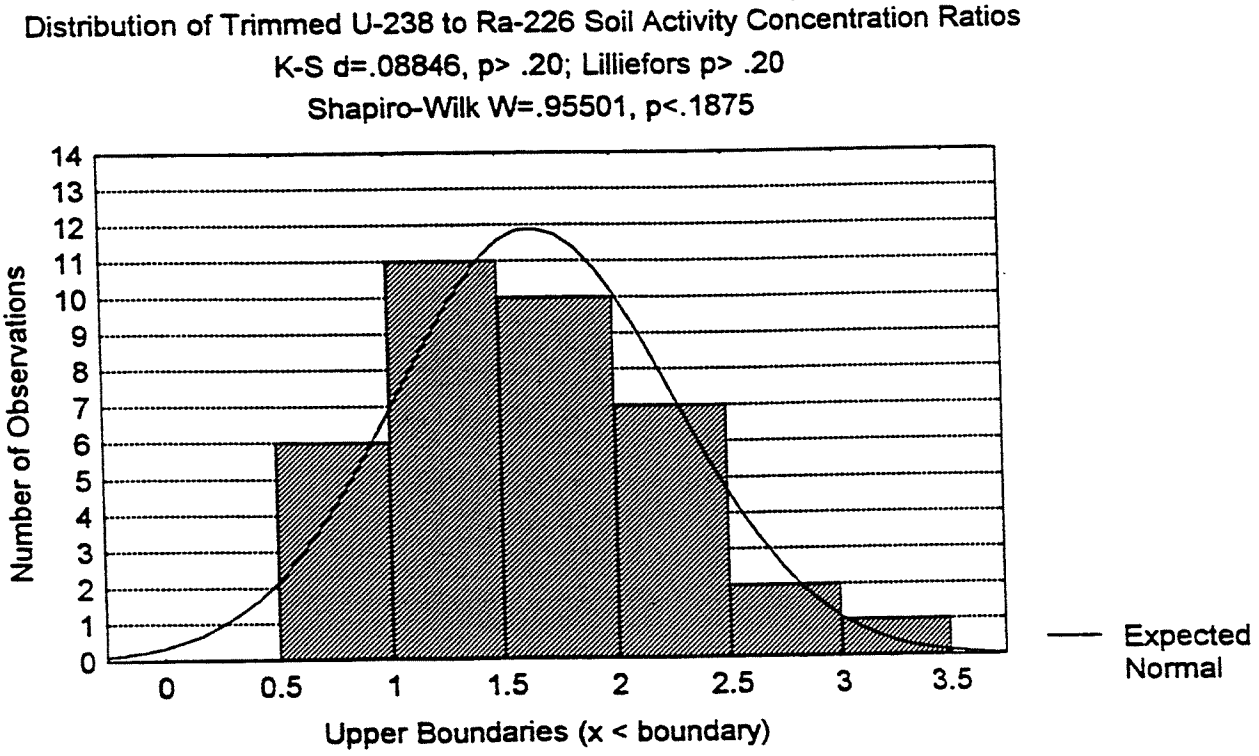

Figure 36

Normal Probability Plot for the Distribution of
Log-Transformed U-238 Soil Activity Concentrations
in the Vicinity of Albuquerque, NM

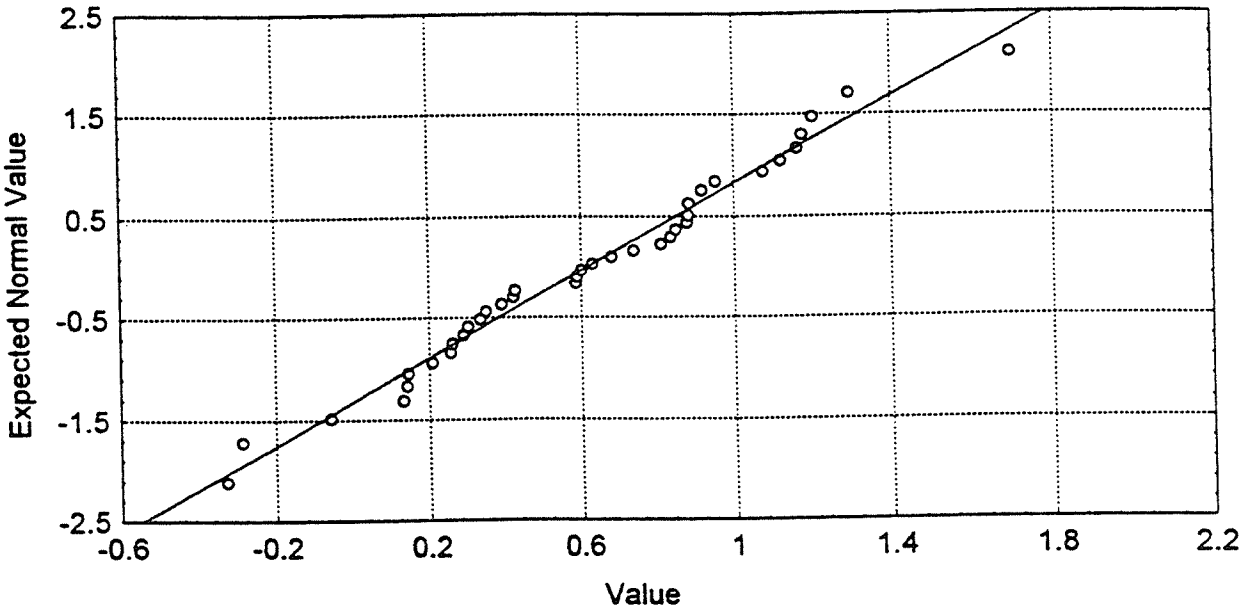

Figure 37

Distribution of (ln) U-238 Soil Activity Concentrations
K-S d=.08683, p> .20; Lilliefors p> .20
Shapiro-Wilk W=.98186, p<.8491

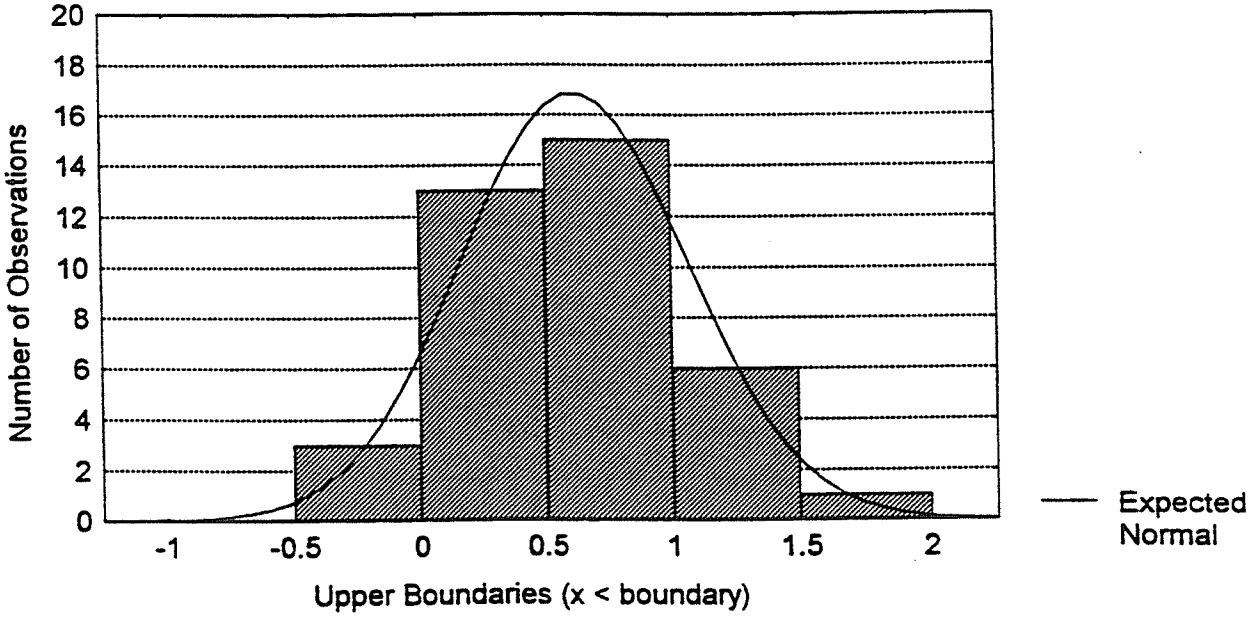

Figure 38

Distribution of Trimmed U-238 Soil Activity Concentrations
K-S d=.13860, p> .20; Lilliefors p<.10
Shapiro-Wilk W=.94862, p<.1173

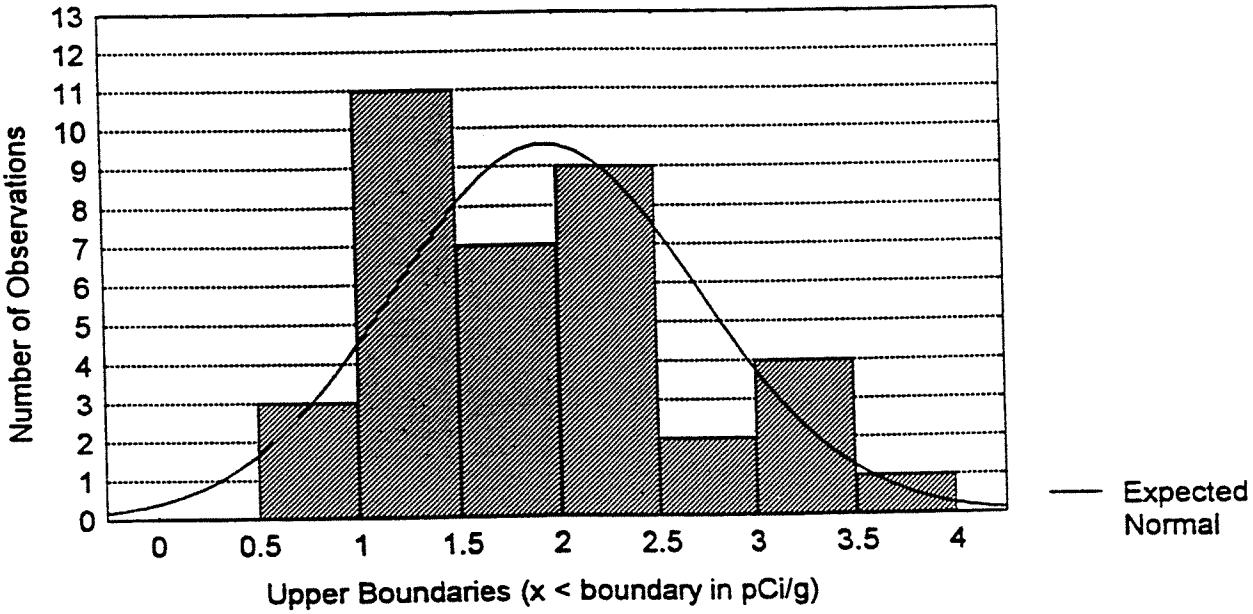

Figure 39

Distribution of Trimmed U-238 Soil Activity Concentrations
Kolmogorov-Smirnov d = .0765388, p = n.s.
Chi-Square: 1.697302, df = 2, p = .4280015

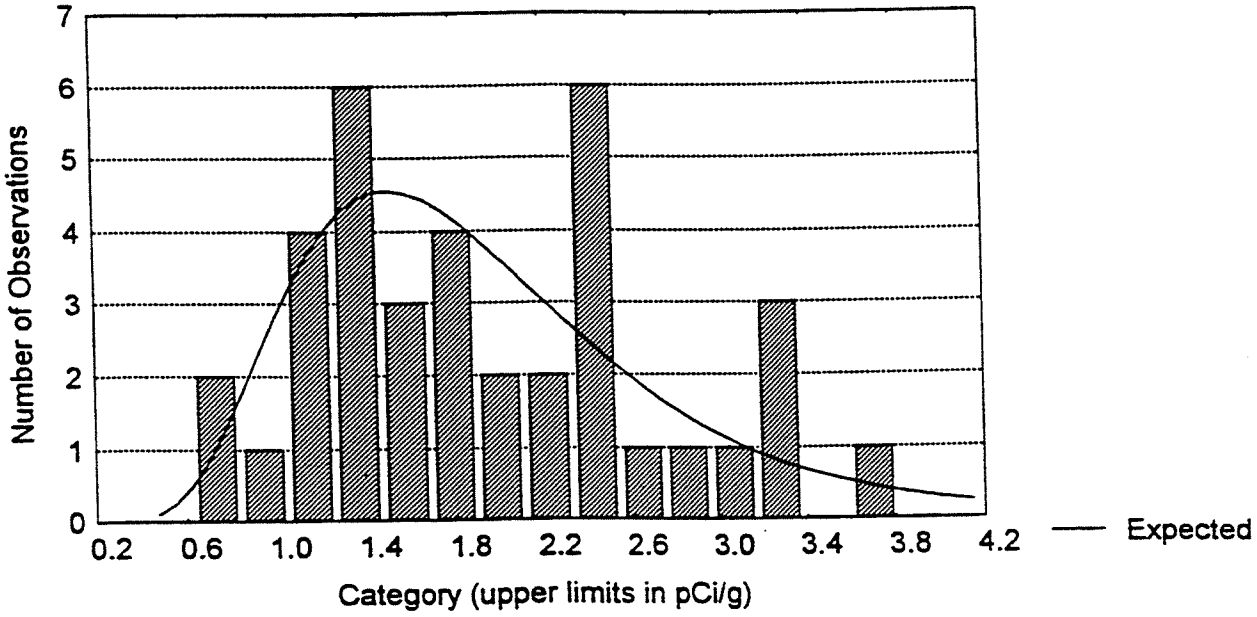

Figure 40

Spatial Distribution of Th-232 Soil Activity Concentrations
in the Vicinity of Albuquerque, NM

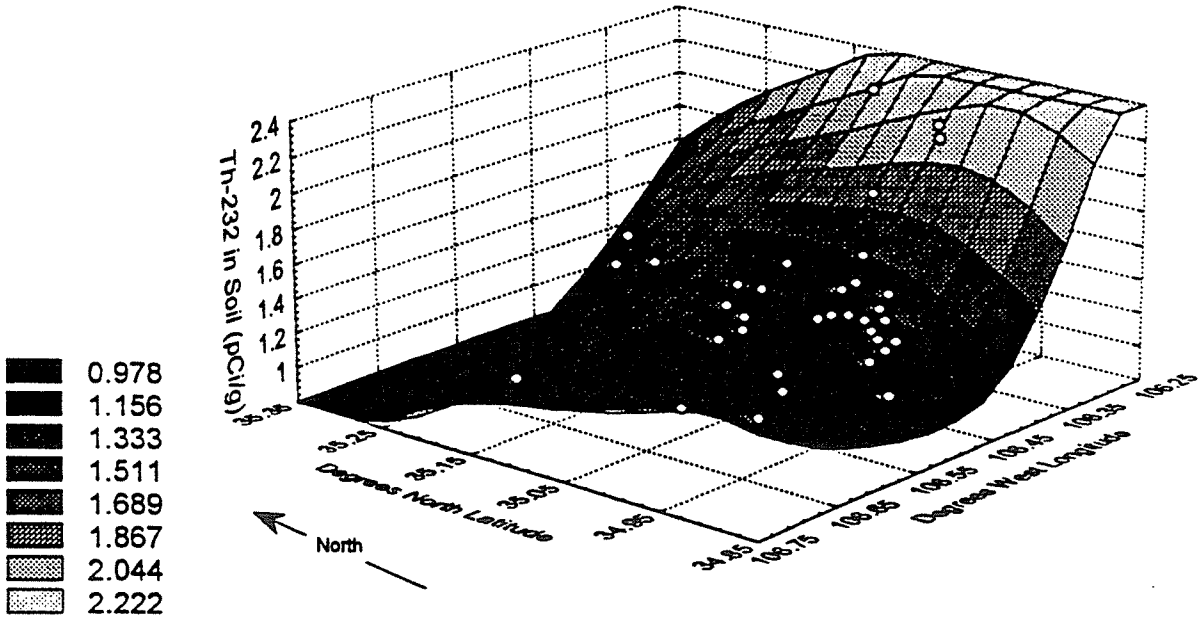

Figure 41

Spatial Distribution of Th-232 Soil Activity Concentrations
in the Vicinity of Albuquerque, NM

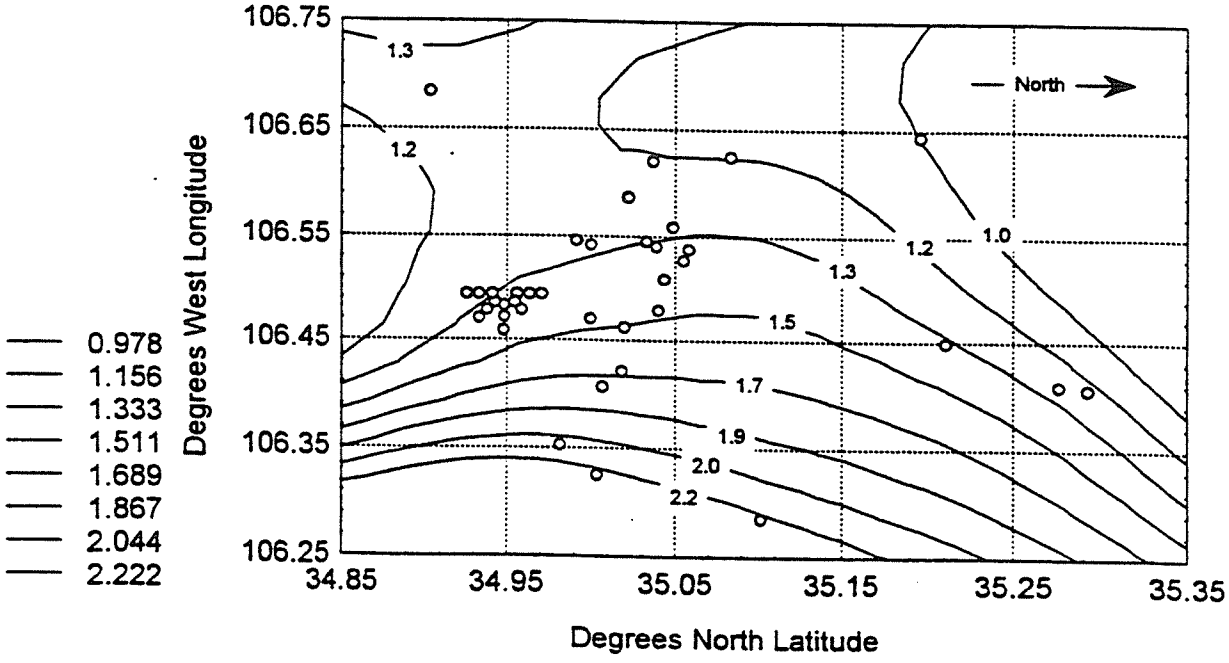

the region that includes Sandia Peak and north slope of the Sandia Range. Those values fall within the inner basin range of about 1.0 to 1.5 pCi/g. Concentration values in the western Manzano slope canyons and eastern slope ranged from less than 1.7 to over 2.2 pCi/g. Positive skew is again apparent in the bow-and-whisker diagrams, relieved by log-transformation of the data (Figures 42 and 43). Testing did not identify any outlying point up to the highest risk level, 10%, investigated. However, as seen in Figure 44, log-transformed data demonstrated greater oscillation around a fitted normal line than was apparent for any previously examined nuclide. This scatter, combined with the appearance of the lognormally fitted histogram of untransformed data in Figure 45 again suggested that at least two separate soil population distributions may have been sampled in the study, one centered around a mean of about 1.4 pCi/g, and another whose mean equaled or exceeded about 2.3 pCi/g. The higher values are largely limited to the Central Highlands.

3.1.5 ^{40}K in Soils

The spatial distribution of ^{40}K soil activity concentrations was very dissimilar to the regional patterns previously illustrated. The highest values were observed in soils of the mid-longitudes of the study area, as seen in Figures 46 and 47. This region is that part of the piedmont-fan slope nearest the mountain escarpments to the west, and the region lying at the northern foot of the Sandias. Values in this region ranged from about 14.3 to 17.6 pCi/g. Values in the Central Highlands portion of the region range from about 13.2 to 15.4 pCi/g, while values in the bulk of the valley and west mesa regions range from 9.9 to 13.2 pCi/g.

The statistical distribution, as apparent in the box-and whisker diagrams (Figures 48 and 49) and probability plots (Figures 50 and 51), suggests little deviation from normalcy. Distributions modelled as normal and lognormal fittings also suggest multimodalities (Figures 52 and 53), although this was not readily apparent in numerical analysis. Based on appearances of the histograms, at least two distinct populations may have been sampled, one centered at a mean of about 14 pCi/g, and another whose mean falls nearer 19 pCi/g. However, tests of outliers yielded no extrema that could be trimmed from the data set at the highest (10%) risk level evaluated.

Figure 42

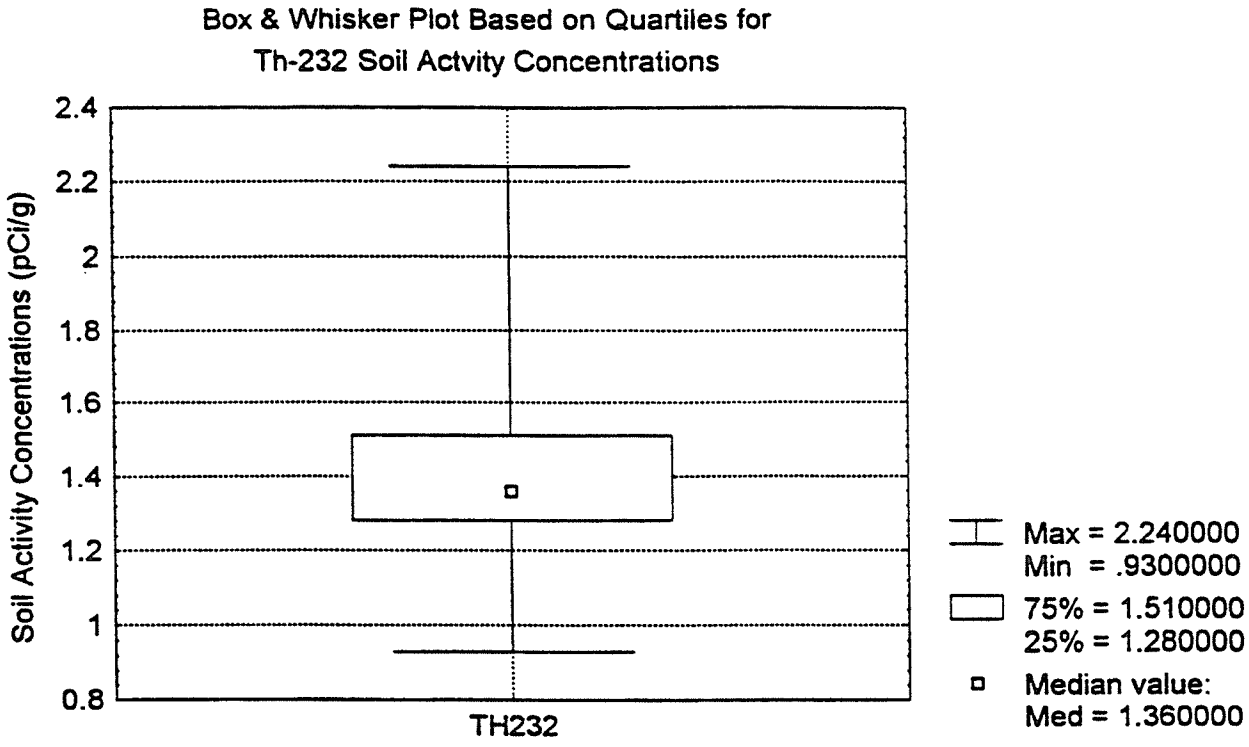

Figure 43

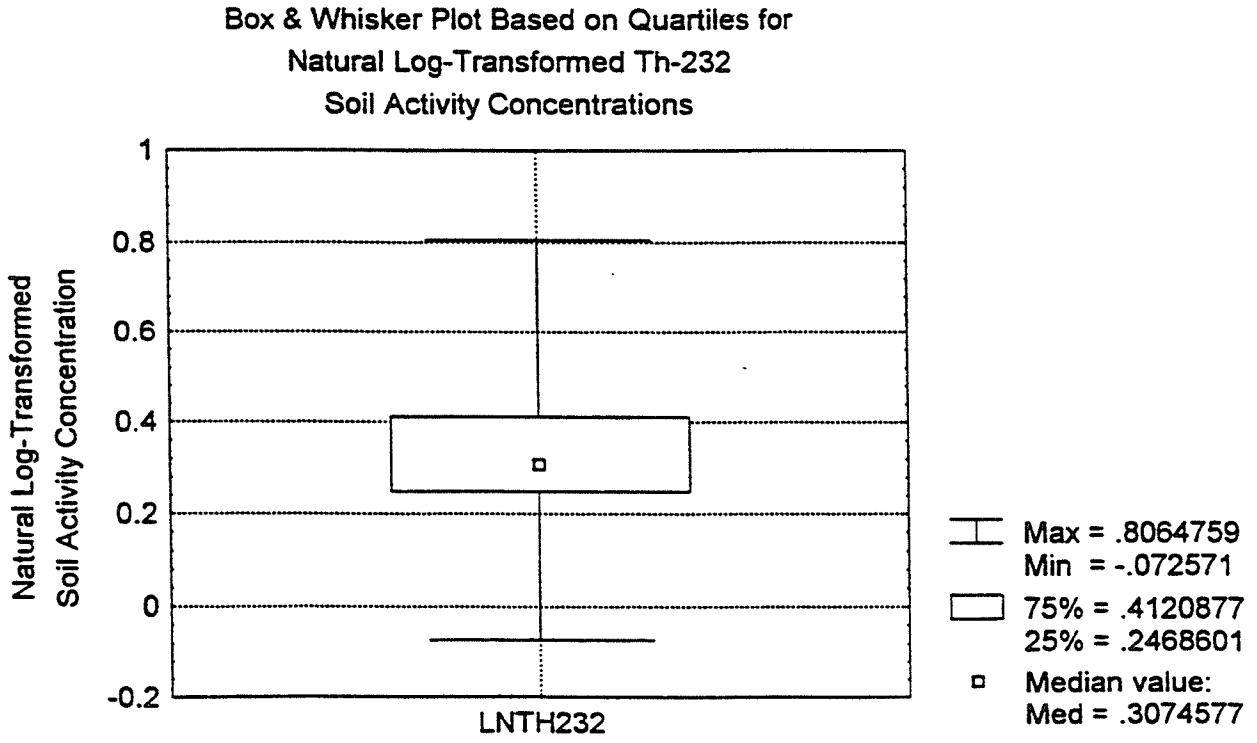

Figure 44

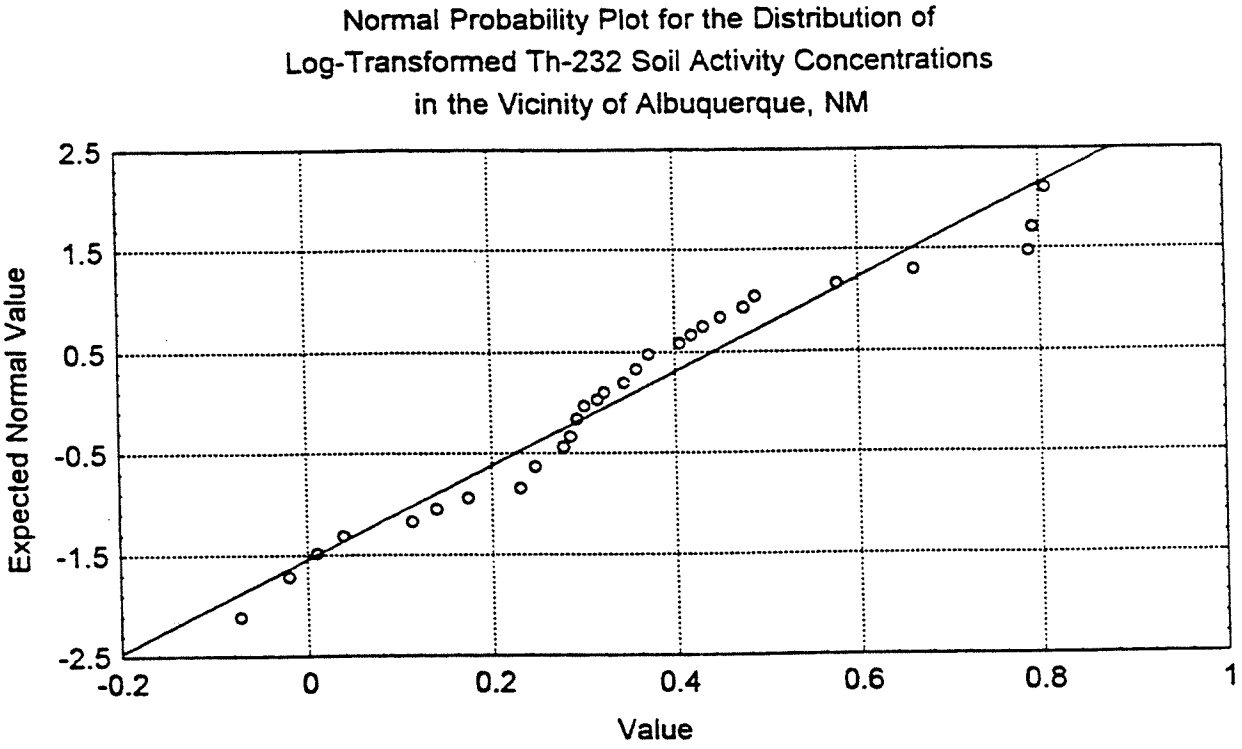

Figure 45

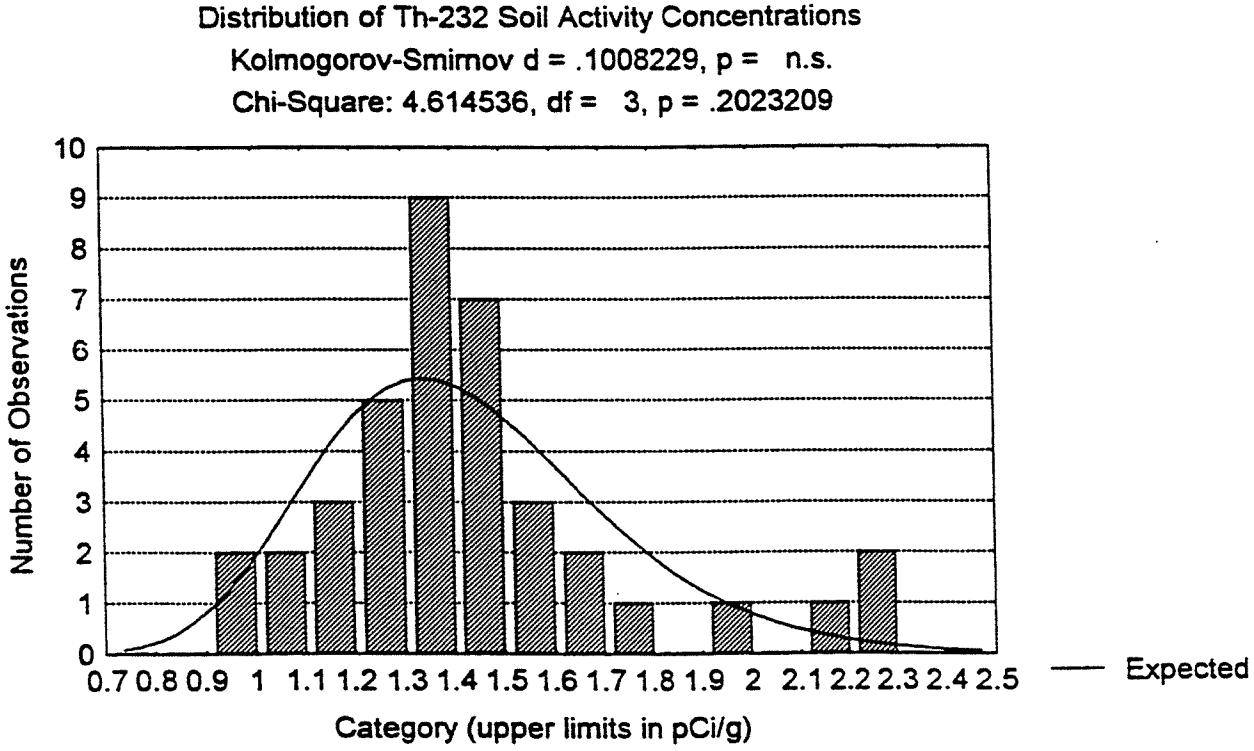

Figure 46

Spatial Distribution of K-40 Soil Activity Concentrations
in the Vicinity of Albuquerque, NM

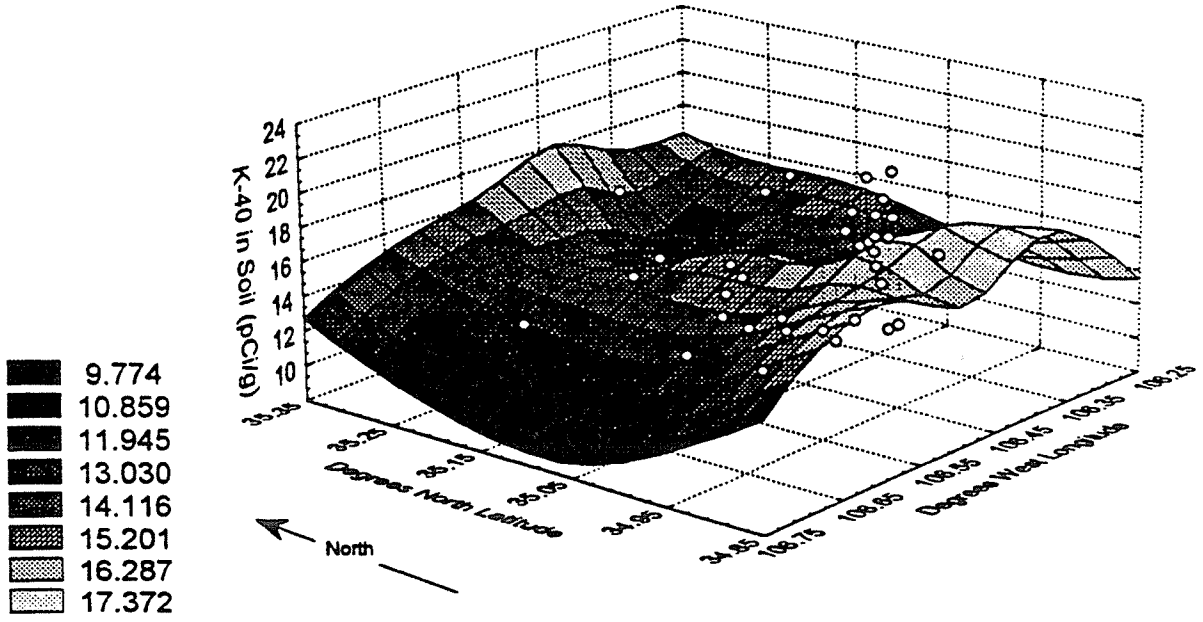

Figure 47

Spatial Distribution of K-40 Soil Activity Concentrations
in the Vicinity of Albuquerque, NM

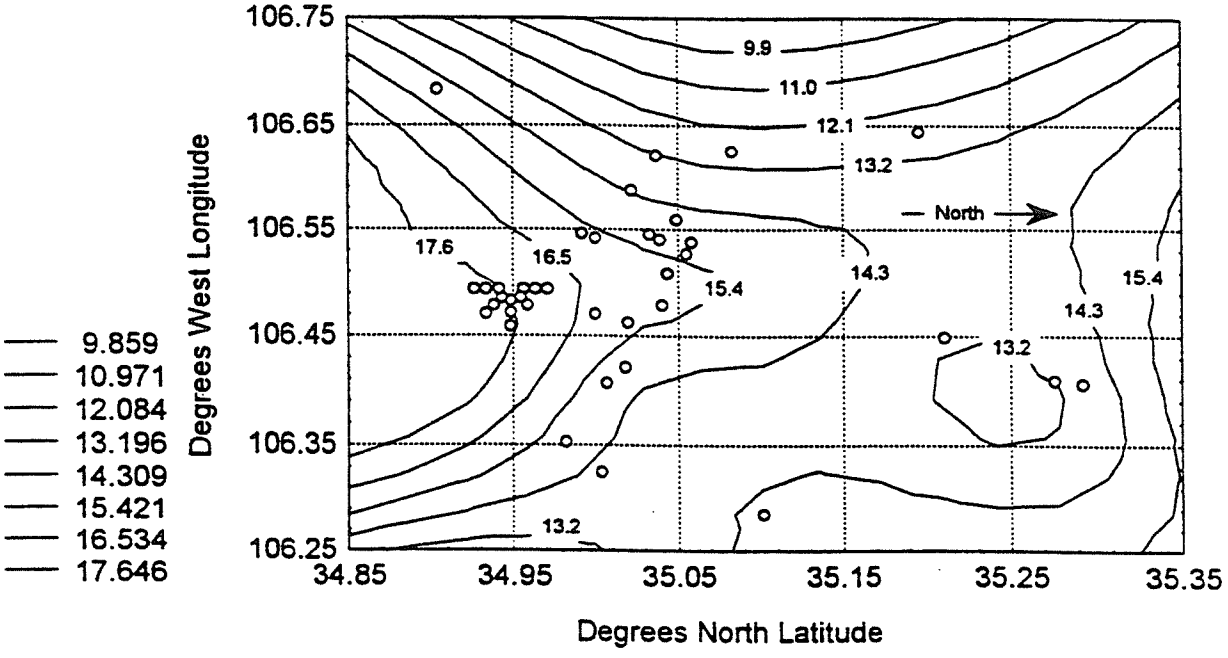

Figure 48

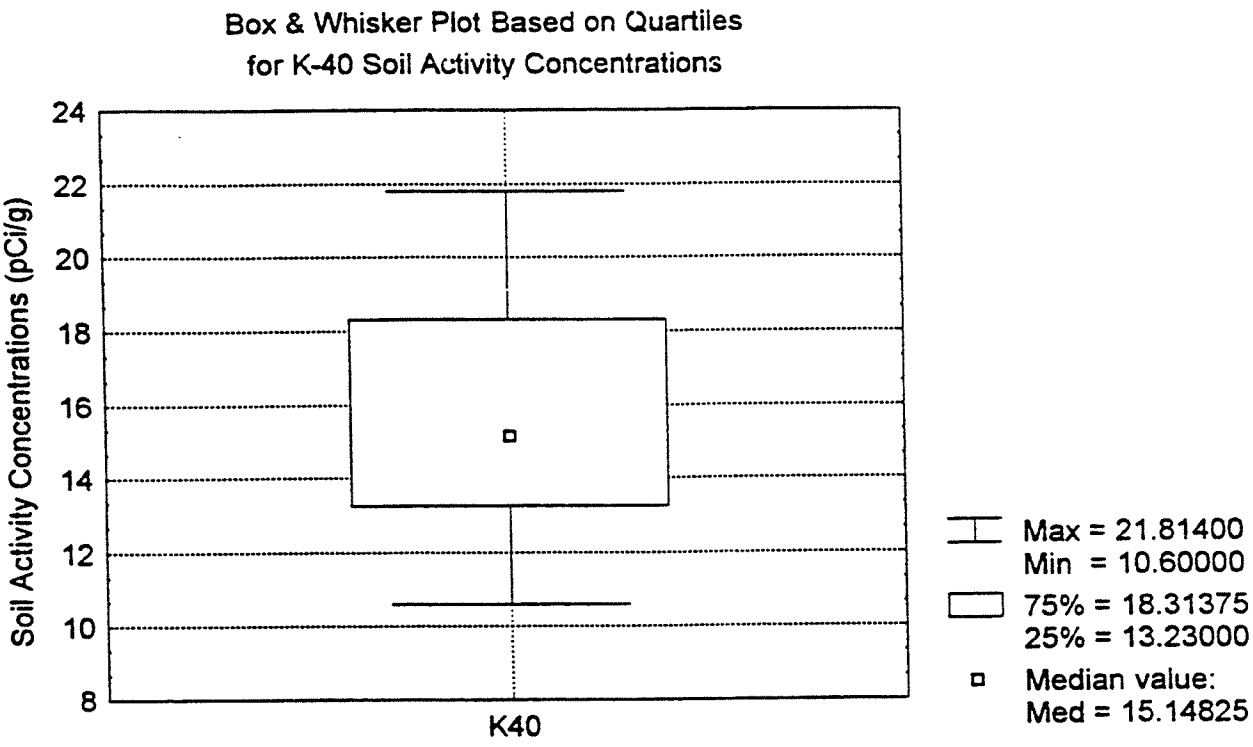

Figure 49

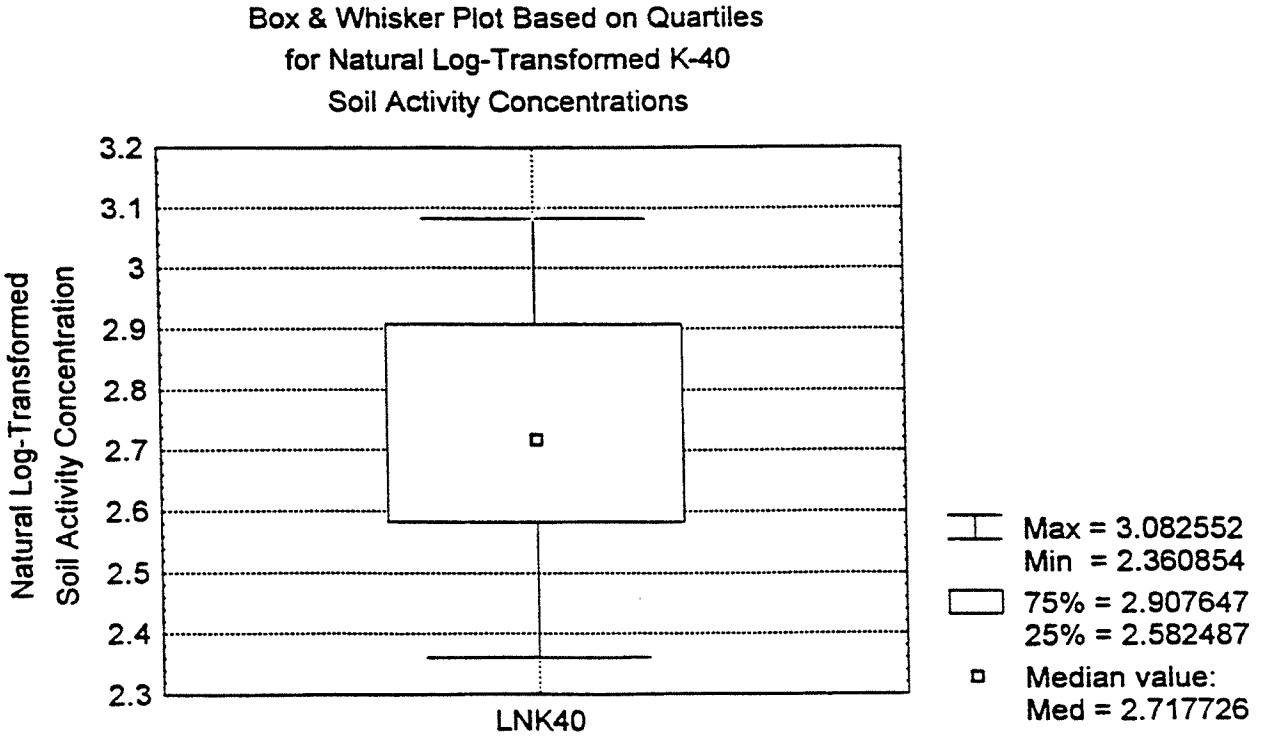

Figure 50

Normal Probability Plot for the Distribution of
K-40 Soil Activity Concentrations in the
Vicinity of Albuquerque, NM

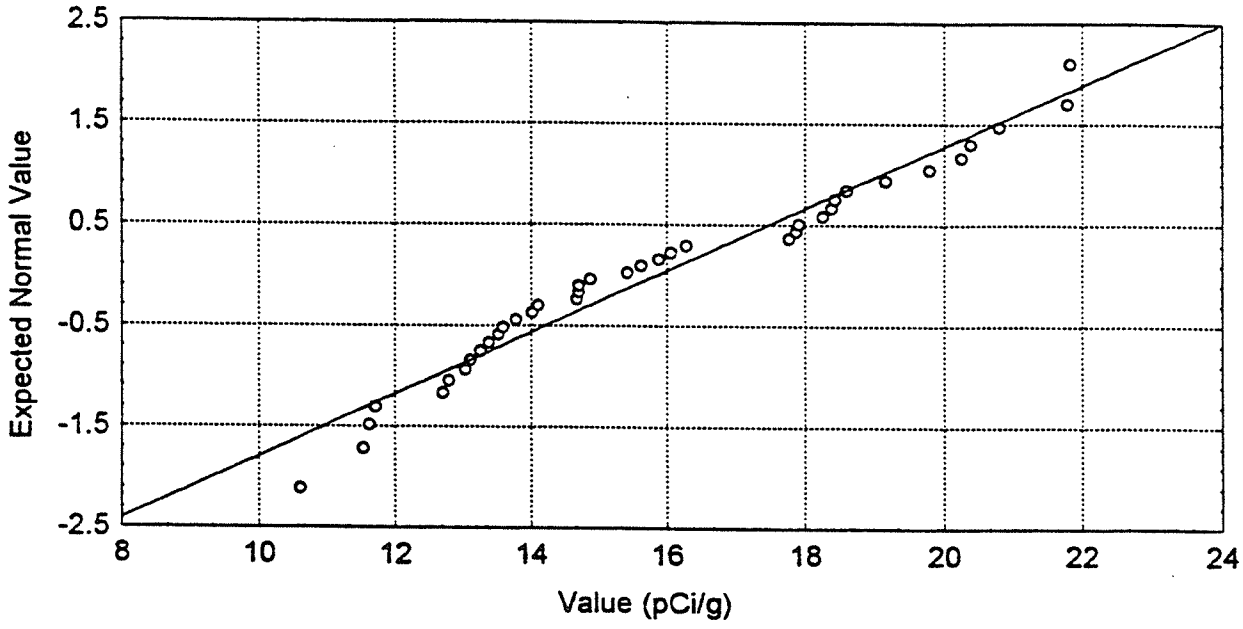

Figure 51

Normal Probability Plot for the Distribution of
Log-Transformed K-40 Soil Activity Concentrations
in the Vicinity of Albuquerque, NM

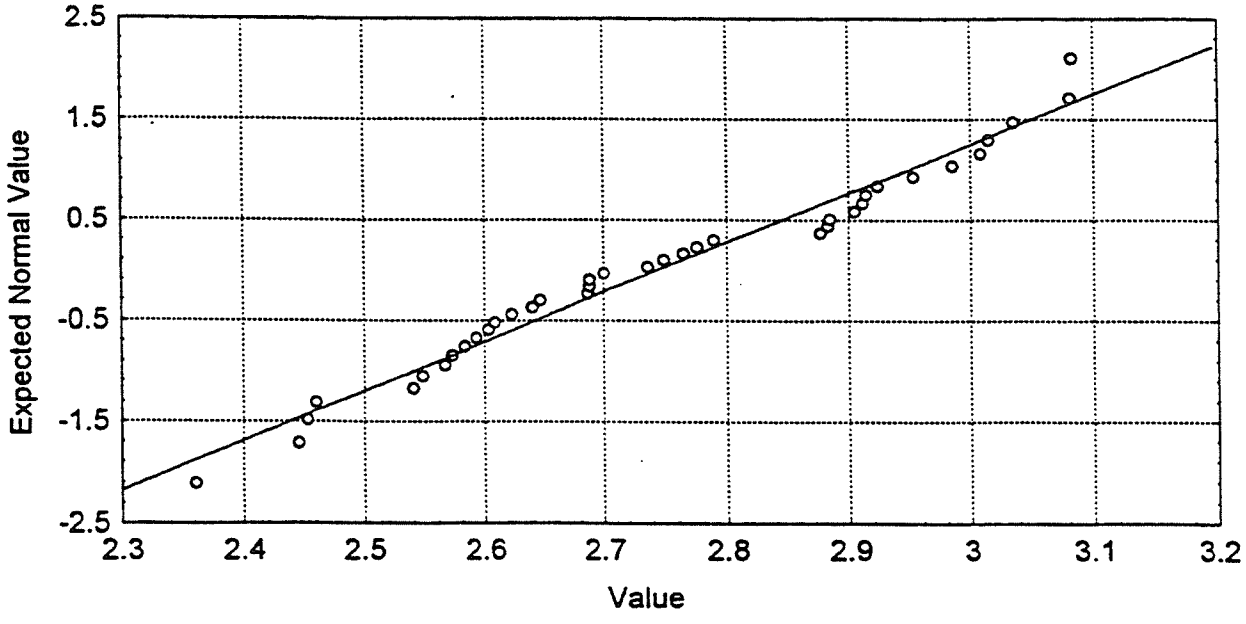

Figure 52

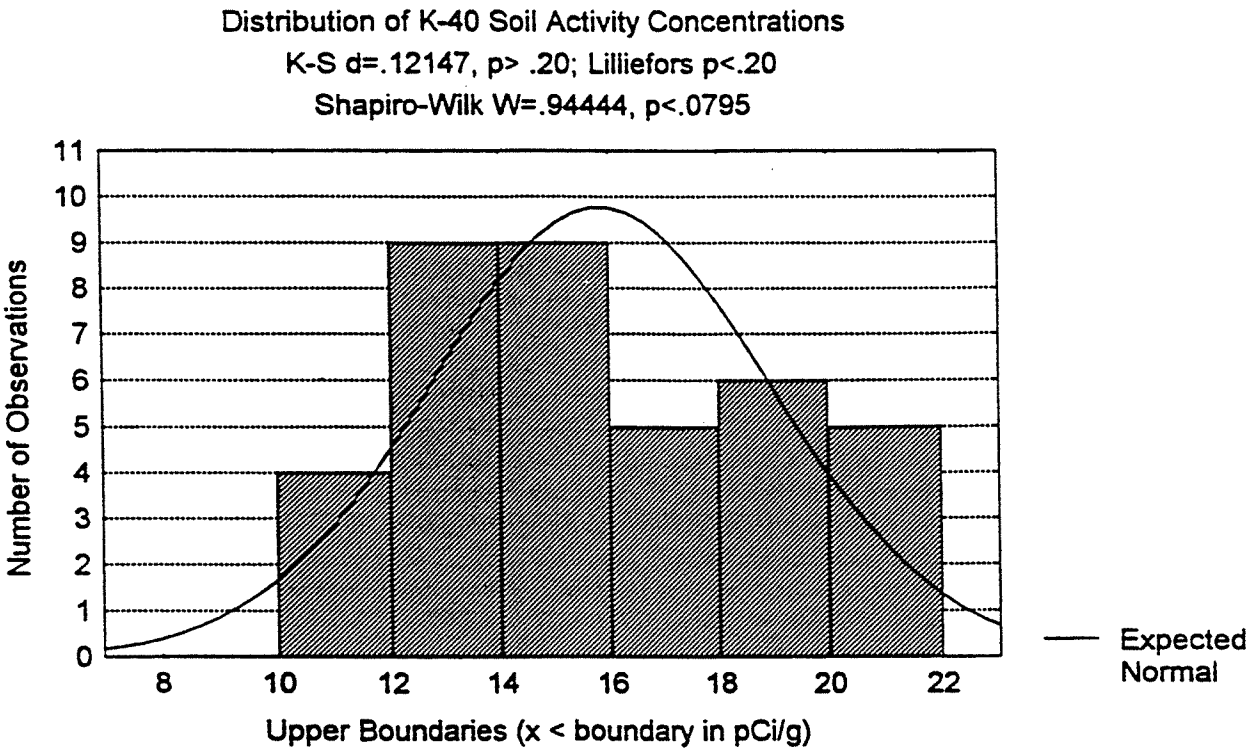

Figure 53

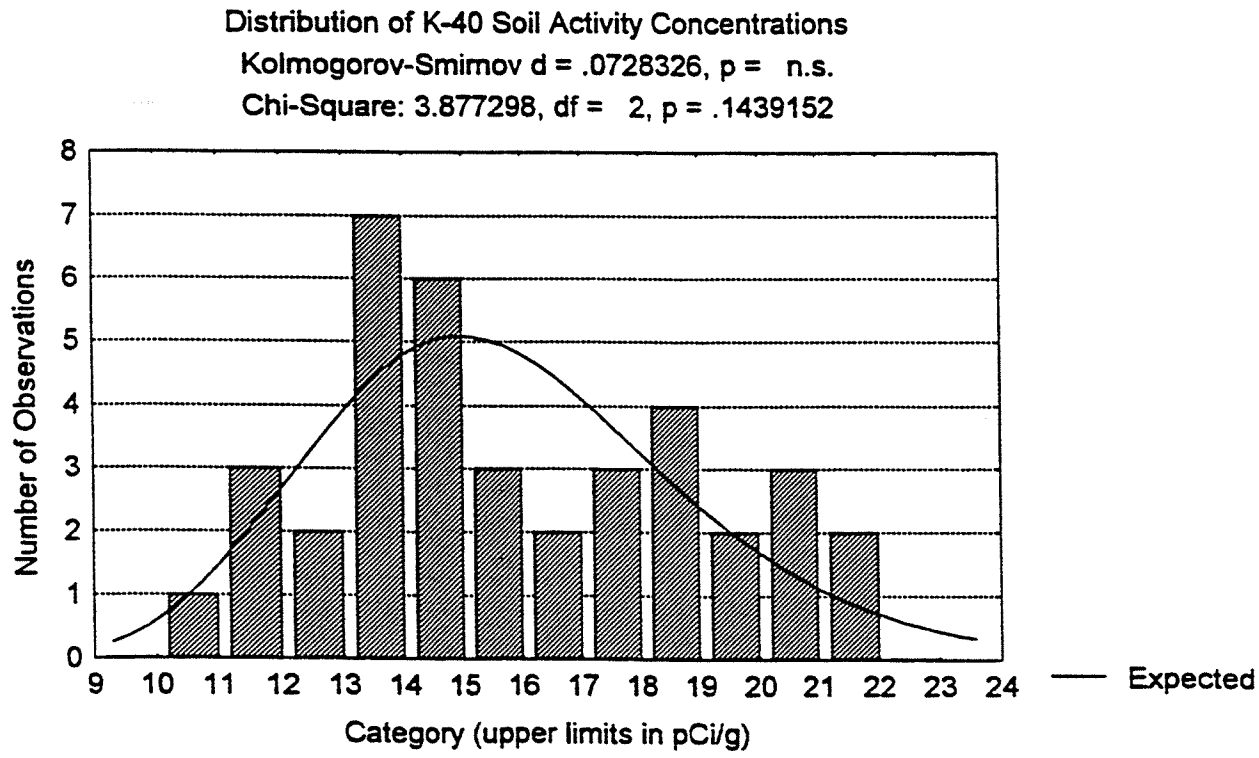

3.1.6 ^{137}Cs in Soils

Special attention was devoted in the study to the description and evaluation of environmentally distributed ^{137}Cs. That nuclide represented the only specific indicator of anthropogenic radiation impacts evaluated in the study. The spatial distribution of ^{137}Cs soil activity concentrations displayed regional patterns distinct from all of the preceding cases. The ^{137}Cs patterns suggested the influence of altitude control, as may be inferred from Figures 54 and 55. The regional study maximum was found at the sampling point of maximum elevation, Sandia Peak and most higher concentration values were also associated with higher elevations, largely in the eastern portion of the study region. To investigate the apparent trend, ^{137}Cs soil activity concentrations was plotted as a function of altitude in Figure 56. The plot displayed a increasing relationship within the scatter, analyzed by piecewise linear regression with quasi-newtonian parametric estimation using a least squares loss function. That analysis yielded a correlation coefficient of 93.7% and accounted for 87.7% of the variance in concentration values based on the effects of altitude alone.

An environmental parameter related to space and altitude was also estimated in the study: soil moisture calculated as weight (mass) fraction of the soil. Analysis of ^{137}Cs soil activity concentrations as a function of soil moisture was performed as above and depicted in Figure 57. The generally increasing relationship suggested by the graph and subsequent analysis was not as close as that using altitude. That analysis yielded a correlation coefficient of 91.0% and accounted for 82.8% of variance. It thus appeared that altitude and environmental conditions leading to higher soil moisture both exerted some degree of control over the regional distributions of the anthropogenic radionuclide in soil. Direct graphical inference between the two soil activity concentration values plotted at the approximate latitude of 35.2° N controlled the appearance of the distribution in Figure 55 in a way that is probably artificial. Independent soil data for a location in northern Albuquerque that falls within this portion of the region indicated that ^{137}Cs soil concentrations on the order of $\leq$ 0.2 pCi/g have been found consistently over time (128,129,130). This suggests that the iso-concentration contours descending along the Sandia escarpment may indeed be much steeper, possibly reflecting the steep descent in altitude.

The internal distribution of the data also demonstrates the most distinctive trends in the study. Outlier tests were performed as described above with the log-transformed data

Figure 54

Spatial Distribution of Cs-137 Soil Activity Concentrations
in the Vicinity of Albuquerque, NM

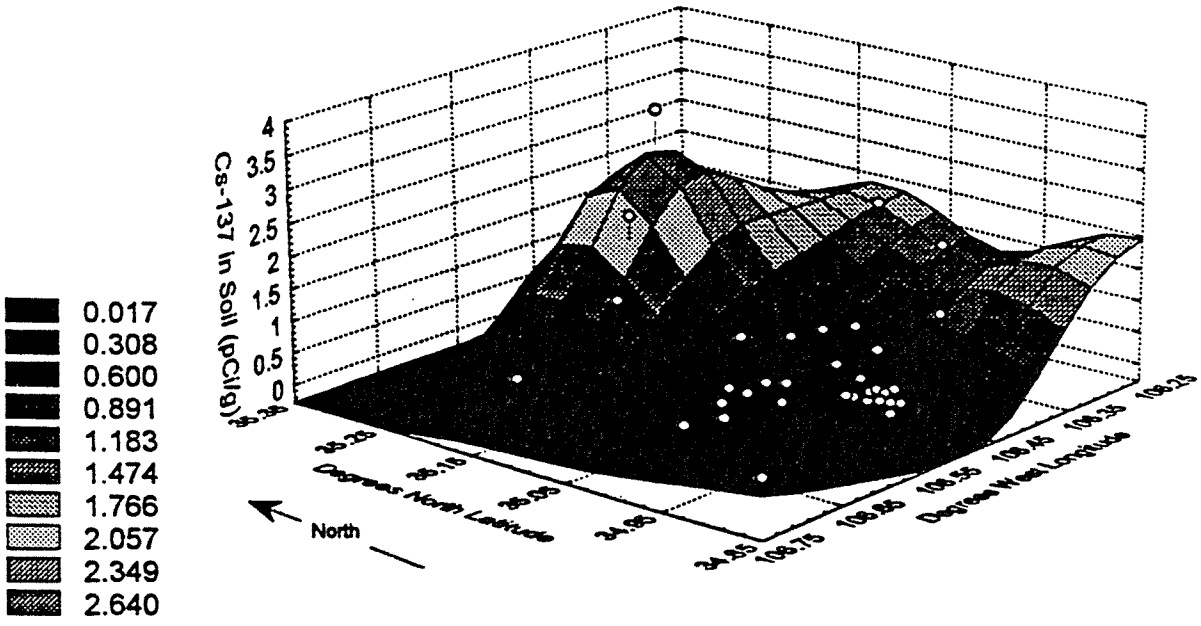

Figure 55

Spatial Distribution of Cs-137 Soil Activity Concentrations
in the Vicinity of Albuquerque, NM

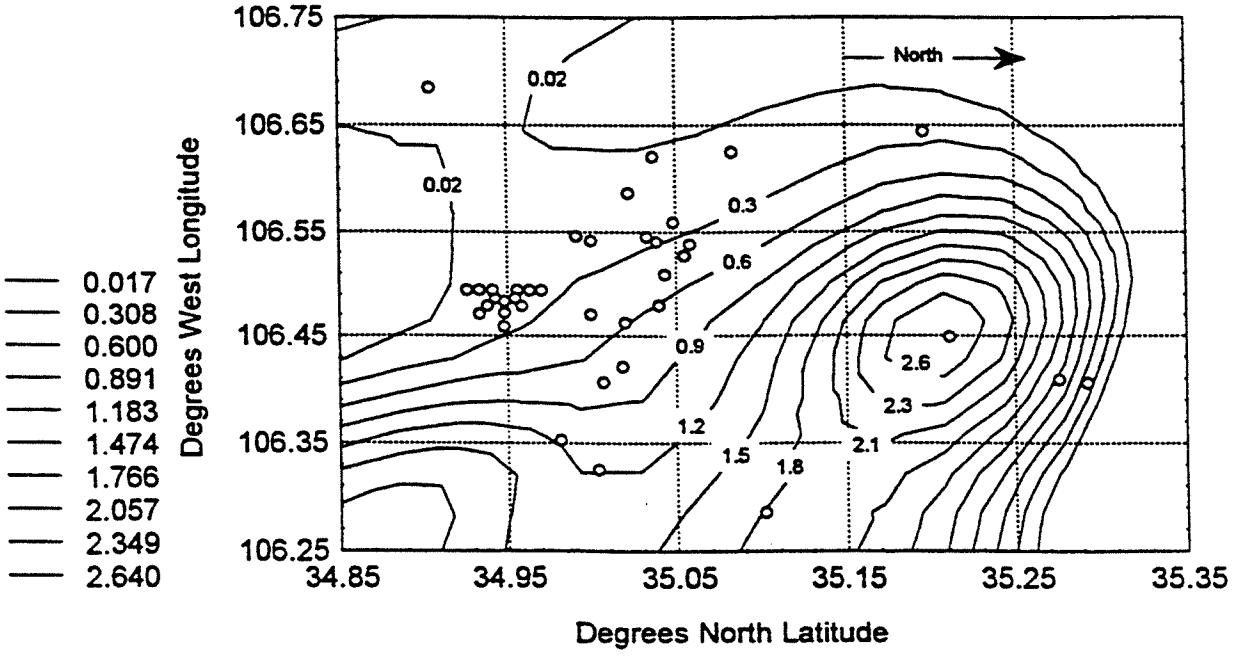

Figure 56

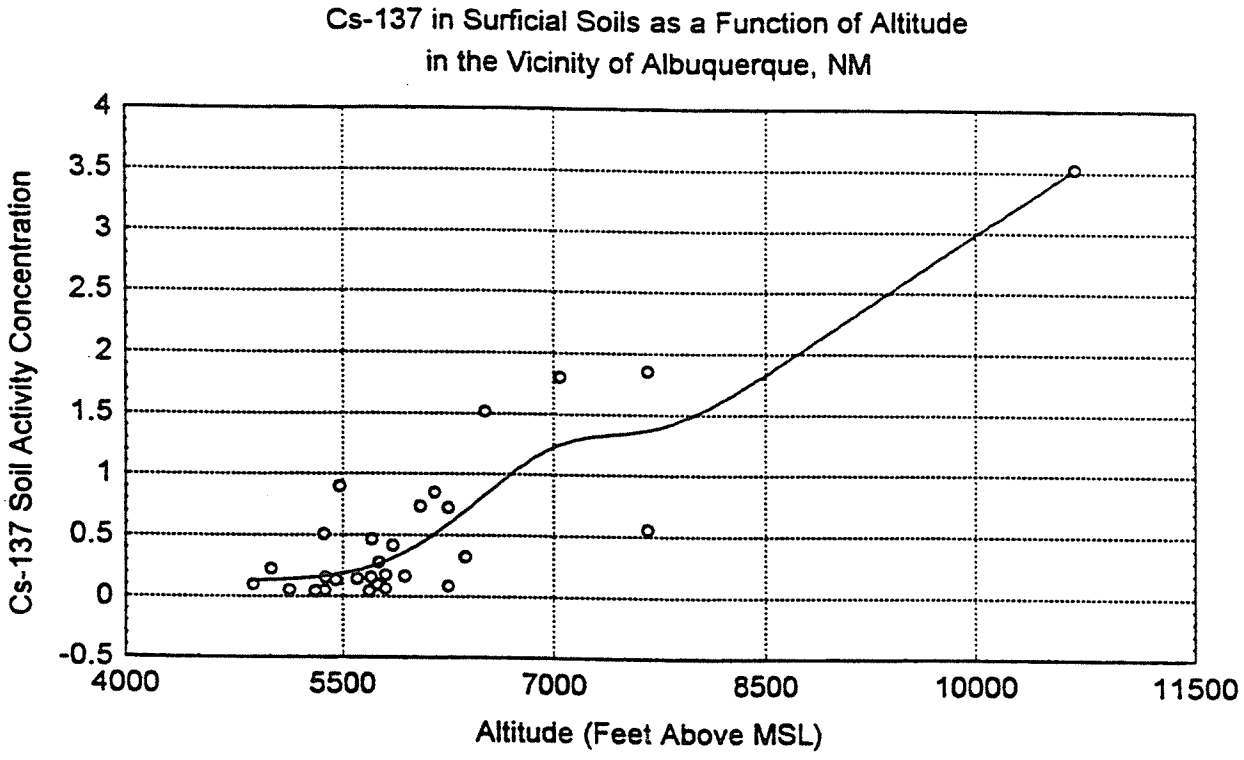

Figure 57

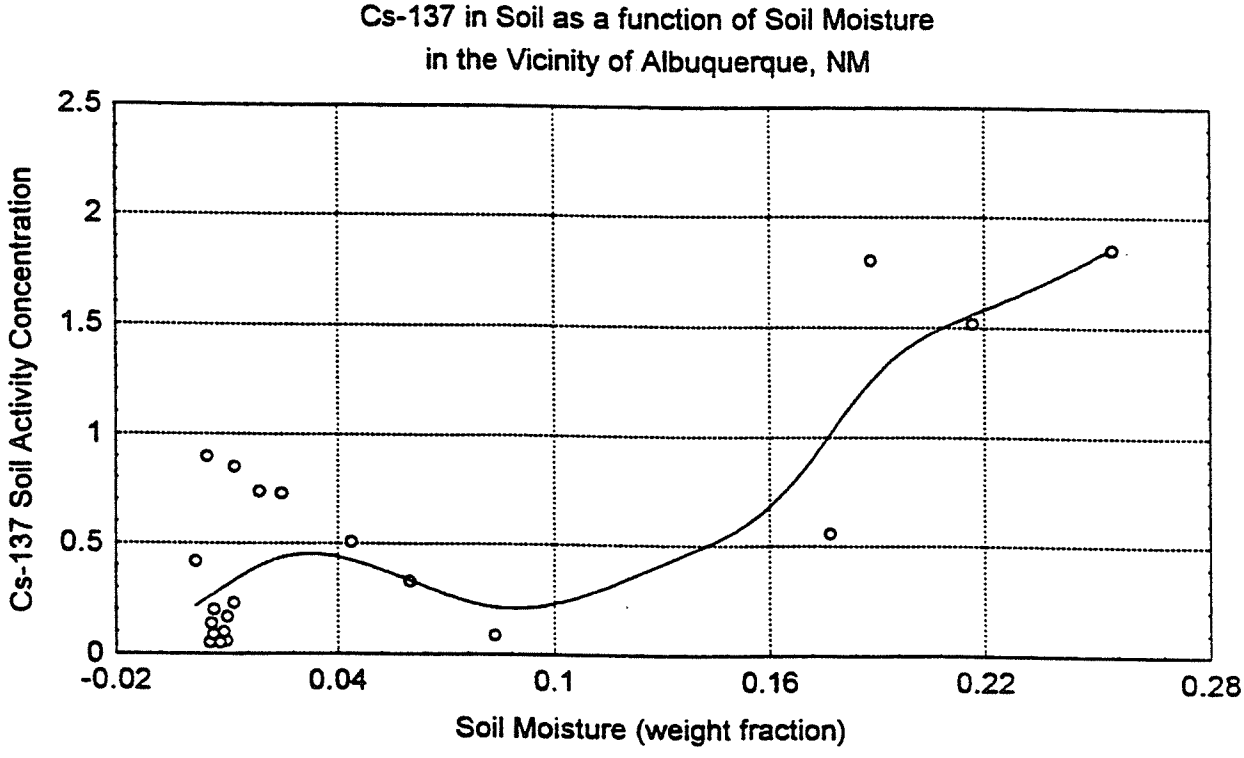

resulting in rejection of four data points, all associated with high sampling altitudes. Outlier and skew effects were readily apparent in Figures 58 and 59, which depict box-and-whisker plots for untrimmed raw and trimmed log-transformed ^{137}Cs soil activity concentrations. The data plots display extreme right skew in distribution; a trend that was significantly modified by a combination of log-transformation and outlier rejection, in this instance at the 0.5% risk level. The complementary probability plots are depicted in Figures 60 and 61. The outliers are apparent, lying beyond the "knee" in the plot of untransformed data. The resultant optimized distributions are apparent as log-transforms in Figure 62 and as raw data in Figure 63.

3.2 *In situ* Exposure Rate Measurement Techniques

The two methodologies employed to make environmental gamma radiation measurements, TLDs and HPIC, have been discussed above. TLDs were deployed in a long-term study with a duration of five calendar quarters, while the HPIC was deployed at any one measurement site for only a brief time.

The quarter-by-quarter results for environmentally deployed TLDs are contained in Tables 9 through 12. The sites are divided arbitrarily into sites on KAFB and sites off KAFB. The latter are described as Albuquerque Vicinity Sites. The quarterly variation for multiple TLDs at each of the sites ranged from 1.8 to 18.9%, expressed as coefficient of variance (COV). Overall, quarterly COVs were less than the 15% variability ascribed by the manufacturer, and precision at the 95% confidence level was within the ANSI recommended tolerance. The annual average COV for sites on KAFB was 9.8%, and for Albuquerque Vicinity Sites was 11.7%. The quarterly and annual variability at most sites did not exceed that value expected on an annual basis due to intrinsic natural variability: 11 mR/y (1.3 μR/h) (123). TLDs sited nearest operating DOE nuclear facilities showed the highest variations in exposure rate over time.

Directional or angular dependence was examined for environmental TLD deployment in an experiment described in Section 2.3.1, above. The site selected for this experiment was TLD Station 18, Four Hills: KAFB Well 11. Conversion of TLD response to exposure rate was accomplished using the five quarter average calibration values inferred from Figure 11. It was expected that solar fading would be maximal in south oriented and west oriented TLDs. The greater solar effects of southern exposure should be intuitive, but the greater solar fading for west directed TLDs may not be as readily apparent. The latter results from the more intense daily insolation

Figure 58

Box & Whisker Plot Based on Quartiles for
Cs-137 Soil Activity Concentrations

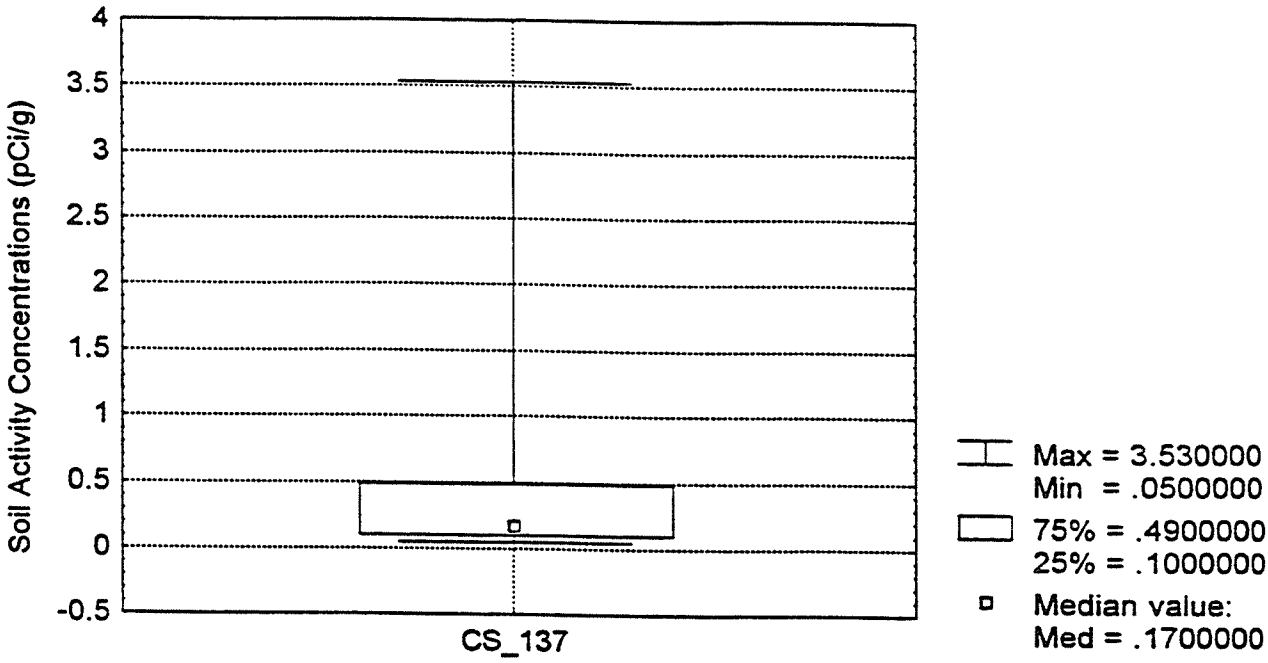

Figure 59

Box & Whisker Plot Based on Quartiles
for Trimmed Log-Transformed Cs-137
Soil Activity Concentrations

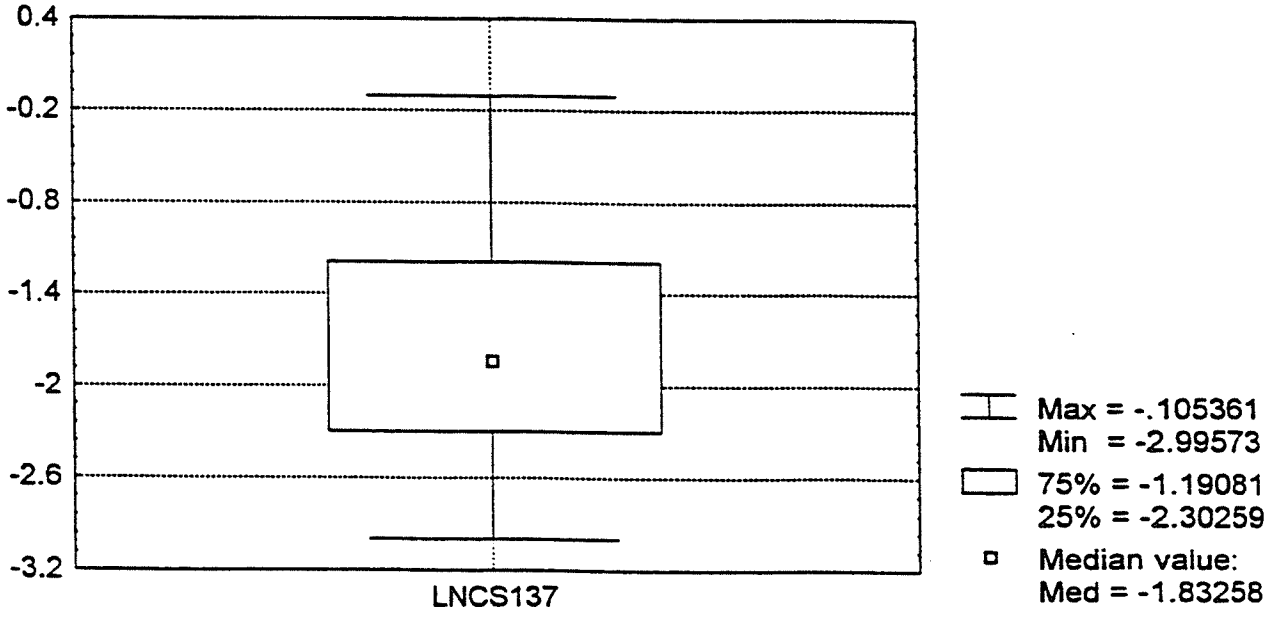

Figure 60

Normal Probability Plot for the Distribution of
Cs-137 Soil Activity Concentrations in the
Vicinity of Albuquerque, NM

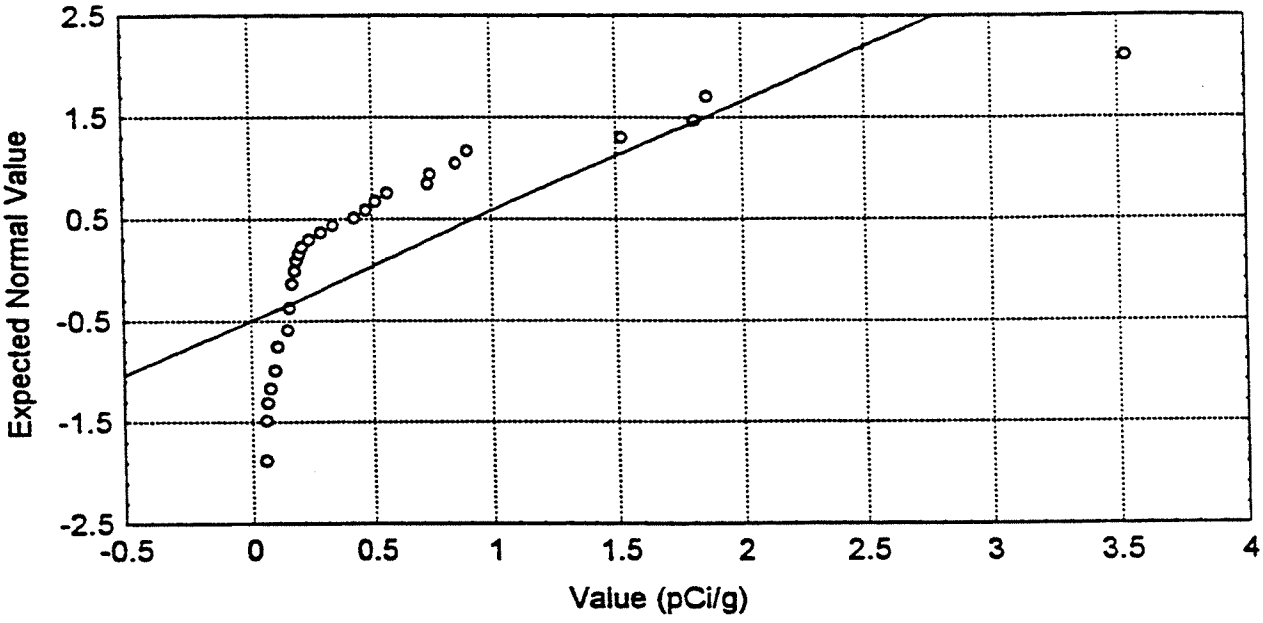

Figure 61

Normal Probability Plot for the Distribution of Trimmed
Log-Transformed Cs-137 Soil Activity Concentrations
in the Vicinity of Albuquerque, NM

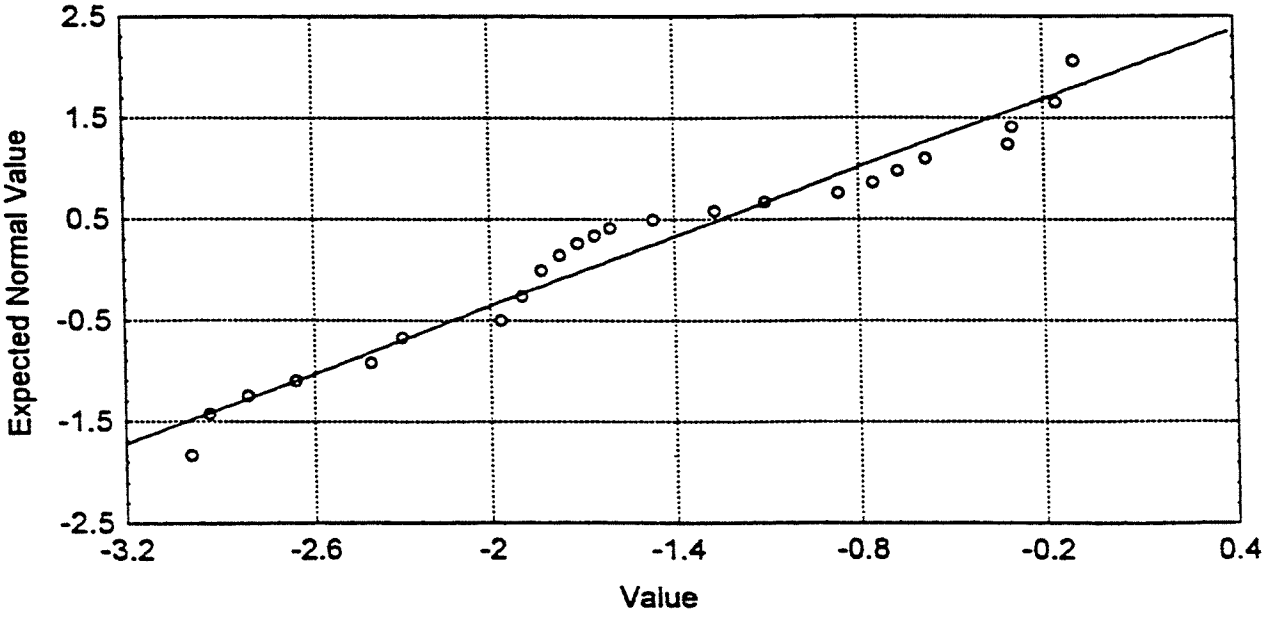

Figure 62

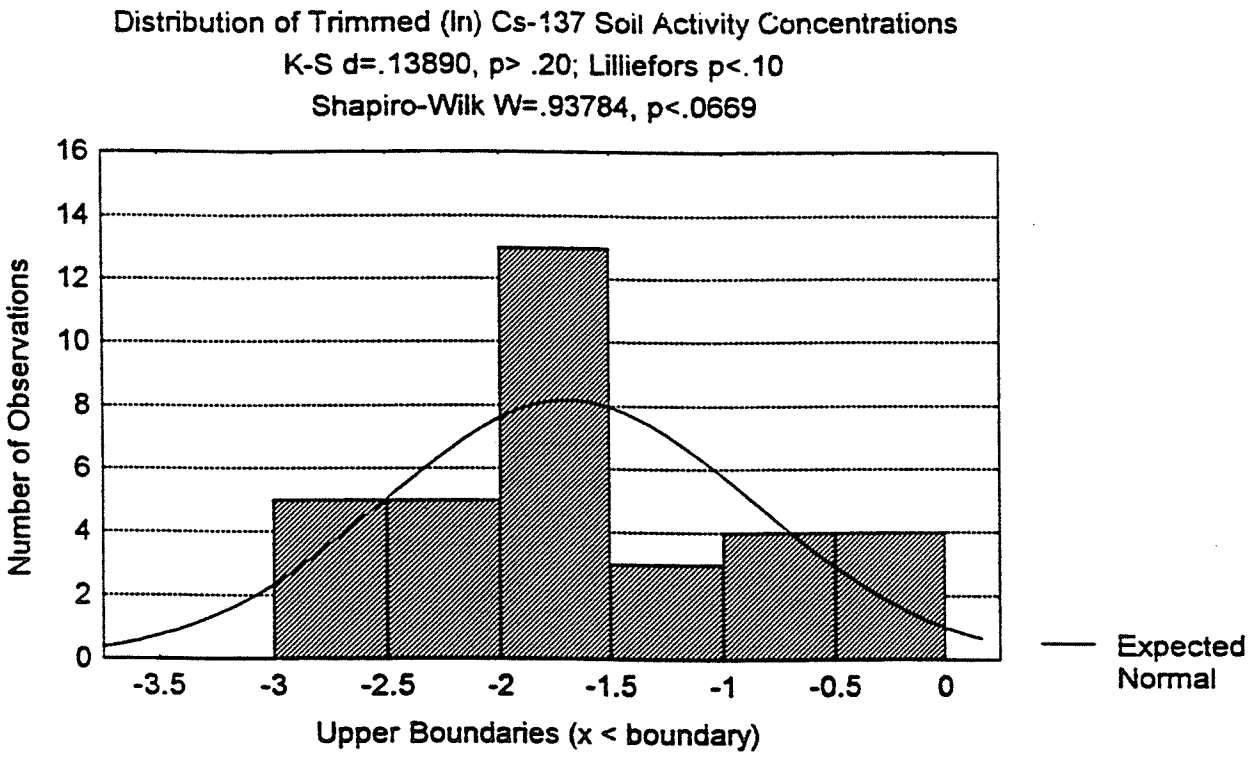

Figure 63

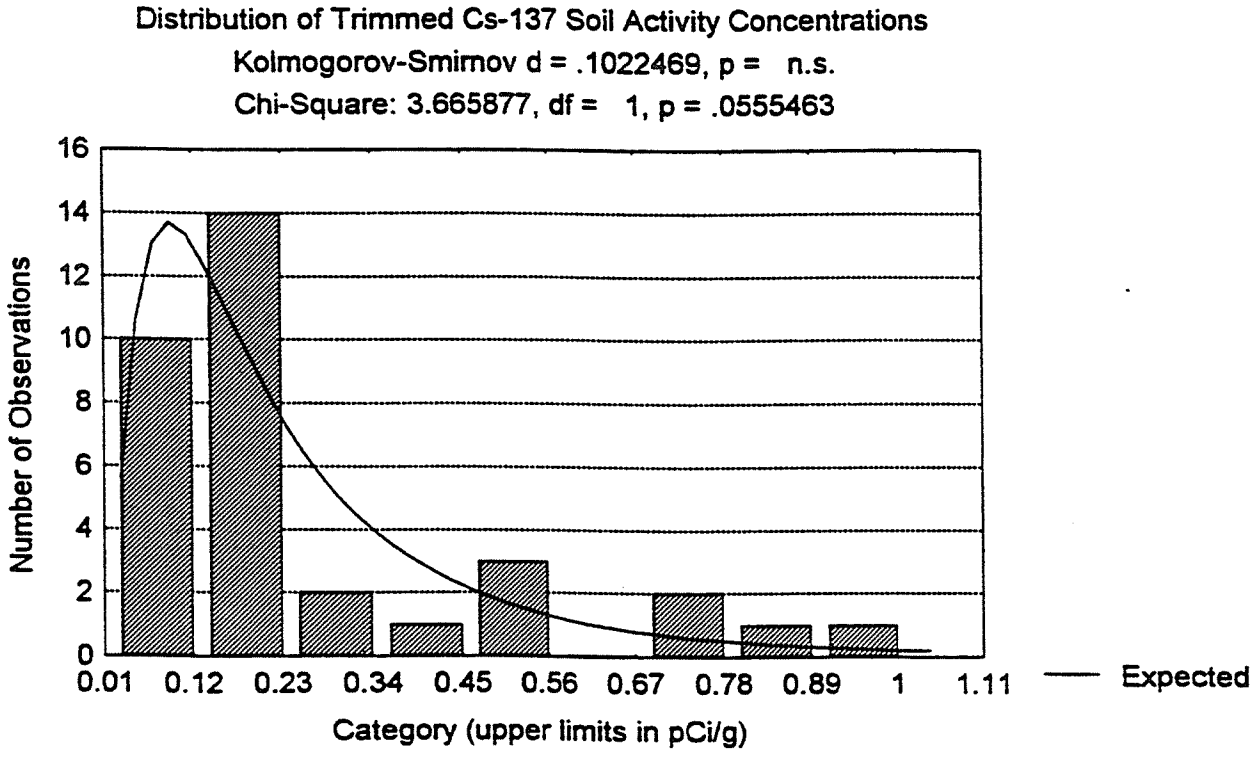

experienced on western New Mexico mountain slopes, discussed above in Environmental Setting. Evaluation of the results suggested very little appreciable difference resulting from TLD orientation. The average exposure rate value over all directed TLDs was 13.6 ± 1.4 μR/h (COV = 10%). Contrary to expectations, the south and west facing TLDs actually indicated slightly higher exposure rate measurements, as is apparent in the box-and whisker plots in Figure 64. The distributions for TLDs in each of the orientations closely fit the normal model, with Shapiro-Wilkinson's W ranging from 0.94 to 0.98 and little positive or negative skew. To preserve and evaluate any inherent variability in the procedure, an outlier test to qualify data points for inclusion was not performed.

The spatial distribution of average annual TLD exposure rates suggests a trend of general increase from west to east, but the representation suffers somewhat from the concentration of sampling points in the central longitudes and central to northern latitudes in the study region (Figures 65 and 66). The spatial distribution of HPIC measurements, which were more areally extensive but represented a shorter time scale of measurement, is depicted in Figures 67 and 68. The surfaces and contours represented in the figures shows a closer relationship to the trends observed in soils measurements and to the effects of elevation. Since cosmic radiation increases as the atmosphere thins with elevation, it was expected that measurement site altitude should exert an appreciable influence. Changes in altitudes may also reflect changes in soil characteristics and radionuclide concentrations.

Both TLD and HPIC exposure rate measurements were analyzed versus altitude as piecewise linear regressions, using quasi-Newtonian parametric estimation. The results are graphically represented in Figures 69 and 70. TLD and HPIC measurements varied weakly as a function of altitude and did not yield a monotonically increasing relationship as might be expected based solely on the increase of cosmic radiation. Altitude alone accounted for no more than 61.7% of observed variance in average TLD rates with a correlation coefficient of 78.6%. Likewise, altitude alone accounted for only 61.3% of the variance in HPIC rates, with a correlation of 78.3%. It is apparent by inspection of the figures that the combination of effects attributable to altitude exerted only limited influence on the overall exposure rate measurements.

The TLD and HPIC techniques employed have been compared cursorily through linear regression analysis, as depicted in Figure 12. The distribution bounds for both techniques may been seen in the box-and-whisker plots depicted in Figures 71 and 72. It was readily apparent that the bulk of HPIC

Figure 64

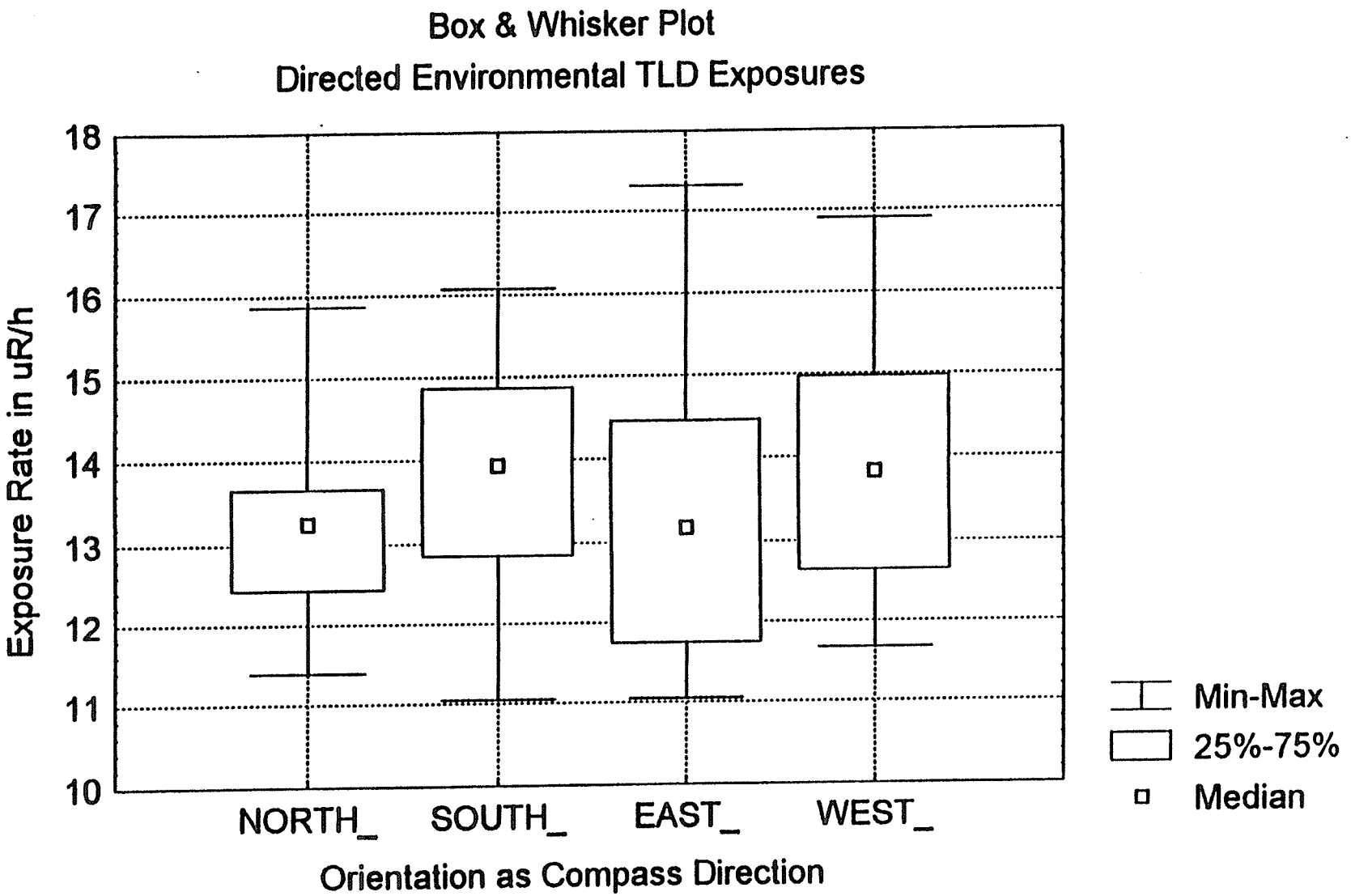
Box & Whisker Plot
Directed Environmental TLD Exposures
Exposure Rate in uR/h
18
17
16
15
14
13
12
11
10
NORTH_
SOUTH_
EAST_
WEST_
Orientation as Compass Direction
Min-Max
25%-75%
Median

Figure 65

Spatial Distribution of Time-Averaged TLD Exposure Rate (uR/h)
Measurements in the Vicinity of Albuquerque, NM

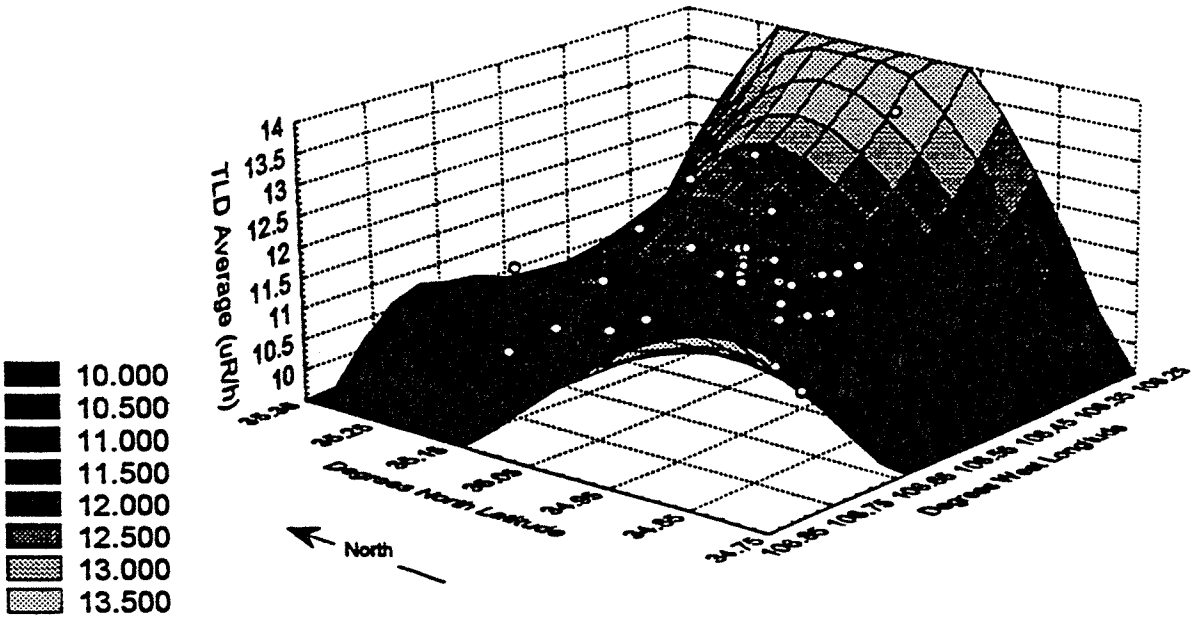

Figure 66

Spatial Distribution of Time-Averaged TLD Exposure Rate (uR/h)
Measurements in the Vicinity of Albuquerque, NM

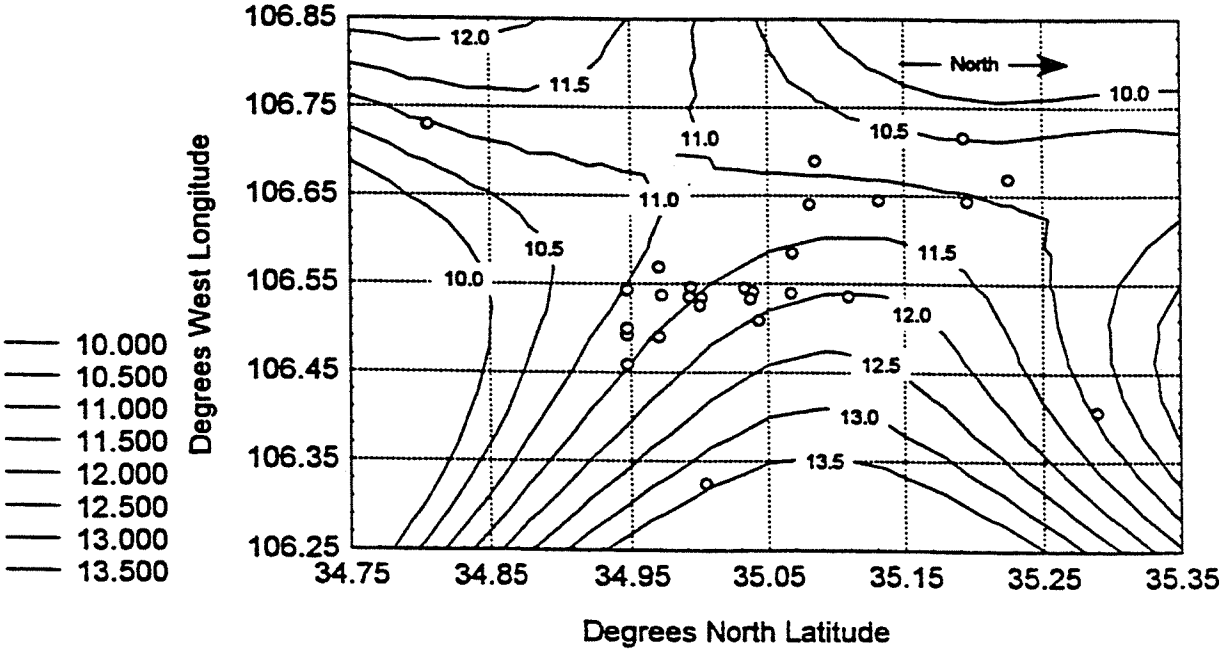

Figure 67

Spatial Distribution of HPIC Exposure Rate
Measurements in the Vicinity of Albuquerque, NM

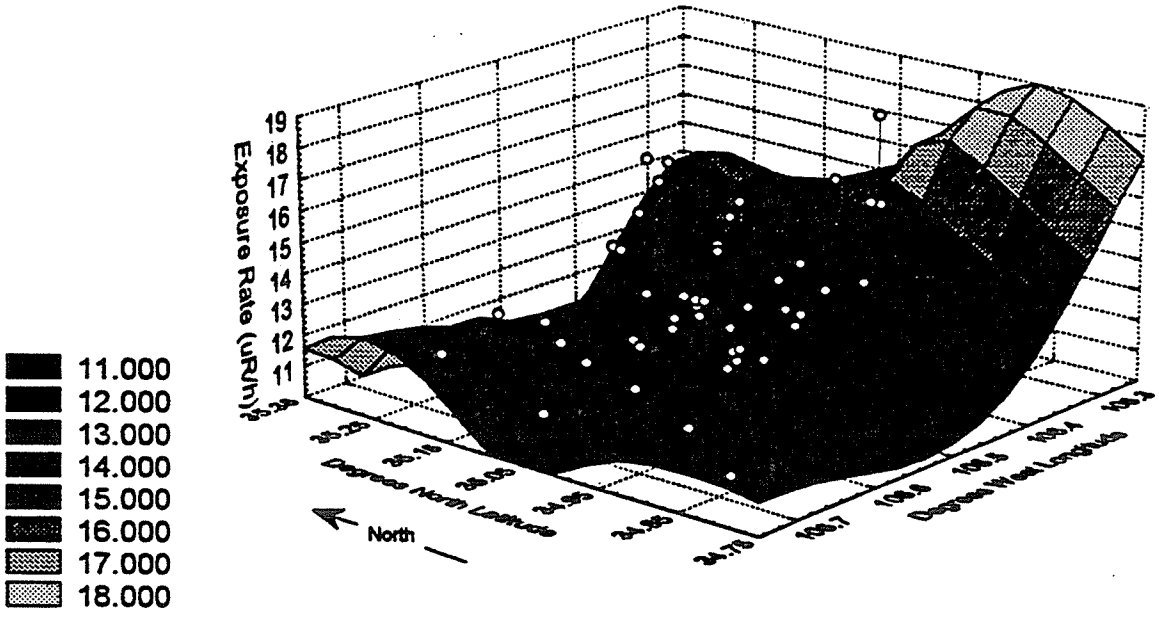

Figure 68

Spatial Distribution of HPIC Exposure Rate
Measurements in the Vicinity of Albuquerque, NM

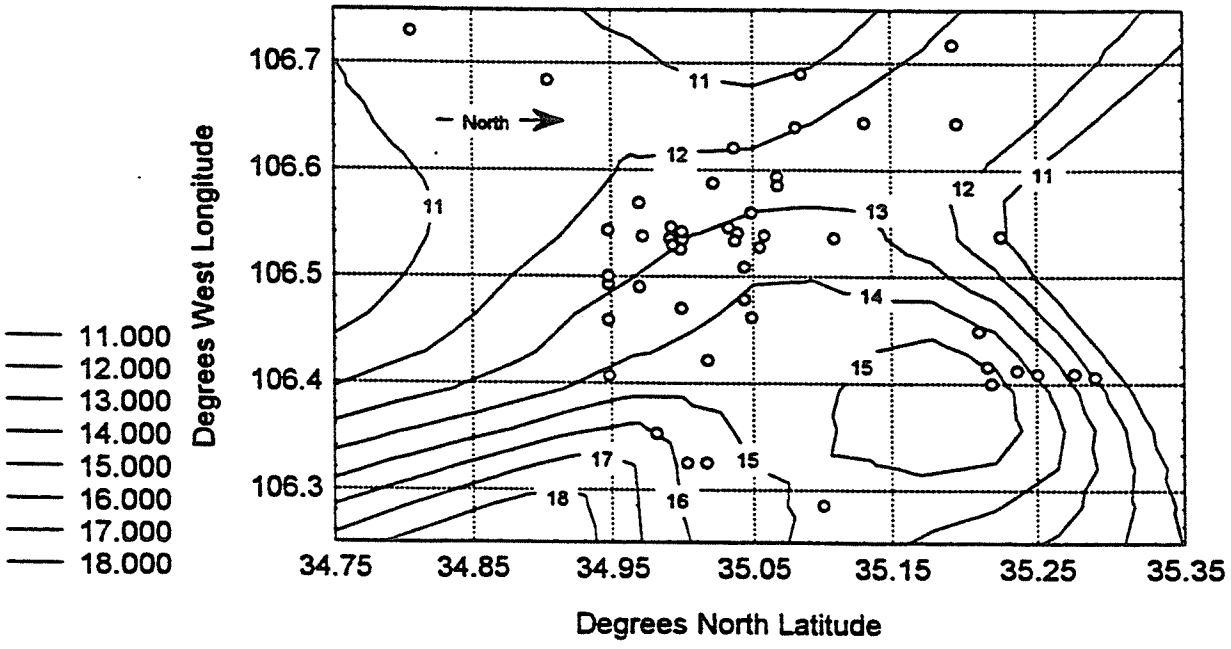

Figure 69

Variation with Elevation of Average TLD Exposure Rates
in the Vicinity of Albuquerque, NM

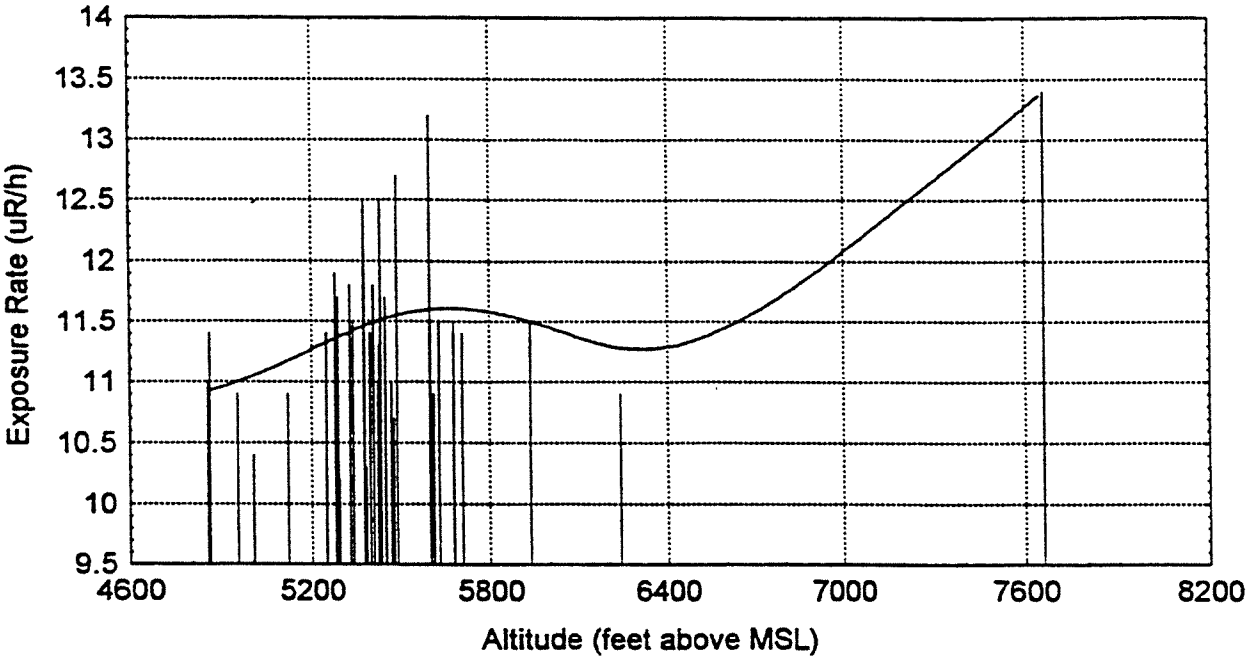

Figure 70

Variation with Elevation of HPIC Measured Exposure
Rates in the Vicinity of Albuquerque, NM

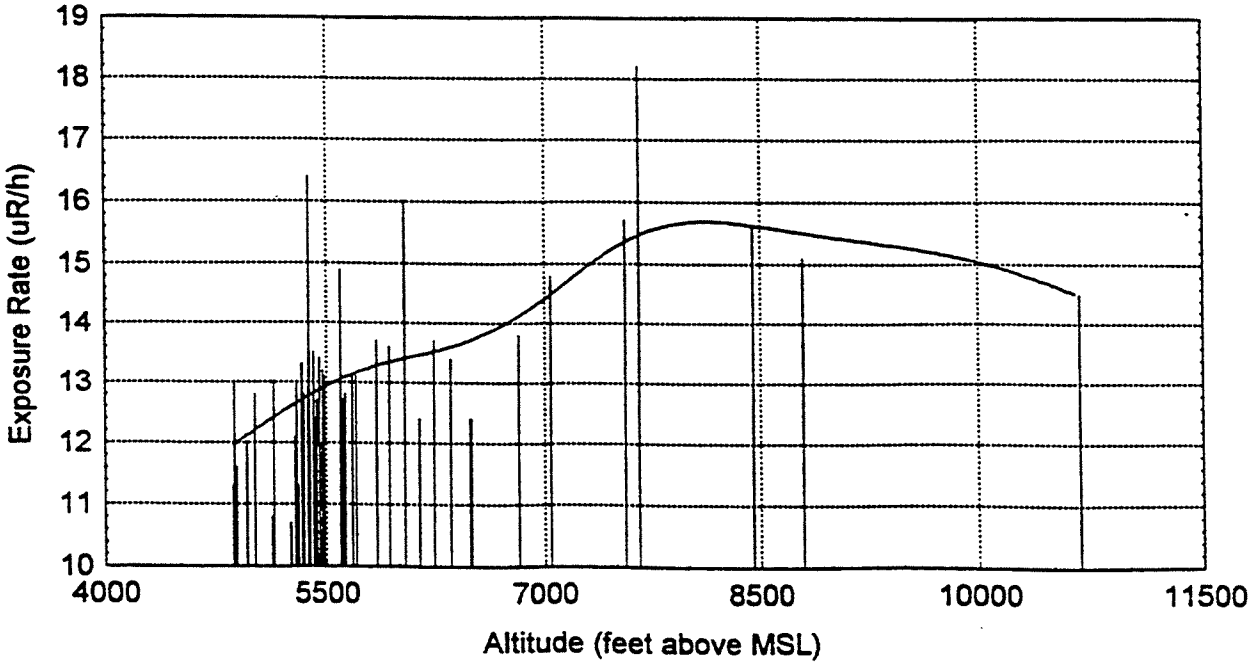

Figure 71

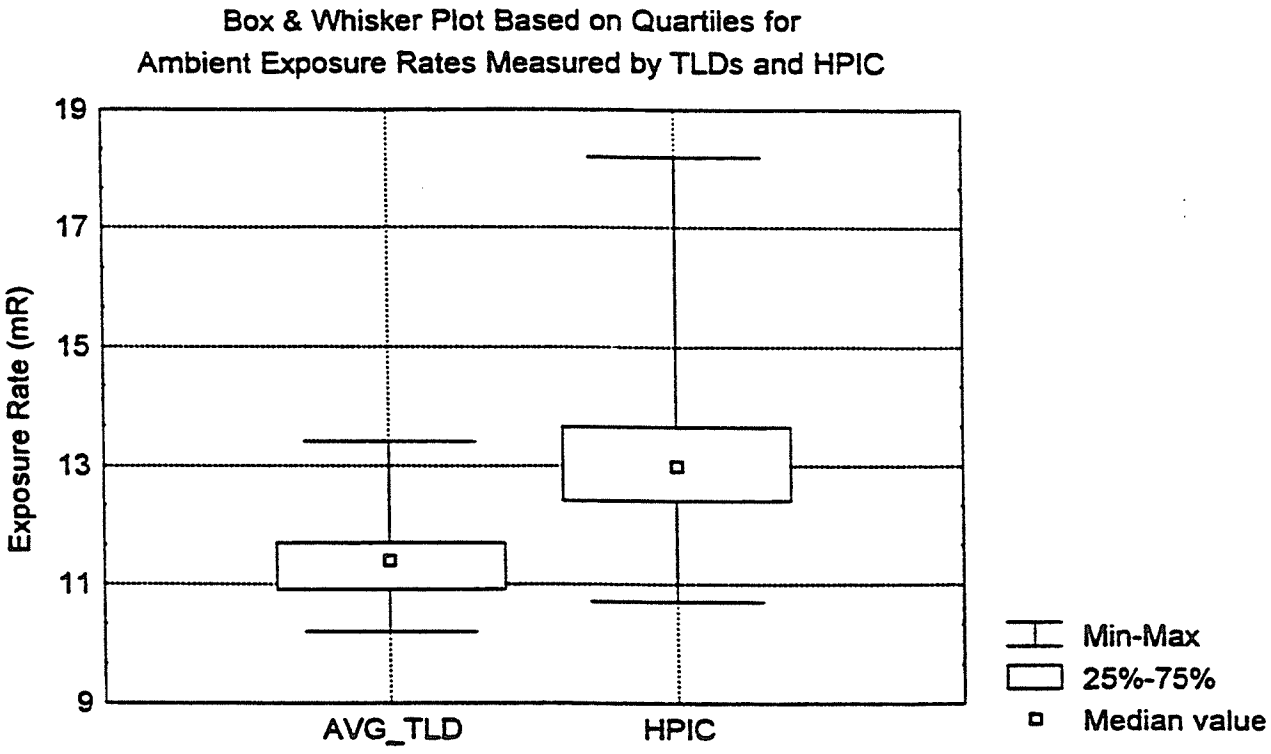

Figure 72

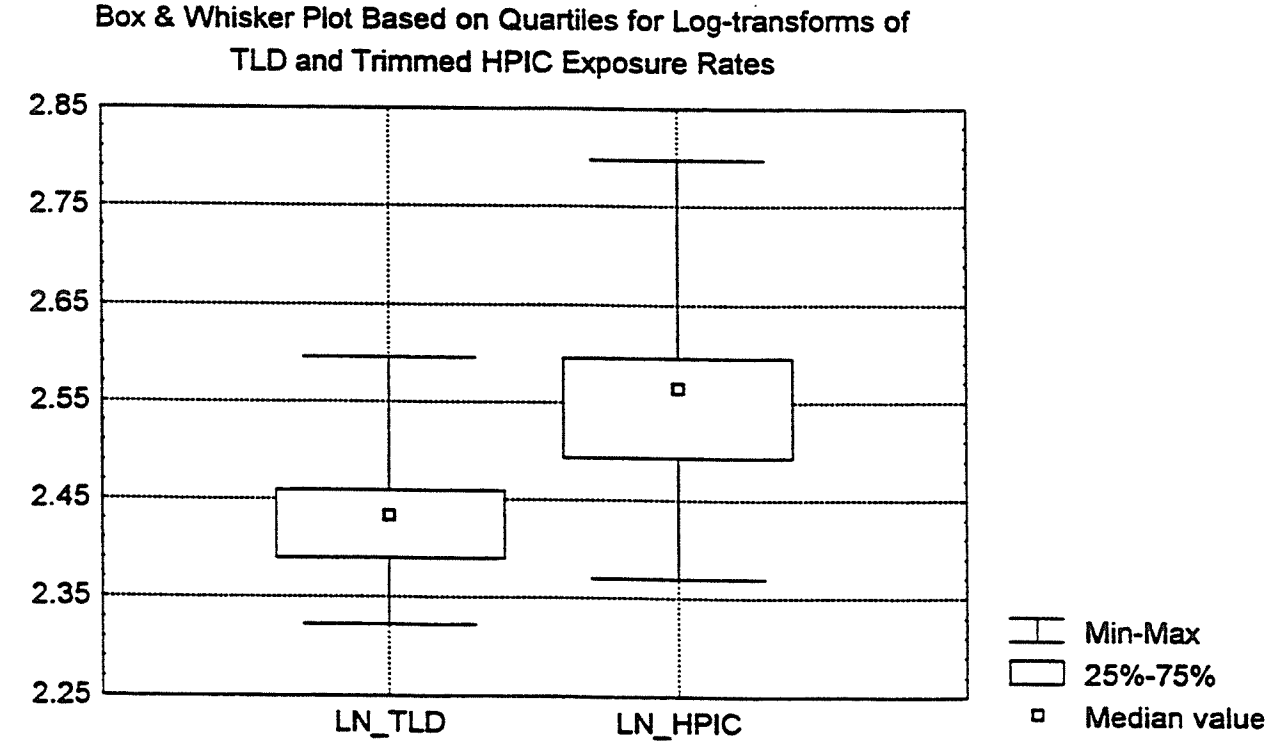

measurement value exceeded the TLD measurement values, although the comparison conditions are somewhat unfair. The HPIC sample population included almost twice as many sites as the TLD sample population, many of which were at unrelated locations. For greater clarity, a station-by-station comparison between TLD and HPIC measurements is also made in Tables 13 and 14. The relative percent differences (RPD) calculated for each station ranged from +1.2% to -20.5%: positive RPDs indicate a higher TLD response, while negative TLDs indicate a higher HPIC response. When average RPDs are calculated for on-KAFB and Albuquerque vicinity sub-samples, the results of -9.2% and -7.2%, respectively, may be accounted for by the varying responses of the techniques to their mutual calibration standard: ^{137}Cs. Based on our previous discussions, the TLD response to the natural spectrum may have been underestimated on the order of 5-10%, while the HPIC response may have been overestimated by about 3%. These variations would be adequate to account for the magnitudes of average RPDs, as well as most of the individual RPDs. Extending to the data the uncertainty due to natural variability of about 2 μR/h for hourly measurements, and the equivalent of 1.3 μR/h for measurements over a year, the TLD and HPIC measurements are generally comparable.

The internal distribution of annual average TLD data obtained in the study may be seen as log-transforms in Figures 73 and 74. A reasonable fit to a lognormal distribution is indicated. This is also apparent for the distribution of trimmed HPIC data, as may be observed in Figures 75 and 76. The fits obtained were comparable with those obtained for log-transformed soil data. The fine structure in the distributions was more readily apparent in Figures 77 and 78, depicting fitted lognormal distribution curves superimposed on histograms of raw TLD and HPIC data frequencies. The suggestion of separate data populations in these plots is not as readily apparent as in various soil data distributions. An extreme value trimmed from the HPIC data set using the critical T_n at the 2.5% risk level was also obtained at the soil sampling site that yielded the highest radium and thorium series soil activity concentrations. The relative combined influence of radionuclides in soil on TLD and HPIC measurements is explored in the analyses represented in Figures 79 and 80, respectively. This groundshine component of exposure was calculated as a function of ^{226}Ra, ^{232}Th, and ^{40}K, soil activity concentrations using the method referred to previously (104). Calculated groundshine values were tabulated as "Soil Estimates" in Tables 6 and 7. The combined influence of primordial radionuclides in soil alone accounted for 80.0% of observed long-term TLD measurement variance at a correlation of 89.5%, while that influence accounted for no

Figure 73

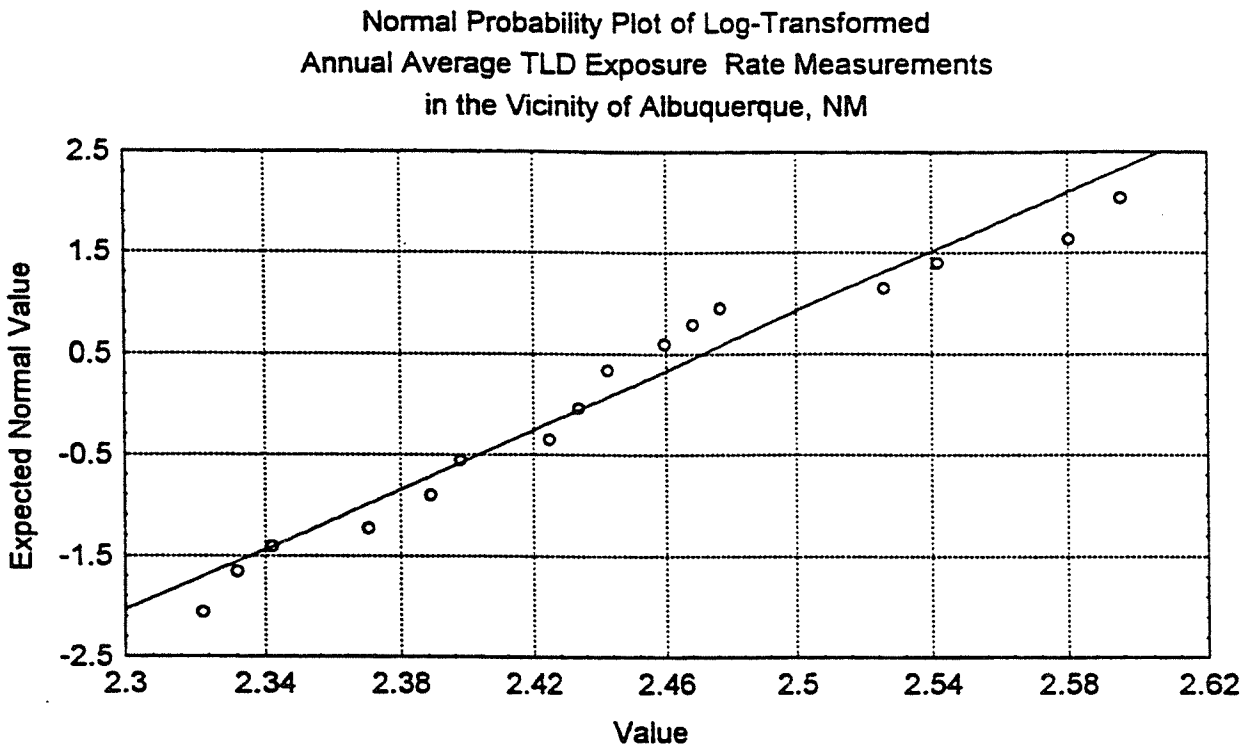

Figure 74

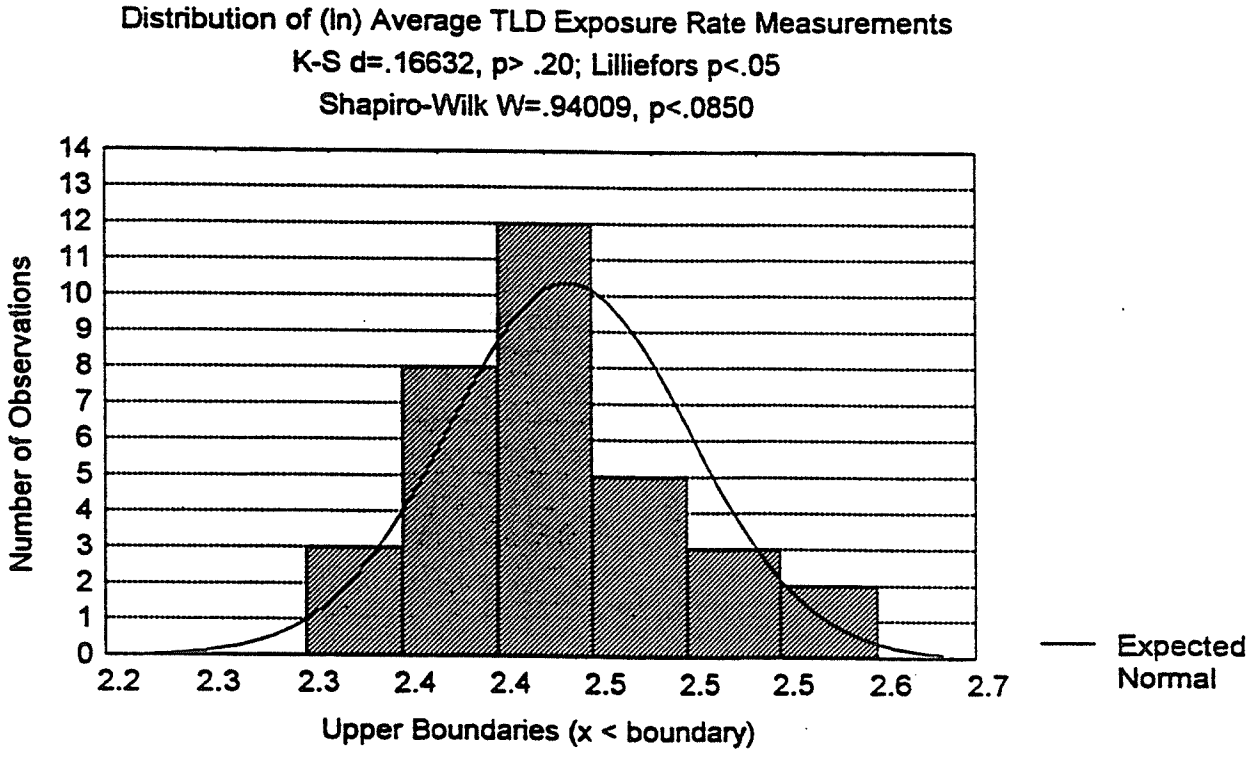

Figure 75

Normal Probability Plot for Trimmed
Log-transformed HPIC Exposure Rates Measured
in the Vicinity of Albuquerque, NM

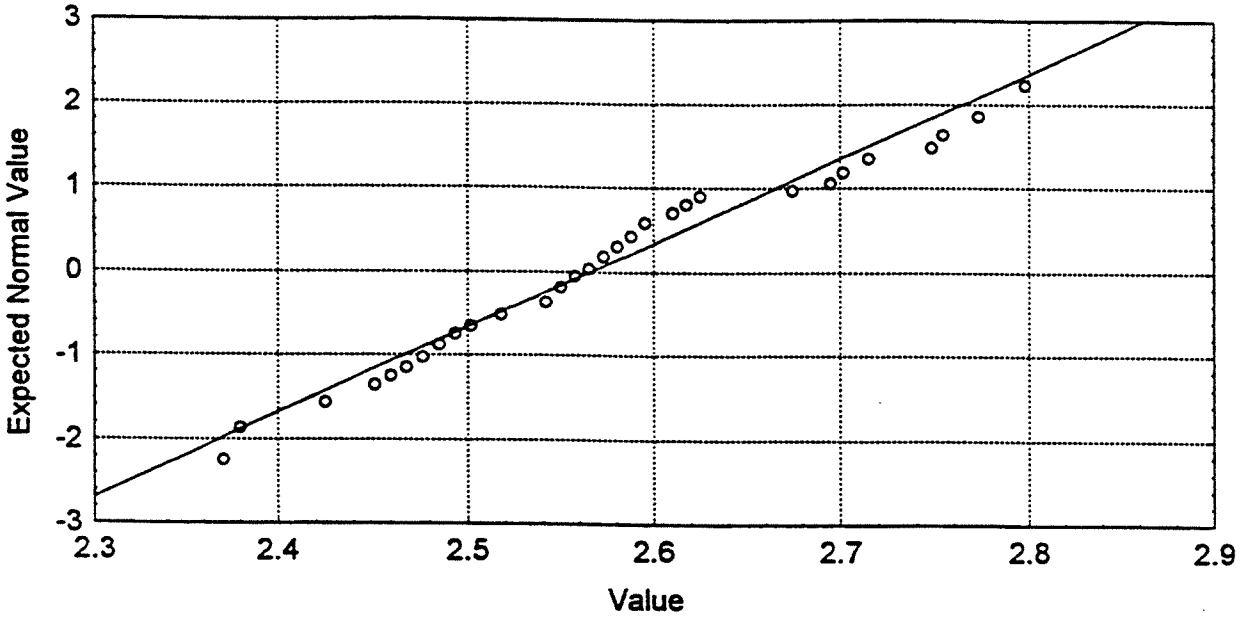

Figure 76

Distribution of (ln) Trimmed HPIC Exposure Rates
K-S d=.13364, p> .20; Lilliefors p<.05
Shapiro-Wilk W=.96075, p<.1495

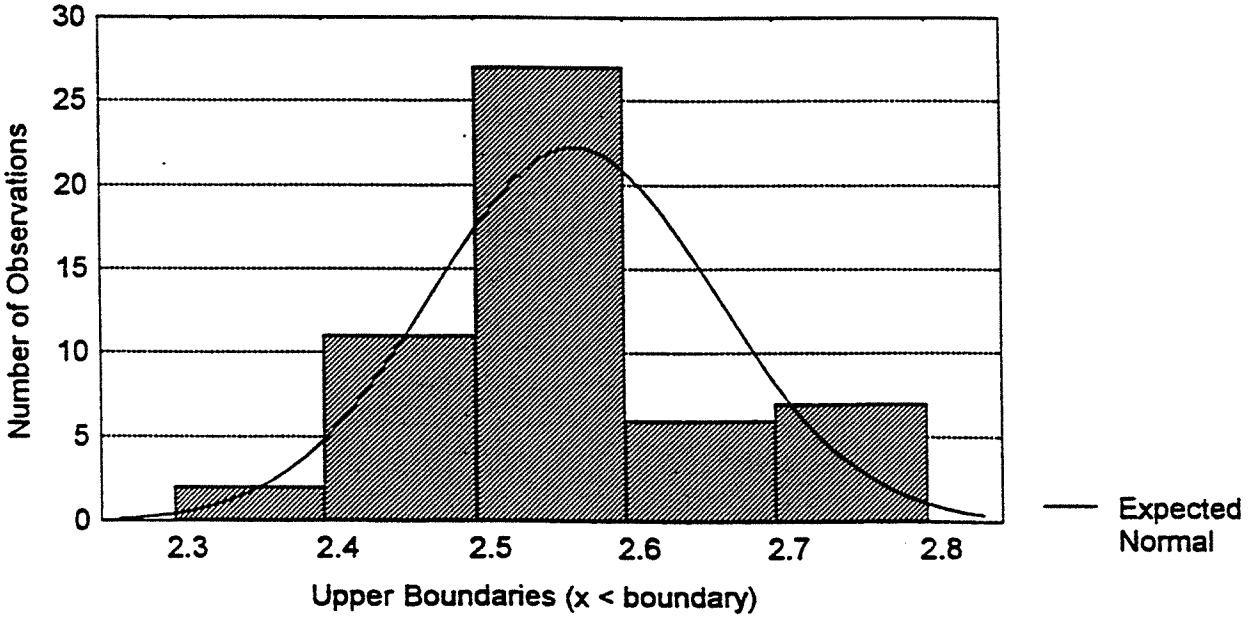

Figure 77

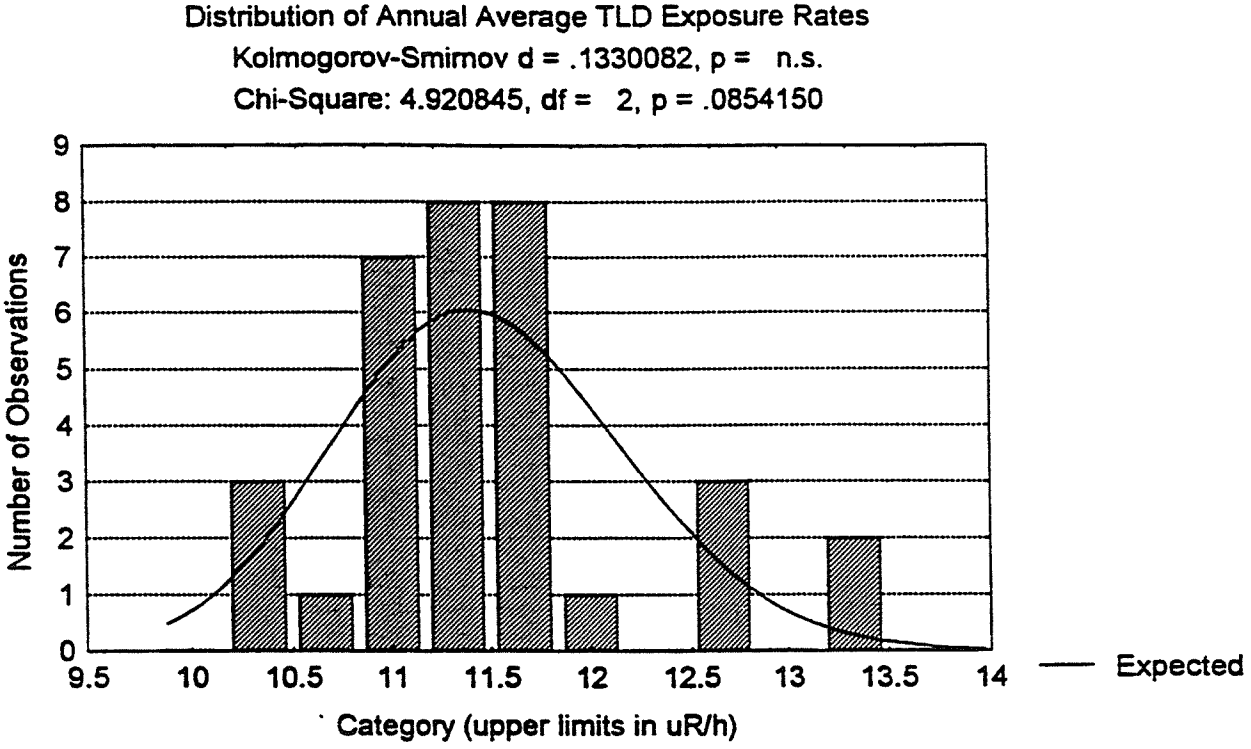

Figure 78

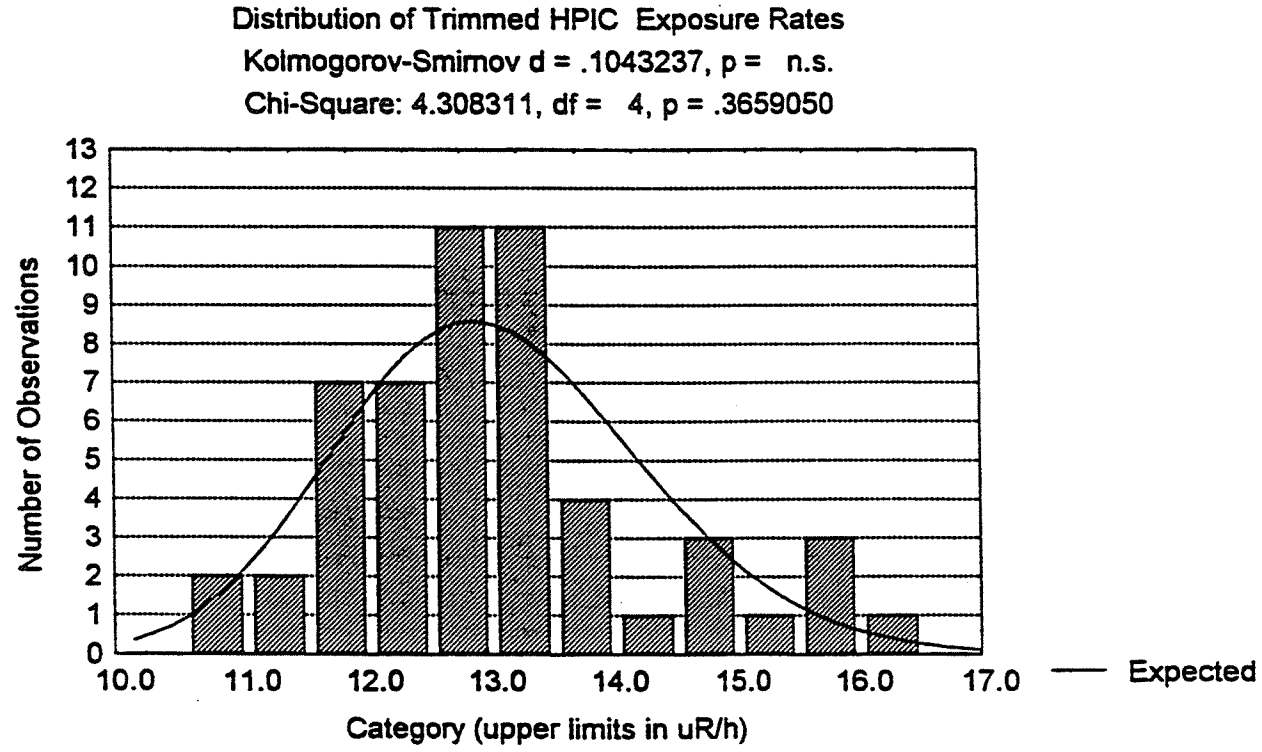

Figure 79

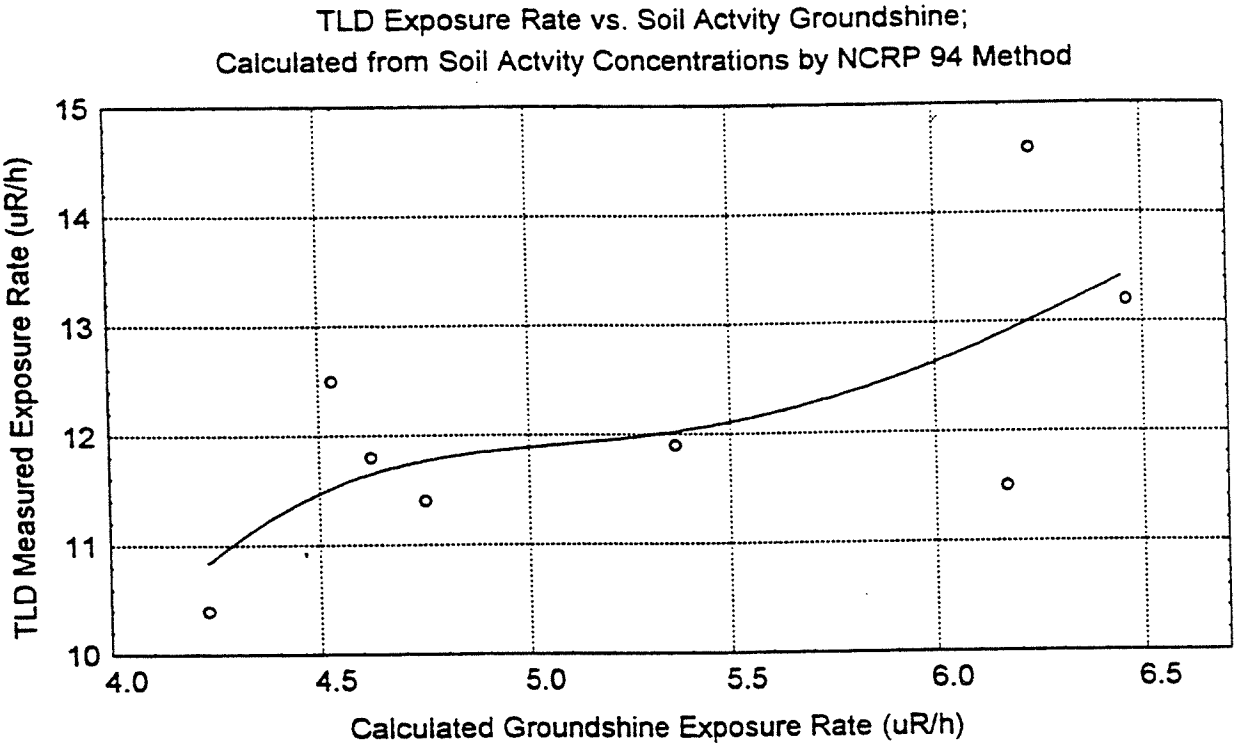

Figure 80

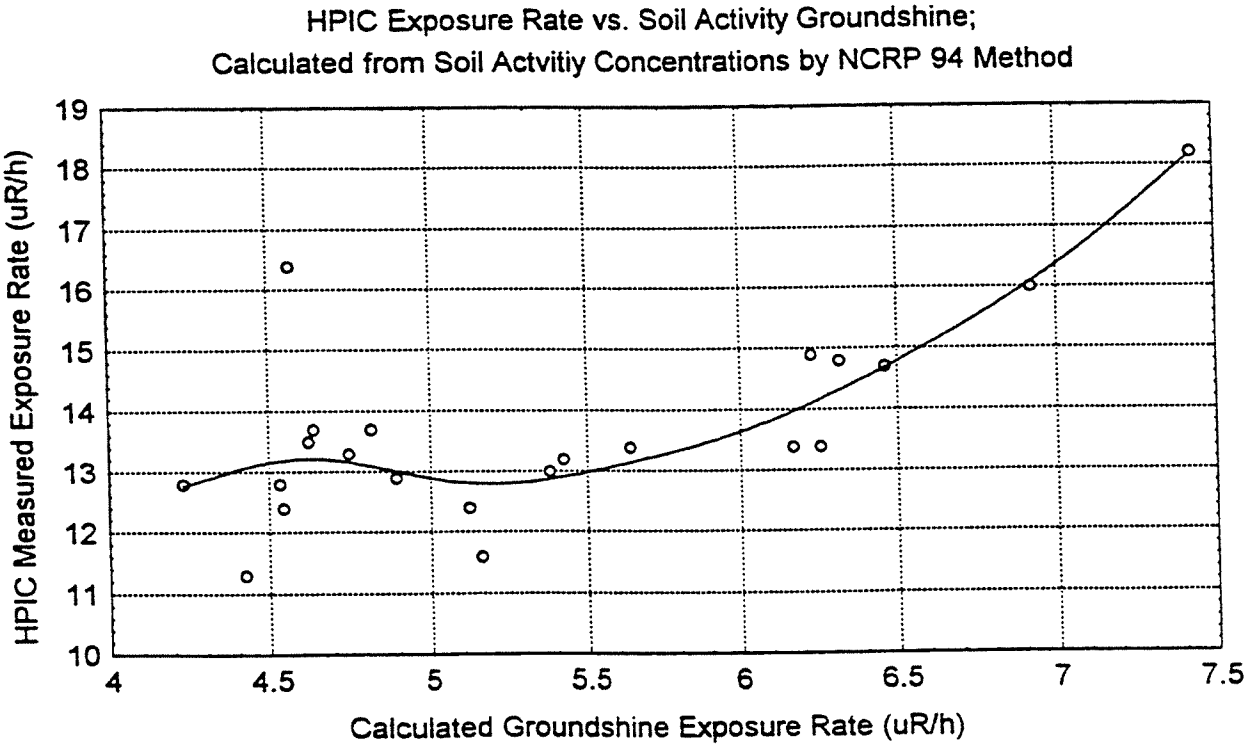

more than 71.3% of short-term HPIC measurement variance at a correlation of 84.4%. The generally increasing trend of measured exposure rates with calculated exposure rates is apparent in the figures, but there was insufficient correlation to infer a strict monolinear relationship. Linear correlations versus soil activity-based calculated exposure rates for TLD and HPIC measured exposure rates were 65.4% and 78.8%, respectively.

3.3 Statistical Summaries, Comparisons and Interpretations

A summary of statistical population estimates is contained in Table 15 for: soil activity concentrations by gamma spectroscopy, activity ratios, and exposure rate measurements derived from this study. Listed in the table are the validated number of measurements (n), arithmetic means (AM), ± 95% confidence limits (CL), the geometric and harmonic means (GM, HM), and sample standard deviations from the mean (dev). Geometric means reflect the lognormal model of population distribution, while harmonic means reflect the relative frequencies of occurrence of values more closely. For most of the distributions, the expectation values are probably best represented by either the geometric or harmonic means.

For purposes of comparison, results of statistical treatment of the soil radiochemical analysis data derived from the WIPP Roadside Study are included in Table 16 (17). The samples were obtained using identical techniques from statewide locations near the proposed WIPP transportation corridor. With the exception of ^{238}U results, all reported nuclides were evaluated from the same gamma peak regions as in the Albuquerque study. Alpha-spectroscopy was used to generate ^{238}U soil activity concentrations in the Roadside Study. Additionally, values for radionuclide activities in similar soils and source rocks from a variety of literature sources, including local to worldwide average and ranges, are included for comparison in Table 17 (14,70,74,106,131,...136).

3.3.1 Naturally Occurring Radionuclides in Soil

The representative values for naturally occurring radionuclides obtained by gamma-spectroscopic analysis of Albuquerque area soils are in general agreement with those reported from a variety of sources both within and outside the immediate vicinity, as may be seen by comparison of values in Tables 15, 16, and 17. High values for the ^{238}U series nuclides are particularly associated with soils in the Central Highlands. As has been mentioned, the potential source rocks

for that area are predominated by the Madera Limestone. Conventional wisdom would suggest that limestone, a chemical sedimentary rock generally of marine depositional origin, would be relatively depleted in concentrations of the metallic radionuclides (104,134). It should be noted, however, that both uranium and thorium as typical chemical species exhibit relatively high solubility in modern sea water, a carbonate buffered system: $3x10^{-3}$ mg/l and $5x10^{-5}$ mg/l, respectively (118). In the converse to a typical terrestrial case, radium is of lesser solubility in sea water, at about $6x10^{-11}$ mg/l, probably a consequence of association with carbonate ions. The depositional environment of the shallow Pennsylvanian seas overlying what is modern New Mexico would favor the introduction of uranium-bearing continental detritus into the pre-diagenetic matrix. Hence, appreciable quantities of uranium, and thorium may have been available in the depositional environment to become incorporated into the calcium carbonate ($CaCO_3$) based sediments.

The occurrence of uraniferous sandstone and limestone deposits in the western extreme of the Central Highlands, to the east of Albuquerque, has been noted by other investigators (137, 138). These have been identified geologically as fracture controlled uranium deposits, associated with the highly fractured Madera Limestone and Abo sandstone The aspect of fracture control of the deposits implies the role of ground water in transporting and concentrating radionuclides. This might provide an explanation to the anomalously high uranium and thorium series nuclide soil activities found in samples from the David Canyon Road site (sample numbers 9405121340 and 9405121350), whose averages were culled as outliers from the sample populations. The outward appearance of the ground surface at that site suggested the action of ground water. Outcropping limestone which provides part of the surface is smoothly undulating, suggesting erosive solvation by water. That appearance contrasted with the blocky appearance of most outcropping limestones in the region, the latter suggesting more mechanical erosion. Ephemeral stream patterns are apparent in the vicinity of the sampling site, although we could not find a spring or seep designated in the available record (36). Soils in the region occur in and around the area of limestone outcrop. Those soils most closely associated with the outcrop had the appearance and consistency of mud during each of several visits to the site. As has been previously discussed, the Madera Limestone is a highly heterogenous formation, and the influence of interbedded materials of distinct lithologic character may also contribute to the higher overall uranium and thorium series activities in soils derived from them. In addition, a number of investigators have implicated the Madera Limestone as a uranium bearing deposit (137,138,139).

An aspect of soil development that has bearing on activity concentrations of radionuclides is the relative organic content. Soils occurring in the forested western Central Highlands and in the upland canyons of the Sandia and Manzano ranges tend to be more enriched in organic matter. The high humus content of Central Highlands soils was readily apparent upon inspection of color and texture, as was the relatively low humic content of the sandier soils found within the basin. The predominant uranium species in the redox and pH regime characteristic of the surficial soil environment is the hexavalent uranyl ion (UO_2^{2+}), with a less extensive occurrence of the tetravalent forms; UO_2 and $U(OH)_4$ (140). Thorium generally occurs in the environment as the tetravalent species, primarily ThO_2. Radium and potassium are limited in their potential oxidation states. They are universally found in the divalent and monovalent forms, respectively.

Uranyl carbonate complexation favors the mobilization of uranium from the mineral component of soils, while the presence of organic matter may further retard its mobility, resulting in the concentration of radionuclides in soils to a degree commensurate with their humic content (141). The effect of soil organic matter on increased mobilization of tetravalent thorium has also been observed (72). Organic acids in the soil humic content exert an additional effect through simple lowering of pH in the mineral-organic interface, a condition which generally favors the mobilization of metals. Conversely, high humus contents with low aeration can result in reductive conditions that may diminish the solubility of metallic radionuclides subject to reduction state alteration. This may occur in deep humic sediments that are consistently water saturated.

Another soil characteristic that may influence naturally occurring radionuclide constituents is clay content. Clay minerals have extensive surface areas and high negative charge to mass ratios, and in soil can act to adsorb positively charged species. This action has been observed to concentrate radium and uranium in clayey soils (72). Micaceous rock materials that may be parent to clay minerals such as illite are found sporadically interbedded in the Madera, and are even better represented in the igneous and metamorphic rocks contributing mineral detritus to the soils of the inner basin. Since grain size decreases in the basin in a westerly direction from the mountain front toward the river, some concentration of radionuclides might be expected with increasing clay content. This trend, however, was not evident in the results of our study. The competing diffusive effects of runoff and leaching of the radionuclide constituents may have overshadowed any concentrating effects.

Maximal ^{238}U concentrations in the soils of the inner basin are somewhat higher than those reported for the potential parent Sandia Granite but are consistent with those reported for rhyolites that may be representative of the meta-rhyolites occurring in the region (14,134). Moreover, it is not uncommon to find that erosion products outwashed from mountain fronts contain higher concentrations of radioactive species than their source rocks (104). Natural ^{232}Th concentrations reported in the study fell within the ranges ascribed to local and worldwide source rocks and soils. The samples of lowest relative activity for all nuclides were generally associated with the western extreme of the study region. Although that area is extensively underlain by Quaternary basalt flows studded by several volcanic plugs, insufficient geologic time has passed to effect erosion of the recalcitrant volcanic rock to predominant soil components. Thus, west mesa, terrace and valley soils did not necessarily reflect the greater relative depletion of local mafic-basalt derived minerals in uranium and thorium series nuclides.

Disequilibrium is apparent between the activity concentrations of ^{238}U in study area soil and those of its daughters: ^{226}Ra and ^{214}Bi. The average extent of that disequilibrium yielded an ^{238}U:^{226}Ra ratio of 1.65 ± 0.73, as recorded in Table 15. Disequilibrium is not uncommon in natural systems where members of decay chains have long half-lives in comparison to the rates of geochemical processes (104). Although ^{234}U was not directly measured, the experience of disequilibrium between it and its parent ^{238}U in the study of natural groundwaters may shed some light on the apparent phenomenon in study soils. It was demonstrated that an average proportion of about 2:1 occurs between parent and daughter nuclides in New Mexico ground waters, implying processes that increase the daughter's mobility despite it being chemically identical to its parent (142). Assuming all other effects to be equal, the resultant radium series nuclides should also reflect this disequilibrium.

The exact mechanism for this phenomenon remains a matter of debate. Like most metals, uranium generally fits poorly in the crystal lattices of silicate minerals. The recoil energy of ^{238}U alpha decay may result in radiation damage, such as has been demonstrated in the case of smoky quartz and thorium alpha-decay. The damage incurred may be sufficient to open the fine structure of soil mineral to the enhanced effects of water mediated transport of daughters. Since ground waters become preferentially enriched in the lighter uranium isotope by a factor of approximately two, It could be predicted that soil minerals like the deeper sediments infused by ground waters would become depleted in the lighter uranium isotope and resultant radium daughter by a similar factor. These

factors agree, approximated to a single significant figure.

^{238}U values were higher overall as estimated by gamma spectroscopic analysis of soils derived from the study region than were reported statewide, as summarized in Table 16. Several factors may account for this. The soils analyzed as part of the Roadside survey were largely sampled within lowlying valleys where the roadbeds of major transportation routes were concentrated. This would result in sampling of soil materials that had experienced greater weathering and chemical leaching. In addition, chemical separation procedures required for the alpha-spectroscopic analysis employed in the Roadside study can introduce chemical recovery losses. There is some indication of this in the reported results. Alpha-spectroscopic ^{238}U results in the Roadside study were lower, overall, than both ^{214}Bi and ^{226}Ra gamma-spectroscopic results presented in the same study by factors of 1.1 to 2.1, respectively. This would otherwise suggest that disequilibrium has occurred favoring the preferential retention of radium in soils as opposed to uranium. It should be noted that the 1001 keV ^{234m}Pa peak used to quantify ^{238}U in soil was the lowest gamma probability yield peak employed in the study. Its results as soil activity concentrations were thus proportionately the most uncertain.

The remaining natural radioisotope, ^{40}K, displayed its maximal concentrations along the base of the mountain escarpments. This is consistent with outwash from potassium-rich sialic rocks including granites and meta-rhyolites. The greater water solubility of potassium would suffice to explain its relative depletion in soils when compared to representative source rocks. Higher average ^{40}K values in soils have been reported from other portions of the Albuquerque area (14). In contrast to the trend of findings for uranium and thorium series nuclides, elevated values of ^{40}K were not generally ascribed to the Central Highlands. Maximal values in our study did not exceed those previously reported values, reproduced here in Table 17.

3.3.2 Anthropogenic Radionuclides in Soil

As noted, the only indicator parameter that is specific for assessing the influence of man-made radiation in our study is ^{137}Cs. Its special utility as an indicator has long been recognized, allowing high specificity detection with a minimum of preparation effort and potential error (105, 143). There are additional specific reasons why ^{137}Cs detection in the environment is important. Among nuclear fission products, it elicits special dosimetric concern due to its high relative fission yields, long physical half-life, and selective uptake

and retention in soft tissue that results in whole body dose (144). The radionuclide demonstrates significant biological reconcentration through the environmental pathways that may lead to eventual human uptake (145,146,147).

During the period of above-ground nuclear weapons testing preceding 1963, the majority of the fission product inventory from nuclear detonations was injected into low to mid-stratospheric levels, where it remained with a residence half-life of six to twelve months before being deposited on the surface of the earth (144). Peak terrestrial fallout levels were observed in 1963 following the global flurry of testing in 1961 and 1962. Later above-ground testing performed by the Chinese and French resulted in deposition primarily in the Southern hemisphere, consistent with the long observed trend of return of fallout to the hemisphere of origin (70). It has been estimated that approximately 1.3×10^9 GBq of ^{137}Cs was released into atmosphere from above-ground weapons testing (69). Global fallout of ^{137}Cs from past weapons testing and the Chernobyl accident has been a particular concern in world regions where, not unlike New Mexico, pastoral agriculture remains a significant component of local food production (70,147,...151). Based on distributions within the study region, it was presumed that ^{137}Cs in sampled soils resulted from fallout deposition. Potential soil sampling sites of known or suspected contamination from Albuquerque area nuclear facilities were avoided. The potential for more recent contribution of fission products from nuclear accidents or discharges was largely ruled out, based on the lack of gamma-peak detection of the more short-lived fission product, ^{134}Cs, during soil sample analysis.

In the general discussion of results, we drew the apparent connections between altitude, region and soil moisture with elevated ^{137}Cs in soils. These connections may be further synthesized to postulate a single credible mechanism for the observed trends in soil: that regional variation in precipitation has influenced soil activity concentrations through patterns of wet deposition of atmospheric fallout. The greatest soil concentrations were associated with regions of greatest rainfall, as inferred from review of the meteorological record. Investigations in other regions of the world have suggested that enhanced ^{137}Cs deposition and resultant soil activity concentrations are associated with regions of increased rainfall (70).

Additional biotic and geochemical factors may play some part in the higher ^{137}Cs soil concentrations found in upland areas. Cesium is found in all natural compounds as a monovalent cation with a radius of 1.67 Å, exhibiting high water solubility and little tendency to form complexes.

Cesium ranks highest in the alkali metal lyotropic series for preferential adsorption to soil surfaces. The occurrence of cesium in representative source rocks may suggest its relative affinity for the mineral components of soils derived from them. The average Cs content of modern sediments is about 6.0 ppm, while its contents in granites and limestones are 5.0-6.8 ppm and 1.0 ppm, respectively (141). This suggests that the predominant mineral component of limestone-derived soils in the uplands of the Central Highlands, Sandia and Manzano Mountains and their canyons, should not retain cesium to a greater extent than granite and meta-rhyolite derived soils in the basin.

Cesium retention in sediments by silts, clays, and micaceous and secondary aluminosilicate minerals such as illites, vermiculites, and biotite has been observed, probably enhanced by trapping of the cation in interleaf spaces or on frayed mineral edges (65,...69,141,150). Although sometimes described as "fixation", the effect of Cs retention in clays is more likely a surface adsorption phenomenon such as ion exchange, rather than true covalent fixation within crystal structure by amorphous substitution for a mineral cation with the same coordination number (140). Although interbedding of micaceous materials can occur in the Madera limestone, the acid intrusive and extrusive Precambrian rocks and their altered forms which contribute detritus to the basin are much richer in these minerals. Micaceous materials were readily apparent upon inspection of most basin soil samples to varying extents but were largely absent in the upland soils east of the ridgeline. Soil acidity can also exert a profound effect on cesium retention through competitive replacement (58,140,150). Humic soils tend to be more acidic, while arid basin soils are calcareous, implying more alkaline conditions. Humic materials may also act to retain cesium in soils. Cation exchange coefficients may be used to compare the relative potentials for cesium interaction between an aluminosilicate mineral that exhibits high cesium retention, illite, and a "typical" humus: 10-40 meq/100 g and over 200 meq/100 g, respectively (140).

The closest geochemical analog for cesium is potassium. They have the same approximate ionic radii, and consequently the same hydrated radii as environmental forms. A similar regional trend in the distribution of potassium as ^{40}K was not observed as for ^{137}Cs, as may be evident by comparing Figures 46,47,54 and 55. Thus, it was inferred that neither the humic content or clay content of soils were primary controlling factors in ^{137}Cs soils distribution. Biotic factors that may influence the concentrations of ^{137}Cs in environmental media include the concentrative effects of lichens, fungi, and other microorganisms (146, 152). There was no device available in

the study to evaluate the relative quantities of these omnipresent organisms, although greater biotic activity may be ascribed to more humic soils.

The representative values for the trimmed and inclusive data sets may be compared to the results of other local area investigators. Available results of soil sampling and analysis for ^{137}Cs by SNL investigators were statistically analyzed by the author without applying outlier rejection (153,...162). The variation of geometric means for ^{137}Cs in soils sampled over an eleven year period is depicted in Figure 81, while the soil data distributions are depicted in Figure 82. Geometric means ranged from 0.15 to 0.41 pCi/g in the SNL sampling. Maxima are apparent in Figure 81 in late 1987 and mid-1992. Interpretation of these maxima must be performed with some care, since the sampled population was significantly increased in 1990 and again in 1991. The results of that increase in creating greater data spread is apparent in Figure 82, particularly beginning with 1991 results. The increased sampled populations incidentally included a greater representation of upland areas in the east portion of the study area. The 11-year average geometric mean for SNL was 0.31 ± 0.35 pCi/g, while the untrimmed geometric mean for our study was 0.25 ± 0.53 pCi/g.

The geometric mean for a one-time study performed by investigators in 1993 near ITRI was 0.13 ± 0.06 pCi/g (163). That study was much more localized in scope, and is apparent in the iso-concentration contour maps and Figure 1 as a half-asterisk shaped cluster of collocated sampling points at the southeast corner of the KAFB military reservation. To directly compare the site-by-site results of collocated samples, regression analyses were performed, the results of which are depicted in Figures 83 and 84 for SNL and ITRI, respectively. The greater overall data spread evident in the SNL comparison may be explained in part by the differences in sampling techniques employed by that facility as compared to the study technique. SNL representatives use a flat trowel which is scraped lightly over the surface of the soil, allowing little depth or areal control. While a greater proportion of collocated sample correlations are included in the 95% confidence region of the figure, larger divergence in the results located outside the region resulted in poor direct linear correlation. The better correlation in the ITRI comparison may be attributable to the similarity of sampling techniques and the more uniform region sampled. To evaluate whether a systematic bias may have been introduced in either set of results, relative percent differences (RPDs) were calculated on a site-by-site basis and grouped for analysis. The distributions of RPDs as compared to expected normal values in Figures 85 and 86 suggest that the deviations in

Figure 81

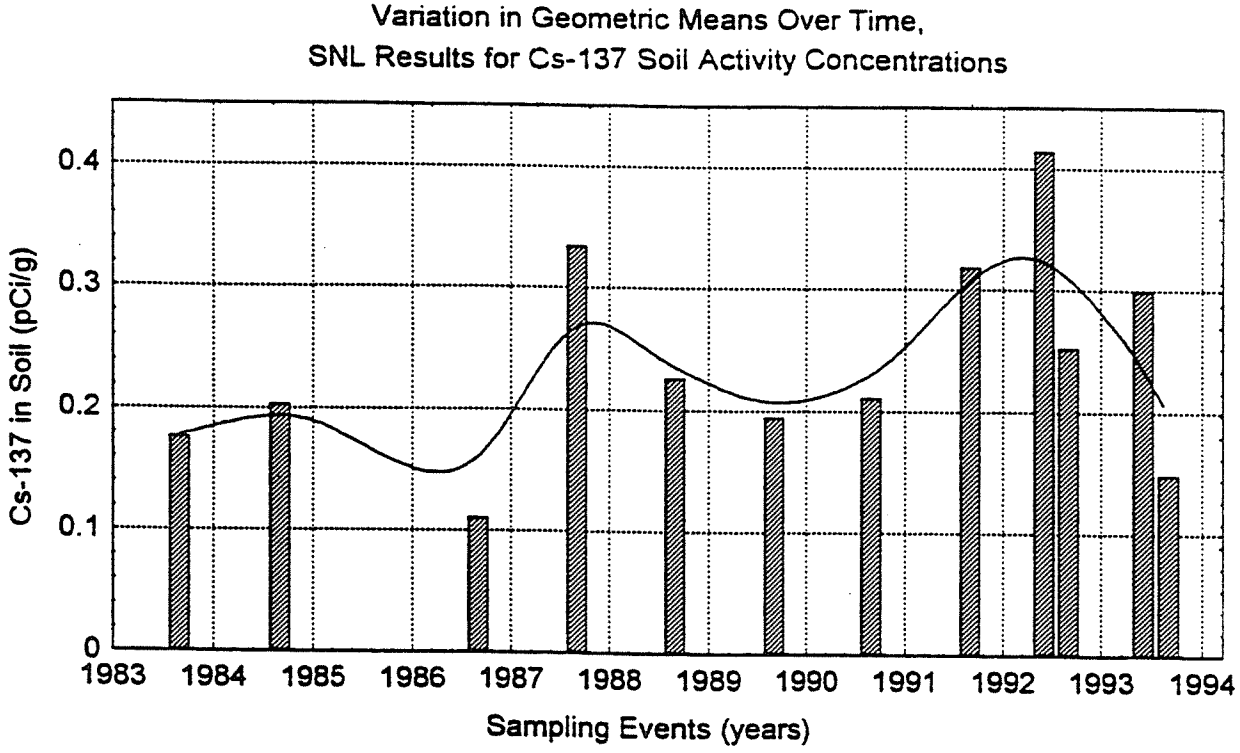

Figure 82

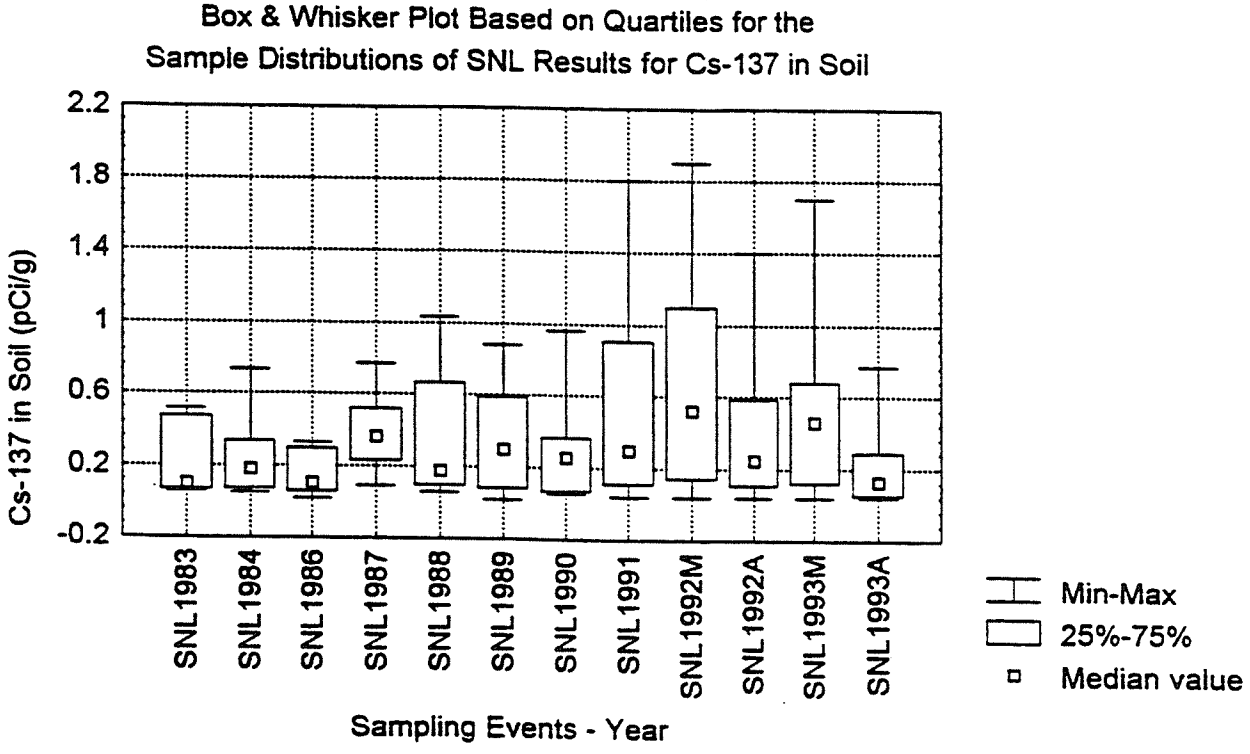

Figure 83

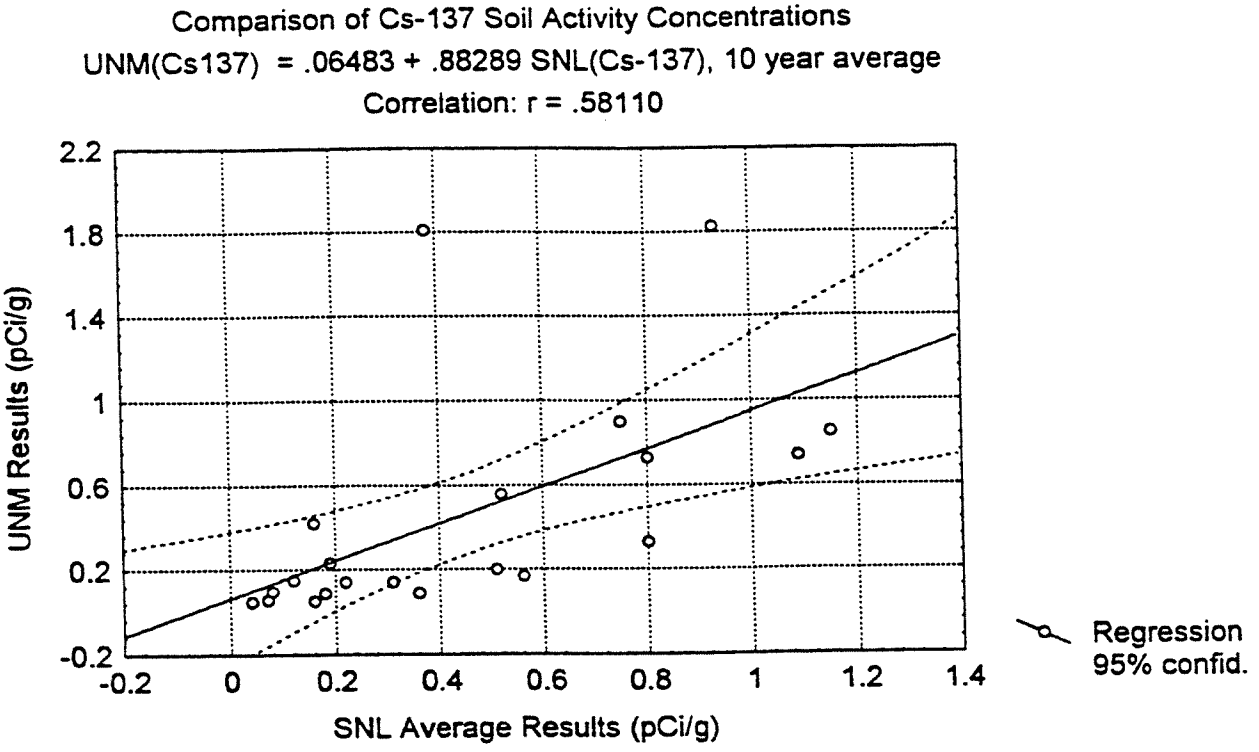

Figure 84

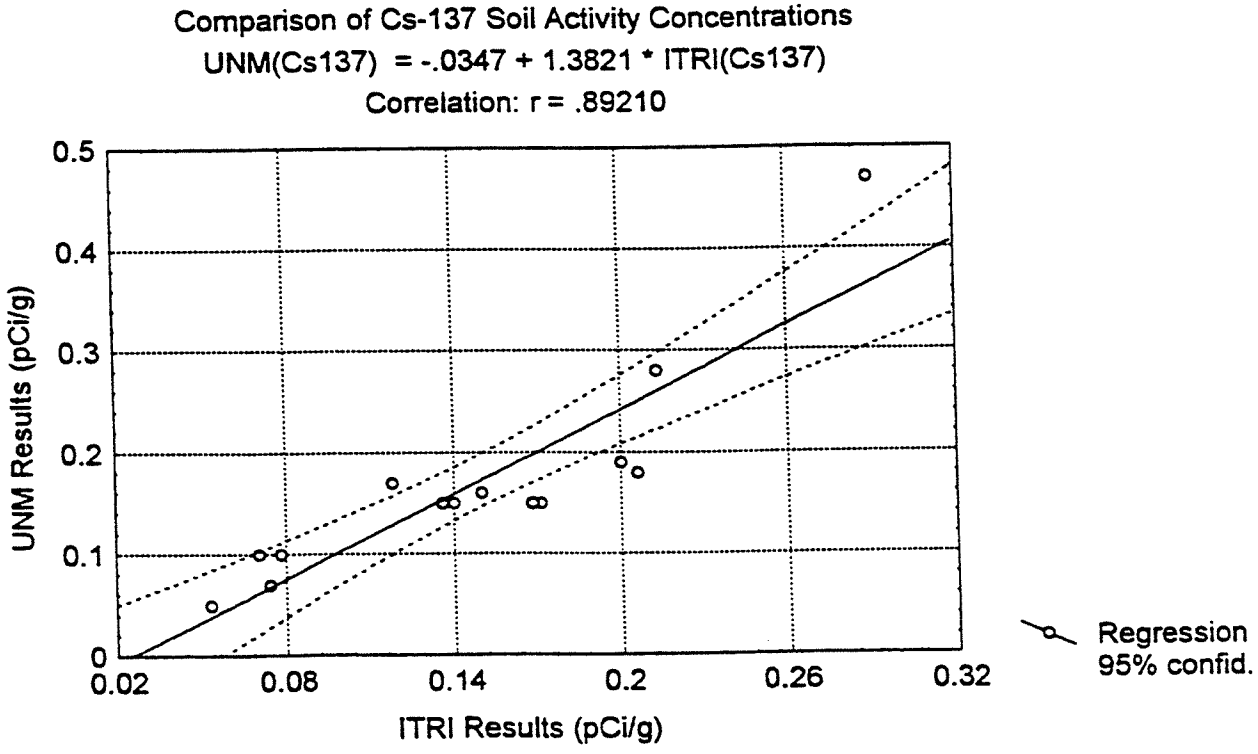

Figure 85

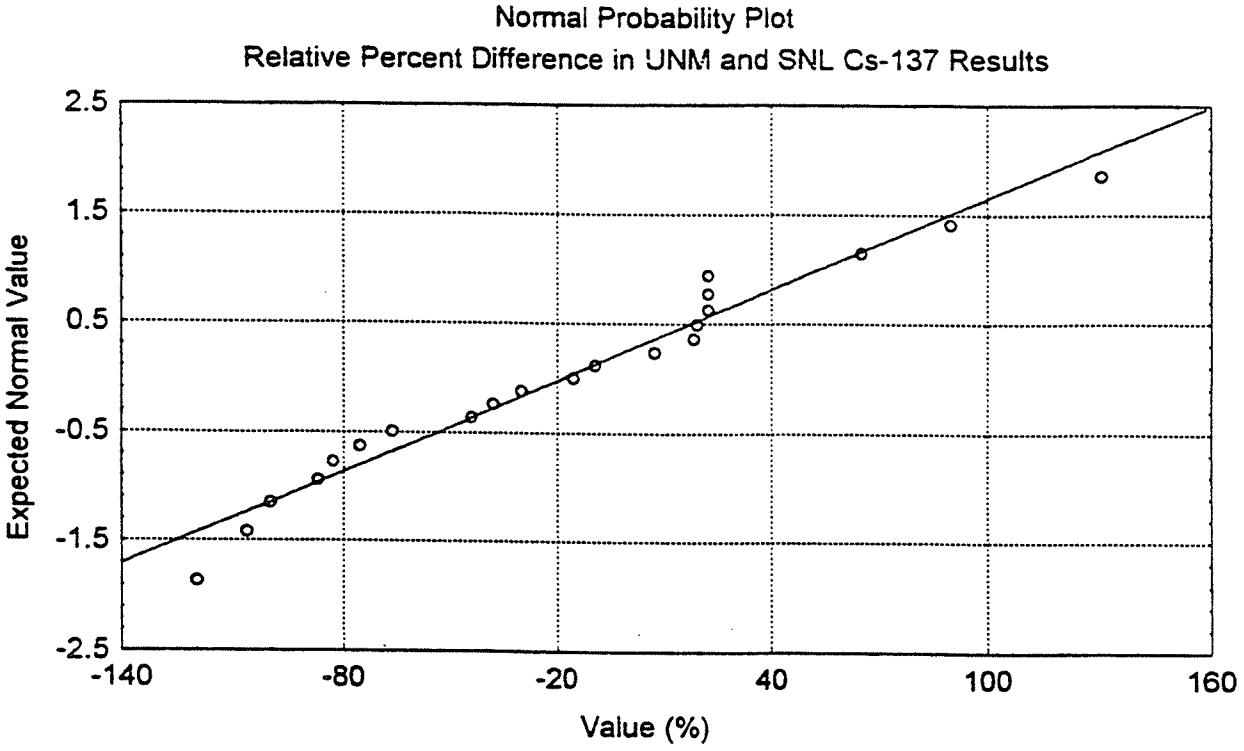

Figure 86

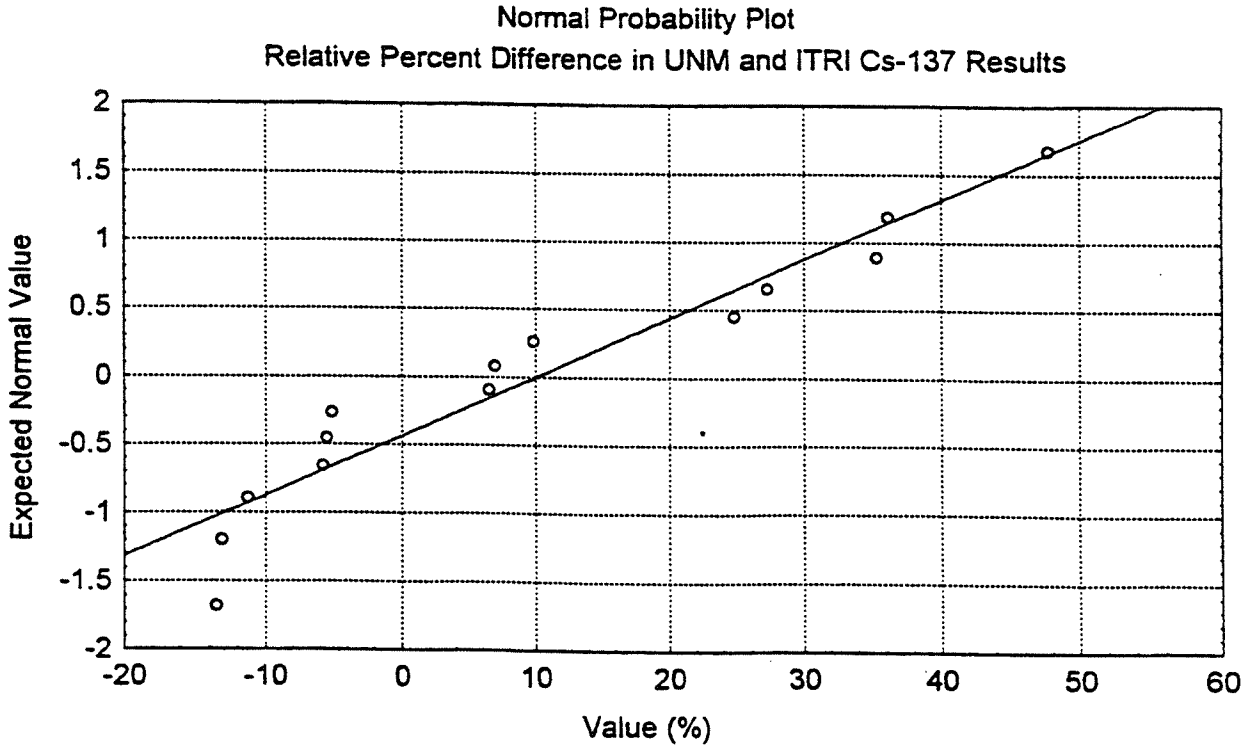

results arose randomly. The average RPD for UNM-SNL results was -18.1% ± 67.0% and for UNM-ITRI results was 10.0 ± 20.6%.

The results of a Los Alamos National Laboratories (LANL) study of fallout radionuclides in soils in Northern New Mexico were also analyzed by the author (135). The combined effects of altitude and west sheltering by north-south trending mountain ranges on the distribution of all fallout nuclide soil activity concentrations were also evident in the LANL study. The average ^{137}Cs value obtained over a twelve year period at the location nearest the study area, Bernalillo, NM, was 0.24 ± 0.14 pCi/g. The data for northern New Mexico were also analyzed to provide ratios for ^{90}Sr and $^{239+240}Pu$ to ^{137}Cs soil activity concentrations that may be used to predict concentrations in our study area. The analysis yielded an arithmetic mean Sr:Cs ratio of 1:1.6, and a geometric mean ratio of 1:2.2. The former value is exactly that reported by the United Nations based on worldwide data (164). The latter value reflects the apparent lognormal distribution of the ratio over the grouped data sets for all four sampling sites.

Uranium (^{235}U) fission produces ^{90}Sr and ^{137}Cs at roughly the same yield, although the yield is about three times smaller for ^{90}Sr than for ^{137}Cs in ^{239}Pu fissions (84). The overall variation in environmental residence times for Sr and Cs, as may affect their ratios, appears to be primarily influenced by run-off transport and to a lesser extent by infiltration (149,165). The Pu:Cs ratios derived from the analysis were apparently distributed normally, yielding an average ratio of $1:3.0 \times 10^{-2}$. That ratio is greater by two orders of magnitude than the ratio ascribed to fresh fallout onto Ukrainian soils from the Chernobyl accident (150).

3.3.3 *In situ* Environmental Exposure Rate Measurements

Intercomparison of TLD and HPIC measurement distributions, as well as the relationship between in-situ exposure rate measurements and the radionuclide contents of underlying soils has been explored with regard to regional and statistical trends. Issues that remain concern the relative performance of the TLD system with respect to an established system, and aspects of temporal variability that are distinguishable from spatial variability.

The established program providing intercomparison was the SNL Environmental Dosimetry Program, which is described in detail elsewhere (102). Materials and methods of TLD deployment differ between the two programs. The SNL program uses natural LiF phosphors in chip form, manufactured by cutting square pieces approximately 5 mm on edge from a

prepared crystalline sheet. While LiF does not possess the high sensitivity of calcium salt and ceramic phosphors frequently used in environmental dosimetry, it exhibits the characteristics of low environmental fading and linear energy response that make it desirable for a variety of dosimetric applications (93,94). Five loose LiF chips in a plastic container are placed within a polypropylene film can that is deployed in the environment within an aluminum tube at an effective height of approximately one meter from ground surface. Deployment periods and calibration procedures were identical between the UNM and SNL programs. The results of Second Quarter, 1993 (2Q 93) to Second Quarter, 1994 (2Q 94) SNL environmental dosimetry were made available for review (166). The two programs, as compared on a five quarter deployment basis, showed remarkably close agreement. This may be seen in Tables 13 and 14. Relative percent differences (RPDs) were calculated on a site-by-site basis, which ranged from -6.1 to 11.2%, averaging 1.6 ± 5.2% overall. Positive RPDs indicate that UNM measurements were greater than SNL measurements, and negative RPDs indicate the converse. While the individual program responses exhibited only fair (70%) linear correlation in Figure 87, using the RPDs for residual analysis suggested that the variation between program results arose through random processes (Figure 88).

Temporal variability in UNM $CaSO_4$(Tm) TLD exposure rate measurements was evaluated by comparing population distributions and geometric means. The quarterly populations were first represented as distinct temporal samples, as seen in Figure 89. It is apparent from the figure that initial variability of the TLD sample population was very high. There has been some suggestion in the literature that the variability in response characteristics of newly manufactured TLD phosphors improves after a period of field-hardening (105). This observation also appears to have held in our example. The data enclosing the median and 25 to 75 percentiles appear to approach maxima in fourth quarter 1993 and second quarter 1994. This is also apparent in the geometric means of the sample population, as seen in Figure 90. This trend supports our earlier suppositions that winter inversion periods during the fourth calendar quarter could contribute to higher exposure measurements while the monsoon rains during third quarter could contribute to lower exposure rate measurements, based on the predicted relative impacts of weather conditions on the evolution of radon and thoron from soils. It is notable that the high second quarter 1994 behavior is not reflected closely in the preceding second quarter of 1993. This may have been a consequence of the more diffuse overall response of second quarter 1993 response, or may reflect the expected increase in the cosmic-ray contribution to free-air exposure. The variation in geometric

Figure 87

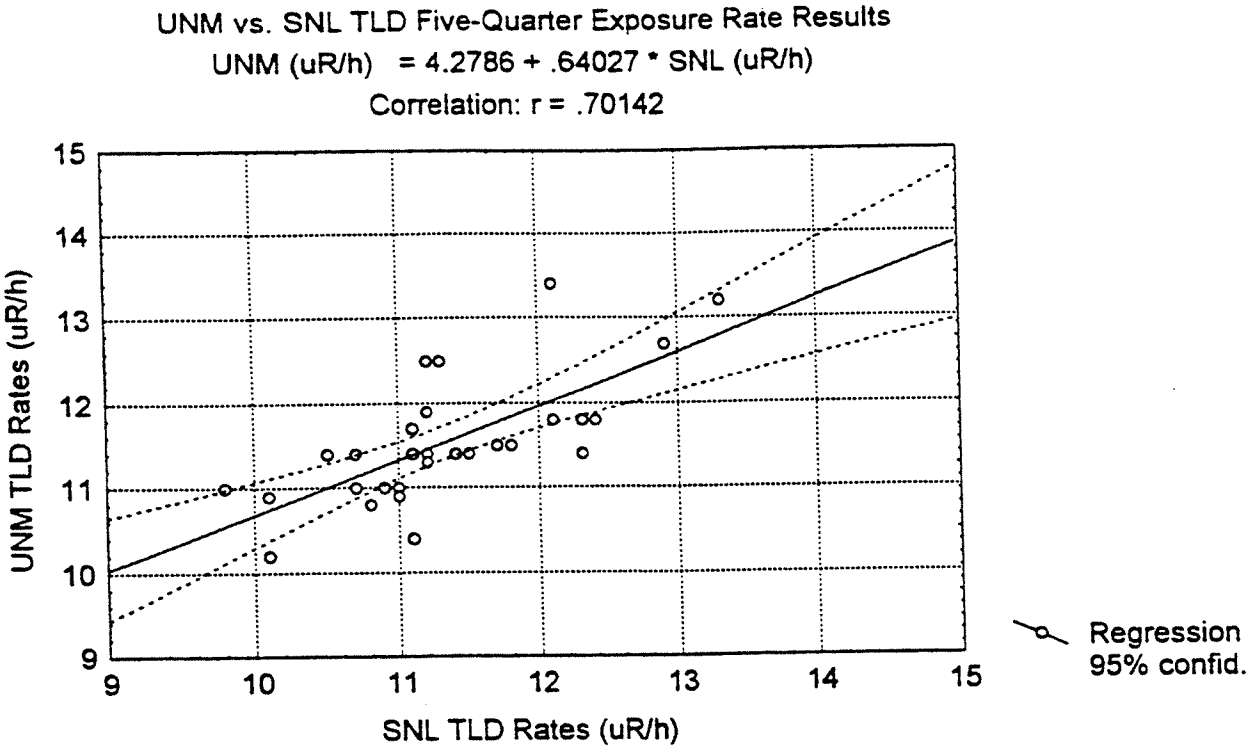

Figure 88

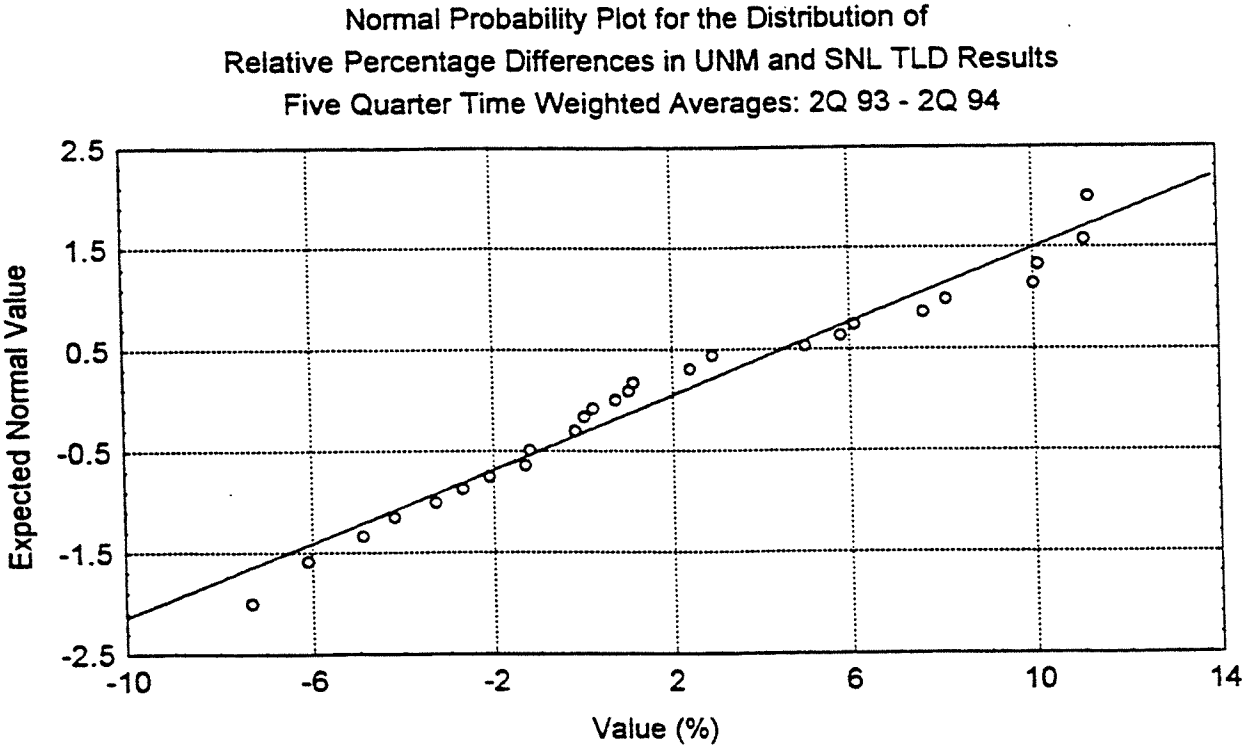

Figure 89

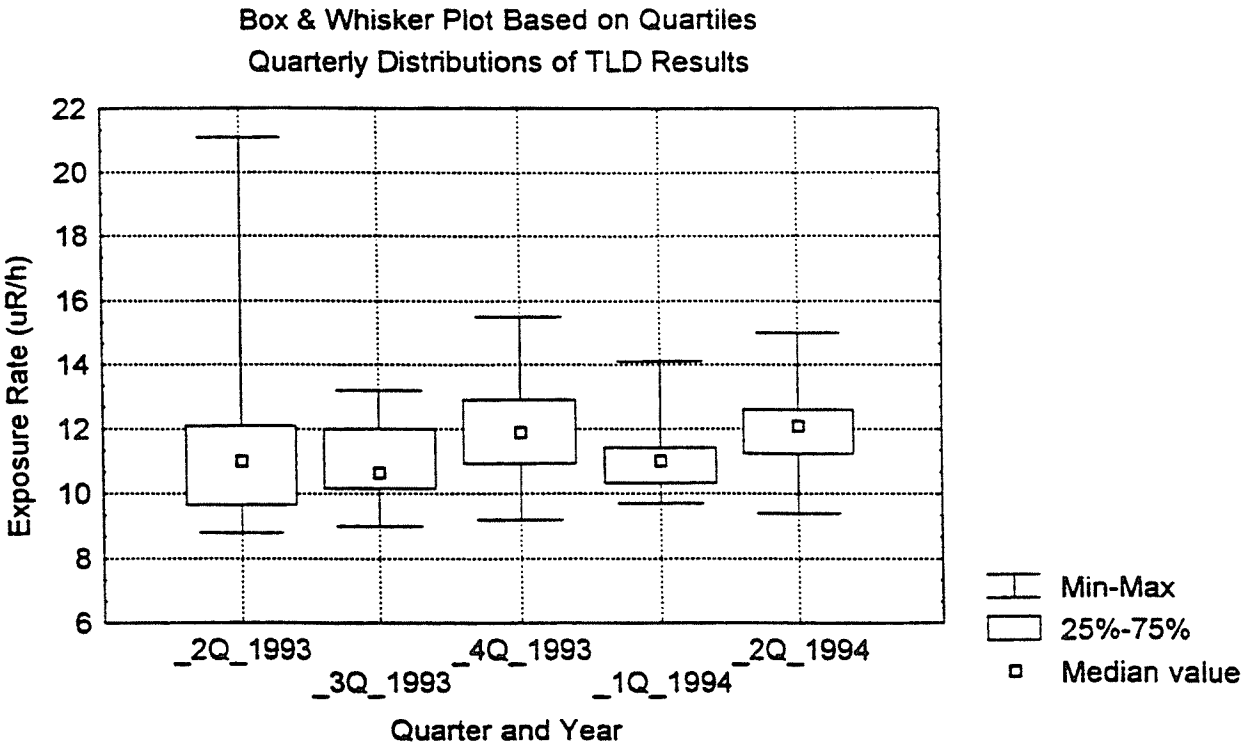

Figure 90

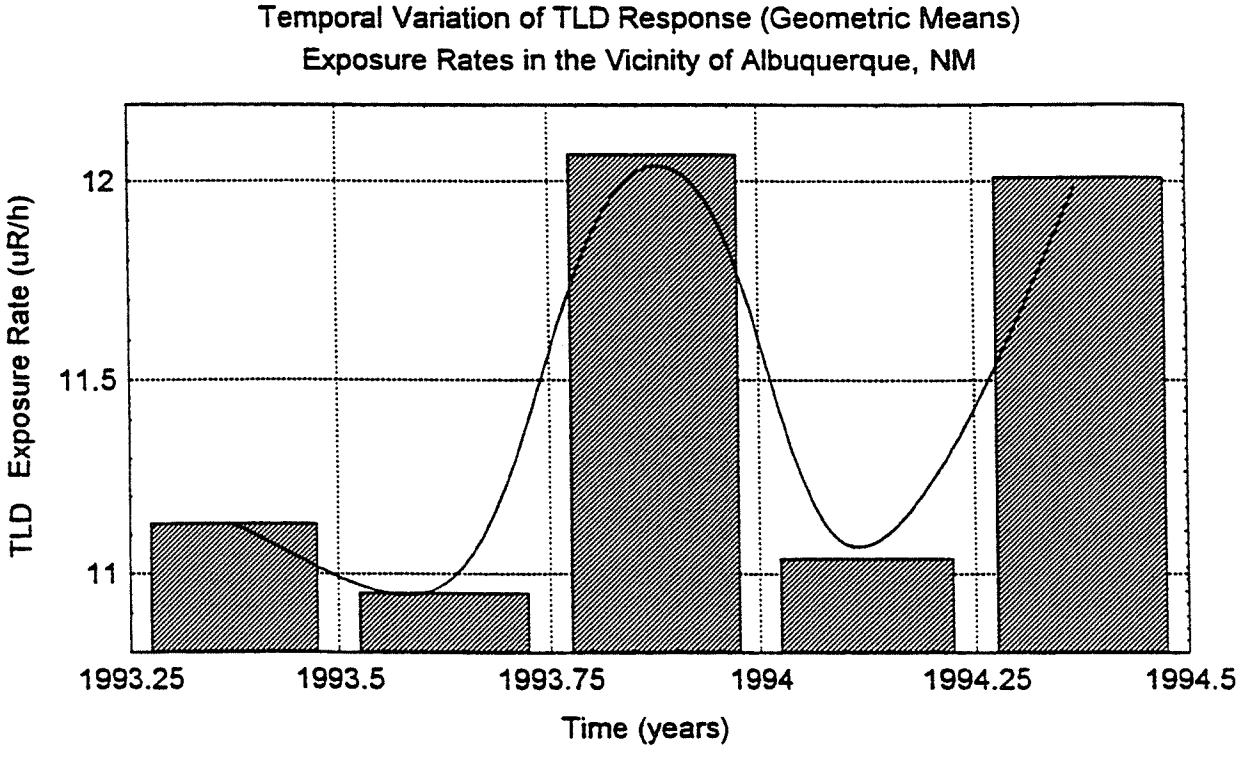

means over time is within that value ascribed to all sources of natural variability, and thus may not be sufficiently great to be of further instructive value in discerning temporal trends (123). A study of longer term using integrating and real time exposure rate measurement at variety of locations could be performed to further evaluate temporal trends.

4. CONCLUSIONS

Information regarding the distribution of environmental radiation and radioactivity in the vicinity of Albuquerque, NM was generated through a concerted, multi-media sampling and monitoring effort spanning two years. In the process of analysis, distinct trends emerged with respect to the spatial distribution of natural and man-made radionuclides. It became apparent that ^{137}Cs soil activities are disparately elevated in the easternmost portion of the study region and show a close relationship to altitude. Research into meteorological trends revealed a mechanism for the disparate findings. Although the majority of weapons test fallout certainly approached the Albuquerque Basin from its origin at the Nevada Test Site to the west, higher rainfall in the east would promote greater wet deposition of atmospheric materials in the eastern highlands and slopes of the mountain ranges that bound the eastern extreme of the basin. This finding is contrary to the experience of altitude controlled deposition patterns on the western slopes of the Rocky Mountains north of the New Mexico, as impacted by Nevada Test Site fallout. The occurrence of uraniferous geological deposits in the eastern portion of the study region also appear to contribute to higher soil activities of uranium and thorium series nuclides and elevated exposure rates. The overall variations in radionuclide soil activities were generally reflected in the regional distributions of free-air exposure rates measured at a height of one meter from ground surface.

Typical numerical values and ranges for radionuclides in soil and *in situ* exposure rate measurements were evaluated. Geometric and harmonic means for the measurement parameters over the entire study area follow: ^{226}Ra, 1.15 and 1.12 pCi/g; ^{214}Bi, 1.19 and 1.16 pCi/g; ^{235}U, 0.06 pCi/g (both) ; ^{238}U, 1.80 and 1.65 pCi/g; ^{232}Th, 1.40 and 1.37 pCi/g; ^{40}K, 15.5 and 15.3 pCi/g; ^{137}Cs, 0.18 and 0.14 pCi/g; TLD Rates, 11.4 μR/h (both); and HPIC rates 13.0 μR/h (both). The values for ^{238}U and ^{232}Th series nuclides, as well as ^{137}Cs and exposure rates were higher on the slopes of the Sandia and Manzano Mountains and Central Highlands than in the Albuquerque Basin. These observations are associated with elevated concentrations of the primordial radionuclides in source rocks and to the effects of meteorology. ^{40}K maxima were associated with the western foothills and bajadas. This appears to have been the result of mountain front outwash of debris from potassium rich igneous rocks. Ranges for the basin up to the western escarpment of the mountain ranges follow: ^{226}Ra and ^{214}Bi, 0.8-1.4 pCi/g; ^{235}U, $\leq$0.05-0.0.06 pCi/g; ^{238}U, 0.9-1.9 pCi/g; ^{232}Th, 1.0-1.5 pCi/g; ^{40}K, 9.9-17.6 pCi/g; ^{137}Cs 0.06-0.4 pCi/g; TLD Rates, 10-12 μR/h; and HPIC rates 11-14 μR/h. Ranges for the mountains and highlands follow: ^{226}Ra and ^{214}Bi,

1.3-2.7 pCi/g; ^{235}U, 0.07-0.12 pCi/g; ^{238}U, 2.3-3.3 pCi/g; ^{232}Th, 1.7-2.2 pCi/g; ^{40}K, 13.2-15.4 pCi/g; ^{137}Cs 0.5-3.5 pCi/g; TLD rates, 10-13.5 μR/h; and HPIC rates 11-18 μR/h.

An important overall finding suggested by the results of this study was that background exposure rates and concentrations of radionuclides sampled and monitored at locations outside the eastern boundary of the Albuquerque Basin do not reflect the range of background conditions observed within the basin, where area nuclear facilities are sited. This would not necessarily detract from the value of continued monitoring of those locations. They represent important local indicators of potential impacts of nuclear facilities and events in the vicinity of Albuquerque and beyond. However, caution is urged in the interpretation of results. If used as background values to evaluate residual radionuclide contamination from basin sources, they would exhibit positive bias and suggest a higher than actual background. The results of our study showed good general agreement with the results of a wide variety of local to global investigators. The regional and statistical distributions generated may provide a practical area database for additional investigations, including those associated with the decommissioning of nuclear facilities and remediation of environmental contamination sites in the vicinity of Albuquerque, New Mexico.

5. REFERENCES

(1) Huffert, A.M., et al; "Background as a Residual Criterion for Decommissioning; Appendix A to the Generic Environmental Impact Statement in Support of Rulemaking on Radiological Criteria for Decommissioning of NRC-Licensed Facilities"; NUREG-1501 (1994)

(2) 40 CFR 195: "Radiation Site Cleanup Regulations; Advance Notice on Proposed Rulemaking"; Federal Register 58(202)54474-54476; (1993)

(3) USEPA; "Issues Paper on Radiation Site Cleanup Regulations"; United States Environmental Protection Agency Office of Radiation and Indoor Air; EPA 402-R-93-084 (1993)

(4) City of Albuquerque: "Radioactive Discharges to the City of Albuquerque Wastewater System", Report of the Radioactive Waste Discharge Policy Study Group; Albuquerque Wastewater Utility Division (1994)

(5) NMEIB: "New Mexico Radiation Protection Regulations"; New Mexico Environment Department: EIB/RPR 1 (1989)

(6) U.S. Air Force 377th Air Base Wing: "Relative Risk Evaluation Worksheets; KAFB Active IRP Sites (1995)

(7) USDOE: "Comprehensive Environmental Assessment and Response Program; Phase I: Installation Assessment, Sandia National Laboratories - Albuquerque (1987)

(8) USDOE: "Environmental Restoration Program Reconnaissance Data Report, Sandia National Laboratories Albuquerque" (1987)

(9) SNL: "Environmental Restoration Program Proposed List of Solid Waste Management Units Table 2, Module IV RCRA Part B Permit (HSWA Module) and Supporting Information"; Sandia National Laboratories Albuquerque (1993)

(10) ITRI: "Assessment Plan, Hot Ponds: ADS #ALIT-1015" and "Assessment Plan, Lagoons and Groundwater: ADS #ALIT-1019"; Inhalation Toxicology Research Institute (1992)

(11) USDOE; "Environmental Assessment of Medical Isotope Production at Sandia National Laboratories/New Mexico and Los Alamos National Laboratory" Vols. I &II; U. S. Department of Energy, Albuquerque Operations (1995)

(12) Manchego, R. A., et al; "New Mexico Radon Survey, 1987-1989"; New Mexico Environment Department and New Bureau of Mines and Mineral Resources (1991)

(13) Berge, L. A.; "A New Mexico Wellhead Survey on the Occurrence of Radon-222 at Public Water Supplies", An Open Report to Public Water Supply Systems, New Mexico Department of Health Scientific Laboratory Division (1994)

(14) Brookins, D. G.; "Background Radiation in the Albuquerque, New Mexico, U.S.A., Area" *Environ. Geol. Water Sci.* 19(1):11-15; 1992

(15) Brookins, D. G.; "Indoor and Soil Rn Measurements in the Albuquerque, New Mexico, Area" *Health Physics* 51(4):529-533 (1986)

(16) Gilbert, R.O. ; Statistical Methods for Environmental Pollution Monitoring; Van Nostrand Reinhold, New York (1987)

(17) Berge, L. A. and Lusk, J. C.; "Analytic Report Regarding Roadside Sampling by EID-Special Waste"; Radiochemistry, Scientific Laboratory Division (1990)

(18) Kelley, V. C.; "Geology of Albuquerque Basin, New Mexico", New Mexico Bureau of Mines and Mineral Resources: Memoir 33 (1977)

(19) Hawley, J. W., et al.; "Hydrogeological Framework for the Northern Albuquerque Basin", New Mexico Bureau of Mines and Mineral Resources: Open File Report 387 (1992)

(20) Lozinsky, R. P., et al.; "Geologic Overview and Pliocene-Quaternary History of the Albuquerque Basin, Central New Mexico", New Mexico Bureau of Mines and Mineral Resources: Bulletin 137 (1991)

(21) Lozinsky, R. P. and Tedford, R. H., "Geology and Paleontology of the Santa Fe Group, Southwestern Albuquerque Basin, Valencia County, New Mexico", New Mexico Bureau of Mines and Mineral Resources: Bulletin 132 (1991)

(22) Logan, L. M.; "Geochemistry of the Albuquerque Municipal Area, Albuquerque, New Mexico", Independent Study, New Mexico Institute of Mining and Technology, Socorro, NM (1990)

(23) Thorn, C. R., et al; "Geohydrologic Framework and Hydrologic Conditions in the Albuquerque Basin, Central New Mexico", U.S. Geological Survey Water-Resources Investigation Report 93-4149 (1993)

(24) 10 CFR 100; "Reactor Site Criteria; Appendix A: Seismic and Geologic Siting Criteria for Nuclear Power Plants" (1993)

(25) Reiche, P.; "Geology of the Manazanita and North Manzano Mountains, New Mexico"; Geologic Society of America Bulletin 60(7):1183-1212 (1949)

(26) Machette, M. N.; "Quaternary and Pliocene Faults in the La Jencia and Southern Part of the Albuquerque-Belen Basins, New Mexico: Evidence of Fault History from Fault-Scarp Morphology and Quaternary Geology"; New Mexico Geologic Society, 33rd Field Conference Guidebook; pp. 161-169 (1982)

(27) Sanford, A. R., et al; "Seismicity of the Rio Grande Rift in New Mexico"; Ch. 12 in Neotectonics of North America; The Geologic Society of America, Boulder (1991)

(28) Northrop, S. A.; "Earthquakes of Albuquerque Country"; New Mexico Geologic Society, 33rd Field Conference Guidebook; pp. 171-178 (1982)

(29) Stover, C. W., et al.; "Seismicity Map of the State of New Mexico"; U.S. Geologic Survey Map MF-2035 (1988)

(30) Algermissen, S. T., et al.; "Probabilistic Earthquake Acceleration and Velocity Maps for the United States and Puerto Rico"; U.S. Geologic Survey Map MF-2120 (1990)

(31) Machette, M. N.; "Calcic Soils of the Southwestern United States"; Geological Society of America , Special Paper 203 (1985)

(32) Machette, M. N.; "Dating Quaternary Faults in the Southwestern United States Using Buried Calcic Paleosols"; *Jour. Research U.S. Geol. Survey* 6(3):369-381 (1978)

(33) U.S. Geologic Survey 7.5 Minute Series Topographic Map: Alameda, NM Quadrangle AMS 4654 II NE - Series V881 (1972)

(34) U.S. Geologic Survey 7.5 Minute Series Topographic Map: Albuquerque East, NM Quadrangle AMS 4654 II SE - Series V881(1972)

(35) U.S. Geologic Survey 7.5 Minute Series Topographic Map: Albuquerque West, NM Quadrangle AMS 4654 II SW - Series V881 (1972)

(36) U.S. Geologic Survey 7.5 Minute Series Topographic Map: Escabosa, NM Quadrangle AMS 4753 IV NE - Series V881 (1972)

(37) U.S. Geologic Survey 7.5 Minute Series Topographic Map: Hubble Spring, NM Quadrangle AMS 4653 I NE - Series V881 (1974)

(38) U.S. Geologic Survey 7.5 Minute Series Topographic Map: Isleta, NM Quadrangle AMS 4653 II NW - Series V881 (1972)

(39) U.S. Geologic Survey 7.5 Minute Series Topographic Map: Los Lunas, NM Quadrangle AMS 4653 I SW - Series V881 (1972)

(40) U.S. Geologic Survey 7.5 Minute Series Topographic Map: Los Lunas SE, NM Quadrangle AMS 4653 I SE - Series V881 (1972)

(41) U.S. Geologic Survey 7.5 Minute Series Topographic Map: Sandia Crest, NM Quadrangle AMS 4754 III NW - Series V881 (1972)

(42) U.S. Geologic Survey 7.5 Minute Series Topographic Map: Sandia Park, NM Quadrangle AMS 4754 III NE - Series V881 (1972)

(43) U.S. Geologic Survey 7.5 Minute Series Topographic Map: Sedillo, NM Quadrangle AMS 4754 III SE - Series V881 (1972)

(44) U.S. Geologic Survey 7.5 Minute Series Topographic Map: Tijeras, NM Quadrangle AMS 4754 III SW - Series V881 (1972)

(45) Kelley, V. C.; "Albuquerque, its Mountains, Valley, Water and Volcanoes"; (3rd ed.) New Mexico Bureau of Mines and Mineral Resources, Scenic Trips to the Geologic Past 9 (1982)

(46) USDA: "Soil Survey of Bernalillo County and Parts of Sandoval and Valencia County, New Mexico"; U.S. Department of Agriculture Soil Conservation Service (1977)

(47) Myers, D. A. and McKay, E. J.; "Geologic Map of the Mount Washington Quadrangle, Bernalillo and Valencia Counties, New Mexico"; U.S. Geologic Survey Map I-968 (1970)

(48) Myers, D. A. and McKay, E. J.; "Geologic Map of the North End of the Manzano Mountains, Tijeras and Sedillo Quadrangles, Bernalillo County, New Mexico"; U.S. Geologic Survey Map GQ-886 (1976)

(49) NPDES Storm Water Permit Application for Sandia National Laboratory, New Mexico, October 1992 (1992)

(50) Tuan, Y-F. , et al.; "The Climate of New Mexico", State of New Mexico Planning Office, Santa Fe (1973)

(51) Kunkel, K. E.; "General Climatology" in Waltemeyer, S. D., and Gold, R. L.; "National Water Summary 1988-1989 - Floods and Droughts: New Mexico"; U.S. Geological Survey Water Supply Paper 2375 (1989)

(52) NOAA: "Local Climatological Data: Albuquerque, NM National Weather Service Office", Monthly Summaries of the National Climatic Data Center, Asheville, North Carolina (1981-1993)

(53) Brown, D. E.; "Biotic Communities of the American Southwest - United States and Mexico", in Desert Plants, University of Arizona (1982)

(54) Sivinski, R. and Lightfoot, K.; "Inventory of Rare and Endangered Plants of New Mexico" New Mexico Forestry and Resources Conservation Division, Santa Fe (1992)

(55) SAND90-7098: UC-630; "Revision of Species Inventory Checklists for Sandia National Laboratories, Albuquerque, Bernalillo County, New Mexico, Final Report" (1990)

(56) U.S. Department of Commerce: "1990 Census of Population and Housing; Summary Population and Housing Characteristics, New Mexico"; 1990 CPH-1-33, Washington, DC (1991)

(57) USDA: "New Mexico Agricultural Statistics", U.S. Department of Agriculture, Las Cruces, NM (1988)

(58) SNL: "Sandia National Laboratories, Albuquerque Environmental Monitoring Plan"; prepared for Sandia National Laboratories by IT Corporation (1993)

(59) Riedhauser, S. R.; "An Aerial Radiological Survey of the Sandia National Laboratories and Surrounding Area"; EG&G Energy Measurements for the U. S. Department of Energy; EGG 11265-1030·UC-702

(60) Barth, D.S., and Mason, B.J.; "Soil Sampling Quality Assurance Users Guide"; U.S. Environmental Protection Agency Environmental Systems Monitoring Laboratory; EPA/600/4-84-043 (1984)

(61) AEC Regulatory Guide 4.5; "Measurements of Radionuclides in the Environment-Sampling and Analysis of Plutonium in Soil"; U.S. Atomic Energy Commission (1974)

(62) USEPA: "Characterization Protocol for Radioactive Contaminated Soils" U.S. Environmental Protection Agency, Office of Solid Waste and Emergency Response, 9380.1-10FS (1992)

(63) van Ee, J. J., et al; "A Rationale for the Assessment of Errors in the Sampling of Soils"; U.S. Environmental Protection Agency Environmental Systems Monitoring Laboratory; EPA/600/4-90/013 (1990)

(64) Watson, J. E. (Chair); "Upgrading Environmental Radiation Data", Health Physics Society Committee Report HPSR-1 (1980); EPA 520/1-80-012;(1980)

(65) Velasco, R. H., et al; "Vertical Transport of Radiocesium in Surface Soils: Model Implementation and Dose-Rate Computation"; *Health Physics* 66(1):36-42 (1994)

(66) Bonazzola, C., et al; "Profiles and Downward Migration of Cs-134 and Ru-106 Deposited on Italian Soils After the Chernobyl Accident"; *Health Physics* 64(5):479-484 (1993)

(67) Kirikopoulos, I. L., et al; "Kinetics of Radiocesium Sorption in Lake Sediments" *Health Physics* 66(1):36-42 (1993)

(68) Salbu, B., et al; "The Mobility of ^{137}Cs and ^{90}Sr in Agricultural Soils in the Ukraine, Belarus, and Russia, 1991"; *Health Physics* 67(5): 518-528 (1994)

(69) Carlton, W. H., et al; "Radiocesium in the Savannah River Site Environment" *Health Physics* 67(3):233-244 (1994)

(70) Schuller, P., et al; "^{137}Cs Concentration in Soil, Prairie Plants and Milk from Sites in Southern Chile"; *Health Physics* 64(2):157-161 (1993)

(71) McArthur, R. D., and Miller, F. L.; "Off-Site Radiation Exposure Project Phase II Soils Program"; Desert Research Institute-Water Resources Center, University of Nevada; DOE/NV/10384-23 Rev (1989)

(72) Mortveldt, J.J.; "Plant and Soil Relationships of Uranium and Thorium Decay Series Radionuclides-A Review"; *J. Environ. Qual.* 23:643-650 (1994)

(73) Popp, C. J., et al; "Radionuclide and Heavy Metal Distribution in the 20th Century Sediments of Major Streams in the Eastern Part of the Grants Uranium Region, New Mexico" in "*Proceedings of a Symposium on Water Quality and Pollution in New Mexico*", New Mexico Bureau of Mines and Mineral Resources Hydrologic Report 7, pp. 34-48(1984)

(74) Popp, C. J., et al; "Use of Radiometric (Cs-137, Pb-210), Geomorphic, and Stratigraphic Techniques to Date Recent Oxbow Sediments in the Rio Puerco Drainage Grants Uranium Region, New Mexico" *Environ. Geol. Water Sci.* 11(3):253-269 (1988)

(75) Johns, F. B., et al (Eds.); "Radiochemical Analytical Procedures for Analysis of Environmental Samples"; U.S. Environmental Protection Agency, Environmental Monitoring and Support Laboratory; EMSL-LV-0539-17 (1979)

(76) Krieger, H.L. and Whittaker, E. L.; "Prescribed Methods for Measurement of Radioactivity in Drinking Water"; U.S. Environmental Protection Agency; EPA-600/4-80-032 (1980)

(77) Chieco, N. (Ed.); "EML Procedures Manual"; U.S. Department of Energy Environmental Measurements Laboratory, 27th Edition, Volume 1; HASL-300 (1992)

(78) NCRP 50: Environmental Radiation Measurements; Recommendations of the National Council on Radiation Protection and Measurements (1985)

(79) NCRP 58: A Handbook Of Radioactivity Measurement Procedures; Recommendations of the National Council on Radiation Protection and Measurements (1985)

(80) Van Cleef, D. J.; "Determination of ^{226}Ra in Soil Using ^{214}Pb and ^{214}Bi Immediately After Sealing"; *Health Physics* 67(3):288-289 (1994)

(81) USDOE: "Final Report, Surface Gamma Radiation Surveys for Sandia National Laboratories/New Mexico Environmental Restoration Project"; (figures modified) RUST Geotech for the U.S. Department of Energy (1994)

(82) Heath, R.L.; "Gamma-Ray Spectrum Catalogue, Ge(Li) and Si(Li) Spectrometry"; 3rd Edition, Volume 2; Aerojet Nuclear Company for the U.S. Atomic Energy Commission: ANCR-1000-2 (1974)

(83) Reus, U. and Westmeier, W.; "Catalog of Gamma-Rays from Radioactive Decay, Parts I and II"; *Atomic Data and Nuclear Data Tables* 29(1); (1983)

(84) Walker, W., et al; "Nuclides and Isotopes"; 14th Edition, General Electric Nuclear Company, San Jose (1989)

(85) Slater, D. N.; "Gamma Rays in Order of Increasing Energy"; Butterworths, Washington (1962)

(86) USDHEW; "Radiological Health Handbook"; U.S. Department of Health, Education and Welfare - Public Health Service Publication 2016 (1970)

(87) Shleien, B. (Ed.); The Health Physics and Radiological Health Handbook; Revised Edition, Scinta, Inc., Silver Spring (1992)

(88) Currie, L. A.; "Lower Limit of Detection: Definition and Elaboration of a Proposed Position for Radiological Effluent and Environmental Measurements", National Bureau of Standards; NUREG/CR-4007 (1984)

(89) Miller, K. M., et al; "*In-Situ* Gamma-Ray Spectrometry for the Measurement of Uranium in Surface Soils"; *Health Physics* 67(2):140-150 (1994)

(90) Brune, D., et al; "Improvements in Applied Gamma-Ray Spectrometry by Germanium Semi-Conductor Detector"; *Nukleonik* 7(8): 484-488 (1965)

(91) Mukoyama, T.; "Fitting of Gaussian to Peaks by Non-iterative Method"; *Nuclear Instruments and Methods* 125: 289-291 (1975)

(92) Sasamoto, N., et al; "An Analysis Method of Gamma-Ray Pulse-Height Distributions Obtained with a Ge(Li) Detector"; *Nuclear Instruments and Methods* 125: 507-523 (1975)

(93) Portal, G.; "Preparation and Properties of Principal TL Products"; in Applied Thermoluminescence Dosimetry, pp. 97-123; Adam Hilger Ltd, Bristol (1981)

(94) Busuoli, G.; "General Characteristics of TL Materials"; in Applied Thermoluminescence Dosimetry, pp. 83-95; Adam Hilger Ltd, Bristol (1981)

(95) Piesch, E., G.; "Application of TLD Systems for Environmental Monitoring"; in Applied Thermoluminescence Dosimetry, pp. 197-224; Adam Hilger Ltd, Bristol (1981)

(96) ANSI N545-1975: "Performance, Testing, and Procedural Specifications for Thermoluminescent Dosimetry (Environmental Applications)", American National Standards Institute, New York (1975)

(97) de Planque, G.: "Evaluation of Methods for the Determination of X- and Gamma-Ray Exposures Attributable to a Nuclear Facility Using Environmental TLD Measurements", U.S. Department of Energy for the U. S. Nuclear Regulatory Commission, NUREG/CR-0711, EML-355 (1979)

(98) Struckmeyer, R., and McNamara, N.; "NRC TLD Direct Radiation Monitoring Network", Progress Report, U.S. Nuclear Regulatory Commission, NUREG-0837,(12)4; (1993)

(99) Eisenhower, E. H., et al; "Quality Assurance for Measurements of Ionizing Radiation, Annual Report for FY 1981"; National Bureau of Standards for the U.S. Nuclear Regulatory Commission, NUREG/CR-2560 (1982)

(100) Eisenhower, E. H., et al; "Quality Assurance for Measurements of Ionizing Radiation, Annual Report for FY 1982"; National Bureau of Standards for the U.S. Nuclear Regulatory Commission, NUREG/CR-312 (1983)

(101) Panasonic: "Service Manual, Model TLD Reader UG-716AGL" and "Technical Information on Panasonic TLD"; Matushita Electric Industrial Co., Ltd., TLB-R16-A01 (1989)

(102) Thompson, D.J.; "Description and Procedures of the Environmental Radiation Dosimetry Program", Sandia National Laboratories, SAND-1916·UC-41 (1987)

(103) Lewis, W. T.; "Operation of the Gamma and Neutron Source Range Facility", Activity Specific ES&H Operating Procedure, SP472288 Issue A, Sandia National Laboratories Organization 7715 (1992)

(104) NCRP 94: Exposure of the Population in the United States and Canada from Natural Background Radiation; Recommendations of the National Council on Radiation Protection and Measurements (1987)

(105) ICRU 22: Measurement of Low-level Radioactivity; Recommendations of the International Commission on Radiation Units and Measurements (1972)

(106) NCRP 57: Instrumentation and Monitoring Methods for Radiation Protection; Recommendations of the National Council on Radiation Protection and Measurements (1978)

(107) De Campo, J. A., et al; "High Pressure Ionization Chamber Systems for the Measurement of Environmental Radiation Exposure Rates"; U.S. Atomic Energy Commission, Health and Safety Laboratory, HASL-260 (1972)

(108) Berger, J.; "Manual for Conducting Radiological Surveys in Support of License Termination: Draft Report for Comment"; U.S. Nuclear Regulatory Commission Division of Regulatory Applications, NUREG/CR-5849 (1992)

(109) Reuter-Stokes: "RSS-112 PIC Environmental Radiation Monitoring Station Operating Manual", Version 1.5; Reuter-Stokes, Twinsburg, OH (1991)

(110) Porstendorfer, J., et al; "Daily Variations of the Radon Concentration Indoors and Outdoors and the Influence of Meteorological Parameters"; *Health Physics* 67(3):283-287 (1994)

(111) Grasty, R. L.; "Summer Outdoor Radon Variations and their Relationship to Soil Moisture" *Health Physics* 62(2):185-193 (1993)

(112) Morris, R. C. and Fraley, L.; "Soil Permeability as a Function of Vegetative Type and Soil Water Content" *Health Physics* 66(6): 691-698 (1994)

(113) Brutsaert, W.; Evaporation into the Atmosphere; Theory, History, and Applications; D. Reidel, Dordrecht (1982)

(114) Harbeck, G. E.; "A Practical Field Technique for Measuring Reservoir Evaporation Using Mass-Transfer Theory"; U. S. Geological Survey Professional Paper 272-E (1962)

(115) Brisson, N., and Perrier, A.; "A Semiempirical Model of Bare Soil Evaporation for Crop Simulation Models" *Water Res Research* 27(5):719-727 (1991)

(116) Knapp, H. V.; "Evaporation and Transpiration", in Handbook of Applied Meteorology, D.D. Houghton (Ed), pp 537-554; John Wiley and Sons, New York (1985)

(117) Danali-Cotsaki, S., and Margomenou-Leonidopoulou; "^{222}Rn in Greek Spa Waters: Correlation with Rainfall and Seismic Activities"; *Health Physics* 64(6):605-612 (1993)

(118) Lide, D. R. (Ed.); CRC Handbook of Chemistry and Physics, 73rd edition, CRC Press, Boca Raton (1992)

(119) Ahluwalia, H. S.; "Cosmic Ray Modulation Near the Onset and Maximum Phases of the Solar Activity Cycle 22" *Planet. Space Sci* 40(9):1227-1234; (1992)

(120) Ahluwalia H. S.; "Solar Polar Field Reversals and Secular Variation of Cosmic Ray Intensity" in Solar and Interplanetary Dynamics, M. Dryer and E. Tandberg-Hansen, Eds., pp. 79-86 (1980)

(121) Ahluwalia, H. S.: "Solar Activity and the Natural States of the Heliosphere"; International Union of Pure and Applied Physics, 21st International Cosmic Ray Conference, 6.1-3:5-8 (1990)

(122) National Oceanic and Atmospheric Administration-National Geophysical Data Center E/GC2; Telecommunication Information Sheet: Monthly Mean 2800 MHz Solar Radio Flux, Sunspot Numbers and Climax Cosmic Ray Data 1983-1993 (1993)

(123) Spiers, F. W., et al; "A Guide to the Measurement of Environmental Gamma-Ray Dose Rate"; British Committee on Radiation Units and Measurements (BCRU) (1991)

(124) ASTM: "Standard Recommended Practice for Dealing with Outlying Observations" ASTM E178-75 (1975)

(125) Grubbs, F. E., and Beck, G; "Extension of Sample Sizes and Percentage Points for Significance Testing of Outlying Observations" *Technometrics* 14(4):847-854; (1972)

(126) Ott, L.; An Introduction to Statistical Methods and Data Analysis; Duxbury Press, North Scituate (1977)

(127) Gilbert, R. O., and Kinnison, R. R.; "Statistical Methods for Estimating the Mean and Variance from Radionuclide Data Sets Containing Negative, Unreported, or Less-than Values" *Health Physics* 40(3): 377-390; (1981)

(128) Shankar, A. S., and Thompson, J.J.; "Site Environmental Monitoring Report-1989"; Inhalation Toxicology Research Institute, Albuquerque, NM (1990)

(129) Shankar, A. S., and Thompson, J.J.; "Site Environmental Monitoring Report-1990"; Inhalation Toxicology Research Institute, Albuquerque, NM (1991)

(130) Bennett, W. C., et al; "Site Environmental Monitoring Report-1991"; Inhalation Toxicology Research Institute, Albuquerque, NM (1992)

(131) UNSCEAR 1988: United Nations Scientific Committee on the Effects of Atomic Radiation: "Sources, Effects and Risks of Ionizing Radiation", Report to the General Assembly. United Nations: New York (1988)

(132) Quindós, L. S., et al; "Natural Radioactivity in Spanish Soils" *Health Physics* 66(2): 194-200 (1994)

(133) Ibrahiem, N. M., et al; "Measurement of Radioactivity Levels in Soil in the Nile Delta and Middle Egypt" *Health Physics* 64(6):620-627 (1993)

(134) Wollenberg, H. A., et al, "Application of Airborne Gamma Spectrometric Survey Data to Estimating Terrestrial Gamma-Ray Dose Rates: an Example in California" *Health Physics* 64(1):10-16 (1994)

(135) Purtymun, W. et al; "Background Concentrations of Radionuclides in Soils and River Sediments in Northern New Mexico, 1974-1986" Los Alamos National Laboratory: La-111134-MS UC-11 (1987)

(136) USDOE: "National Uranium Resource Evaluation (NURE) Data for the Albuquerque 2° Quadrangle; Stream Sediment", Bendix Grand Junction Operations (1984)

(137) McLemore, V. T., and Chenoweth, W. L.; "Uranium Resources in New Mexico" New Mexico Bureau of Mines and Mineral Resources Resource Map 18 (1989)

(138) McLemore, V. T.; "Uranium and Thorium Occurrences in New Mexico: Distribution, Geology, Production, and Resources"; New Mexico Bureau of Mines and Mineral Resources Open File Report 183 (1983)

(139) Brookins, D. G. and Della Valle, R. S.; "Uranium Abundance in Some Precambrian and Phanerozoic Rocks from New Mexico"; pp. 353-362 in Rocky Mountain Association of Geologists' Guidebook to the 1977 Field Conference (1977)

(140) Dragun, J.; The Soil Chemistry of Hazardous Materials; Hazardous Materials Control Research Institute, Silver Spring, MD (1988)

(141) Ames, L. L., and Dhanpat, R.; "Radionuclide Interactions with Rock and Soil Media; Volume 1: Processes Influencing Radionuclide Mobility and Retention"; EPA 520/6-78-007 (1978)

(142) Berge, L. A., "Is the Assumption for a U-234:U-238 Ratio = 1.0 Valid for Common Groundwater", New Mexico Scientific Laboratory Division; presented at the 34th Annual Conference on Bioassay, Analytical and Environmental Radiochemistry, Las Vegas (1988)

(143) US DHEW, Public Health Service: "Environmental Contamination by Radioactive Substances" Report to the Director, National Center for Radiological Health (1967)

(144) NCRP 52: Cesium-137 from the Environment to Man: Metabolism and Dose; Recommendations of the National Council on Radiation Protection and Measurements (1977)

(145) NCRP 76: Radiological Assessment: Predicting the Transport, Bioaccumulation, and Uptake by Man of Radionuclides Released to the Environment; Recommendations of the National Council on Radiation Protection and Measurements (1985)

(146) Hofmann, W., et al; "Cs-137 Concentrations in Lichens Before and After the Chernobyl Accident" *Health Physics* 64(1):70-73 (1993)

(147) Åhman, B. and Åhman, G.; "Radiocesium in Swedish Reindeer after the Chernobyl Fallout; Seasonal Variations and Long-Term Decline" *Health Physics* 66(5):503-512 (1994)

(148) Kirchner, G.; "Transport of Iodine and Cesium Via the Grass-Cow-Milk Pathway After the Chernobyl Accident" *Health Physics* 66(6):653-665 (1994)

(149) Fabbri, S., et al; "Transfer Kinetics of ^{90}Sr, ^{134}Cs and ^{137}Cs from Forage Contaminated by Chernobyl Fallout to Milk of Cows" *Health Physics* 66(4):375-379 (1994)

(150) Hoshi, M., et al; "Fallout Radioactivity in Soil and Food Samples in the Ukraine: Measurements of Iodine, Plutonium, Cesium and Strontium Isotopes" *Health Physics* 67(2):187-191 (1994)

(151) Bunzl, K., et al; "Residence Times of Global Weapons Testing Fallout ^{237}Np in a Grassland Soil Compared to $^{239+240}Pu$, ^{241}Am, and ^{137}Cs" *Health Physics* 68(1):89-93 (1995)

(152) Zajic, J. E.; Microbial Biogeochemistry; Ch. 11: "Uranium Biogeochemistry"; Academic Press, New York (1969)

(153) Culp, T. A., et al; "1993 Site Environmental Report, Sandia National Laboratories, Albuquerque, New Mexico"; SAND94-1293·UC-630 (1994)

(154) Culp, T. A., et al; "1992 Site Environmental Report, Sandia National Laboratories, Albuquerque, New Mexico"; SAND93-1448·UC-630 (1993)

(155) Culp, T. A., et al; "1991 Site Environmental Report, Sandia National Laboratories, Albuquerque, New Mexico"; SAND92-0939·UC-630 (1992)

(156) Hwang, S., et al; "1990 Site Environmental Report, Sandia National Laboratories, Albuquerque, New Mexico"; SAND91-0592·UC-630 (1991)

(157) Hwang, S., et al; "1989 Site Environmental Report, Sandia National Laboratories, Albuquerque, New Mexico"; SAND90-0301·UC-630 (1990)

(158) Millard, G., et al; "1988 Site Environmental Report, Sandia National Laboratories, Albuquerque, New Mexico"; SAND89-1368·UC-630 (1989)

(159) Millard, G., et al; "1987 Site Environmental Report, Sandia National Laboratories, Albuquerque, New Mexico"; SAND88-0697·UC-20e (1988)

(160) Millard, G., et al; "1986 Site Environmental Report, Sandia National Laboratories, Albuquerque, New Mexico"; SAND87-0606·UC-20e (1987)

(161) Millard, G. C., et al; "1984 Site Environmental Report, Sandia National Laboratories, Albuquerque, New Mexico"; SAND85-0550·UC-20e (1985)

(162) Millard, G. C., et al; "1983 Site Environmental Report, Sandia National Laboratories, Albuquerque, New Mexico"; SAND84-0429·UC-20e (1984)

(163) Letter to Mr. Lloyd Aker, NMED, December 23, 1994 from A. C. Grace, ITRI; Transmitting Draft ITRI Background Sampling Site Results (1994)

(164) UNSCEAR 1982: United Nations Scientific Committee on the Effects of Atomic Radiation: "Sources, Effects and Risks of Ionizing Radiation", Report to the General Assembly. United Nations: New York (1982)

(165) Joshi, S. R.; "Prediction of Runoff Transport of Fallout ^{90}Sr" *Health Physics* 66(3):253-256 (1994)

(166) Ward, D.; Sandia Environmental TLD Monitoring Program, Interperiod Exposure Reports: Second Quarter 1993 through Second Quarter 1994 (1994)

Appendix I:

Tables

Table 1): Soil Sample Data

Sample Identification			Latitude:	Longitude:	Altitude:	Dry Mass:	Moisture:	Count Time:	Soil	Setting -
Sample Time ID	Facility ID	AIV	Degrees N	Degrees W	Feet > MSL	g	w/w %	Seconds	Type	Geomorph.
9308080945	S19	1	34.9478	106.4596	5935	1448	-	67686.0	Aeol/Alv Sand	Foothill-Fan
9312081630	I1	2	34.9558	106.4937	5700	984	-	24023.6	Aeol/Alv Sand	Foothill-Fan
9312090002	I2	3	34.9545	106.4860	5740	908	-	54835.5	Aeol/Alv Sand	Foothill-Fan
9312091417	I7	4	34.9585	106.4785	5800	1019	-	27315.3	Aeol/Alv Sand	Foothill-Fan
9312091510	I6	5	34.9633	106.4937	5695	1020	-	58432.6	Aeol/Alv Sand	Foothill-Fan
9312091625	I10	6	34.9705	106.4937	5680	993	-	56117.4	Aeol/Alv Sand	Foothill-Fan
9312100003	I3	7	34.9482	106.4828	5750	996	-	25152.2	Aeol/Alv Sand	Foothill-Fan
9312101130	I8	8	34.9482	106.4720	5840	915	-	51541.3	Aeol/Alv Sand	Foothill-Fan
9312101215	I13	9	34.9482	106.4613	5900	1108	-	59106.1	Aeol/Alv Sand	Foothill-Fan
9312120004	I4	10	34.9428	106.4860	5725	1005	-	63609.4	Aeol/Alv Sand	Foothill-Fan
9312131035	I9	11	34.9378	106.4785	5767	995	-	32180.6	Aeol/Alv Sand	Foothill-Fan
9312121145	I14	12	34.9330	106.4708	5800	1025	-	26956.8	Aeol/Alv Sand	Foothill-Fan
9312121450	I11	13	34.9330	106.4937	5680	890	-	25866.4	Aeol/Alv Sand	Foothill-Fan
9312130005	I5	14	34.9585	106.4785	5680	1070	-	27429.1	Aeol/Alv Sand	Foothil-Fan
9312131605	I15	15	34.9258	106.4937	5680	879	-	60234.1	Aeol/Alv Sand	Foothill-Fan
9405051000	S2	16	34.9922	106.5463	5370	1490	0.0436	57577.8	Aeol/Alv Sand	Bajada
9405051049	S2d	17	34.9922	106.5463	5370	1502	0.0033	35500.0	Aeol/Alv Sand	Bajada
9405051218	S52	18	34.9996	106.5418	5380	1287	0.0100	24371.2	Aeol/Alv Sand	Bajada
9405051330	S63	19	35.0177	106.4217	6240	1373	0.0249	60763.8	Sandy loam	Canyon
9405051415	S34	20	35.0062	106.4070	6360	1195	0.0598	15209.5	Sandy loam	Canyon
9405051457	S59	21	35.0485	106.5597	5375	1525	0.0052	90828.7	Aeol/Alv Sand	Bajada-Terrace

Table 2): Soil Sample Data

Sample Identity/Location Values:						Sample/Analysis Characteristics:				
Sample Identification			Latitude:	Longitude:	Altitude:	Dry Mass:	Moisture:	Count Time:	Soil	Setting -
Sample Time ID	Facility ID	AIV	Degrees N	Degrees W	Feet > MSL	g	w/w %	Seconds	Type	Geomorph.
9405051530	S58	22	35.0578	106.5383	5450	1410	0.0055	164149.6	Aeol/Alv Sand	Bajada-Terrace
9405060925	S16	23	35.0432	106.5092	5600	1708	0.0041	95099.2	Sand/DC Granite	Foothills
9405061000	S64	24	35.0398	106.4797	6040	1618	0.0188	58291.1	Sand/DC Granite	Saddle
9405061036	S12	25	35.0196	106.4628	6143	1482	0.0120	246502.6	Sand-Quartzite	Saddle
9405061315	S65	26	35.0545	106.5272	5475	1575	0.0044	76353.8	Aluvial Sands	Saddle-Terrace
9405090925	S33	27	34.9992	106.4708	5850	1232	0.0013	179280.4	AlvSnds-Schist	Canyon
9405091220	S20	28	35.0325	106.5458	5380	1438	0.0062	72697.3	Aluvial Sands	Arroyo-Terrace
9405091300	S46	29	35.0385	106.5410	5410	1450	0.0062	71412.9	Aluvial Sands	Arroyo-Terrace
9405091415	S61	30	35.0365	106.6212	5307	1408	0.0078	81274.2	Aluvial Sands	Valley-Terrace
9405091420	S61d	31	35.0365	106.6212	5307	1412	0.0079	87486.2	Aluvial Sands	Valley-Terrace
9405100930	S8	32	35.1957	106.6440	5005	1510	0.0118	28556.6	Aluvial Sands	River Valley
9405101240	S60	33	35.0218	106.5878	5134	1426	0.0097	80938.7	Alluvial Sands	Arroyo
9405111145	S11	34	34.9040	106.6843	4880	1307	0.0091	87407.8	Alluvial Sands	River Valley
9405120915	S25	35	35.2923	106.4067	6240	1221	0.0833	58761.5	Alluvial Sands	Bajada-Arroyo
9405120940	S68	36	35.2755	106.4092	6500	926	0.2166	86223.8	Humic Loam-LS	Canyon
9405121115	S9	37	35.1008	106.2860	7040	858	0.1883	102931.6	Humic Loam-LS	Canyon
9405121310	S10	38	35.0032	106.3255	7660	1184	0.1766	80440.2	Humic Loam-LS	Intrmont.-Mesa
9405121340	S62	39	34.9812	106.3527	7660	994	0.2554	65915.1	Humic Loam-LS	Eastern Foothill
9405121350	S62d	40	34.9812	106.3527	7660	1002	0.2352	68001.4	Humic Loam-LS	Eastern Foothill
9409176500	S68d	41	35.2755	106.4092	6500	1039	-	27700.8	Humic Loam-LS	Canyon
9409171130	U1	42	35.2102	106.4497	10678	764	-	65721.9	Humic Loam-LS	Sandia Peak

ANTICIPATED NUCLIDE	Table 3): Detection Characteristics		
	Expected Peak Energy keV	Detector Efficiency cpg	Gamma Yield g/dis
X-rays	17-25	ND	1.00E+00
Th-227	50	ND	8.00E-02
Th-234	63.3	ND	6.00E-03
X-ray complex	79-81	3.68E-02	1.00E+00
Ac-227*	122.43	3.38E-02	9.00E-02
Pa-234	131.2	3.10E-02	2.00E-01
Ra-223**	143.85	3.00E-02	1.10E-01
U-235 (40%)	185.7	2.65E-02	5.75E-01
Ra-226 (60%)	186	2.65E-02	4.30E-02
Ac-228***	209.28	2.40E-02	4.43E-02
Pb-212****	238.6	2.17E-02	4.46E-01
Rn-219	272	1.96E-02	8.90E-02
Pb-214	295.09	1.80E-02	1.90E-01
Ac-228	327.97	1.62E-02	3.40E-02
Ac-228	338.296	1.55E-02	1.50E-01
Pb-214	351.9	1.50E-02	3.60E-01
Ac-228	409.4	1.30E-02	2.20E-02
Ac-228	463	1.12E-02	4.60E-02
Pos Annil/Tl-208	511	1.03E-02	2.30E-01
Tl-208	583.1	9.10E-03	8.60E-01
Bi-214	609.3	9.00E-03	4.60E-01
Cs-137	661.7	8.30E-03	8.50E-01
Bi-212	727.264	7.80E-03	7.00E-02
Bi-214	768.45	7.60E-03	4.86E-02
Ac-228	794.928	7.40E-03	4.80E-02
Tl-208	860.53	6.70E-03	1.25E-01
Ac-228	911.1	6.90E-03	2.50E-01
Ac-228	968.9	6.20E-03	2.00E-01
U-238 (234m-Pa)	1001	6.00E-03	8.00E-03
Bi-214	1120.3	5.50E-03	1.50E-01
Bi-214	1238.1	5.40E-03	5.92E-02
Bi-214	1280.97	5.30E-03	1.47E-02
Bi-214	1377.651	4.70E-03	4.10E-02
Bi-214	1385.32	4.60E-03	8.50E-03
Bi-214	1407.99	4.60E-03	2.50E-02
K-40	1462	4.50E-03	1.10E-01
Bi-214	1509.24	4.20E-03	2.19E-02
Ac-228	1587.9	3.80E-03	3.55E-02
Bi-212	1620.6	3.70E-03	1.80E-02
Bi-214	1661.3	3.60E-03	1.14E-02
Bi-214	1729.2	3.50E-03	3.05E-02
Bi-214	1764.51	3.50E-03	1.59E-01
Bi-214(sum)	1847.49	3.50E-03	2.16E-02
Bi-214	2117	3.50E-03	1.21E-02
Bi-214	2204.1	3.50E-03	4.99E-02
Bi-214	2447.71	3.50E-03	1.55E-02
Tl-208	2614.48	3.50E-03	9.98E-01

*Th-231 @ 124, Th-229 @ 124.7 (0.0162), Ra-223 @ 121.22 (0.0012);
**Th-230 @ 144.2 keV (0.007), Ac-227 @ 144.2 keV (0.0327);
***Ac-227 @ 210.7 (0.0112);
**** Ra-224 @ 241 (0.037), Pb-214 @ 241.9 (0.075)

Table 4): Soil Sample Analytical Results
All Concentrations in pCi/g

Nuclide:	Ra-226 @ 186 keV			U-235 @ 185.7 keV			Th-232 @ 238.6 keV			Bi-214 @ 609.3 keV		
Sample/Time ID	Soil Activity Conc.	Standard Deviation (Sigma)	Lower Limit of Detection	Soil Activity Conc.	Standard Deviation (Sigma)	Lower Limit of Detection	Soil Activity Conc.	Standard Deviation (Sigma)	Lower Limit of Detection	Soil Activity Conc.	Standard Deviation (Sigma)	Lower Limit of Detection
9308090945	0.99	0.06	0.09	0.05	0.003	0.005	0.93	0.02	0.01	0.97	0.02	0.02
9312081630	1.34	0.13	0.19	0.07	0.007	0.009	1.63	0.04	0.02	1.31	0.05	0.05
9312090002	1.40	0.09	0.12	0.07	0.006	0.010	1.78	0.03	0.01	1.35	0.04	0.03
9312091417	1.19	0.11	0.17	0.06	0.010	0.010	1.38	0.03	0.02	1.20	0.04	0.05
9312091510	1.19	0.08	0.11	0.06	0.004	0.010	1.43	0.02	0.01	1.25	0.04	0.03
9312091625	1.13	0.09	0.12	0.06	0.004	0.010	1.33	0.03	0.01	1.24	0.03	0.03
9312100003	1.40	0.14	0.18	0.07	0.010	0.010	1.34	0.04	0.02	1.12	0.04	0.05
9312101130	1.21	0.09	0.13	0.06	0.004	0.010	1.45	0.03	0.01	1.28	0.03	0.03
9312101215	1.19	0.08	0.11	0.06	0.004	0.010	1.52	0.02	0.01	1.32	0.03	0.03
9312120004	0.90	0.06	0.11	0.04	0.030	0.010	1.33	0.02	0.01	1.16	0.04	0.03
9312131035	1.25	0.10	0.16	0.06	0.005	0.008	1.41	0.03	0.02	1.25	0.04	0.04
9312121145	1.32	0.10	0.17	0.07	0.005	0.008	1.28	0.04	0.02	1.48	0.05	0.05
9312121450	1.61	0.14	0.19	0.08	0.010	0.010	1.57	0.04	0.02	1.69	0.06	0.05
9312130005	1.09	0.09	0.16	0.05	0.005	0.008	1.19	0.03	0.02	1.04	0.04	0.04
9312131605	1.05	0.07	0.12	0.05	0.003	0.010	1.28	0.03	0.01	1.19	0.03	0.03
9405051000	0.81	0.05	0.05	0.04	0.002	0.003	1.04	0.01	0.01	0.82	0.01	0.01
9405051049	0.80	0.06	0.06	0.04	0.003	0.003	1.07	0.01	0.01	0.85	0.02	0.01
9405051200	0.83	0.09	0.09	0.04	0.004	0.004	1.12	0.02	0.01	0.80	0.02	0.02
9405051330	1.14	0.06	0.05	0.06	0.003	0.003	1.45	0.02	0.01	1.24	0.02	0.01
9405051415	1.69	0.14	0.12	0.08	0.010	0.010	1.94	0.04	0.02	1.71	0.04	0.03
9405051457	0.99	0.05	0.05	0.05	0.003	0.002	1.28	0.01	0.01	0.99	0.01	0.01

Table 5): Soil Sample Analytical Results
All Concentrations in pCi/g

Nuclide:	Ra-226 @ 186 keV			U-235 @ 185.7 keV			Th-232 @ 238.6 keV			Bi-214 @ 609.3 keV		
Sample/Time ID	Soil Activity Conc.	Standard Deviation (Sigma)	Lower Limit of Detection	Soil Activity Conc.	Standard Deviation (Sigma)	Lower Limit of Detection	Soil Activity Conc.	Standard Deviation (Sigma)	Lower Limit of Detection	Soil Activity Conc.	Standard Deviation (Sigma)	Lower Limit of Detection
9405051530	1.09	0.04	0.04	0.05	0.002	0.002	1.43	0.01	0.01	1.07	0.01	0.01
9405060925	1.01	0.04	0.04	0.05	0.002	0.002	1.50	0.01	0.01	1.08	0.01	0.01
9405061000	1.21	0.07	0.05	0.06	0.003	0.003	1.61	0.02	0.01	1.30	0.02	0.01
9405061036	1.08	0.03	0.04	0.05	0.001	0.002	1.28	0.01	0.004	1.02	0.01	0.01
9405061315	1.08	0.06	0.05	0.05	0.003	0.002	1.54	0.01	0.01	1.11	0.01	0.01
9405090925	1.27	0.04	0.04	0.06	0.002	0.002	1.34	0.01	0.01	1.31	0.01	0.01
9405091220	1.00	0.06	0.05	0.05	0.003	0.002	1.41	0.02	0.01	1.17	0.02	0.01
9405091300	0.93	0.04	0.05	0.05	0.002	0.002	1.32	0.01	0.01	1.00	0.01	0.01
9405091415	0.88	0.04	0.05	0.04	0.002	0.002	1.00	0.01	0.01	0.77	0.01	0.01
9405091420	0.81	0.04	0.05	0.04	0.002	0.002	1.02	0.01	0.01	0.81	0.01	0.01
9405100930	0.74	0.07	0.07	0.04	0.003	0.004	0.98	0.02	0.01	0.79	0.02	0.02
9405101240	0.98	0.05	0.13	0.05	0.003	0.007	1.37	0.01	0.02	1.10	0.01	0.01
9405111145	0.99	0.05	0.05	0.05	0.002	0.002	1.26	0.01	0.01	1.09	0.01	0.01
9405120915	1.01	0.06	0.06	0.05	0.003	0.003	1.15	0.02	0.01	1.10	0.02	0.01
9405120940	1.65	0.05	0.06	0.08	0.002	0.003	1.54	0.01	0.01	1.81	0.02	0.01
9405121115	1.72	0.05	0.05	0.09	0.003	0.003	2.24	0.01	0.01	1.81	0.02	0.01
9405121310	1.75	0.05	0.05	0.09	0.002	0.003	2.21	0.01	0.01	1.83	0.02	0.01
9405121340	2.44	0.08	0.06	0.12	0.004	0.003	2.16	0.02	0.01	2.44	0.02	0.01
9405121350	2.21	0.05	0.06	0.11	0.003	0.003	2.22	0.02	0.01	2.59	0.02	0.01
9409176500	1.41	0.10	0.4	0.07	0.005	0.005	1.16	0.03	0.01	1.34	0.03	0.02
9409171130	1.50	0.08	0.06	0.07	0.003	0.003	1.34	0.02	0.01	1.45	0.02	0.02

Table 6): Soil Sample Analytical Results
All Concentrations in pCi/g

Nuclide:	Cs-137 @ 661.7 keV			U-238 @ 1001 keV			K-40 @ 1462 keV			Exposure Rates		
Sample/Time ID	Soil Activity Conc.	Standard Deviation (Sigma)	Lower Limit of Detection	Soil Activity Conc.	Standard Deviation (Sigma)	Lower Limit of Detection	Soil Activity Conc.	Standard Deviation (Sigma)	Lower Limit of Detection	Soil Estimate uR/h	HPIC Measured uR/h	Fraction Est/Meas
9308090945	0.17	0.01	0.02	ND	-	1.35	19.14	0.22	0.71	6.6	13.6	0.49
9312081630	0.47	0.03	0.09	5.45	2.12	1.49	17.90	0.43	1.27	8.6	-	-
9312090002	0.10	0.02	0.04	1.42	0.48	0.83	21.78	0.34	0.89	9.6	-	-
9312091417	0.18	0.02	0.02	ND	-	1.29	17.87	0.38	1.16	7.9	-	-
9312091510	0.16	0.02	0.01	1.53	0.76	0.71	19.77	0.28	0.83	8.4	-	-
9312091625	0.15	0.02	0.09	ND	-	1.52	18.60	0.43	1.30	7.9	-	-
9312100003	0.28	0.02	0.08	2.30	1.04	1.41	18.38	0.41	1.23	7.7	-	-
9312101130	0.17	0.02	0.05	ND	-	0.86	20.38	0.32	0.91	8.5	-	-
9312101215	0.19	0.02	0.01	3.65	0.77	0.67	21.81	0.27	0.80	9.0	-	-
9312120004	0.15	0.01	0.04	1.34	0.66	0.71	18.25	0.26	0.55	7.7	-	-
9312131035	0.10	0.02	0.07	ND	-	1.15	18.43	0.36	1.08	8.1	-	-
9312121145	0.07	0.01	0.08	ND	-	1.30	13.36	0.33	1.17	7.4	-	-
9312121450	0.15	0.01	0.04	ND	-	0.75	16.05	0.25	0.85	8.8	-	-
9312130005	0.15	0.02	0.07	3.05	1.05	1.23	17.76	0.37	1.13	7.2	-	-
9312131605	0.05	0.01	0.04	2.93	1.22	0.79	13.57	0.24	0.87	7.0	-	-
9405051000	0.21	0.01	0.02	1.48	0.68	0.19	13.50	0.12	0.33	5.8	12.8	0.45
9405051049	0.22	0.01	0.03	1.48	0.62	0.26	13.73	0.18	0.39	6.0	12.8	0.47
9405051200	0.16	0.01	0.04	2.42	0.79	0.41	14.01	0.20	0.50	6.0	12.8	0.47
9405051330	0.73	0.01	0.02	1.16	0.74	0.19	11.62	0.11	0.34	7.1	13.7	0.52
9405051415	0.33	0.02	0.07	3.24	1.36	0.67	14.70	0.28	0.69	9.5	13.4	0.71
9405051457	0.53	0.01	0.01	2.41	0.77	0.14	13.77	0.10	0.30	6.7	12.9	0.52

Table 7): Soil Sample Analytical Results
All Concentrations in pCi/g

Nuclide:	Cs-137 @ 661.7 keV			U-238 @ 1001 keV			K-40 @ 1462 keV			Exposure Rates		
Sample/Time ID	Soil Activity Conc.	Standard Deviation (Sigma)	Lower Limit of Detection	Soil Activity Conc.	Standard Deviation (Sigma)	Lower Limit of Detection	Soil Activity Conc.	Standard Deviation (Sigma)	Lower Limit of Detection	Soil Estimate uR/h	HPIC Measured uR/h	Fraction Est/Meas
9405051530	0.14	0.01	0.01	2.50	0.63	0.105	16.27	0.08	0.28	7.5	13.4	0.56
9405060925	0.15	0.01	0.01	1.82	0.65	0.08	20.25	0.11	0.29	8.3	14.7	0.57
9405061000	0.74	0.01	0.01	ND	-	1.65	20.80	0.15	0.32	9.0	16.0	0.56
9405061036	0.85	0.01	0.004	1.79	0.38	0.04	11.71	0.06	0.26	6.4	12.4	0.52
9405061315	0.90	0.11	0.31	1.88	0.77	0.10	15.42	0.11	0.31	7.7	13.2	0.59
9405090925	0.42	0.01	0.01	2.24	0.59	0.11	11.54	0.07	0.28	7.0	13.7	0.51
9405091220	0.20	0.01	0.01	2.42	0.89	0.17	13.09	0.11	0.32	7.2	13.3	0.54
9405091300	0.09	0.01	0.01	0.95	0.43	0.17	13.01	0.11	0.32	6.7	13.5	0.49
9405091415	0.03	0.01	0.01	1.37	0.33	0.15	12.51	0.10	0.31	5.5	11.3	0.48
9405091420	0.05	0.01	0.01	ND	-	1.05	12.97	0.10	0.30	5.7	11.3	0.50
9405100930	0.23	0.01	0.03	0.72	0.86	0.27	12.68	0.16	0.43	5.5	12.8	0.43
9405101240	0.06	0.01	0.02	1.97	0.56	1.57	15.87	0.12	0.14	7.4	13.0	0.57
9405111145	0.10	0.01	0.01	2.09	0.60	0.15	14.88	0.11	0.31	7.0	11.6	0.60
9405120915	0.09	0.01	0.02	ND	-	2.10	15.62	0.14	0.35	6.8	12.4	0.55
9405120940	1.69	0.01	0.02	2.88	0.53	0.17	10.16	0.12	0.35	8.0	12.4	0.64
9405121115	1.81	0.02	0.02	3.20	0.70	0.15	14.67	0.15	0.34	10.3	14.8	0.70
9405121310	0.56	0.01	0.02	2.59	0.50	0.14	14.10	0.13	0.33	10.2	14.9	0.69
9405121340	1.88	0.02	0.02	2.60	0.92	0.19	14.42	0.15	0.37	11.1	18.2	0.61
9405121350	1.83	0.02	0.02	3.51	0.81	0.22	14.83	0.14	0.36	11.5	18.2	0.63
9409176500	1.54	0.02	0.05	1.79	1.13	0.44	11.03	0.15	0.53	6.5	12.4	0.52
9409171130	3.53	0.02	0.01	3.33	0.91	0.29	13.23	0.13	0.42	7.4	14.5	0.51

Table 8): Albuquerque Regional Integrated Exposure Rates - TLD Environmental Fade Characteristics Study
Period: 2Q 1993, Comparison of Monthly, Bimonthly and Quarterly Rates
M: 4/7 - 5/13/93, B: 5/13 - 7/7/93 Q(S): 4/7 - 7/7/93

STATION	ID No.: SNL (S) ITRI (I)	Monthly (36 d)		Bimonthly (55 d)		Quarterly (91 d)		Monthly/Bimonthly Time Weighted Sum	
		Net uR/hr	Sigma uR/hr	Net uR/hr	Sigma uR/hr	Net uR/hr	Sigma uR/hr	TWS uR/hr	TWS vs. Quarterly RPD%
(0) Background	(NA)	1.5	2.1	1.6	1.3	1.5	0.3	1.6	-4.03
(1) Northwest of SNL TA II Gate, KAFB	2022 (S)	12.3	0.5	9.7	0.4	9.1	0.9	10.7	-17.90
(3) South of SNL TA IV, KAFB	4203 (S)	11.6	0.5	10.2	0.9	10.5	1.3	10.8	-2.42
(5) North of TA V Stack, KAFB	8004 (S)	12.5	0.6	12.3	0.6	11.4	0.6	12.4	-8.59
(6) SNL Mixed Waste Landfill, TA III	3006 (S)	12.2	1.3	12.8	0.2	11.4	0.3	12.6	-10.20
(9) SNL TA V North Exclusion Fence, KAFB	5005 (S)	12.1	0.7	12.7	0.3	9.4	0.7	12.5	-32.58
(10) East of SNL HERMES Facility, KAFB	5006 (S)	12.1	0.7	12.4	0.4	9.6	0.9	12.3	-27.93
(11) SNL TAV South Exclusion Fence, KAFB	5007 (S)	12.8	0.9	9.0	0.8	11.6	0.5	10.5	9.45
(13) North of USGS Seismological Laboratory, KAFB	8032 (S)	11.6	0.8	*	*	12.0	0.7	11.9	3.33
(16) Tijeras Canyon East of TA IV, KAFB	8005 (S)	11.3	0.5	11.2	1.5	11.9	0.7	11.2	5.55
(17) Tijeras Canyon East of TA II, KAFB	8006 (S)	11.1	0.7	10.4	0.5	11.4	0.4	10.7	6.34
(18) Four Hills: KAFB Well 11, KAFB	8009 (S)	13.7	0.8	12.7	1.6	13.6	0.4	13.1	3.71
	Averages	12.1	0.7	11.3	0.7	11.1	0.7	11.7	-6.5
(**) Averages from Field Deployed TLDs	All Field Sites	POP DEV	0.7	POP DEV	1.4	POP DEV	1.3	POP DEV	0.9
		TOTAL D	2.6	TOTAL D	3.1	TOTAL D	2.8	RPD DEV	14.4

*NOTE: TLD for this location was unreadable in this period;
TWS was calculated from monthly and quarterly data as best estimate.

Table 9) CaSO4(Tm) Thermoluminescent Dosimeter Quarterly Results for Sites on Kirtland Air Force Base, Albuquerque, NM

STATION	Site ID No. SNL (S) or ITRI(I)	2Q 1993			3Q 1993			4Q 1993		
		TLD uR/h	Sigma uR/h	COV %	TLD uR/h	Sigma uR/h	COV %	TLD uR/h	Sigma uR/h	COV %
(1) Northwest of SNL TA II Gate, KAFB	2022 (S)	9.6	0.9	9.5	10.1	1.0	9.9	13.3	1.2	9.2
(2) South Corner of SNL TA II, KAFB	2023 (S)	10.6	0.4	4.0	11.9	0.5	4.0	10.9	1.2	9.2
(3) South of SNL TA IV, KAFB	4203 (S)	11.1	1.3	12.1	10.8	1.5	13.7	11.7	2.1	18.1
(4) Pennsylvania Av Bridge at Tijeras Arroyo, KAFB	8008 (S)	12.1	0.5	4.5	10.7	0.6	6.3	12.3	1.9	15.2
(5) North of TA V Stack, KAFB	8004 (S)	12.1	0.6	5.0	10.5	0.7	6.3	14.1	0.4	3.0
(6) SNL Mixed Waste Landfill, TA III	3006 (S)	12.1	0.3	2.5	11.3	0.3	3.0	14.5	1.6	11.1
(7) SNL Radioactive Waste Management Facility, TA III	3007/8 (S)	9.5	0.5	5.0	10.3	0.5	5.1	13.6	0.7	4.9
(8) SNL Building 6505, TA III	3001 (S)	9.2	0.7	8.1	10.3	0.8	8.0	12.1	1.5	10.1
(9) SNL TA V North Exclusion Fence, KAFB	5005 (S)	10.0	0.8	7.7	10.0	0.8	8.4	15.0	1.5	10.1
(10) East of SNL HERMES Facility, KAFB	5006 (S)	10.3	1.0	9.8	10.0	1.1	11.0	10.9	1.3	11.6
(11) SNL TAV South Exclusion Fence, KAFB	5007 (S)	12.4	0.5	4.0	10.3	0.5	5.3	10.9	1.8	16.2
(12) SNL Coyote Range Headquarters, KAFB	6005 (S)	12.1	0.8	6.7	12.2	0.9	7.2	10.8	0.4	3.5
(13) North of USGS Seismological Laboratory, KAFB	8032 (S)	12.7	0.7	5.8	11.0	0.8	7.3	11.6	0.4	3.3
(14) McCormick Ranch Gate, KAFB	8007 (S)	10.9	0.6	5.7	10.1	0.7	6.7	9.2	0.5	5.8
(15) Isleta Reservation Gate, KAFB	8031 (S)	11.9	0.2	1.7	10.6	0.7	6.4	10.9	0.7	6.1
(16) Tijeras Canyon East of TA IV, KAFB	8005 (S)	12.7	0.8	6.2	9.7	0.2	2.3	11.5	0.8	6.8
(17) Tijeras Canyon East of TA II, KAFB	8006 (S)	12.1	0.4	3.6	11.5	0.9	7.4	12.2	0.9	7.4
(18) Four Hills: KAFB Well 11	8009 (S)	14.5	0.4	2.9	11.2	0.5	4.2	15.5	0.8	4.9
(19) KAFB Boundary, North of Officer's Club	8014 (S)	nd	nd	nd	12.2	0.5	3.7	11.9	0.7	5.8
(20) SE of ITRI, KAFB Reservation Boundary	D1 (I)	nd	nd	nd	10.0	0.5	4.5	12.1	0.6	4.6
(21) S of ITRI Lagoons, Reservation Boundary	D2 (I)	nd	nd	nd	11.8	0.5	3.9	11.3	0.4	3.4
(22) SW of ITRI, KAFB Reservation Boundary	D3 (I)	nd	nd	nd	10.1	0.5	4.5	10.2	0.6	6.4
(**) Averages of Field Values	Reported	11.4	0.6	5.8	10.8	0.7	6.3	12.1	1.0	8.0

Table 10) CaSO4(Tm) Thermoluminescent Dosimeter Quarterly Results for Sites on Kirtland Air Force Base, Albuquerque, NM

STATION	Site ID# SNL (S) ITRI(I)	1Q 1994			2Q 1994			Time Period Sample Average		
		TLD uR/h	Sigma uR/h	COV %	TLD uR/h	Sigma uR/h	COV %	TLD uR/h	Sigma uR/h	COV %
(1) Northwest of SNL TA II Gate, KAFB	2022 (S)	11.0	0.6	5.5	13.2	1.0	7.3	11.4	1.7	15.1
(2) South Corner of SNL TA II, KAFB	2023 (S)	14.1	2.1	14.9	11.5	0.2	2.1	11.8	1.4	11.7
(3) South of SNL TA IV, KAFB	4203 (S)	11.1	0.8	7.0	12.1	2.2	17.9	11.4	0.5	4.6
(4) Pennsylvania Av Bridge at Tijeras Arroyo, KAFB	8008 (S)	11.2	0.8	7.0	12.5	2.1	16.9	11.8	0.8	6.6
(5) North of TA V Stack, KAFB	8004 (S)	11.1	0.6	5.1	14.7	0.4	3.1	12.5	1.8	14.7
(6) SNL Mixed Waste Landfill, TA III	3006 (S)	11.0	1.1	10.3	13.6	1.7	12.7	12.5	1.5	12.0
(7) SNL Radioactive Waste Management Facility, TA III	3007/8 (S)	10.4	0.8	7.5	13.1	1.7	12.7	11.4	1.8	16.2
(8) SNL Building 6505, TA III	3001 (S)	10.7	0.8	7.5	14.8	1.3	8.6	11.4	2.2	18.9
(9) SNL TA V North Exclusion Fence, KAFB	5005 (S)	11.2	1.0	9.2	12.3	1.4	11.0	11.7	2.1	17.8
(10) East of SNL HERMES Facility, KAFB	5006 (S)	10.8	0.5	4.4	11.8	2.1	17.7	10.8	0.7	6.4
(11) SNL TAV South Exclusion Fence, KAFB	5007 (S)	10.9	0.4	4.1	10.6	0.5	4.9	11.0	0.8	7.4
(12) SNL Coyote Range Headquarters, KAFB	6005 (S)	10.6	0.6	6.1	11.3	0.6	5.4	11.4	0.7	6.4
(13) North of USGS Seismological Laboratory, KAFB	8032 (S)	10.5	0.7	7.1	11.5	0.7	6.5	11.5	0.8	7.2
(14) McCormick Ranch Gate, KAFB	8007 (S)	10.2	0.9	8.7	10.5	0.7	6.5	10.2	0.6	6.2
(15) Isleta Reservation Gate, KAFB	8031 (S)	10.8	0.8	7.4	10.9	0.6	5.6	11.0	0.5	4.6
(16) Tijeras Canyon East of TA IV, KAFB	8005 (S)	12.4	0.5	4.4	12.7	1.4	10.7	11.8	1.3	10.8
(17) Tijeras Canyon East of TA II, KAFB	8006 (S)	11.0	0.6	5.1	10.6	0.6	5.8	11.5	0.7	6.0
(18) Four Hills: KAFB Well 11	8009 (S)	12.4	1.3	10.6	12.3	0.2	1.5	13.2	1.8	13.4
(19) KAFB Boundary, North of Officer's Club	8014 (S)	11.2	1.3	10.6	9.8	0.7	6.8	11.3	1.1	9.5
(20) SE of ITRI, KAFB Reservation Boundary	D1 (I)	12.7	1.1	9.1	11.5	0.7	6.5	11.6	1.2	10.0
(21) S of ITRI Lagoons, Reservation Boundary	D2 (I)	11.6	1.5	13.3	11.4	0.6	5.5	11.5	0.2	1.9
(22) SW of ITRI, KAFB Reservation Boundary	D3 (I)	12.2	1.0	8.1	11.2	0.7	6.4	10.9	1.0	9.0
(**) Averages of Field Values	Reported	11.3	0.9	7.9	12.0	1.0	8.3	11.4	1.1	9.8

Table 11) CaSO4(Tm) Thermoluminescent Dosimeter Quarterly Results for Albuquerque Vicinity Sites

STATION	Site ID No. SNL (S) or ITRI(I)	2Q 1993			3Q 1993			4Q 1993		
		TLD uR/h	Sigma uR/h	COV %	TLD uR/h	Sigma uR/h	COV %	TLD uR/h	Sigma uR/h	COV %
(23) AFD Station 11, 5403 Southern SE, Albuquerque	9016 (S)	11.8	0.1	0.8	12.6	0.6	4.8	12.6	0.6	4.8
(24) Los Lunas FD, Los Lunas	9027 (S)	8.9	0.6	6.7	12.1	0.5	4.1	12.2	0.6	4.9
(25) AFD Station 2, 301 High Street SE, Albuquerque	9011 (S)	9.7	0.4	4.1	10.3	0.9	8.7	12.1	1.0	8.3
(26) AFD Station 6, 523 Griegos NW, Albuquerque	9018 (S)	10.9	0.9	8.3	10.2	0.5	4.9	12.9	0.6	4.7
(27) Sandoval County VFD Station 10, Placitas	9019 (S)	9.6	1.1	11.5	10.2	0.8	7.8	11.9	1.1	9.2
(28) Corrales VFD, Corrales Rd., Corrales	9021 (S)	8.8	0.7	8.0	9.0	0.6	6.7	11.5	1.1	9.6
(29) Rio Rancho VFD, 19th Avenue, Rio Rancho	9033 (S)	10.9	0.9	8.3	12.3	0.4	3.3	11.6	0.4	3.4
(30) AFD Station 9, 9601 Menaul NE, Albuquerque	9017 (S)	11.1	0.5	4.5	13.2	1.5	11.4			
(31) AFD Station 7, 116 47th St. NW, Albuquerque	9029 (S)	9.2	1.4	15.2	12.3	0.6	4.9			
(32) USFS Oak Flats Campground, NM 14 10 mi S of I40	9010 (S)				13.2	0.8	6.1	14.6	0.6	4.1
(33) Albuquerque West Side, Paradise Hills	(NA)	11.2	0.3	2.7				10.9	0.6	5.5
(**) Averages of Field Values	Reported	10.2	0.7	7.0	11.5	0.7	6.3	12.3	0.7	6.1

Table 12) CaSO4(Tm) Thermoluminescent Dosimeter Quarterly Results for Albuquerque Vicinity Sites

STATION	Site ID# SNL (S) ITRI(I)	1Q 1994			2Q 1994			Time Period Sample Average		
		TLD uR/h	Sigma uR/h	COV %	TLD uR/h	Sigma uR/h	COV %	TLD uR/h	Sigma uR/h	COV %
(23) AFD Station 11, 5403 Southern SE, Albuquerque	9016 (S)	12.8	0.4	3.1	9.8	1.0	7.3	11.9	1.2	10.5
(24) Los Lunas FD, Los Lunas	9027 (S)	9.7	0.6	6.2	11.9	0.2	2.1	11.0	1.5	14.1
(25) AFD Station 2, 301 High Street SE, Albuquerque	9011 (S)	9.9	0.5	5.1	12.4	2.2	17.9	10.9	1.3	11.7
(26) AFD Station 6, 523 Griegos NW, Albuquerque	9018 (S)	10.5	0.6	5.7	12.5	2.1	16.9	11.4	1.2	10.7
(27) Sandoval County VFD Station 10, Placitas	9019 (S)	10.2	0.3	2.9	12.9	0.4	3.1	11.0	1.4	12.6
(28) Corrales VFD, Corrales Rd., Corrales	9021 (S)	10.3	0.5	4.9	12.5	1.7	12.7	10.4	1.6	15.3
(29) Rio Rancho VFD, 19th Avenue, Rio Rancho	9033 (S)	10.1	0.5	5.0	12.0	1.7	12.7	11.4	0.9	7.8
(30) AFD Station 9, 9601 Menaul NE, Albuquerque	9017 (S)	11.6	0.7	6.0	15.0	1.3	8.6	12.7	1.8	13.8
(31) AFD Station 7, 116 47th St. NW, Albuquerque	9029 (S)	10.1	0.3	3.0	12.1	1.4	11.0	10.9	1.5	13.9
(32) USFS Oak Flats Campground, NM 14 10 mi S of I40	9010 (S)	11.6	0.7	6.0	14.3	2.1	17.7	13.4	1.4	10.1
(33) Albuquerque West Side, Paradise Hills	(NA)	9.7	0.9	9.3	9.4	0.5	4.9	10.3	0.9	8.6
(**) Averages of Field Values	Reported	10.6	0.5	5.2	12.3	1.3	10.4	11.4	1.3	11.7

Table 13) CaSO4(Tm) Thermoluminescent Dosimeter Ambient Exposures Averaged from 2nd Quarter 1993 to 2nd Quarter 1994, with HPIC Method Comparisons: Sites on Kirtland Air Force Base

STATION	Site ID No.: SNL (S) ITRI (I)	Exposure Rates					GPS Spatial Coordinates		
		AVG TLD uR/h	HPIC uR/h	RPD %	AVG SNL (uR/h)	RPD %	Latitude North degrees	Longitude West degrees	Elevation feet
(1) Northwest of SNL TA II Gate, KAFB	2022 (S)	11.4	13.2	-14.3	11.5	-0.2	35.0385	106.5410	5410
(2) South Corner of SNL TA II, KAFB	2023 (S)	11.8	13.4	-12.7	12.1	-2.7	35.0403	106.5412	5410
(3) South of SNL TA IV, KAFB	4203 (S)	11.4	13.3	-15.7	11.4	-0.2	35.0325	106.5458	5380
(4) Pennsylvania Av Bridge at Tijeras Arroyo, KAFB	8008 (S)	11.8	13.0	-10.0	12.3	-4.2	35.0293	106.5463	5290
(5) North of TA V Stack, KAFB	8004 (S)	12.5	12.7	-1.6	11.2	11.2	35.0003	106.5348	5435
(6) SNL Mixed Waste Landfill, TA III	3006 (S)	12.5	12.8	-2.4	11.3	10.0	34.9922	106.5465	5380
(7) SNL Radioactive Waste Management Facility, TA III	3007/8 (S)	11.4			10.7	6.1	34.9718	106.5375	5400
(8) SNL Building 6505, TA III	3001 (S)	11.4	11.7	-2.4	11.2	2.4	34.9912	106.5356	5435
(9) SNL TA V North Exclusion Fence, KAFB	5005 (S)	11.7	11.9	-1.7	11.1	5.0	34.9995	106.5320	5450
(10) East of SNL HERMES Facility, KAFB	5006 (S)	10.8	11.8	-9.2	10.8	0.0	34.9987	106.5257	5480
(11) SNL TAV South Exclusion Fence, KAFB	5007 (S)	11.0	12.0	-8.5	11.0	0.2	34.9932	106.5293	5470
(12) SNL Coyote Range Headquarters, KAFB	6005 (S)	11.4	13.1	-13.9	11.1	2.9	34.9697	106.4908	5710
(13) North of USGS Seismological Laboratory, KAFB	8032 (S)	11.5	13.6	-17.1	11.8	-3.3	34.9473	106.4597	5935
(14) McCormick Ranch Gate, KAFB	8007 (S)	10.2	11.9	-15.6	10.1	1.1	34.9698	106.5688	5293
(15) Isleta Reservation Gate, KAFB	8031 (S)	11.0	12.1	-9.3	10.9	1.0	34.9473	106.5432	5425
(16) Tijeras Canyon East of TA IV, KAFB	8005 (S)	11.8	13.3	-12.0	12.4	-4.9	35.0367	106.5333	5330
(17) Tijeras Canyon East of TA II, KAFB	8006 (S)	11.5	12.8	-10.9	11.7	-2.1	35.0405	106.5327	5340
(18) Four Hills: KAFB Well 11	8009 (S)	13.2	14.9	-12.3	13.3	-1.3	35.0432	106.5092	5600
(19) KAFB Boundary, North of Officer's Club	8014 (S)	11.3	12.4	-9.5	11.2	0.7	35.0672	106.5397	5430
(20) SE of ITRI, KAFB Reservation Boundary	D1 (I)	11.6	13.1	-12.4	NA	NA	34.9473	106.4935	5680
(21) S of ITRI Lagoons, Reservation Boundary	D2 (I)	11.5	12.8	-10.5	NA	NA	34.9473	106.5007	5630
(22) SW of ITRI, KAFB Reservation Boundary	D3 (I)	10.9	12.7	-15.0	NA	NA	34.9473	106.5058	5610
(**) Averages of Field Values	Reported	11.4	12.5	-9.2	11.4	1.1	34.9978	106.5270	5478

Table 14) CaSO4(Tm) Thermoluminescent Dosimeter Average Results for Second Quarter 1993 to Second Quarter 1994 Ambient Exposures with HPIC Method Comparisons; Albuquerque Vicinity Sites

STATION	Site ID No.: SNL (S) ITRI (I)	Exposure Rates					GPS Spatial Coordinates		
		AVG TLD uR/h	HPIC uR/h	RPD %	AVG SNL uR/h	RPD %	Latitude North degrees	Longitude West degrees	Elevation feet
(23) AFD Station 11, 5403 Southern SE, Albuquerque	9016 (S)	11.9	12.1	-1.5	11.2	5.8	35.0678	106.5853	5280
(24) Los Lunas FD, Los Lunas	9027 (S)	11.0	11.3	-3.1	9.8	11.1	34.8053	106.7303	4852
(25) AFD Station 2, 301 High Street SE, Albuquerque	9011 (S)	10.9	12.0	-9.8	11.0	-1.2	35.0808	106.6408	4950
(26) AFD Station 6, 523 Griegos NW, Albuquerque	9018 (S)	11.4	13.0	-13.1	12.3	-7.3	35.1313	106.6450	4860
(27) Sandoval County VFD Station 10, Placitas	9019 (S)	11.0	12.4	-12.3	10.7	2.4	35.2897	106.4066	6240
(28) Corrales VFD, Corrales Rd., Corrales	9021 (S)	10.4	12.6	-20.5	11.1	-6.1	35.1957	106.6440	5005
(29) Rio Rancho VFD, 19th Avenue, Rio Rancho	9033 (S)	11.4	10.7	6.2	10.5	8.1	35.2255	106.6698	5250
(30) AFD Station 9, 9601 Menaul NE, Albuquerque	9017 (S)	12.7	13.1	-2.9	12.9	-1.2	35.1093	106.5360	5490
(31) AFD Station 7, 116 47th St. NW, Albuquerque	9029 (S)	10.9	10.8	1.2	10.1	7.6	35.0852	106.6903	5120
(32) USFS Oak Flats Campground, NM 14 10 mi S of I40	9010 (S)	13.4	14.9	-10.4	12.1	10.1	35.0030	106.3255	7660
(33) Albuquerque West Side, Paradise Hills	(NA)	10.3	12.2	-16.9	NA	NA	35.1930	106.7176	5385
(**) Averages of Field Values	Reported	11.5	12.4	-7.2	11.3	3.7	35.1353	106.5972	5652

Table 15): Statistical Summaries
Albuquerque Area Environmental Measurements

Analyte	n	AM	-0.95CL	+0.95CL	GM	HM	Deviation
Nuclide (pCi/g):							
Ra-226	37	1.17	1.09	1.26	1.15	1.12	0.26
Bi-214	37	1.21	1.13	1.30	1.19	1.16	0.26
U-235	37	0.06	0.05	0.06	0.06	0.06	0.01
U-238	37	1.95	1.69	2.20	1.80	1.65	0.77
Th-232	38	1.44	1.33	1.54	1.40	1.37	0.31
K-40	38	15.7	14.7	16.7	15.5	15.3	3.1
Cs-137	34	0.26	0.18	0.35	0.18	0.14	0.24
Activity Ratio:							
U-238:Ra-226	37	1.65	1.44	1.85	-	-	0.73
Ra-226:Bi-214	38	0.96	0.94	0.99	-	-	0.08
Exposure Rate(uR/h):							
TLD-North	30	13.2	12.8	13.6	-	-	0.98
TLD-South	30	13.9	13.4	14.4	-	-	1.25
TLD-East	30	13.3	12.7	13.9	-	-	1.54
TLD-West	30	13.9	13.3	14.5	-	-	1.55
5-Q Average TLD	33	11.5	11.2	11.7	11.4	11.4	0.74
HPIC	53	13.1	12.8	13.0	13.0	13.0	1.27

Table 16): Statistical Summaries
New Mexico Statewide Environmental Measurements

Analyte	n	AM	-0.95CL	+0.95CL	GM	HM	Deviation
				Nuclide (pCi/g):			
Ra-226	41	1.28	1.12	1.43	1.16	1.01	0.48
Bi-214	41	0.69	0.61	0.76	0.64	0.60	0.02
U-235	41	0.05	0.05	0.06	0.05	0.04	0.02
U-238 (alpha-spec.)	40	0.61	0.53	0.69	0.56	0.51	0.25
Th-232	41	1.04	0.90	1.18	0.94	0.83	0.44
K-40	41	12.6	11.5	13.7	12.1	11.4	3.6
Cs-137	41	0.21	0.16	0.27	0.17	0.13	0.17

Table 17) Comparative Rock and Soil Concentrations

Material	Location	^{238}U	^{226}Ra	^{232}Th	^{40}K	^{137}Cs	Ref
Soils	Worldwide	–	0.8 (0.4-1.9)	0.7 (0.2-1.4)	10.0 (2.7-18.9)	–	131
Soils	US-Canada	1.8	-	1.0	10.8	-	104
Mafic Rocks	"	0.3	-	0.4	8 - 11	-	104
Sialic Rocks	"	1.0	-	1.9	29.7-40.5	-	104
Limestone	"	0.7	-	0.2	2.0	-	104
Soils	Spain	–	1.1 (0.2-8.4)	1.1 (0.1-6.8)	15.6 (0.8-55.1)	-	132
Soils	Chile	-	-	-	-	0.1-0.5	70
Soils	Nile Valley	0.3 - 0.7	-	0.3 - 1.3	5.0 - 10.2	-	133
Granite	California	0.8	-	1.0	18.4	-	134
Rhyolite	California	1.9	-	2.5	31.0	-	134
Basalt	"	0.3	-	0.3	5.9	-	134
Precambrian Sediments	"	0.6	-	1.0	15.1	-	134
Soils, Q/T Sediments	"	0.7	-	0.9	15.9	-	134
Soils	Rio Puerco Valley, NM	-	0.9-1.3	1.2	-	0.1-0.3	74
Soils	Rio Grande Valley, NM	-	-	-	-	0.2-0.8	135
Granite	Sandia Mtns New Mexico	1.2	-	1.8	29.4	-	14
Soils	Albuquerque New Mexico	1.6	-	1.4	23.6	-	14
Sediments	Albuquerque New Mexico	1.7	-	1.8	-	-	136

Table 18)
1994 EPA Performance Evaluations, Code UT

June 1994 Round

Nuclide	Prepared Concentration pCi/l	Control Precision pCi/l	UNM Concentration pCi/l	Standard Deviation	RPD %
Co-60	50.0	8.7	41.4	1.1	18.8
Zn-65	134.0	22.6	139.3	4.8	-3.9
Ru-106	252.0	43.4	238.3	9.5	5.6
Cs-134	40.0	8.7	41.5	0.3	-3.7
Cs-137	49.0	8.7	47.8	2.5	2.5
Ba-133	98.0	17.3	96.7	9.7	1.3

November 1994 Round

Nuclide	Prepared Concentration pCi/l	Expected Precision pCi/l	UNM Concentration pCi/l	Standard Deviation	RPD %
Co-60	59	5	47.4	0.1	21.8
Zn-65	100	10	93.4	4.7	6.8
Cs-134	24	5	23.8	0.1	0.8
Cs-137	49	5	37.5	0.4	26.6
Ba-133	73	7	64.9	8.1	11.7